PACIFIC EARTHQUAKE ENGINEERING
RESEARCH CENTER

Stochastic Characterization and Decision Bases under Time-Dependent Aftershock Risk in Performance-Based Earthquake Engineering

Gee Liek Yeo

C. Allin Cornell

Department of Civil and Environmental Engineering
Stanford University

PEER 2005/13
JULY 2005

Stochastic Characterization and Decision Bases under Time-Dependent Aftershock Risk in Performance-Based Earthquake Engineering

Gee Liek Yeo
Department of Civil and Environmental Engineering
Stanford University

C. Allin Cornell
Department of Civil and Environmental Engineering
Stanford University

PEER Report 2005/13
Pacific Earthquake Engineering Research Center
College of Engineering
University of California, Berkeley

July 2005

ABSTRACT

This report addresses the broad role of aftershocks in the Performance-based Earthquake Engineering (PBEE) process. This is an area which has, to date, not received careful scrutiny nor explicit quantitative analysis.

We begin by introducing Aftershock Probabilistic Seismic Hazard Analysis (APSHA). APSHA, similar to conventional mainshock PSHA, is a procedure to characterize the time-varying aftershock ground motion hazard at a site. We next show a methodology to quantify, in probabilistic terms, the multi-damage-state capacity of buildings in different post-mainshock damage states. A time-dependent building "tagging" policy (permitting or restricting occupancy) is then developed based on the quantification of life-safety threat in the aftershock environment using the probability of collapse as a proxy for fatality risk.

We also develop formal stochastic financial life-cycle cost models in both the post- and pre-mainshock environment. We include both transition and disruption costs in our model. Transition costs can be attributed to one-time financial losses due to structural and nonstructural damage to the building, and can also include the costs of evacuation of the occupants of a building. Disruption costs can be attributed to the downtime and limited functionality of the damaged building. We begin with the traditional Poisson model for temporally homogeneous mainshocks and extend it to nonhomogeneous aftershocks. Further, the model is generalized to include renewal processes for modeling mainshock occurrences and Markov-chain descriptions of the damage states of a building. The analysis procedures are nonhomogeneous Markov and semi-Markov decision analysis and stochastic dynamic programming (Howard (1971)).

Finally, we introduce a decision analytic framework under improving states of information for both the post- and pre-mainshock environment. We emphasize the role of information in potentially improving our decision-making capability. Decision bases include the expected life-cycle cost and rate of collapse in the aftershock environment. We also introduce the concept of the value of information to determine if obtaining more information is financially desirable, which can potentially improve the quality of the decision.

ACKNOWLEDGEMENTS

This work was supported in part by the Earthquake Engineering Research Centers Program of the National Science Foundation under award number EEC-9701568 through the Pacific Earthquake Engineering Research Center (PEER).

Any opinions, findings, and conclusions or recommendations expressed in this material are those of the author(s) and do not necessarily reflect those of the National Science Foundation.

CONTENTS

LIST OF FIGURES

LIST OF TABLES

1 Introduction

Earthquakes are rare natural catastrophes which have severe societal consequences in terms of fatalities and casualties, financial losses and business interruption when they occur. There are professionals from diverse disciplines such as seismology, structural engineering and social science who are committed to rational seismic risk management. Modern methods including Probabilistic Seismic Hazard Analysis (PSHA), damage and collapse analysis of buildings, fatality/casualty and financial loss estimation etc., all in formal, explicit probabilistic terms, attempt to identify and analyze all details and dimensions of the problem. A current title for this process is *Performance-based Earthquake Engineering* (PBEE), in its broad sense.

This report will address an entire facet of that large problem which has, to date, not received careful scrutiny nor explicit quantitative analysis: namely, the role of aftershocks in the broad PBEE process. After an earthquake of large magnitude (referred to as the mainshock), many induced events or aftershocks will occur. The mean rate of aftershocks, which is mainshock-magnitude, m_m, dependent, decreases with increasing elapsed time t from the occurrence of the mainshock. Thus, we will expect the interarrival times between aftershocks to be much shorter just after the main event. The aftershock magnitudes follow the same general relative frequency law as other earthquakes (i.e., the Gutenberg-Richter law). Aftershocks also typically occur close to the original rupture zone. Hence if the mainshock was near the structure of interest, so will be at least some of this family of aftershocks. The ground motions from aftershocks show the typically high event-to-event variability, implying the potential for larger motions from small magnitudes. The number, size, proximity and variability of aftershocks may represent a significant ground motion hazard. Aftershock ground motions may cause weakening and/or collapse of structures perhaps already damaged (but not yet repaired) by the mainshock. A schematic of the aftershock environment is shown in Figure 1.1.

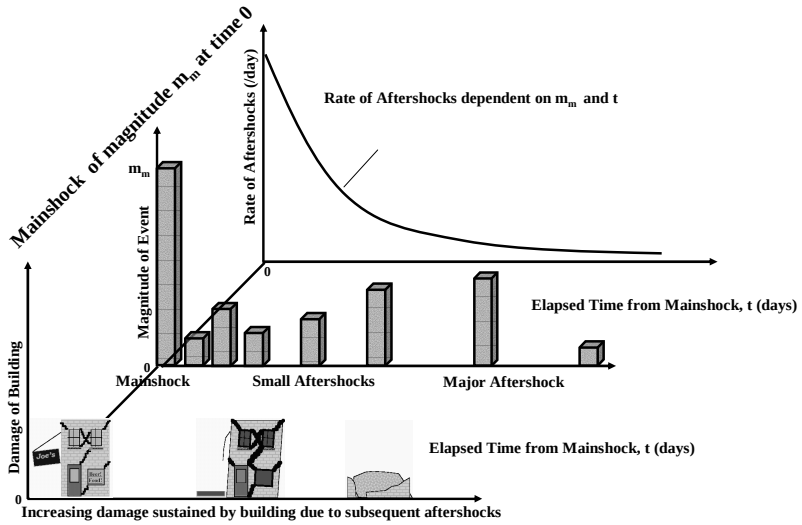

Figure 1.1: A schematic plot of the aftershock environment.

Aftershocks (implicitly or explicitly) also affect decisions to evacuate (possibly damaged) buildings because of the inferred life safety threat. For example, a magnitude 6.7 earthquake occurred in Algeria on 21^{st} May 2003 which killed over 1000 people and injured 7000 people. Many thousands more people were evacuated after the mainshock for fear of collapse of the damaged buildings in an aftershock. This situation is illustrated in Figure 1.2.

Also, Gallagher et al. (1999) provided guidelines on the safety evaluation of earthquake-damaged buildings as well as conditions for permitting entry into such buildings that may be structurally unsound based on the aftershock earthquake occurrence rates obtained for California in Reasenberg and Jones (1989) and Reasenberg and Jones (1994). Such building evacuations affect (a) public safety in post-quake recovery (e.g., closed hospitals and power distribution facilities) and (b) business and housing disruptions ("downtime losses"), which are among, if not *the*, major contributor to earthquake financial losses. See, for example, Comerio (2000).

Therefore, aftershock ground motion hazard, structural behavior of damaged buildings, evacuation (building "tagging") decisions, financial loss estimation, etc., all deserve special attention to identify and improve our understanding and processing of the role of aftershocks in earthquake engineering and earthquake risk management. This study of aftershocks will

Figure 1.2: Evacuated occupants in Algeria earthquake.

in many ways parallel that of the more familiar study of modern PBEE which has to date been restricted to mainshocks. The broad global study of PBEE is illustrated by the Pacific Earthquake Engineering Research (PEER) Center and its developments.

1.1 PBEE/PEER

Performance-based earthquake engineering (PBEE) has been an area of active research in the United States. PEER is currently spearheading an effort to develop a quantitative PBEE methodology which will allow stakeholders to make better informed decisions by providing them with probabilistic descriptions of system-level performance metrics. In order to achieve this ambitious objective, the performance assessment and design process has been divided into simpler elements in terms of the description, definition and quantification of earthquake intensity measures (IMs), engineering demand parameters (EDPs), damage measures (DMs) and decision variables (DVs). Commonly used examples of the above parameters are peak ground acceleration and first-mode spectral acceleration (IMs), interstory drift ratios, inelastic component deformations and floor acceleration spectra (EDPs), damage states of structural and nonstructural elements (DMs) and fatalities, financial losses and downtimes (DVs). A consistent probabilistic framework is used to explicitly and rigorously quantify the inherent uncertainties and randomness in all the above-mentioned variables.

See Moehle and Deierlein (2004) and Porter (2003) for details on PEER's methodology.

The PEER PBEE methodology developed for mainshocks can be expressed in the form of a triple integral based on the total probability theorem as shown in Equation 1.1.

$$\upsilon(DV) = \iiint G(DV|DM)dG(DM|EDP)dG(EDP|IM)|d\lambda(IM)| \tag{1.1}$$

This equation is commonly referred to as the "PEER Equation". Here, $\lambda(IM)$ is the mean annual rate of exceeding a given IM level and is obtained from a conventional Probabilistic Seismic Hazard Analysis (PSHA). $G(EDP|IM)$ is the shorthand notation for the complementary cumulative probability distribution function of EDP conditioned on a given level of IM, i.e., $G(EDP|IM) = P[EDP \geq y|IM = x]$ while in the continuous case, $|dG(EDP|IM)| = f_{EDP|IM}(y|x)dy$ is the conditional probability density function times dy. $G(DM|EDP)$ and $G(DV|DM)$ are defined in a similar manner. Each of the four components in Equation 1.1 is designed to require inputs from a specific discipline, for example, $\lambda(IM)$ from seismologists and geotechnical engineers, $G(EDP|IM)$ from structural engineers and $G(DV|DM)$ from cost estimators. The output of Equation 1.1 is $\upsilon_{DV}(DV \geq x)$ (or simply $\upsilon(DV)$), the mean annual rate of exceeding a given level of $DV = x$. Probabilistic information of DV can be used by building owners and stakeholders to make better seismic-risk related decisions. Note that IM, EDP, DM and DV can potentially also be vectors.

The PEER Equation involves pair-wise sequences of four random variables. It assumes one-step, or *Markov*, memory in the individual components such that we do not need to condition on all previous components but only on the last one. For example, it assumes that $G[DM > x|EDP = y$ and $IM = z]$ is equal to $G[DM > x|EDP = y]$, i.e., a function of only y. This presumes that EDP is "sufficient" with respect to DM and thus IM does not need to be included in the equation. See Cornell (2004).

The PEER Equation has been developed for mainshocks which are commonly modeled as homogeneous Poisson processes with time-independent mean rate of occurrences or intensity functions. Also, since PSHA is usually performed using the mean annual rates of mainshock occurrences, the resulting probabilistic description of DV is usually also defined on an annual basis. This mean annual basis is also consistent with current safety criteria which are commonly expressed in terms of mean annual fatality frequencies, e.g., following Okrent (1987). Consequently, because of the duration of one year which is implicit in the PEER Equation and because of the rarity of mainshocks, the likelihood of multiple mainshock

events is small. If the duration of interest is chosen to be other than one year (say T), then the mean number of events exceeding $DV = x$ in T becomes $v(DV)T$. If T is significantly longer than one year (for example, the life-span of the building), then multiple mainshocks are more likely. In this case, after one mainshock that has damaged the building, the PEER Equation implicitly assumes that the damaged building is repaired to its original pre-mainshock state (usually considered to be intact) before the occurrence of the next mainshock. Such a formulation permits the direct computation of expected life-cycle cost which is also commonly used as a building design criterion. However, if the DV is financial losses, the PEER Equation contains no explicit consideration of the time-value of money, since future financial losses are not discounted back to the present-day value.

The PEER Equation can be extended to take into account multiple mainshocks within the life-span of a structure with financial losses discounted at an appropriate discount rate. For example, if we wish to compute the expected total financial loss TL over the life-span of the building $t_{\max}$ with α as the annual constant deterministic discount rate and L as the financial losses given a mainshock, we can use Equation 1.2.

$$\begin{aligned} & E(TL; t_{\max}) \\ &= \int_0^{t_{\max}} \int_{DM} \int_{EDP} \int_{IM} E(Le^{-\alpha t}|DM) dG(DM|EDP) dG(EDP|IM) |d\lambda(IM)| dt \\ &= \frac{1 - e^{-\alpha t_{\max}}}{\alpha} \int_{DM} \int_{EDP} \int_{IM} E(L|DM) dG(DM|EDP) dG(EDP|IM) |d\lambda(IM)| \end{aligned} \tag{1.2}$$

This is similar to the formulation of expected life-cycle cost in Rosenblueth (1976) except that he assumed $t_{\max} = \infty$ such that the leading multiplier to the triple integral simplifies to $1/\alpha$. This formulation relaxes some limitations of the PEER Equation.

Wen and Kang (2001) also developed a formulation similar to Equation 1.2 as an input to rational (pre-mainshock) design criteria. Such a formulation provides us with a quantitative decision-making procedure where we select optimal building designs based on the minimization of expected life-cycle cost which includes the initial cost of design and construction and the cost of potential damage and failure during the building's life-span. The level of damage sustained by the building determines the functionality, and consequently, the downtime, of the structure. Business disruption financial losses from non-operable buildings should be included in the cost of damage as well. Wen and Kang (2001) incorporates

life-safety considerations in their methodology by including financial losses due to injuries and fatalities based on the economic value of human life. We shall revisit these models in Chapter 5.

1.2 Significance of Aftershocks in PBEE

In Section 1.1, we discussed financial losses, life-safety and downtimes in the context of mainshocks. However, these factors may also be very dependent on the real or threatened post-earthquake performance of (possibly mainshock-damaged) buildings in the aftershock environment where there is a significantly increased rate of earthquake occurrence. To the author's knowledge, before the studies here, these elements had not been addressed by PEER or other investigators. They do deserve closer scrutiny as aftershocks could potentially pose excessive life-safety threat to building occupants and contribute significantly to financial losses and downtime.

For example, after a mainshock, the life-safety threat that an occupant is exposed to could be considerably higher than before the occurrence of the mainshock, either because of the number, proximity, etc. of subsequent aftershocks or because of building damage, or both. Similarly, financial losses are also highly dependent on the downtime of the building which is in turn dependent on the "tag" given the building after the mainshock. After an earthquake, buildings might suffer significant damage without collapse. Hence, there is a need to inspect such buildings to decide if it is necessary to evacuate their occupants based on the damage sustained by the buildings. The decision is denoted by a tag, green, yellow or red, on the door to the building. A building that has suffered significant structural damage in the mainshock could be yellow or red-tagged, necessitating the evacuation of all building occupants. This building-tagging issue has been addressed in Bazzurro et al. (2004a) and Luco et al. (2004). Also, buildings that have not been structurally damaged might require a period of time of closure for clean-up of damaged nonstructural building components to restore building functionality. Furthermore, buildings that have been structurally damaged and are yellow or red-tagged will require more detailed inspection and/or engineering analysis to perhaps confirm that the building is still in fact structurally sound, or repair might be required to restore the structural integrity before re-occupancy of the building can be permitted. Thus, the downtime due to the nonfunctionality of the building may significantly increase the financial losses due to loss of revenue. In some cases, unless the

continued functionality of the building is essential to the building owner, it might take two years or more before re-opening of the mainshock-damaged building. Comartin (2004) and Comerio (2000) have documented examples of such cases of significant business disruption in mainshock-damaged buildings.

Also, the emergency situation in the post-mainshock environment brings with it a series of decisions that need to be addressed in a short period of time. These include the building-tagging and evacuation decisions which we have discussed earlier as well as inspection, analysis and repair decisions and re-occupancy decisions. Such decisions are fundamentally dependent on the life-safety threat due to occupancy of the possibly mainshock-damaged building. The predominant ground motion hazard may very well be that due to aftershocks, at least initially. The decisions made in the post-mainshock environment can have a significant impact on both life-safety and financial losses. For example, the evacuation of building-occupants would reduce the life-safety threat posed by that building but increase the financial losses due to delay of resumption of normal operations. On the other hand, the decision to evacuate a facility critical to post-quake recovery (such as a hospital or electrical substation) may reduce the safety of those dependent on its operation during the recovery period. Also prolonged evacuation of building occupants in residences may increase exposure to public health problems. Such trade-offs should in principle be considered in the policy and process of decision making. Moreover, these decisions can be made or re-considered at any time after the mainshock. For example, allowing re-occupancy of a damaged building is a decision which can be influenced by the gradually decaying aftershock ground motion threat. Thus, it is desirable to develop a methodology that will allow us to determine the optimal action and when it should be taken after the mainshock.

Such decisions might be information-sensitive as well. For example, early rapid inspections might provide only limited information about the damage state of the building such that different probabilities should be given to different damage states, representing the then-current epistemic uncertainty. Detailed inspections thereafter might allow one to quantify the damage state with more confidence, i.e., the probabilities assigned to different states might be revised substantially, narrowing the range of possible states. Such information may allow better decisions to be made about the tag of the building which is in turn dependent on the damage sustained by the structure due to the mainshock. Thus, it is desirable when dealing with aftershocks to develop a methodology which addresses the impact and value of additional information on post-quake decision making as well.

Because the performance of mainshock-damaged buildings in the aftershock environment may have such a significant impact on the post-quake functionality and economic consequences of an earthquake, aftershock considerations should perhaps also have substantial influence on pre-mainshock design criteria and pre-mainshock decision making. An example of pre-mainshock decision would be whether or not to retrofit prior to the occurrence of a mainshock or whether to expend additional funds to provide a structure with enhanced aftershock performance (e.g., to introduce self-centering connections that reduce the residual displacements that are known to increase building capacity to withstand aftershocks. See Kwan and Billington (2003a), Kwan and Billington (2003b) and Luco et al. (2004).). A methodology for pre-mainshock decision making incorporating such post-quake functionality issues is also a desirable objective.

Based on the discussion above, it is clear that the proposed formulation for the aftershock risk assessment problem should be developed in terms of both life-safety and financial losses and that it should address the critical decisions that need to be made at various times after a mainshock. It should also address the pre-mainshock decisions that are dependent on post-quake functionality of structurally damaged buildings. The development of such a methodology will be the focus of this report.

1.3 Challenges of Aftershock Risk Analysis

The aftershock environment poses several conceptual challenges that are different from those in the mainshock environment. Aftershock ground motion hazard and the induced undesirable building behavior hazard are nonhomogeneous in time: they are at their maximum immediately after the mainshock and decrease after that. The magnitude distribution of aftershocks is independent of the elapsed time after the mainshock, so aftershocks of large magnitudes are still possible a long time after the mainshock. The mean rate and the magnitude distribution of aftershocks are dependent on the mainshock magnitude and the probability distribution of aftershock locations are dependent on the mainshock rupture zone geometry. Because of the increased mean rate of aftershocks, the variability in ground motions and the damage sustained by the structure, aftershocks of smaller magnitudes can potentially produce larger site ground motion intensity measure (IM) values and larger engineering demand parameter (EDP) values than the mainshock.

For example, the 1983 California Coalinga earthquake had an aftershock of moment

magnitude 5.9 resulting in a PGA of 0.43g at the Pleasant Valley pump plant. This observed PGA exceeded the PGA of 0.31g at the same site due to the mainshock of moment magnitude 6.5 about two months earlier (USGS (1986)). The Coalinga example is a case of a site with typical, limited degree of instrumentation. An example with dense instrumentation is that of the 2004 Japan Niigata earthquake where an aftershock of moment magnitude 6.3 resulted in a PGA of 0.15g, whereas the mainshock of moment magnitude 6.6 resulted in a PGA of 0.1g half an hour earlier (PGA values obtained from the COSMOS Virtual Data Center). This is simply a single example. There may well be other sites with similar differences during the sequence of aftershocks.

Because of this potential for larger ground motions due to aftershocks, even buildings that have not been damaged by the mainshock have some likelihood of being damaged due to the occurrence of an aftershock. Mainshock-damaged buildings are even more susceptible to incremental damage due to aftershocks because their reduced structural capacity reduces the threshold of the ground motion intensity needed to cause further damage.

Even though systematic data collection of building damage progression in mainshocks and subsequent aftershocks has apparently been non-existent, there are several examples of aftershocks resulting in further damage or even collapse reported in literature. For example, the 1999 Turkey Kocaeli earthquake with a mainshock of moment magnitude 7.4 had a documented example of an aftershock of moment magnitude 5.9 almost one month later which killed seven people, injured at least 239 people and caused dozens of buildings to collapse in three cities near the epicenter of the aftershock (USGS (2000)). Figure 1.3 excerpted from USGS (2000) shows an example of a building in Gölcük which was somewhat damaged by the mainshock, and which subsequently collapsed due to the aftershock of moment magnitude 5.9 almost one month later.

Another documented example is the moment magnitude 5.7 Italy Molise earthquake on October 31 2002 which had an aftershock the next day with a similar moment magnitude of 5.7. Figure 1.4 shows an example of a column (highlighted in the left-hand picture) in a four-story building which was not damaged significantly by the mainshock, but which suffered severe joint damage shown in the right-hand picture during the aftershock.

Further, Lew et al. (2000) reported the collapse of a mainshock-damaged gasoline service station in an aftershock in the 1999 Taiwan Chi-Chi earthquake. Lastly, a nine-story reinforced concrete building which had already been severely damaged in the 1995 Japan Kobe earthquake, is also reported in Whittaker et al. (1997) to have overturned due

(a) After mainshock of magnitude 7.4 on August 17, 1999

(b) After aftershock of magnitude 5.9 on September 13, 1999

Figure 1.3: Pictures of a building which suffered slight damage due to the 1999 Turkey Kocaeli mainshock that fully collapsed due to a smaller magnitude aftershock almost one month later. Photographs excerpted from USGS (2000).

to the occurrence of an aftershock.

Two cases in which an aftershock following the mainshock was responsible for the predominant damage in an entire community are Bakersfield, California in the 1952 Kern County event sequence (Dreger and Savage (1998)) and Big Bear, California in the 1992 Landers event sequence[1] (Hauksson et al. (1993)). In both cases the aftershock was of significantly smaller magnitude than the mainshock but it was located much closer to the built-up community.

Thus, before the completion of repair, a mainshock-damaged building could be progressively further damaged due to the aftershock ground motions experienced at the site, thus incurring more financial losses, becoming more susceptible to life-threatening collapse, causing evacuation or delaying re-occupancy. All these characteristics need to be addressed when developing the probabilistic assessment of the decision variables, DVs, in the aftershock environment.

Based simply on the preceding observations, we can now propose an aftershock PBEE framing equation, Equation 1.3, analogous to the PEER Equation in Equation 1.1 discussed

[1]The distance (50 km) of the Big Bear event from the fault trace of the Landers event has led to controversy as to whether this should be considered an aftershock at all. It was, however, only 3 hours after the Landers event and it occurred within 2 fault dimensions of Landers, which together are sufficient to make it fit certain formal definitions of an aftershock (Hauksson et al. (1993)).

(a) After mainshock of magnitude 5.7 on October 31, 2002

(b) After aftershock of magnitude 5.7 on November 1, 2002

Figure 1.4: Pictures of a column which was only slightly damaged due to the 2002 Italy Molise mainshock but that suffered severe spalling, bar buckling and a residual vertical deformation at the top of the column due to an aftershock one day later. Photographs courtesy of Mucciarelli and Gallipoli, University of Basilicata, Italy and Dr. Paolo Bazzurro.

above.

$$\upsilon_a^{t_{\max}}(DV|MI,SI) = \int_{DM}\int_{EDP}\int_{IM}\int_{i} G_a(DV|DM,i)dG_a(DM|EDP,i) \cdot dG_a(EDP|IM,i)d\lambda_a^{t_{\max}}(IM,i|MI)dG_a(i|MI,SI) \tag{1.3}$$

It takes into consideration many of the above characteristics. Its purpose is to capture and display, more precisely but still only symbolically, the structure of dependency of various elements of the problem upon one another. The subscript a refers specifically to the aftershock environment. As discussed earlier, decision making in the post-event environment is information sensitive and we incorporate our state of information in Equation 1.3 using the notations MI and SI. The notation MI represents the current state of information about the mainshock and possibly subsequent event-specific aftershock sequence information and parameter values (this will be discussed in Chapter 2). This information might include the mainshock magnitude, location and rupture zone geometry which will allow us to better define the aftershock environment. MI could also include information on the mainshock

site intensity measure, IM, which will provide us with better information about the state of the building, both in terms of the severity of damage and the initial capacity of the building (since it was perhaps capable of withstanding $IM = x$ in the mainshock). The notation SI represents the information about the damage state, i, of the building. This information could be obtained from various levels of inspection and engineering analysis, ranging from simpler less-detailed inspections and static pushover analysis to detailed floor-to-floor inspections and nonlinear dynamic time history analysis. SI could potentially be improved by information obtained from structural health monitoring devices which provide data on peak and residual deformations of the building. Such information will allow us to better understand the condition of the damaged building thus potentially improving our dynamic modeling capability.

$\lambda_a^{t_{\max}}(IM, i|MI)$ in Equation 1.3 is the mean number of aftershocks exceeding a given IM in post-mainshock time interval $[0, t_{\max}]$ for a building in damage state i, given our current state of information about MI. As discussed, this number depends on mainshock magnitude. We include the dependence on i in this step of the formulation for structural-period dependent IM (such as first-mode period spectral acceleration) because the period of a mainshock-damaged building might be lengthened. $|dG_a(i|MI, SI)|$ is the probability that the building is in damage state i after the mainshock given the current state of information about MI and SI. The inclusion of $|dG_a(i|MI, SI)|$ means that we have an additional integral over all possible post-mainshock damage states i. Similar formulations hold for the remaining terms analogous to those in the PEER Equation, except that we need to explicitly consider the damage state i in the computation. For example, the likelihood of exceeding a particular value of maximum interstory drift (assuming it is taken to be the EDP) depends on the state of the structure if it is damaged; here, $dG_a(EDP|IM, i)$ replaces the simpler $dG(EDP|IM)$ in Equation 1.1 where it is implicitly assumed that the structure is intact.

Equation 1.3 provides us with a description of the interaction among components of the probability distribution of DV in the aftershock environment. Each component in Equation 1.3 will be discussed in the chapters of the report to follow. Like the PEER Equation, this equation is largely only symbolic. It helps one to identify some of the differences between the mainshock and the aftershock problems. For example, unlike Equation 1.1, time explicitly appears in Equation 1.3 via t_{max}. The increased mean rate of aftershocks after a mainshock of large magnitude suggests that multiple aftershocks are more likely as t_{max} increases, which increases the chance of incremental damage to the structure as we are more likely to

encounter aftershock ground motions of large intensity. For demonstration, we assume here that the capacity of a structure in damage state i is deterministic and can be expressed in terms of the intensity measure of interest. We denote this capacity as IM^i_{cap}. We assume also that we can compute the probability of the site intensity measure, IM, exceeding a specified value y given the occurrence of an aftershock, denoted as $P(IM > y|aftershock)$. The method to evaluate this probability will be discussed in Chapter 2 where we consider random aftershock ground motions from aftershocks of random magnitudes at random locations (conditioned on MI). Denoting the collapse damage state as n, the probability of collapse of the building given an aftershock, $P'_{in}|aftershock$, is thus $P(IM > IM^i_{cap}|aftershock)$. The probability of no collapse given an aftershock, denoted as $\overline{P}'_{in}|aftershock$, is simply $1 - P'_{in}|aftershock$.

We are interested in the computation of the probability $P(\overline{C})$ of the no collapse event $\overline{C}$ in the aftershock environment in the time interval $[0, t_{\max}]$. The expected number of aftershocks is denoted by $\nu_a^{t_{\max}}$. $P(\overline{C})$ can be calculated using Equation 1.4.

$$
\begin{aligned}
& P(\overline{C}) \\
= & \left[\begin{array}{c} P(\text{no event}) + P(1 \text{ event}) P(\overline{C}|1 \text{ event}) + P(2 \text{ events}) P(\overline{C}|2 \text{ events}) \\ + \ldots + P(m \text{ events}) P(\overline{C}|m \text{ events}) + \ldots \end{array} \right] \\
= & \left[\begin{array}{c} e^{-\nu_a^{t_{\max}}} + \nu_a^{t_{\max}} e^{-\nu_a^{t_{\max}}} \left(\overline{P}'_{in}\right) + \frac{\left(\nu_a^{t_{\max}}\right)^2}{2!} e^{-\nu_a^{t_{\max}}} \left(\overline{P}'_{in}\right)^2 \\ + \ldots + \frac{\left(\nu_a^{t_{\max}}\right)^m}{m!} e^{-\nu_a^{t_{\max}}} \left(\overline{P}'_{in}\right)^m + \ldots \end{array} \right] \\
= & e^{-\nu_a^{t_{\max}}} \left[1 + \nu_a^{t_{\max}} \left(\overline{P}'_{in}\right) + \frac{\left[\nu_a^{t_{\max}} \left(\overline{P}'_{in}\right)\right]^2}{2!} + \ldots + \frac{\left[\nu_a^{t_{\max}} \left(\overline{P}'_{in}\right)\right]^m}{m!} + \ldots \right] \\
= & e^{-\nu_a^{t_{\max}}} \left[\exp\left(\nu_a^{t_{\max}} \overline{P}'_{in} \right) \right] \\
= & e^{-\nu_a^{t_{\max}} P'_{in}}
\end{aligned}
\tag{1.4}
$$

Here, we have suppressed the condition given the occurrence of an aftershock. Notice that for *no* collapse of the building, if there are m aftershock events, the ground motion intensity measure must be less than IM^i_{cap} all m times, an event with probability $\left(\overline{P}'_{in}\right)^m$, which decays geometrically with m. Equation 1.4 shows the effect that the multiple aftershocks – each with its own random magnitude, location and ground motion – can have on decreasing the probability of no collapse, $P(\overline{C})$ (and consequently, increasing the probability of collapse

in our example).[2]

Thus, the effects of multiple aftershocks can be captured by the term $t_{\max}$ in the formulation. It should be pointed, too, that Equation 1.3 is not as complete as one might like. One might prefer the time of the decision to also enter the Equation 1.3 formulation, e.g., when making a re-occupancy decision seven days after the mainshock. Further, Equation 1.3 implicitly assumes that should the building be further damaged in an aftershock, it will be "repaired" back to state i before the occurrence of any subsequent aftershocks. This may be adequate in some cases especially if the only DV of interest is collapse related (e.g., life safety). It is a less realistic assumption, however, in the immediate post-mainshock environment where aftershocks are more frequent. At the high risk of becoming too complicated to be of even symbolic value, the above representation could be further extended to the more general case using an embedded Markov chain formulation (see Chapters 5 and 6) where we allow for the possibility of transitions from one damage state to another due to aftershock occurrences. While the framework equation will remain as it is, this study as a whole will not be limited to the conditions implied by Equation 1.3.

The ability to formulate and analyze the aftershock problem allows earthquake engineering policy-making decisions to be made based on probabilistic descriptions of DV. As shown in Equation 1.3, DV is dependent on the damage state i of the building after a mainshock because the probabilities $dG_a(EDP|IM, i)$ etc. will change if the state i changes. Hence, the quantification of DV (and subsequent decision making) may be improved with the ability to obtain more information about the damage state i of the building after the mainshock. Decision analytic tools (described in details in Chapter 6) exist to allow us to quantify how new information can potentially change (update) the probabilities of damage states i and hence the probabilistic descriptions of DV, thus possibly influencing the decision-making process thereafter. More detailed information is always of value but it comes at a price. For example, detailed inspections which provide us with more information about i also cost more than simpler inspections. Tools will be described in Chapter 6 which will allow us to quantify the value of possible new information to help decide if it is financially desirable to invest in obtaining more information.

We can also insert the aftershock scenario into more familiar pre-mainshock DV assessment. Following the lead of past engineering studies such as Rosenblueth (1976), Ang and

[2]The effect of random capacity can be included by multiplying the results in Equation 1.4 by the probability density function of the capacity, $f_{IM^i_{cap}}(s)$, and integrating over all possible values of s.

Leon (1996) and Wen and Kang (2001), we could base pre-mainshock decision analyses on a minimization of expected financial losses. As discussed above, the incorporation of aftershocks allows us to explicitly consider the downtime losses due to limited post-mainshock functionality associated with damage from the mainshock and due to potential incremental damage from aftershocks. But decisions should be made based on individual life-safety considerations as well (e.g., following Paté-Cornell (1984)). Instead of simply using an implicit economic value of human life in cost-minimization analysis, we use in addition a constraint on the mean rate of individual life loss. The results in this work allow for a procedure based on minimization of expected financial losses subject to a constraint on minimal level of individual life-safety. The focus of the report will be on buildings such as offices, residences and industrial facilities including electrical power distribution facilities essential for post-quake recovery. Analogous ideas also apply to other structures as well, such as bridges which are currently being studied by Mackie and Stojadinovic (2004).

1.4 Report Organization

The remaining chapters will discuss in depth the analysis of the various elements that have been brought up in this chapter. Chapter 2 introduces Aftershock Probabilistic Seismic Hazard Analysis (APSHA), a procedure by which aftershock ground motion hazard can be evaluated. Several methodologies to quantify the performance of (possibly) mainshock-damaged buildings in the aftershock environment will be discussed in Chapter 3. Chapter 4 describes a risk management tagging policy based on the quantification of life-safety threat in the aftershock environment using the probability of collapse as a proxy for fatality risk. A formulation of financial losses in the aftershock and pre-mainshock scenarios will be presented in Chapter 5. Finally a decision analytic framework under improving states of information will be introduced in Chapter 6. Each chapter will be illustrated by a continuing example of a specific multistory building. Chapter 7 will summarize conclusions and limitations and suggest further work.

2 Aftershock PSHA

This chapter presents a method of Aftershock Probabilistic Seismic Hazard Analysis (APSHA) similar to conventional "mainshock" PSHA in that it estimates the likelihoods of ground motion intensity (in terms of PGA, spectral accelerations or other ground motion intensity measures) due to future earthquakes. This proposed methodology differs from conventional mainshock PSHA in that mainshock occurrence rates remain constant for a conventional (homogeneous Poisson) earthquake occurrence model while aftershock occurrence rates decrease with increased elapsed time from the initial occurrence of the mainshock. In addition, the aftershock ground motion hazard at a site depends on the magnitude and location of the causative mainshock, and the location of aftershocks is limited to an aftershock zone which is also dependent on the location and magnitude of the initial mainshock. APSHA is useful for post-earthquake safety evaluation where there is a need to quantify the rates of occurrences of ground motions caused by aftershocks following the initial rupture. This knowledge will permit, for example, more informed decisions to be made for building tagging, including entry of damaged buildings for rescue, repair or normal occupancy. Building tagging will be the subject of discussion in Chapter 4.

2.1 Introduction

In conventional PSHA, the annual probability of exceedance of a given ground motion intensity measure (typically PGA or the first-mode spectral acceleration) is evaluated for a given structural period and damping ratio. The mainshock occurrence rates are assumed to be time-invariant constant values, and a homogeneous Poisson earthquake occurrence model is generally used. Conventional mainshock PSHA, typically based on a truncated exponential magnitude model or a characteristic magnitude model or both, is an established process that is well documented in literature. See, for example, Kramer (1995). Mainshock

PSHA is performed by first considering the geometry of the neighboring faults with respect to the site of concern as well as the annual rates of earthquakes on these faults. The basic formulation of PSHA requires the development of an earthquake model to address the randomness of the times of occurrences as well as the randomness of the earthquake magnitudes. The randomness of the distance from the site to the possible rupture planes and the distribution of possible ground motions given an earthquake of a particular magnitude and distance are also addressed in standard mainshock PSHA procedures.

In the post-mainshock situation, however, aftershock occurrence rates are no longer time-invariant. Aftershock rates are at their maximum immediately following the occurrence of the mainshock, and they decrease with increasing elapsed time from the mainshock. Aftershock rates are dependent on the magnitude of the causative mainshock. The subsequent aftershock ground motion hazard at a site is also dependent on the location and magnitude of the initial mainshock, which defines the aftershock zone in which aftershocks are expected to occur. In this chapter, we propose a method of calculating the post-mainshock ground motion hazard at a site which we refer to as Aftershock Probabilistic Seismic Hazard Analysis, or APSHA for short, where we take the above factors into consideration. This method enables us to estimate the likelihood of severe ground motions at a site due to aftershocks.

There are several recent examples of studies where the results of APSHA would have proved useful.

Gallagher et al. (1999) presented an ATC technical brief titled "Earthquake Aftershocks-Entering Damaged Buildings" which provided guidelines on the safety evaluation of earthquake damaged buildings as well as conditions for permitting entry into such buildings that may be structurally unsound. These guidelines are based purely on the aftershock earthquake occurrence rates obtained for California in Reasenberg and Jones (1989) and Reasenberg and Jones (1994) as a function of magnitude and time. However, the hazard at the site of concern cannot be adequately described without the explicit consideration of the location of the aftershock hazard zone relative to the site and the possible ground motion intensities at the site. Both these factors are considered in the proposed method.

FEMA, in conjunction with the SAC steel project, has published a report titled "Recommended Post-Earthquake Evaluation and Repair Criteria for Welded Steel Moment-Frame Buildings". FEMA (2000) provides guidelines on post-earthquake occupancy criteria for damaged structures based on their ability to resist collapse after the mainshock. In the report, a "presumed postearthquake hazard curve" for a mainshock-damaged building is

presented based on the annual probability of exceedance of the first-mode spectral acceleration in an aftershock, assuming simply that the probable maximum intensity value for aftershock-induced ground shaking at the building site is the same as that experienced in the original damaging mainshock and that the variability in this intensity is normally distributed with a coefficient of variation of 50%. A more precise methodology to quantify the aftershock ground motion hazard is required.

The proposed method of APSHA is similar to conventional mainshock PSHA in terms of the treatment of uncertainty in magnitude, source-to-site distance and ground motion intensity. The detailed description of conventional PSHA will not be discussed in this chapter. The reader is presumed to be familiar with conventional PSHA as described, for example, in Kramer (1995). We will explicitly incorporate the unique characteristics of aftershock ground motion hazard mentioned earlier in the formulation of APSHA.

2.2 Methodology

It has been generally observed that several earthquakes occur as a cluster within a limited period of time and confined to a limited interval in space. For the purpose of this study, we assume that we can classify all earthquakes as foreshocks, mainshocks and aftershocks. The mainshock is generally defined to be the earthquake in a sequence which has the largest magnitude. The foreshocks are usually very limited in number. Our focus is on the aftershock sequence. For the purpose of this study, we are interested in the aftershocks in the days and perhaps months following the occurrence of a mainshock, and the resulting increased ground motion hazard at the site.

Immediately following the occurrence of a mainshock, the rate of occurrences of aftershocks is at its maximum, and then decreases with increasing elapsed time from the occurrence of the mainshock. This decay is of a power-law form which is generally referred to as the modified Omori law in which the instantaneous aftershock rate per day is expressed as a function of $(t+c)^p$, where t is the number of elapsed days from the occurrence of the mainshock and c and p are constant values for a particular aftershock sequence. See Omori (1894) and Utsu (1995). Because of the time-varying rate of aftershocks immediately following a mainshock, a nonhomogeneous Poisson process is used to model aftershock occurrences.

The modified Omori law has been used by a number of researchers to model aftershock

rates immediately after the occurrence of a mainshock. For example, Merz (1973) used the modified Omori law to model aftershock rates in evaluating the contribution of aftershocks to the total engineering seismic hazard (in terms of ground motion exceedance probabilities) at a site.

More recently, Reasenberg and Jones (1989) and Reasenberg and Jones (1994) fitted 62 California aftershock sequences with mainshock magnitudes m_m greater than 5.0 to the modified Omori law using the method of maximum likelihood. The mean aftershock rates are described by the modified Omori law (elapsed-time dependence) and by the Gutenberg-Richter relationship (aftershock magnitude probability distribution). They used all aftershocks with moment magnitude $m \geq m_m - 3$ to estimate a and p, and $m \geq 2$ to estimate b. They refer to this model as the "generic California" aftershock model. Here, $\gamma(t, m; m_m)$, the mean instantaneous daily rate of aftershocks with moment magnitude m or larger at time t following a mainshock of moment magnitude m_m, can be calculated using Equation 2.1.

$$\gamma(t, m; m_m) = \frac{10^{a+b(m_m-m)}}{(t+c)^p} \tag{2.1}$$

The generic California aftershock sequence has parameters $a = -1.67, b = 0.91, p = 1.08$ and $c = 0.05$.

The b-value describes the relative likelihood of large and small mainshocks or aftershocks. For example, USGS (1999) obtained a b-value of 0.91 for mainshocks in the San Francisco Bay Region. The generic aftershock sequence for California studied by Reasenberg and Jones also has a b-value of 0.91. Thus, because b-values are usually quite similar in value, the relative likelihood of large and small aftershocks is approximately the same as the relative likelihood of large and small mainshocks.

If we define $a_0 = a + bm_m$, $\alpha = a_0 \ln 10$ and $\beta = b \ln 10$, Equation 2.1 simplifies to Equation 2.2.

$$\gamma(t, m; m_m) = \frac{e^{\alpha-\beta m}}{(t+c)^p} \tag{2.2}$$

$|\gamma_m(t, m; m_m)|$ is the absolute value of the partial derivative of $\gamma(t, m; m_m)$ in Equation 2.2 with respect to m, and it is the instantaneous daily rate density of aftershocks of magnitude m at time t following a mainshock of magnitude m_m. $|\gamma_m(t, m; m_m)|$ is defined in Equation 2.3.

$$|\gamma_m(t, m; m_m)| = \left|\frac{\partial \gamma(t, m; m_m)}{\partial m}\right| = \frac{e^{\alpha}}{(t+c)^p}\beta e^{-\beta m} \tag{2.3}$$

In this representation of the generic California model, $\frac{e^{\alpha}}{(t+c)^p}$ is the mean instantaneous daily rate of aftershocks at time t following the mainshock of magnitude m_m, and $\beta e^{-\beta m}$ is the exponential probability density function of aftershock magnitudes. Here, $m \geq 2$ because Reasenberg and Jones used aftershocks with moment magnitude of 2.0 or more to estimate the value of β in the modified Omori law of the generic California model.

A more useful representation of $|\gamma_m(t, m; m_m)|$ will require us to introduce lower and upper bound aftershock magnitudes of m_l and m_u to the exponential probability density function in Equation 2.3. m_l represents the minimum aftershock magnitude of engineering interest, typically taken to be 5.0. m_u represents the upper bound magnitude of the fault in consideration. For the case of aftershocks, m_u is typically considered to be the mainshock magnitude, m_m. See Reasenberg and Jones (1989). Truncating the exponential probability density function at m_l and m_u, and taking $m_u = m_m$, we get Equation 2.4.

$$|\gamma_m(t, m; m_m)| = \frac{10^{a+b(m_m-m_l)} - 10^a}{(t+c)^p}\frac{\beta e^{-\beta(m-m_l)}}{1-e^{-\beta(m_m-m_l)}},\ m_l \leq m \leq m_m \tag{2.4}$$

We can also represent $|\gamma_m(t, m; m_m)|$ using Equation 2.5 where $\mu(t; m_m)$ is the instantaneous daily rate density of aftershocks with magnitudes between m_l and m_m at time t following a mainshock of magnitude m_m, and is equal to $\frac{10^{a+b(m_m-m_l)}-10^a}{(t+c)^p}$.

$$|\gamma_m(t, m; m_m)| = \mu(t; m_m) f_M(m; m_m),\ m_l \leq m \leq m_m \tag{2.5}$$

The function, $f_M(m; m_m) = \frac{\beta e^{-\beta(m-m_l)}}{1-e^{-\beta(m_m-m_l)}}$, is the truncated exponential probability density function of aftershock magnitudes, with truncations at m_l and m_m. The mean number of aftershocks with magnitudes between m_l and m_m in the time interval $[t, t+T]$ following a mainshock of magnitude m_m (denoted as $\mu^*(t, T; m_m)$) can be found using Equation 2.6.

$$\mu^*(t, T; m_m) = \int_t^{t+T} \mu(\tau; m_m) d\tau = \frac{10^{a+b(m_m-m_l)} - 10^a}{p-1}\left[(t+c)^{1-p} - (t+T+c)^{1-p}\right] \tag{2.6}$$

For seismic hazard analysis, we first define the site ground motion intensity measure as Y. In conventional mainshock PSHA, the rate of mainshocks is a constant value in time.

If we denote the mean annual rate of mainshocks with magnitudes between m_l and m_u by υ, we can compute the mean number of mainshocks exceeding site ground motion y in duration T, denoted as $\widetilde{\upsilon}(y,T)$, using Equation 2.7. T is usually one year in mainshock PSHA such that in Equation 2.7, the term T does not appear. Details of PSHA can be found in Kramer (1995).

$$\widetilde{\upsilon}(y,T) = \upsilon T \int_R \int_{m_l}^{m_u} P(Y > y|m,r) f_{R|M}(r|m) f_M(m) dr dm \tag{2.7}$$

In Equation 2.7, we have assumed that only one source contributes to the mainshock hazard at the site. It is straightforward to extend the formulation to include the contributions from multiple sources by summing the contributions to the total hazard from all such sources. We also need to assume a spatial distribution of earthquakes of random magnitudes up to m_u, coupled with a suitable attenuation law for the ground motion intensity measure of interest. In Equation 2.7, $f_M(m)$ is the probability density function of mainshock magnitudes (with upper and lower magnitude bounds at m_l and m_u). $f_{R|M}(r|m)$ is the conditional probability density function of the closest distance between the site and the plane of rupture given an event of a particular magnitude. Lastly, $P(Y > y|m,r)$ is the conditional probability of exceeding a particular ground motion intensity measure given an event of a particular magnitude at a particular distance from the site. This conditional probability is usually evaluated assuming that the distribution of the ground motion intensity measure given M and R is lognormal, where $E(\ln y)$ and $\sigma_{\ln(Y)}$ are obtained from a suitable attenuation law.

Analogously, in APSHA, we want to calculate the mean number of aftershocks in $[t, t+T]$ exceeding site ground motion y, where there is explicit dependence on both t and T. We represent this mean number as $\widetilde{\mu}(y,t,T;m_m)$ which can be calculated using Equation 2.8.

$$\widetilde{\mu}(y,t,T;m_m) = \mu^*(t,T;m_m) \int_R \int_{m_l}^{m_m} P(Y > y|m,r) f_{R|M}(r|m) f_M(m;m_m) dr dm \tag{2.8}$$

Note that the formulation for APSHA is almost identical to that of conventional PSHA, except that $\widetilde{\upsilon}(y,T)$ is replaced by $\widetilde{\mu}(y,t,T;m_m)$, which is a function of t, T and m_m.

Provided Equation 2.5 holds, Equation 2.8 is quite general. In practice, the aftershock zone is defined in a complex manner. It has also been observed that aftershocks tend to

occur more frequently at the ends of the rupture zones of the initial mainshock. See Hough and Dreger (1995) for details. Such complexity in the definition of the aftershock zone can be considered in APSHA.

From Equations 2.7 and 2.8, it is clear that we can explicitly compute the site hazard (mainshock or aftershock) by uncoupling the expected number of events in the duration of interest and the probability of exceeding a specified ground motion given an event. Hence, to perform APSHA in existing mainshock hazard analysis computer programs, one simply needs to replace the expected number of mainshocks (which is elapsed-time invariant) by the expected number of aftershocks (which is time varying) in the duration of interest. The maximum magnitude of the aftershock magnitude probability distribution and the aftershock zone also needs to be revised accordingly. Finally, the aftershock spatial distribution needs to be defined, using perhaps multiple homogeneous sub-sources. After the aftershock magnitudes, locations and rates have been defined, probabilistic ground motion analysis otherwise identical to conventional mainshock PSHA procedures needs to be carried out. In particular, one can estimate the probability of exceeding a given site ground motion intensity measure from an aftershock of random magnitude at a random location by setting $\mu^*(t, T; m_m) = 1$ in Equation 2.8.

The time-varying nature of aftershock ground motion hazard has also been studied recently in Weimer (2000) and Gerstenberger et al. (2002). His focus has been on generating real-time aftershock PGA maps, in which the parameters of the modified Omori law are updated periodically via Bayesian analyses to reflect the on-going aftershock sequence as the parameters a, b, c and p and the aftershock zone may be sequence dependent. Availability of such a real-time system would facilitate the use of aftershock ground motion hazard in making engineering decisions. It is under development in the U.S. Geological Survey (USGS).

Thus, APSHA provides us with the aftershock hazard curve that can be compared to the mainshock hazard curve obtained from conventional mainshock PSHA. In order to gain insight and familiarity with the nature and level of aftershock ground motion hazard, in the example to follow, we shall study the effects of elapsed time, duration, mainshock magnitude and site locations on aftershock ground motion hazard. We shall also study the sensitivity of aftershock hazard to changes in the period of the structure by comparing it to the base case for PGA. The effects of correlation between mainshock and aftershock ground motion epsilons, ε_{MS} and ε_{AS}, (details and concepts to be elucidated in a later section) on

aftershock hazard will also be studied.

2.3 Example

The example in this section serves to demonstrate the proposed APSHA procedures and to gain understanding as to the nature of this threat, in particular relative to the mainshock hazard. The site used for this example is part of Stanford University, which is in close proximity to the San Andreas Fault and in the vicinity of the Hayward and other faults. The site is located at $R = 10$ km off the San Andreas Fault. We assume that a characteristic mainshock of magnitude $m_m = 7.0$ has ruptured the Mid-Peninsula Segment of the San Andreas Fault in the computation of aftershock ground motion hazard. We assume that the aftershock magnitude distribution follows a truncated exponential model and that the maximum aftershock magnitude is equal to the mainshock magnitude. Aftershock occurrences are restricted to the fault plane itself with a specified line at constant depth as the aftershock zone. Here, the aftershock zone is defined to be the extent of the rupture of the initial mainshock. In other cases, if the rupture zone of the mainshock is not yet well defined, the rupture length can be estimated using the relationship between the magnitude of the mainshock and its corresponding rupture length in Wells and Coppersmith (1994).

Two cases of APSHA will be considered. In both, we use the generic California model developed by Reasenberg and Jones. The first case assumes aftershocks are equally likely to occur at any location on the linear aftershock zone. The second case assumes aftershocks are twice as likely to occur at the ends of the rupture zone as compared to its interior, where the "end" of the rupture zone is taken to be equal to one-fourth of the entire length. The attenuation relationship developed in Abrahamson and Silva (1997) for rock sites is used for APSHA. One objective is to develop insight into the aftershock hazard problem by showing a series of alternate ways of plotting APSHA results, especially given the fact that there are two competing time parameters (t and T) due to the nonhomogeneity of the aftershock rate in time. Our base case example assumes $t = 7$ days, $T = 365$ days and $m_m = 7.0$; these parameters will be used unless mentioned otherwise.

Figure 2.1 is a schematic layout of the site adjacent to the midpoint of the 85 km long segment of the fault that has been ruptured by the initial mainshock. The linear aftershock zone is assumed to be on the ruptured segment at a perpendicular distance R of 10 km.

For comparison, we consider the mainshock hazard analysis that has been performed for

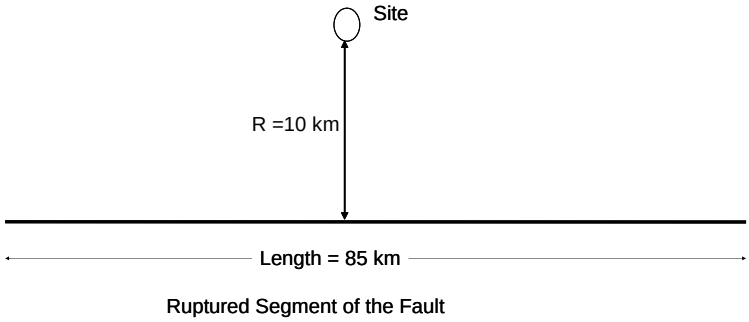

Figure 2.1: Schematic of site layout and linear aftershock zone.

the Stanford site mentioned above by Woodward-Clyde Consultants by considering the San Andreas, Hayward, Rodgers Creek, Calaveras and San Gregorio Faults in Woodward-Clyde (1991). A minimum earthquake magnitude of 5.0 was used to define the limits of engineering interest. A characteristic earthquake model was employed. The resulting mainshock hazard curve is shown in Figure 2.2.

It is worthwhile noting that other options can also be used for the modeling of future mainshock earthquake occurrences where the annual rates are elapsed-time-dependent and where some degree of memory can be associated with earthquake occurrences. For example, memory of the "quasi-cyclic" type (where the inter-arrival time coefficient of variation <1) can be used to model mainshock occurrences where, with the rupture, there will be a subsequent hazard reduction along the segment, followed by a gradual increase. This reduction, to some extent, offsets the aftershock hazard which will be at its maximum immediately after the occurrence of the initial rupture. Such a time-dependent model has been used in, for example, USGS (2003), and will not be considered in this chapter.

2.3.1 Comparison of Mainshock Hazard to Aftershock Hazard

We demonstrate the significant difference that may exist between mainshock hazard and aftershock hazard by performing APSHA for the scenario described above. The aftershock hazard curves are obtained for the base case example with $t = 7$ days and $T = 365$ days using Equation 2.8. Note that the aftershock hazard computed here does not include the mainshock hazard that is still present from other sources (the Hayward Fault, for example) nor does it include the residual mainshock hazard from the San Andreas Fault itself. The

two cases for APHSA together with the mainshock hazard curve are shown in Figure 2.2.

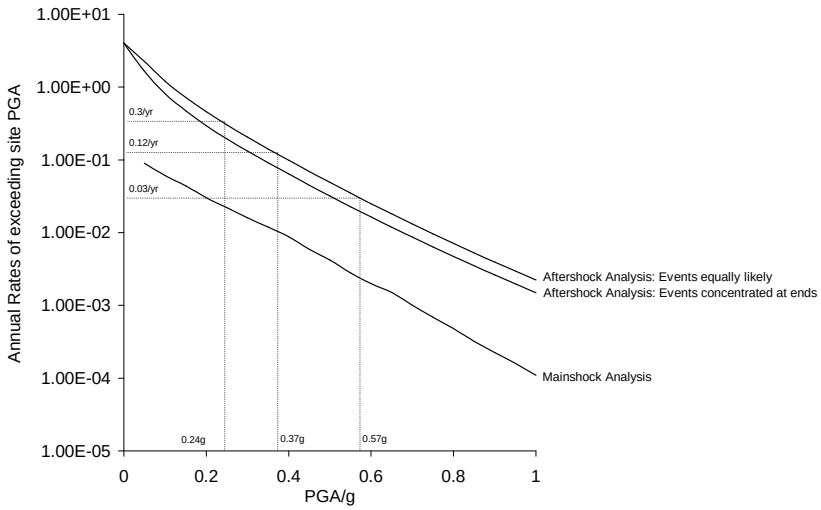

Figure 2.2: Comparison of mainshock and aftershock site hazard curves (as functions of PGA), where aftershock hazard is evaluated at $t = 7$ days with $T = 365$ days for aftershocks equally likely to occur at any location on the linear aftershock zone and for aftershocks concentrated at the ends of the linear aftershock zone. The mainshock magnitude is assumed to be 7.0.

From Figure 2.2, it can be seen that in the year starting one week after the initial mainshock, aftershock ground motion hazard on the linear aftershock zone (i.e., the Mid-Peninsula segment) is considerably higher, about ten times, than the total pre-mainshock hazard at the site. If we further compute the total post-mainshock hazard by including the mainshock hazard from other sources and the residual mainshock hazard from the San Andreas Fault, the resulting difference would even be more significant.

It can also be seen that the two cases of aftershock hazard computation described earlier result in similar values. The case with equally likely aftershock locations results in higher aftershock hazard as compared to the case where aftershock locations are concentrated at the ends of the linear aftershock zone. This can be attributed to the location of the site which is located midway along the linear aftershock zone. More aftershocks are predicted closer to the site by the equally-likely model. In subsequent examples, we shall use only the equally-likely case.

One can also estimate the rate of exceeding the mainshock site PGA in the aftershock environment from Figure 2.2. For example, the predicted median mainshock site PGA using

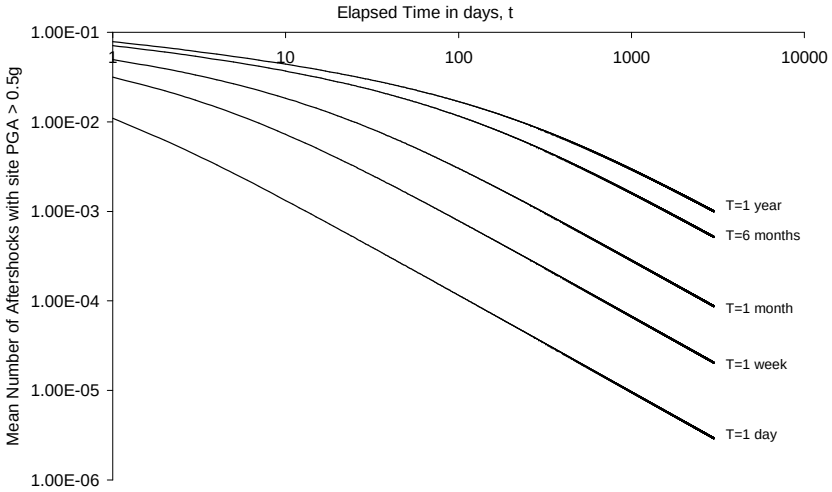

Figure 2.3: Mean number of aftershocks (as a function of elapsed time, t) with site PGA $>$ 0.5g in specified durations T.

the attenuation law is 0.37g and the predicted median PGA $\pm$ one standard deviation is [0.24g, 0.57g]. These points are shown in Figure 2.2. One can then estimate the rate of exceeding the predicted median PGA and predicted median PGA $\pm$ one standard deviation to be about 0.12/year, 0.03/year and 0.3/year, respectively, for our base case aftershock example. These numbers can be compared to the assumption made in FEMA (2000) discussed above, where the first number is 0.5, not 0.12. This base case example does not include the entire post-mainshock time frame (1 to ∞ days), however.

2.3.2 Effects of Duration (T) on Aftershock Hazard

To study the effects of different durations T on the aftershock hazard at the site, the same linear aftershock zone is considered with T equal to one day, one week, one month, six months and one year. The resulting total aftershock ground motion hazard is shown in Figure 2.3 and is presented as a function of elapsed time from the initial rupture, t. An exceedance of 0.5g PGA is considered. Here, we calculate the total aftershock ground motion hazard in terms of the mean number of aftershocks in the duration (T) with site PGA greater than 0.5g, instead of annual rates of exceeding site PGA used previously (where, specifically, $T = 365$ days). Based on the earlier observation that the aftershock ground motion hazard can be calculated by uncoupling the expected number of aftershocks in the

duration of interest and the probability of exceeding a specified PGA given an aftershock (based on Equation 2.8), the results in Figure 2.3 for an exceedance PGA of 0.5g is in fact proportional to any other PGA ground motion levels for fixed values of t, T and m_m.

As can be seen from Figure 2.3, the aftershock hazard at the site is higher when the duration considered is longer, and the difference becomes more pronounced with increasing elapsed number of days from the initial rupture of the fault segment. This can be attributed to the fact that aftershocks tend to occur much more frequently a short time period after the initial rupture. Hence, the aftershock hazard does not differ significantly a short time period after the initial rupture when different durations are considered because the aftershocks are concentrated in the first few days after the initial mainshock. As the elapsed number of days from the initial rupture increases, aftershocks occur less frequently and the durations considered become more significant in determining the difference in aftershock hazard. Also, the aftershock hazard is relatively insensitive to the duration of interest provided it is about six months or longer.

In order to facilitate the comparison of the aftershock hazard in various durations, we next normalize the aftershock hazard in one week, one month, six months and one year with respect to the aftershock hazard in one day. The results are shown in Figure 2.4. In the first 10 days after the mainshock, the resulting ratios are fairly close to one another, indicating, again, that aftershocks are concentrated in the first few days after the occurrence of the mainshock. After the first 10 days, the resulting ratios with respect to the aftershock hazard in one day become much larger in values as compared to the first 10 days after the mainshock. The ratios approach a constant value (7 for the duration of one week, 30 for the duration of one month, 180 for the duration of six months and 365 for the duration of one year) after more than 1,000 elapsed days from the mainshock. These steady-state ratios are simply the length of the respective durations (in days), and this can be attributed to the fact that the instantaneous aftershock daily rates approaches almost a constant value after more than 1,000 days after the mainshock. Of course, the mean instantaneous aftershock rates are effectively negligible by that time.

In Figure 2.5, we have maintained the end time constant at one year, and evaluated the aftershock hazard of exceeding a site PGA of 0.5g as a function of elapsed time. This means that we consider the mean number of aftershocks from days 1 to 366, days 2 to 366, days 3 to 366 and so on in evaluating the aftershock hazard at the site. For comparison to Figure 2.3, we have included the aftershock hazard of exceeding a site PGA of 0.5g from t through

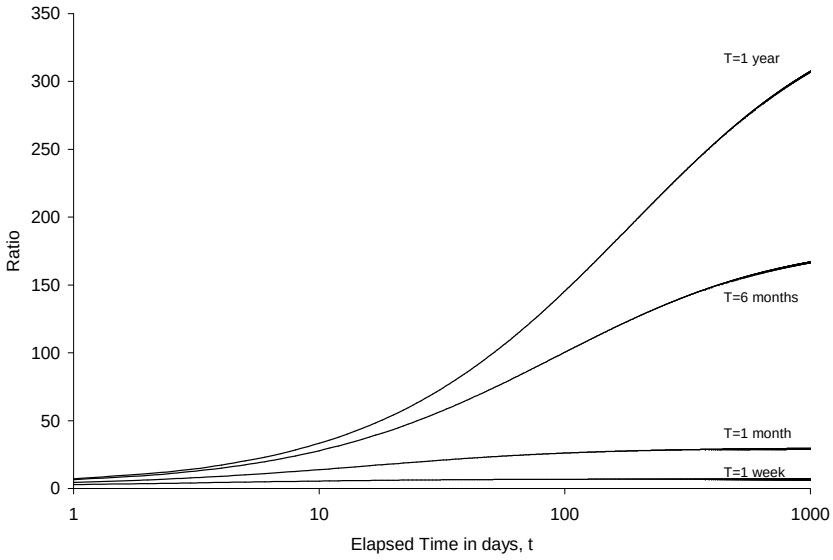

Figure 2.4: Ratios of expected number of aftershocks resulting in site PGA > 0.5g for $T =$ one week, one month, six months and one year to the expected number of aftershocks resulting in site PGA > 0.5g in one day, as a function of the elapsed time, t, of the first day in the duration of interest.

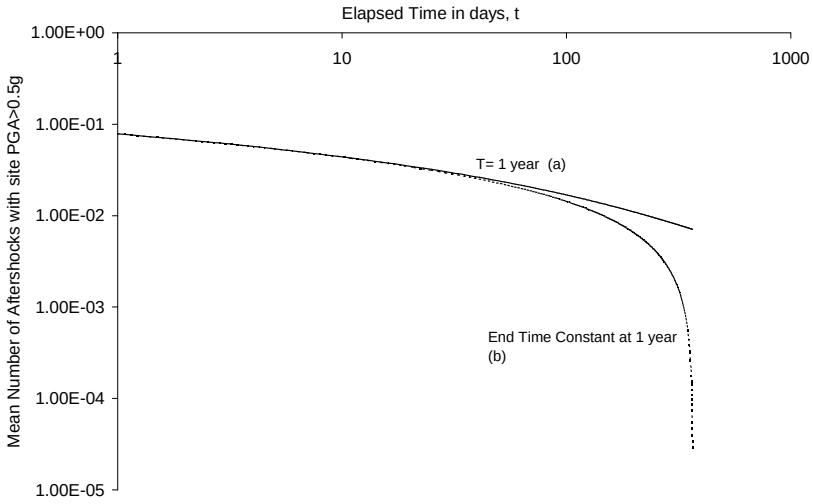

Figure 2.5: Mean number of aftershocks (as a function of elapsed time t) with site PGA $>$ 0.5g. The duration T is constant at one year in the first case (a), and the end time is constant at one year in the second case (b).

$t + 1$ year, i.e., from days 1 to 366, days 2 to 367, days 3 to 368 and so on. From Figure 2.5, we can see that the two methods of evaluating aftershock hazard demonstrate similar results for less than 100 elapsed days after the mainshock, from which point, the aftershock hazard curves for the two cases deviate significantly. Again, this can be attributed to the fact that the aftershock rate is much higher in the short time period after the mainshock.

2.3.3 Effects of Elapsed Time from Initial Rupture (t) on Aftershock Hazard

As mentioned earlier, aftershock hazard is at its maximum immediately after the occurrence of the mainshock and this hazard decreases with increasing elapsed time from the initial rupture of the fault segment. We now study the effects of elapsed time from the mainshock, t, on aftershock hazard. Aftershock hazard is also dependent on the duration, T. We keep T constant at 365 days while considering PGA exceedance values of 0.3g, 0.5g and 0.7g, roughly bracketing the number likely to have been experienced in the mainshock. The results are shown in Figure 2.6.

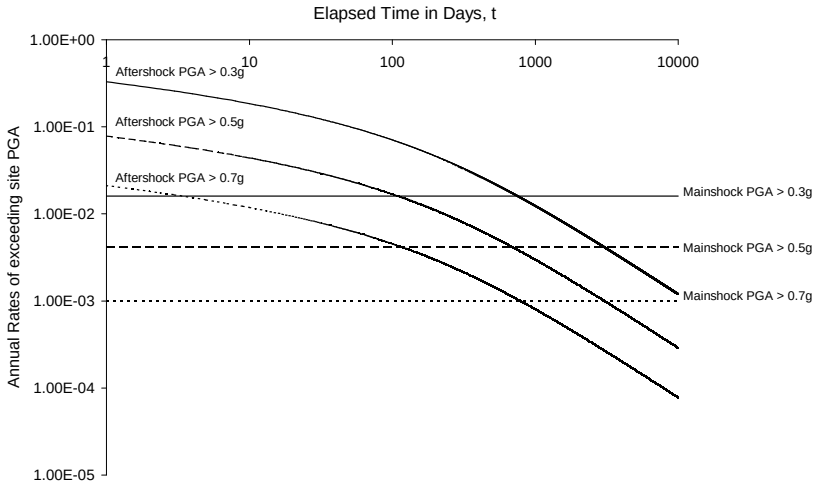

Figure 2.6: Aftershock hazard as a function of t for site PGA= 0.3g, 0.5g and 0.7g, and $T = 365$ days. The aftershock hazard is compared to the pre-mainshock hazard of exceeding the respective PGA values.

It can be seen that one-year aftershock hazard decreases relatively slowly in the first 100 days from the initial occurrence of the mainshock, and that it decreases more rapidly after that. It can also be seen that it takes more than one year for aftershock hazard to decrease to

the original level of total pre-mainshock hazard before the occurrence of the initial rupture. For example, for the case of exceeding a site PGA value of 0.3g, it takes about 1000 days for the aftershock hazard to decrease to the level of pre-mainshock hazard before the initial mainshock rupture. It takes more than 30 years for the aftershock hazard to become a negligible ($< 10\%$) contribution to the total (mainshock and aftershock) hazard.

We next study the aftershock hazard (as a function of PGA) one day, one week and one month after the mainshock, where T is equal to one year. We present the results in Figure 2.7. Because of the separability of the functions of time and ground motion amplitude in

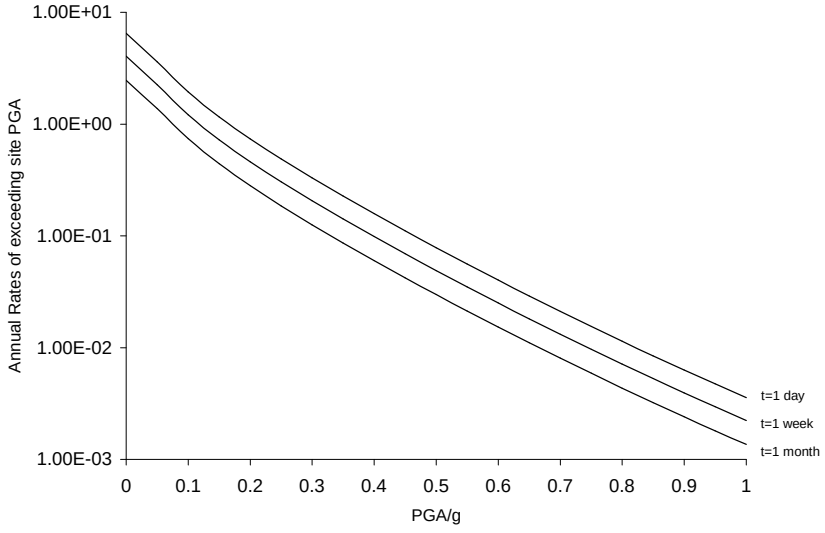

Figure 2.7: Aftershock hazard as a function of site PGA for $t = 1$ day, 1 week and 1 month after the mainshock. $T = 365$ days.

Equation 2.8, the hazard for these curves are scalar multiples of one other. Therefore, we can normalize the results with respect to the base case, i.e., $t = 7$ days or one week after the mainshock. We find that the annual aftershock hazard one day after the mainshock is 1.6 times that of the annual aftershock hazard one week after the mainshock, and that the annual aftershock hazard one month after the mainshock is 0.6 times that of the annual aftershock hazard one week after the mainshock.

2.3.4 Similarity of APSHA to Mainshock PSHA

From Figure 2.2, we see that the base case aftershock ground motion hazard is almost a scalar multiple of the mainshock hazard for all PGA levels. In our example, the Mid-Peninsula segment is the dominant source of a damaging mainshock ground motion at the site. This means that the mainshock hazard at the site obtained using Equation 2.7 considering all seismic sources can be estimated quickly by considering only the Mid-Peninsula segment. Since the aftershock zone is also defined to be on the same Mid-Peninsula segment (i.e., the same source-to-site geometry for both cases), the double integrals in Equations 2.7 and 2.8 are almost equal, if not for the difference in upper bound earthquake magnitudes used in both equations. The difference between the double integrals is likely to be small due to the decreasing contribution from earthquakes of increasing magnitudes. Also, as discussed earlier, the aftershock ground motion hazard can be calculated by uncoupling the expected number of aftershocks in the duration of interest and the probability of exceeding a specified PGA given an aftershock. Thus, the ratio of the base case aftershock hazard to the mainshock hazard for all PGA levels is almost constant, in this case, approximately equal to the ratio of $\mu^*(t, T; m_m)$ in Equation 2.8 to υT in Equation 2.7. Thus, if the mainshock hazard at the site is dominated by one single fault segment, and if this segment were to rupture, the resulting aftershock ground motion hazard at the site can be rapidly approximated by multiplying $\frac{\mu^*(t,T;m_m)}{\upsilon T}$ to the existing mainshock hazard at the site for all PGA levels, using the values of t and T of interest. A better methodology to facilitate rapid estimation of aftershock hazard at a site after a major earthquake is to perform mainshock PSHA, before the mainshock has occurred, for all likely rupture scenarios using $\upsilon T = 1$ and the maximum magnitude on the fault segment. Then, after the occurrence of the mainshock, one simply needs to multiply $\mu^*(t, T; m_m)$ to the set of mainshock hazard results obtained earlier corresponding to the actual mainshock rupture scenario, to obtain an estimate of the resulting aftershock hazard for all PGA levels.

To facilitate the direct comparison of APSHA to mainshock PSHA over the same fault segment (so that the double integrals in Equations 2.7 and 2.8 are almost identical with the same source-to-site geometry, except for the change in upper-bound earthquake magnitude), we consider three different formulations for mainshock PSHA in which we obtain an approximately equivalent characterization of the site mainshock hazard from all possible sources from the Woodward-Clyde studies by restricting mainshocks to the Mid-Peninsular segment and matching the 2% in 50 years site PGA value (0.82g) obtained from the Woodward-Clyde

studies. The three formulations differ only in the mainshock magnitude distribution and are:

1. Mainshock PSHA case 1: Mainshock magnitudes are assumed to have a truncated exponential distribution between 5.0 and 6.75 and a deterministic characteristic magnitude of 7.0. The rate of characteristic events is equal to 0.0067/year, taken from USGS (1990). The annual rate of mainshocks with magnitudes between 5.0 and 6.75 is evaluated (by trial and error) to be 0.144/year to match the Woodward-Clyde 2% in 50 years site PGA value of 0.82g.

2. Mainshock PSHA case 2: Mainshock magnitudes are assumed to have a truncated exponential magnitude distribution between 5.0 and 7.0. The rate of earthquakes between 5.0 and 7.0 is evaluated (again by trial and error) to be 0.256/year to match the Woodward-Clyde 2% in 50 years site PGA value of 0.82g. In this case, the mainshock hazard results are a direct multiple of the corresponding aftershock hazard results (for $m_m = 7.0$) as the double integrals in Equations 2.7 and 2.8 are exactly the same, since the upper-bound earthquake magnitude are both equal to 7.0 with the same site-to-source geometry as well.

3. Mainshock PSHA case 3: Mainshock magnitudes are assumed to have a truncated exponential distribution between 5.0 and 6.75, with no consideration of potential characteristic events. We take the annual rate of mainshocks with magnitudes between 5.0 and 6.75 to be 0.144/year, obtained from mainshock PSHA case 1 previously. In this case, we are assuming that future characteristic mainshocks on the Mid-Peninsular segment are precluded. This assumption is approximately consistent with quasi-cyclic models that have been discussed earlier. Previous results in this example do not make this assumption.

The three approximate mainshock PSHA cases are shown in Figure 2.8, together with the mainshock hazard curve obtained from the Woodward-Clyde studies. By design, the three curves from mainshock PSHA case 1, case 2 and the Woodward-Clyde studies intersect at 0.82g. Note that the approximate hazard curves from mainshock PSHA cases 1 and 2 are in general agreement with the hazard curve obtained from the Woodward-Clyde studies which considered all possible seismic sources. The approximate methods work well if the hazard at the site is dominated by a single nearby fault, as is the case for our site in

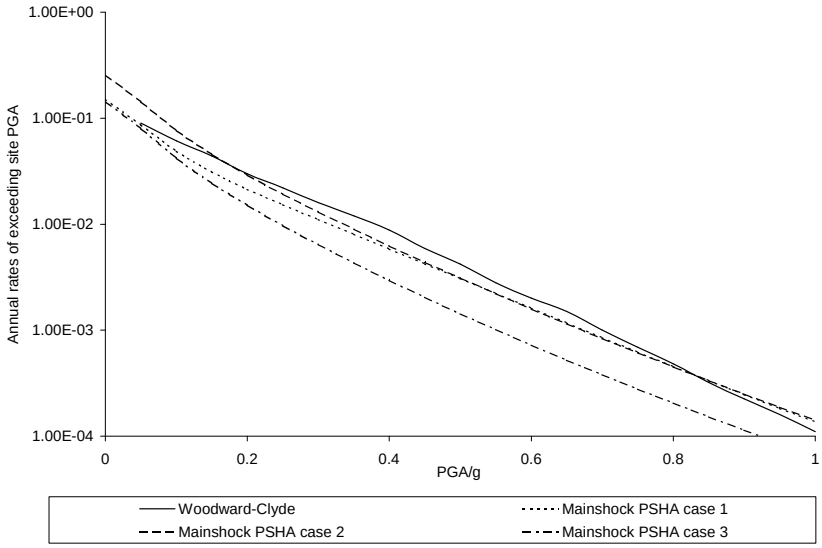

Figure 2.8: Approximate mainshock hazard curves by restricting mainshocks to the Mid-Peninsular segment.

consideration. Note also that the preclusion of future characteristic events (mainshock PSHA case 3) makes little difference when compared to the mainshock hazard results in the other cases, and consequently, the ratio of the aftershock hazard to pre-mainshock hazard is not significantly increased as well.

2.3.5 Effects of Mainshock Magnitude (m_m) and Site Location on Aftershock Hazard

The magnitude of the initial rupture is studied next to display its effects on aftershock hazard. We consider mainshock magnitudes m_m of 6.0, 7.0, 7.5 and 8.0. The base-case aftershock hazard curves are shown in Figure 2.9. It is clear that aftershock hazard is highly dependent on m_m. With increasing m_m values, the increase in aftershock hazard can be attributed mainly to an increase in the mean rate of aftershocks (dependent only on m_m) and, to a significantly less extent, a factor due to the implied increase in the upper bound aftershock magnitude (where the factor is dependent on both m_m and PGA level). This explains why the aftershock hazard curves are almost parallel. We shall now study

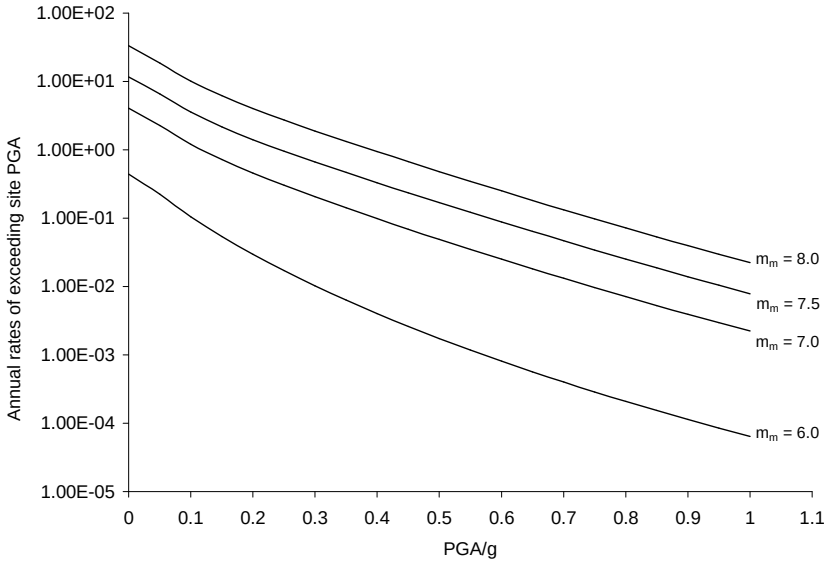

Figure 2.9: Effects of mainshock magnitudes m_m on aftershock hazard as a function of site PGA with base case values of $t = 7$ days and $T = 365$ days.

these effects in detail[1].

Next, we normalize the aftershock hazard in Figure 2.9 by the mainshock hazard for three different sites at R equal to 10 km, 30 km and 50 km using mainshock PSHA case 2. The results are shown in Figure 2.10. Importantly, the ratio of aftershock hazard to mainshock hazard becomes insensitive to location and is almost constant for all levels of PGA, for larger mainshock magnitudes especially. This insensitivity occurs because both aftershock and mainshock hazard are considered over the same fault segment where the integration over M and R for both cases in the process of PSHA (using Equation 2.7 for mainshock hazard analysis and Equation 2.8 for APSHA) are almost identical except for the changes in the upper bound aftershock magnitude. Indeed, the primary reason for introducing the Case 2 approximation above was so that mainshock and aftershock hazard could be compared in

[1]An increase in m_m might potentially increase the mainshock rupture length and, consequently, the length of the aftershock zone. An increase in the length of the aftershock zone will result in a reduction of the aftershock hazard at the site. This effect has not been considered here. The increase in aftershock hazard due to an increase in the mean rate of aftershocks (with increasing values of m_m) is independent of this effect. The increase in aftershock hazard due to the implied increase in the upper bound aftershock magnitude would be reduced if this effect had been taken into account. Thus, the factor due to the implied increase in the upper bound aftershock magnitude studied in this section (without consideration of this effect) serves as a conservative estimate of the resulting increase in aftershock hazard with increasing values of m_m.

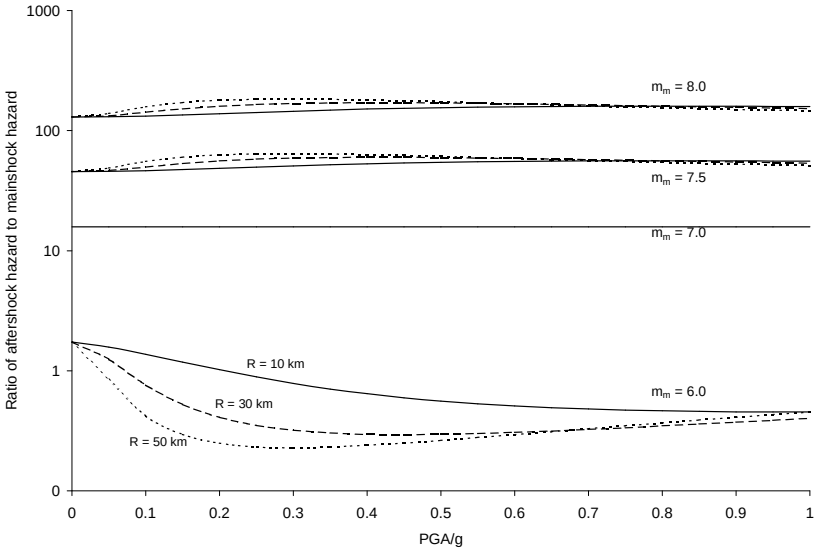

Figure 2.10: Ratio of PGA aftershock hazard to mainshock hazard for different site locations. $R = 10$ km is the solid line, $R = 30$ km is the dashed line and $R = 50$ km is the dotted line.

this explicit way. Thus, the increase in aftershock hazard can be attributed mainly to the increase in the mean aftershock rate with increasing values of m_m which does not depend on the ground motion level. The increase in the mean aftershock rate with an increase in m_m can be easily computed using Equation 2.6 for t, T constant. The (generally) secondary effect caused by the increase in the upper bound of the aftershock magnitude distribution is shown in Figure 2.11. As an example, for the case where $m_m = 8.0$, the total increase in the aftershock hazard from the base case at a PGA of 0.8g is about 10 times from Figure 2.10. This total factor is approximately equal to the product of 1.2 obtained from Figure 2.11 and the ratio of Equation 2.6 for $m_m = 8.0$ to $m_m = 7.0$ (t, T constant), which is approximately 8.25. The latter is clearly the primary contributor to the net increase. At lower levels of PGA, the increased mean aftershock rate contributes proportionately even more significantly to the increase in the aftershock hazard.

2.3.6 Effects of Structural Periods (T_0) on Aftershock Hazard

Up to now, we have studied aftershock hazard with respect only to site PGA, i.e., at a structural period T_0 of 0s. We next study the aftershock hazard as a function of spectral accelerations (Sa) with respect to structural periods of 0.5s, 0.75s, 1.0s and 1.5s. The

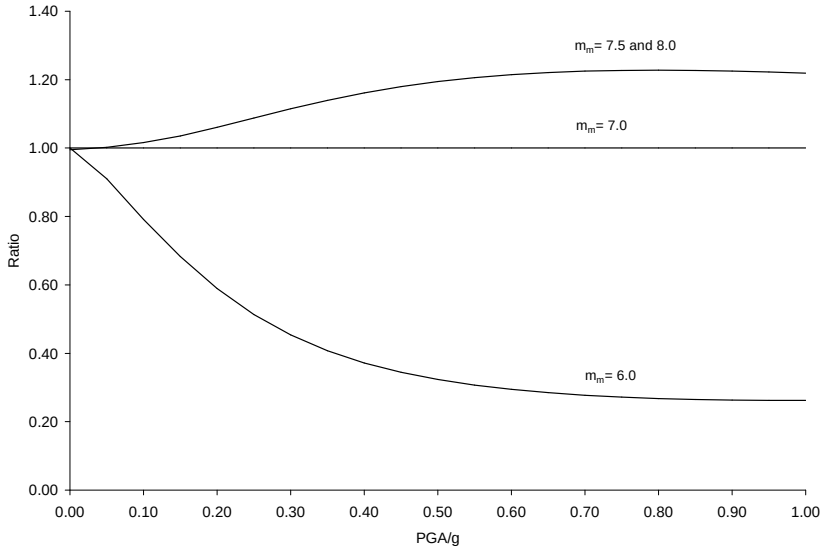

Figure 2.11: Change in aftershock hazard due to changes in the upper bound aftershock magnitude for $m_m = 6.0, 7.5$ and 8.0. Results are normalized to base case of $m_m = 7.0$.

aftershock hazard for the base case at different values of T_0 is shown in Figure 2.12. We can see that the aftershock hazard at a period of 0.5s is higher than that of the base case of 0s, i.e., the case with respect to site PGA. At periods between 0.75s and 1s, the aftershock hazard is reasonably similar to the base case of PGA for all Sa levels. At periods greater than or equal to 1.5s, the aftershock hazard is considerably lower as compared to the PGA base case.

We next study spectral shape ratios, as defined by the ratio of $Sa(T_0)$ to PGA. The results are shown in Figure 2.13 for the 2% in 50 years level. The first three cases are obtained from the attenuation law in Abrahamson and Silva (1997) by considering a fixed R of 30 km, and by varying the earthquake magnitudes from 5.0 to 6.0 and 7.0. The uniform hazard APSHA spectral shape ratio is obtained from the base case example previously discussed. Uniform hazard spectral ratios based on mainshock PSHA cases 1 and 3 are also shown. The PSHA cases (both mainshock and aftershock) can be considered a weighted average of the rates obtained from different events of different magnitudes. Bearing this in mind, it can be seen that the APSHA case is dominated by the higher magnitude events as the spectral shape ratios are closest to the spectral shape ratios obtained from the deterministic case where the event magnitude is assumed to be 7.0. Mainshock PSHA

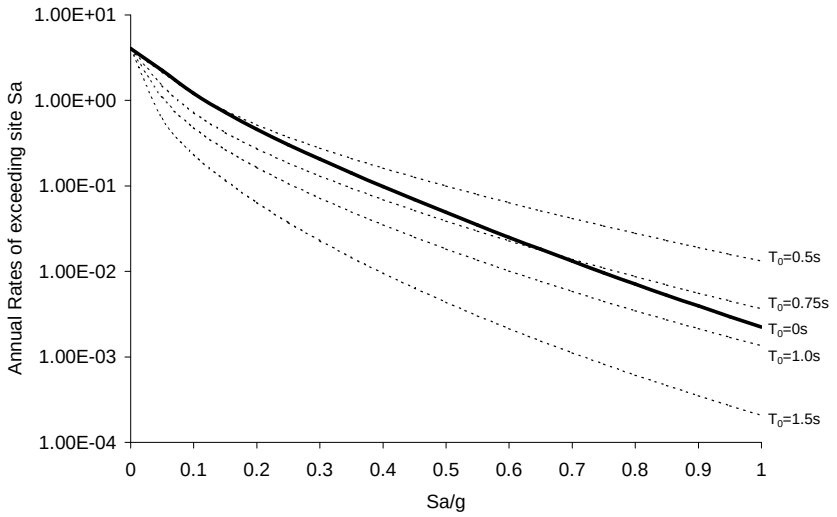

Figure 2.12: Base case aftershock hazard as a function of Sa for various structural periods, T_0.

case 1 demonstrates the fact that the mainshock hazard is dominated by higher-magnitude characteristic events when compared to mainshock PSHA case 3 which assumes there are no characteristic events. Note also that the APSHA spectral ratios are very close to the mainshock PSHA ratios. This suggests that the ratio of aftershock hazard to mainshock hazard should also be very similar not only for PGA, as studied in detail above, but also for all values of T_0.

We carry out the process of normalizing the aftershock hazard with respect to the mainshock hazard in a manner similar to Figure 2.10 for PGA, but for $T_0 = 0.75$s to verify the above claim. The results are shown in Figure 2.14. Note that the ratio of aftershock hazard to mainshock hazard also becomes relatively insensitive to location and is almost equal to the value obtained from the PGA case for all Sa levels. The contribution to the increase in aftershock hazard due to an increase in the upper bound of the aftershock magnitude distribution (similar to Figure 2.11) for Sa at $T_0 = 0.75$s is shown in Figure 2.15 together with the results obtained from Figure 2.11 for PGA.

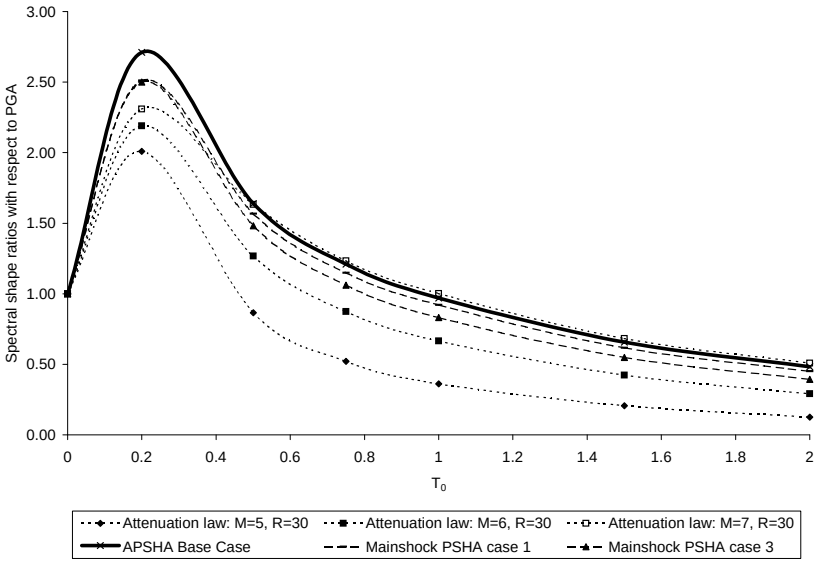

Figure 2.13: Spectral shape ratios with respect to PGA at the 2% in 50 years hazard level.

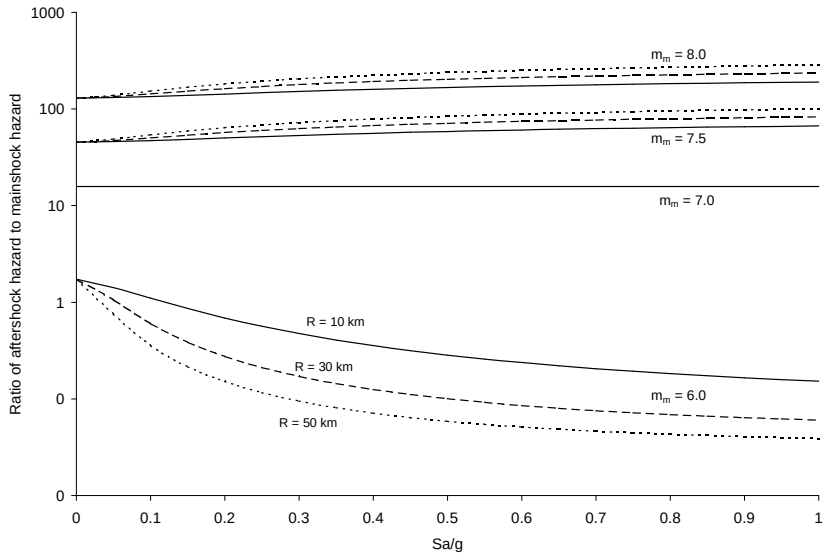

Figure 2.14: Ratio of aftershock hazard to mainshock hazard for different site locations for $T_0 = 0.75$s spectral acceleration. $R = 10$ km is the solid line, $R = 30$ km is the dashed line and $R = 50$ km is the dotted line.

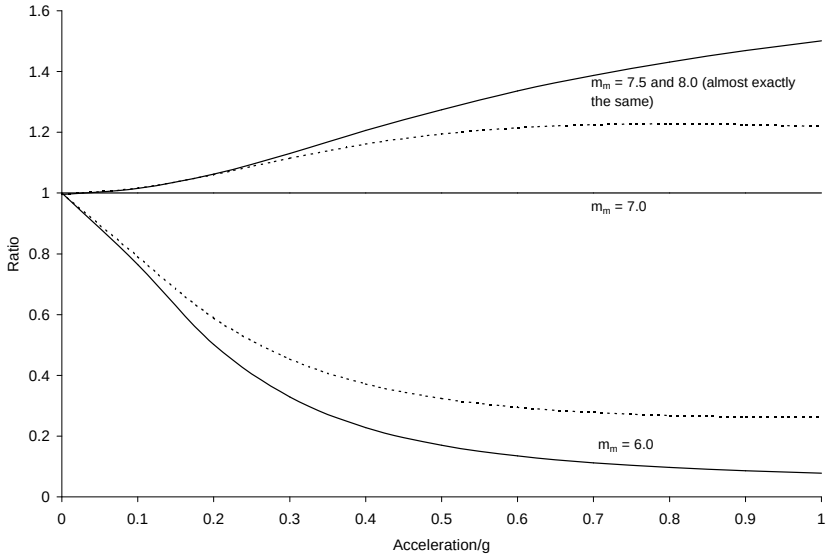

Figure 2.15: Change in aftershock hazard (normalized to base case of $m_m = 7.0$) due to changes in the upper bound aftershock magnitude ($m_m = 6.0, 7.5$ and 8.0) for PGA (dotted line) and spectral acceleration at $T_0 = 0.75$s (solid line).

2.3.7 Summary and Approximate APSHA

Based on the above example, for those cases where a single nearby fault (segment) is the dominant source of a damaging mainshock ground motion, the normalized aftershock hazard is relatively insensitive to a number of factors. This insensitivity permits one to conclude that the aftershock hazard is approximately a fixed multiple of the mainshock hazard for all ground motion levels, all values of T_0 and all site locations. For example, our base case APSHA example (with $t = 7$ days, $T = 365$ days and m_m=7.0) is approximately 20 times that of the pre-mainshock hazard (from Figures 2.10 and 2.14) for both PGA and $T_0 = 0.75$s at all levels of PGA and Sa, and for $R = 10, 30$ and 50 km. If we are interested in assessing the ratio of aftershock hazard to mainshock hazard one day after the mainshock and the duration of interest is in the order of one year (i.e., $t = 1$ and $T = 365$ days), we need to further multiply the mainshock hazard by a factor of 1.6 which can be either obtained from Figure 2.7 or Figure 2.4. Similarly, one can adjust for other values of t and T using Figure 2.4. To adjust for other mainshock magnitudes, one can use Figure 2.10 or 2.14. The ability to estimate aftershock hazard from the available mainshock hazard (due to a single dominant fault segment) in this approximate but rapid way has practical implications, for

example, for post-earthquake building tagging, a subject of discussion in Chapter 4. We believe it also fosters an appreciation for the nature of aftershock ground motion hazard and its relationship to the more familiar mainshock hazard.

2.4 Effects of Correlation between Mainshock Epsilon (ε_m) and Aftershock Epsilon (ε_a) on Aftershock Hazard

The expected intensity of the ground shaking at a site of known site conditions is generally estimated from an attenuation relationship. For example, in the APSHA examples that we have considered above, we have utilized the attenuation relationship developed in Abrahamson and Silva (1997) for rock sites. Such attenuation relationships are generally developed by using nonlinear regressions of empirical recordings from events of different magnitudes (M), source-to-site distances (R) and other variables (θ) such as local soil conditions, fault types etc. Such empirical recordings demonstrate a significant amount of scatter for the same M and R values. This variability is modeled by assuming the form (for the linear spectral acceleration at a site Sa, which is oscillator frequency and damping dependent) in Equation 2.9.

$$\ln Sa = g(M, R, \theta) + \varepsilon \sigma_{\ln Sa}^{attenuation} \tag{2.9}$$

The random variable epsilon (ε) is defined as the number of (logarithmic) standard deviations ($\sigma_{\ln Sa}^{attenuation}$) by which the (logarithmic) ground motion deviates from $g(M, R, \theta)$, the median value predicted by the attenuation relationship given M, R and θ. ε is generally modeled as a standard Gaussian variable.

Given the above formulation for the attenuation relationship, Equation 2.7 for mainshock PSHA (assuming one seismic source) could be more formally written as Equation 2.10.

$$\widetilde{\upsilon}(y, T) = \upsilon T \int_{-\infty}^{+\infty} \int_{R} \int_{m_l}^{m_u} I(Sa > y | m, r, \varepsilon) f_{M,R,\varepsilon}(m, r, \varepsilon) d\varepsilon dr dm \tag{2.10}$$

In Equation 2.10, $I(Sa > y|m, r, \varepsilon)$ is an indicator function which is equal to one if $Sa > y$ for a given m, r and ε, and zero otherwise. Upon observing that ε is independent of M and R such that $f_{M,R,\varepsilon}(m, r, \varepsilon) = f_{M,R}(m, r) f_{\varepsilon}(\varepsilon)$ and integrating over all values of ε, it is straightforward to show that Equation 2.10 reduces to Equation 2.7.

The above formulation serves to illustrate the role that ε plays in the evaluation of the

seismic hazard at the site in the mainshock situation. In the aftershock scenario, based on our previous formulation, we have implicitly assumed that $\varepsilon_{aftershock}$ is also modeled as a standard Gaussian variable which is independent of $\varepsilon_{mainshock}$. In reality, if we assume complete knowledge of the Sa at the site after the mainshock (for example, with the presence of a instrument at the site), we would be able to compute $\varepsilon_{mainshock}$ based on Equation 2.9, i.e., $\varepsilon_{mainshock} = \frac{\ln Sa - g(M,R,\theta)}{\sigma_{\ln Sa}^{attenuation}}$. Knowledge of $\varepsilon_{mainshock}$ at a site might in principle provide us with further information of $\varepsilon_{aftershock}$ at the same site in the event of the occurrence of an aftershock. These two ε's might be correlated due, for example, to certain commonalities in source, path, or site factors. Thus, we would want to be able to model the conditional probability distribution of $\varepsilon_{aftershock}$ given knowledge of $\varepsilon_{mainshock}$ at the site in consideration.

Both $\varepsilon_{mainshock}$ and $\varepsilon_{aftershock}$ have been modeled as standard Gaussian variables. We chose to model their joint probability distribution as a standard bivariate Gaussian distribution with probability density function given by Equation 2.11.

$$f_{\varepsilon_m,\varepsilon_a}(\varepsilon_m,\varepsilon_a) = \frac{1}{2\pi\sqrt{1-\rho^2}} \exp\left[-\frac{1}{2(1-\rho^2)}(\varepsilon_m^2 - 2\rho\varepsilon_m\varepsilon_a + \varepsilon_a^2)\right] \tag{2.11}$$

Here, for notational brevity, we denote $\varepsilon_{mainshock}$ as ε_m and $\varepsilon_{aftershock}$ as ε_a. ρ is the correlation coefficient (with values from -1 to 1) between ε_m and ε_a such that if ρ is equal to 1, $\varepsilon_m = \varepsilon_a$ and if ρ is equal to 0, ε_a is independent of ε_m. Thus, if ρ is equal to 0, we obtain the original formulation for APSHA as discussed in the previous sections. Equation 2.11 can be written as Equations 2.12 or 2.13.

$$f_{\varepsilon_m,\varepsilon_a}(\varepsilon_m,\varepsilon_a) = f_{\varepsilon_m}(\varepsilon_m) f_{\varepsilon_a|\varepsilon_m}(\varepsilon_a|\varepsilon_m) \tag{2.12}$$

$$f_{\varepsilon_m,\varepsilon_a}(\varepsilon_m,\varepsilon_a) = \frac{1}{\sqrt{2\pi}} \exp(-\frac{1}{2}\varepsilon_m^2) \frac{1}{\sqrt{2\pi(1-\rho^2)}} \exp\left[-\frac{1}{2}\left(\frac{\varepsilon_a - \rho\varepsilon_m}{\sqrt{1-\rho^2}}\right)^2\right] \tag{2.13}$$

By comparing Equations 2.13 and 2.12, since ε_m is a standard Gaussian variable, one can see that Equations 2.14 and 2.15 hold.

$$f_{\varepsilon_m}(\varepsilon_m) = \frac{1}{\sqrt{2\pi}} \exp(-\frac{1}{2}\varepsilon_m^2) \tag{2.14}$$

$$f_{\varepsilon_a|\varepsilon_m}(\varepsilon_a|\varepsilon_m) = \frac{1}{\sqrt{2\pi(1-\rho^2)}} \exp\left[-\frac{1}{2}\left(\frac{\varepsilon_a - \rho\varepsilon_m}{\sqrt{1-\rho^2}}\right)^2\right] \tag{2.15}$$

Hence, $f_{\varepsilon_a|\varepsilon_m}(\varepsilon_a|\varepsilon_m)$ is also a normal distribution with the parameters given in Equations 2.16 and 2.17.

$$E(\varepsilon_a|\varepsilon_m) = \rho\varepsilon_m \tag{2.16}$$

$$\sigma_{\varepsilon_a|\varepsilon_m}(\varepsilon_a|\varepsilon_m) = \sqrt{1-\rho^2} \tag{2.17}$$

Thus, if we have knowledge of the mainshock Sa and hence ε_m, in APSHA, we could model the distribution of ε_a given ε_m based on Equations 2.15, 2.16 and 2.17.

For APSHA, we integrate over all possible values of ε_a using the conditional probability distribution function of ε_a given ε_m as derived in Equation 2.15. In this case, the conditional probability distribution given M and R is still lognormal but with the parameters in Equations 2.18 and 2.19.

$$E\left(\ln Sa_{aftershock}|Sa_{mainshock}\right) = g(M,R,\theta) + \rho\varepsilon_m\sigma^{attenuation}_{\ln Sa_{aftershock}} \tag{2.18}$$

$$\sigma_{\ln Sa_{aftershock}|Sa_{mainshock}} = \sigma^{attenuation}_{\ln Sa_{aftershock}}\sqrt{1-\rho^2} \tag{2.19}$$

Hence, based on the above formulation, one can revise the ground motion analysis portion of the APSHA procedure to take into consideration the conditional probability distribution of ε_a given knowledge of $Sa_{mainshock}$ and hence ε_m.

We use the same site described earlier to demonstrate the difference in the aftershock seismic hazard curves that are obtained if we have knowledge of ε_m under different correlation level assumptions between ε_m and ε_a. We use the base case APSHA example for T_0=0.75s and we assume first that ε_m is equal to 0.5. The results are shown in Figure 2.16 where we obtain the annual rates of exceeding a site Sa due to an aftershock.

We can see from Figure 2.16 that with ρ equal to zero, the aftershock seismic hazard curve is the same as the curve in Figure 2.12. At the other extreme, with ρ equal to one, $\varepsilon_m = \varepsilon_a$ such that there is zero residual uncertainty in ε_a (i.e., $\sigma_{\ln Sa_{aftershock}|Sa_{mainshock}} = 0$), and there is an upper bound to the first mode $Sa_{aftershock}$ that is realizable at the site in the aftershock scenario. That bound is associated with the closest distance R and the largest aftershock magnitude, here assumed to be equal to m_m. Intermediate values of ρ (for example, ρ equal to 0.5 and 0.7) result in seismic hazard curves that lie between the

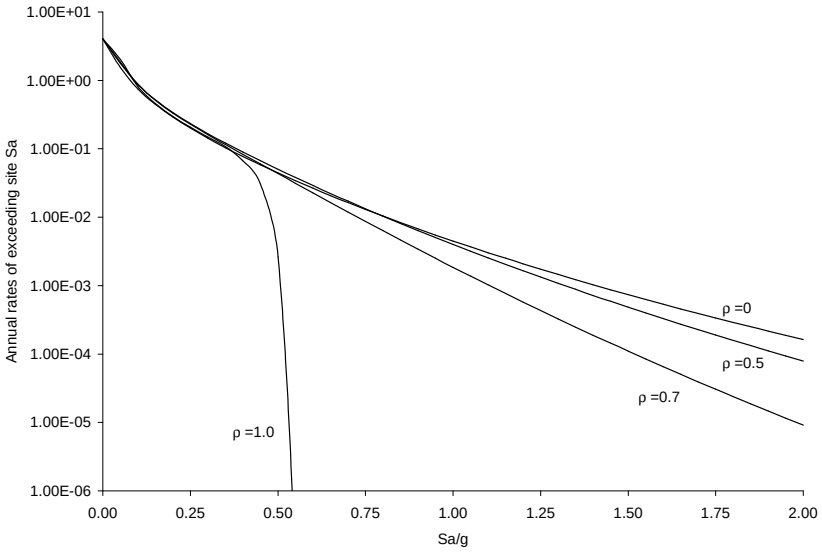

Figure 2.16: Base case aftershock seismic hazard curves for T_0 =0.75s. ε_m is taken to be equal to 0.5 and $\rho = 0, 0.5, 0.7$ and 1.0.

two curves previously described. The most reasonable values for the correlation coefficient between ε_m and ε_a probably lie between 0 and 0.7, for which the hazard in Figure 2.12 is quite insensitive, at least up to about 1g. Thus, these results suggest that despite the correlation that might exist between ε_m and ε_a, for reasonable levels of correlations as described by low to intermediate values of ρ (around 0.5), the resulting effects on aftershock hazard can be considered to be negligible, at least for all but very rare $Sa_{aftershock}$ levels, in which this assumption is conservative.

We next perform parametric studies on the base case site aftershock hazard with $\rho = 0.5$, 0.7 and 1.0 and $\varepsilon_m = -0.5$, 0, 0.5 and 1.0. We compare the results by normalizing it to the case with $\rho = 0$. The results are shown in Figure 2.17. We can see that for reasonable values of ρ (say $\rho = 0$ to 0.7) and $\varepsilon_m = -0.5, 0, 0.5$, the results are less than an order of magnitude away from the base case with $\rho = 0$. This conclusion is true except for rare $Sa_{aftershock}$ levels. Hence, the effects of correlation between ε_m and ε_a might not be significant for practical purposes, except for negative values of ε_m, high ρ values and rare ground motion levels where we might overestimate the aftershock hazard if we use $\rho = 0$ (which serves as a conservative estimate), and for $\varepsilon_m \geq 1.0$ where we might underestimate the aftershock hazard by a factor of two or more.

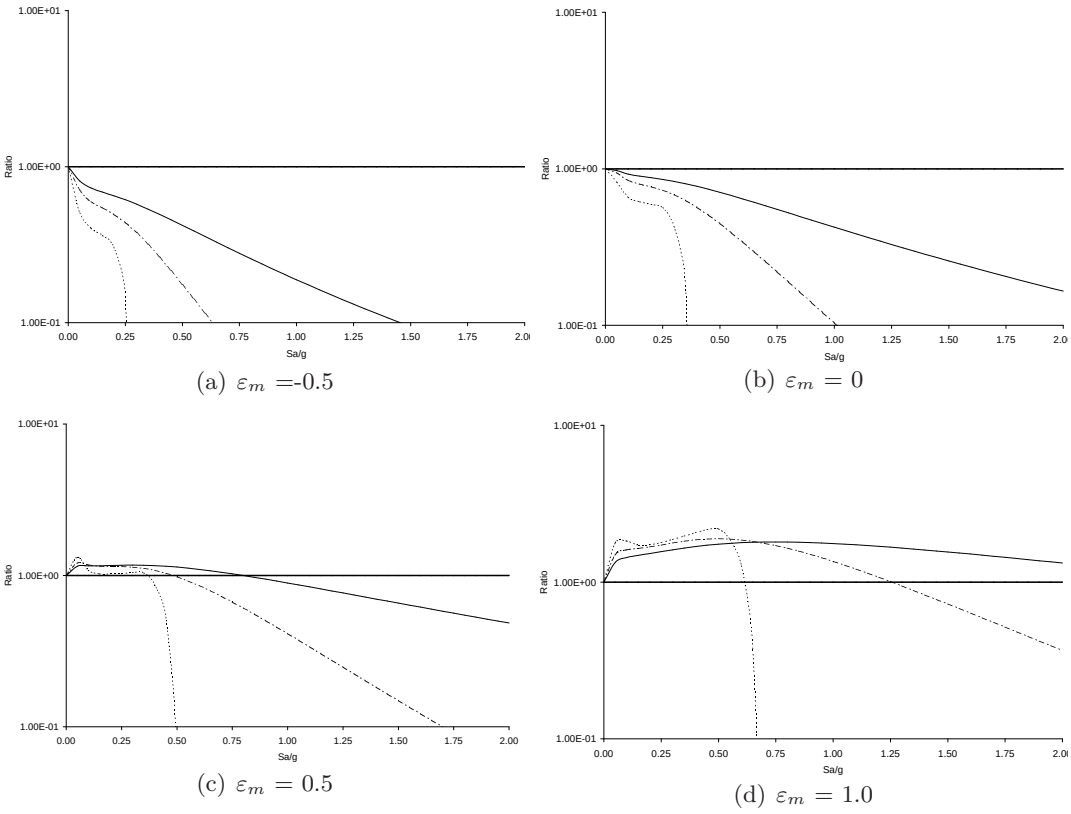

(a) ε_m =-0.5 (b) $\varepsilon_m = 0$

(c) $\varepsilon_m = 0.5$ (d) $\varepsilon_m = 1.0$

Figure 2.17: Ratios of base case aftershock hazard with $\rho = 0.5$ (solid line), 0.7 (dashed line) and 1.0 (dotted line) and $\varepsilon_m = -0.5, 0, 0.5$ and 1.0 to aftershock hazard with $\rho = 0$.

2.5 Conclusion

APSHA is a useful tool for post-earthquake ground motion hazard analysis. Knowing the expected number of aftershocks for exceeding any ground motion intensity measure allows us to quantify the time-varying aftershock hazard explicitly in a manner that will be useful to engineers and decision makers. We see that aftershock hazard can for some time after the mainshock be significantly higher than pre-mainshock hazard and that it depends on elapsed time t, duration T and mainshock magnitude m_m. Aftershock hazard decreases relatively slowly for low values of t and rapidly after $t = 100$ days. It is also not sensitive to T if T is 6 months or more. Aftershock hazard also increases with m_m; the increase is due primarily to the increase in mean aftershock rate, and secondarily to the presumed increase in the upper bound aftershock magnitude. Assuming one fault (or fault segment)

that dominates the pre-mainshock hazard at the site, aftershock hazard becomes relatively insensitive to site location and almost a constant value when we normalize by the mainshock hazard. This insensitivity is true for all levels of ground motion and for all values of T_0, implying that uniform hazard spectral shapes for aftershocks and mainshocks are about the same. These observations allow one to estimate the aftershock hazard at a site rapidly using the base case example presented here plus curves to correct for t, T and m_m. We find that the effects of potential correlation between ε_m and ε_a might not be significant for most practical purposes. We shall make use of APSHA in later chapters for building-tagging and post-earthquake decision making.

3 Performance of Mainshock-Damaged Buildings

In Chapter 2, we proposed a methodology to characterize the aftershock ground motion hazard at a site in terms of a suitable site ground motion intensity measure. In order to make informed building-tagging decisions based on quantifying the life-safety threat faced by a building occupant, we also need a methodology to quantify the performance of (potentially) mainshock-damaged buildings under different levels of ground shaking due to potential aftershocks. The permitted occupancy status of the building should be determined based on the building's residual dynamic capacity to resist aftershocks and the likelihood of an aftershock ground motion exceeding that capacity. The convolution of the aftershock site ground motion hazard from APSHA with the residual capacity of mainshock-damaged buildings in probabilistic terms allows us to quantify the rate of collapse due to aftershocks which can be objectively used as a decision basis for making building-tagging decisions. Building-tagging will be the main topic of discussion in Chapter 4.

In this chapter, we provide a summary of the procedure proposed by Luco et al. (2004) to quantify the probabilistic capacity of mainshock-damaged buildings to withstand future aftershock ground shaking by considering several levels of mainshock-sustained damage. A methodology to calculate the probability of a building in a given damage state progressing to a worse damage state due to the occurrence of an earthquake (either mainshock or aftershock) will be developed in this chapter as well. We shall illustrate the methodology with a case-study building which will be used throughout this report. Interested readers are referred to Luco et al. (2004), Bazzurro et al. (2004a) and Bazzurro et al. (2004b) for more details on the approach as well as a more complete description of the case-study building.

3.1 Methodology

3.1.1 Quantification of Aftershock Capacity of Mainshock-Damaged Buildings

To date, much of structural engineering research has been focussed on the mainshock environment and the quantification of the structural capacity of an intact structure in probabilistic terms. For example, the PEER Equation described in Chapter 1 assumes that a mainshock-damaged building is repaired to its original pre-mainshock state (usually considered to be intact) before the occurrence of the next mainshock. This instant "re-built" assumption is reasonable considering the long interarrival times between mainshocks. This is one reason why structural engineers have traditionally focussed on developing models to quantify the structural capacity of intact buildings only.

In the aftershock environment, the likelihood of aftershocks capable of incremental damage to an already mainshock-damaged building is greatly increased, and there might be insufficient time for the mainshock-damaged building to be repaired back to the original intact state due to likely insufficient manpower resources in the post-mainshock emergency situation. Also, as discussed in Chapter 1, aftershocks (implicitly or explicitly) affect evacuation decisions of (possibly) mainshock-damaged buildings because of the inferred life safety threat due to occupancy of a damaged building which might have less resistance to potential aftershock ground shaking. Hence, it is important to be able to assess the capacity of mainshock-damaged buildings, in probabilistic terms, to quantify the probability that a mainshock-damaged building will be incrementally damaged due to the occurrence of an aftershock. The aftershock environment thus poses a new challenge to current structural engineering analysis capabilities.

We first define several levels of damage sustained by the structure by associating increasing levels of damage with increasing values of peak roof drift ratios. We first denote the (random) peak roof drift ratio after an earthquake as θ. We also assume that we can classify several levels of damage sustained by the structure into discrete damage states DSj, where the peak roof drift ratio associated with DSj is θ_j. We chose to define the damage states based on the peak roof drift ratios in this report. Note that we can also choose to define damage states based on other engineering demand parameters (EDPs) such as the residual drift ratios, and even vectors of EDPs. The discrete damage states based on peak roof drift ratios for a building described in an example to follow correspond to physically

identifiable damage that can be observed in practice.

Now, we propose a methodology to quantify the aftershock capacities of mainshock-damaged buildings based on the discrete damage states described earlier. Luco et al. (2004) and Bazzurro et al. (2004b) define the (random) residual capacity of a building in post-mainshock damage state DSi as the minimum first-mode aftershock ground motion spectral acceleration that would induce collapse, denoted as DSn. (In the particular building model used in the example to follow, no global dynamic collapse ever preceded local collapse). This definition of (dynamic) residual capacity can be extended to the definition of the capacity of a building in DSi going to damage state DSj or worse due to the occurrence of an aftershock. We denote this capacity as $Sa_{cap}^{DSi,DSj}$ and it is the minimum first-mode aftershock ground motion spectral acceleration that would induce the peak roof drift ratio θ_j associated with DSj for a building originally in post-mainshock damage state DSi. Such (random) capacities can be estimated using the following steps.

1. Select a suite of earthquake ground motion records which can be used to represent both mainshocks and aftershocks.

2. Perform nonlinear dynamic time-history analysis using the selected set of ground motions, with suitable levels of scaling in amplitude, on either a full intact multiple-degree-of-freedom (MDOF) model, or an equivalent intact single-degree-of-freedom (SDOF) model, to obtain multiple realizations of each post-mainshock damage state as defined by appropriate peak roof drift ratios. This step is iterative. Each record is scaled until the spectral acceleration is found that causes precisely (with some tolerance) the peak roof drift ratio θ_i associated with each damage state, DSi. If a SDOF model is used, the force-deformation backbone curve should be about the same as that obtained from SPO analysis, with appropriately chosen hysteretic behavior. The resulting output of this step is the curve for the incremental dynamic analysis (IDA) of the intact structure – see, for example, Figure 3.3 to follow. The intersections of the IDA curves with a vertical line associated with damage state DSi, yield the observed values of the capacities $Sa_{cap}^{Intact,DSi}$ of the intact building going to DSi or worse in spectral acceleration terms, thus allowing statistics of $Sa_{cap}^{Intact,DSi}$ to be obtained. This step produces a probability distribution of the mainshock ground motion amplitude that results in the intact building going into damage state DSi or worse for each i. It also provides for each damage state and each record, a model of

the damaged building. These models will be used as the starting point for the next step.

3. Perform nonlinear dynamic time-history analysis using the same set[1] of ground motions, again with suitable levels of scaling, on the multiple realizations of the damaged building models from step 2. For each post-mainshock damage state DSi in step 2, scale iteratively to induce the peak roof drift ratio θ_j to the level associated with each worse damage state DSj, $j > i$. Again, the intersections of the IDA curve for the building in DSi with a vertical line associated with damage state DSj yield the observed values of the capacities $Sa_{cap}^{DSi,DSj}$. This step produces a probability distribution of the aftershock ground motion amplitude that results in the building in post-mainshock damage state DSi going to DSj or worse due to an aftershock.

4. Compute the median capacity of the building going from DSi to DSj or worse, denoted as $\widehat{Sa}_{cap}^{DSi,DSj}$, by considering all the possible pairs of mainshock-damaged building realizations leading to DSi and of aftershock ground motions resulting in further deterioration of the building from DSi to DSj or worse. The dispersion, denoted as $\beta_R^{DSi,DSj}$, is the standard deviation of the logarithm of $Sa_{cap}^{DSi,DSj}$ and can also be obtained as well.

3.1.2 Determination of Transition Probabilities

We shall now use the statistical information of $Sa_{cap}^{DSi,DSj}$ obtained from steps 1-4 in Section 3.1.1 to compute the probability of a building in DSi going to DSj or worse, $j > i$, given an earthquake (mainshock or aftershock) resulting in a random first-mode spectral acceleration, Sa. To facilitate the computation of the above probability, we condition on $Sa = x$ to first compute the probability of a building in DSi going to DSj or worse, given an earthquake resulting in a first-mode spectral acceleration, $Sa = x$, i.e., $P_i(\theta > \theta_j | Sa = x)$. If we further assume that the IDA curves are monotonically increasing (see, for example, Figure 3.3 to follow), then we have:

$$P_i(\theta > \theta_j | Sa = x) = P(Sa_{cap}^{DSi,DSj} < x)$$

[1] In principle, a different set of records might be used to represent the aftershocks.

It is clear that we need to have the probability distribution of $Sa_{cap}^{DSi,DSj}$ to compute the above probability (the computation of $\widehat{Sa}_{cap}^{DSi,DSj}$ and $\beta_R^{DSi,DSj}$ discussed earlier will allow us to fit a lognormal probability distribution to $Sa_{cap}^{DSi,DSj}$, which is the assumption that we will adopt later). Since Sa is itself a random variable, we need to consider all possible values of x such that the probability of a building in DSi going to DSj or worse, given an earthquake resulting in a random Sa with probability density function $f_{Sa}(x)$ is:

$$\int_0^\infty P(Sa_{cap}^{DSi,DSj} < x) f_{Sa}(x) dx \tag{3.1}$$

Alternatively, we can first condition on $Sa_{cap}^{DSi,DSj} = y$. Assuming that the probability density function of $Sa_{cap}^{DSi,DSj}$ is $f_{Sa_{cap}^{DSi,DSj}}(y)$, the probability of a building in DSi going to DSj or worse, given an earthquake resulting in a random Sa can also be calculated to be:

$$\int_0^\infty P(Sa > y) f_{Sa_{cap}^{DSi,DSj}}(y) dy \tag{3.2}$$

$P(Sa > y)$ can be obtained from mainshock PSHA or APSHA. Note that Equations 3.1 and 3.2 are equivalent. We shall adopt Equation 3.2 for the remaining study.

Again, in order to use Equation 3.2 to compute the probability of a building in DSi going to DSj or worse, $j > i$, given an earthquake (mainshock or aftershock), we need to have the probability distribution of $Sa_{cap}^{DSi,DSj}$. Step 4 of Section 3.1.1 provides us with the values of the median capacities $\widehat{Sa}_{cap}^{DSi,DSj}$ and the standard deviation of the logarithm of $Sa_{cap}^{DSi,DSj}$, $\beta_R^{DSi,DSj}$. However, $\beta_R^{DSi,DSj}$ described in Section 3.1.1 only represents the aleatory uncertainty in terms of variability of building response due to different ground motion records. This uncertainty is intrinsic in nature and thus cannot be reduced. We also need to include epistemic uncertainty which represents limited accuracy of the structural analysis procedure and imperfect knowledge of the parameters of the mathematical model of the structure. Such epistemic uncertainty can potentially be reduced with more detailed investigations into the building properties and the model development of the structure etc. We use the term $\beta_U^{DSi,DSj}$ to represent such epistemic uncertainty which reflects professional confidence on the selected mathematical model of the structure and the structural analysis

results. We can compute the net "uncertainty" or dispersion, $\beta_{cap}^{DSi,DSj}$, using Equation 3.3.

$$\beta_{cap}^{DSi,DSj} = \sqrt{\left(\beta_{R}^{DSi,DSj}\right)^2 + \left(\beta_{U}^{DSi,DSj}\right)^2} \tag{3.3}$$

Now that we have obtained values of $\widehat{Sa}_{cap}^{DSi,DSj}$ and $\beta_{cap}^{DSi,DSj}$, we make the assumption that $Sa_{cap}^{DSi,DSj}$ is a lognormal random variable with parameters $\widehat{Sa}_{cap}^{DSi,DSj}$ and $\beta_{cap}^{DSi,DSj}$, following Bazzurro et al. (2004b). The fragility curve of a building in DSi, defined as the conditional probability of a building in DSi exceeding a given damage state DSj for a given level of ground motion intensity (Sa in this case), can then be developed. The fragility curve also represents the cumulative distribution function of the random variable $Sa_{cap}^{DSi,DSj}$ with corresponding probability density function $f_{Sa_{cap}^{DSi,DSj}}(y)$.

The development of fragility curves, which are functions of Sa, allows one to compute the probability of a building originally in DSi going to DSj or worse given a mainshock of magnitude m_m at a closest distance R from the ruptured source. This requires the incorporation of the probability distribution of Sa for a given m_m and R. From a standard attenuation law (e.g., Abrahamson and Silva (1997)), one can obtain $E(\ln Sa_{mainshock})$ and $\sigma_{\ln(Sa_{mainshock})}$ where $Sa_{mainshock}$ is the mainshock first-mode site spectral acceleration which is generally assumed to be lognormally distributed.

To calculate the probability of a building in DSi going to DSj or worse due to a mainshock with magnitude m_m at a closest distance R from the site with random capacity $Sa_{cap}^{DSi,DSj}$, i.e., $P\left(Sa_{cap}^{DSi,DSj} < Sa_{mainshock}\right)$, we can use Equation 3.2. However, because $Sa_{cap}^{DSi,DSj}$ and $Sa_{mainshock}$ are both lognormal random variables, the computation of $P\left(Sa_{cap}^{DSi,DSj} < Sa_{mainshock}\right)$ is much simpler because:

$$\begin{aligned}
& P\left(Sa_{cap}^{DSi,DSj} < Sa_{mainshock} | mainshock\right) = P\left(\frac{Sa_{cap}^{DSi,DSj}}{Sa_{mainshock}} < 1\right) \\
= \; & P\left[\ln\left(\frac{Sa_{cap}^{DSi,DSj}}{Sa_{mainshock}}\right) < 0\right] = P\left[\ln\left(Sa_{cap}^{DSi,DSj}\right) - \ln(Sa_{mainshock}) < 0\right] \\
= \; & P(W < 0) = \Phi\left(\frac{E(\ln Sa_{mainshock}) - \ln\left(\widehat{Sa}_{cap}^{DSi,DSj}\right)}{\sqrt{\left(\beta_{cap}^{DSi,DSj}\right)^2 + \left(\sigma_{\ln(Sa_{mainshock})}\right)^2}}\right)
\end{aligned} \tag{3.4}$$

In Equation 3.4, W is defined to be the random variable $\ln\left(Sa_{cap}^{DSi,DSj}\right) - \ln(Sa_{mainshock})$,

and W is lognormal with median equal to $E(\ln Sa_{mainshock}) - \ln\left(\widehat{Sa}_{cap}^{DSi,DSj}\right)$ and standard deviation of $\ln W$ equal to $\sqrt{\left(\beta_{cap}^{DSi,DSj}\right)^2 + \left(\sigma_{\ln(Sa_{mainshock})}\right)^2}$. Here, $\Phi(x)$ is the widely available Gaussian cumulative distribution function. Then, the probability of transiting from DSi to DSj, denoted as $P'_{ij}|mainshock$, is simply the difference between the probability of a building in DSi going to DSj or worse and the probability of a building in DSi going to $DS(j+1)$ or worse given the occurrence of the above mainshock, i.e., $P\left(Sa_{cap}^{DSi,DSj} < Sa_{mainshock}|mainshock\right) - P\left(Sa_{cap}^{DSi,DS(j+1)} < Sa_{mainshock}|mainshock\right)$.

We can also compute the probability of a building in DSi after the mainshock going into DSj or worse after an *aftershock* of random magnitude at a random location on the aftershock zone after a mainshock of known magnitude and location. We denote $Sa_{aftershock}$ as the potential aftershock site spectral acceleration (at the first mode period)[2]. In Chapter 2, we have described how to obtain $P(Sa_{aftershock} > y|aftershock)$. The probability of a building in post-mainshock damage state DSi going into DSj or worse due to an aftershock of random magnitude at a random location can be calculated using Equation 3.5, similar to Equation 3.2.

$$P\left(Sa_{cap}^{DSi,DSj} < Sa_{aftershock}|aftershock\right) = \int_y P(Sa_{aftershock} > y|aftershock) f_{Sa_{cap}^{DSi,DSj}}(y)dy \tag{3.5}$$

Then, the transition probability of a building in DSi going to DSj due to an aftershock of random magnitude at a random location, denoted as $P'_{ij}|aftershock$, is the difference of $P\left(Sa_{cap}^{DSi,DSj} < Sa_{aftershock}|aftershock\right)$ and $P\left(Sa_{cap}^{DSi,DS(j+1)} < Sa_{aftershock}|aftershock\right)$.

Since a building in damage state DSi has to be in another damage state (possibly the same damage state, DSi, or a different damage state, DSj, $j > i$) after the mainshock or earthquake, $\sum_j P'_{ij}|mainshock = 1$ and $\sum_j P'_{ij}|aftershock = 1$. Also, since we are assuming that the building can only be progressively damaged due to the occurrences of either mainshocks or aftershocks, $P'_{ij}|mainshock = 0$ and $P'_{ij}|aftershock = 0$ for $i > j$ if we further assume no repair operations.

[2]Here, we assume that the building in all possible post-mainshock damage states has the same structural period as that of the intact building. The damaged building can potentially have a longer structural period as compared to that of the intact building. See, for example, Bazzurro et al. (2004a)

3.2 Example

We shall now provide an example to illustrate the above proposed methodology. The case-study building used in this study has also been used in Phase I of a project for the Pacific Earthquake Engineering Research Lifelines (PEER-LL) Program and its co-sponsor Pacific Gas & Electric (PG&E). It is a three-story steel-moment-resisting-frame (SMRF) building constructed in San Francisco in 1989. The first mode period, T_0, is equal to 0.73s. Because of its date of construction, brittle beam-column connections are assumed. Fractures occur at a plastic hinge rotation of 0.01 radians at which point the moment strength drops to 30% of the plastic value. A static pushover (SPO) of the building, excerpted from Bazzurro et al. (2004b), is shown in Figure 3.1. The first shear-tab failure is assumed to occur at a plastic hinge rotation of 0.07 radians, at which point local collapse is assumed to have occurred, the SPO analysis is halted and zero base shear is assumed from this point on. Four post-mainshock damage states with associated peak mainshock roof drift ratios for the building are considered and are indicated on the SPO curve. Damage state 1 ($DS1$) at a peak roof drift ratio of $\theta_1 = 0.009$ corresponds to onset of nonlinear behavior in the building. Damage state 2 ($DS2$) at a peak roof drift ratio of $\theta_2 = 0.016$ corresponds to fracture of exterior beam-column connections of the first floor in the building. Damage state 3 ($DS3$) at a peak roof drift ratio of $\theta_3 = 0.024$ corresponds to fracture of interior connections of the frame (in addition to exterior connections). Damage state 4 ($DS4$) at a peak roof drift ratio of $\theta_4 = 0.048$ corresponds to local failure of a shear-tab, and it represents local collapse.

Luco et al. (2004) performed the procedures described in Section 3.1.1 using an equivalent SDOF system having the same quadrilinear approximation of the SPO curve as shown in Figure 3.1. He used three different types of hysteretic behavior: bilinear, peak-oriented ("Clough") and pinching. The set of ground motions used in the study by Luco et al. (2004) is the set of 30 earthquake recordings used in Vamvatsikos and Cornell (2004). The force-deformation curves of each hysteretic behavior is shown in Figure 3.2.

Not only does performing step 2 in Section 3.1.1 provides us with multiple realizations of post-mainshock damage states, it also provides us with the incremental dynamic analysis (IDA) curve. The results obtained using a pinching building model is shown in Figure 3.3. The associated peak roof drift ratios for each damage state are also shown in Figure 3.3. The median intact capacities, denoted as $\widehat{Sa}_{cap}^{intact,i}$, and the standard deviation of the logarithm of $Sa_{cap}^{intact,i}$, denoted as $\beta_R^{intact,i}$, can be quantified by drawing a vertical line associated with

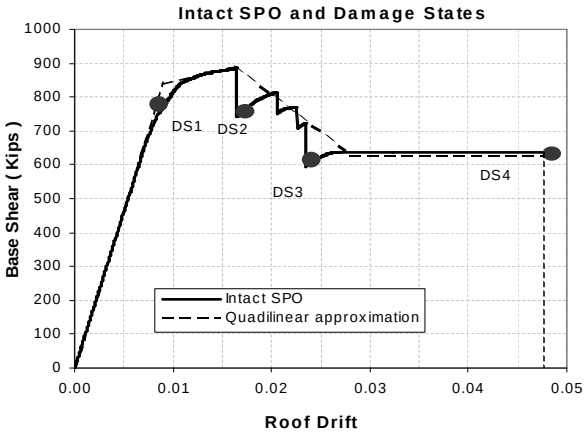

(a) Intact

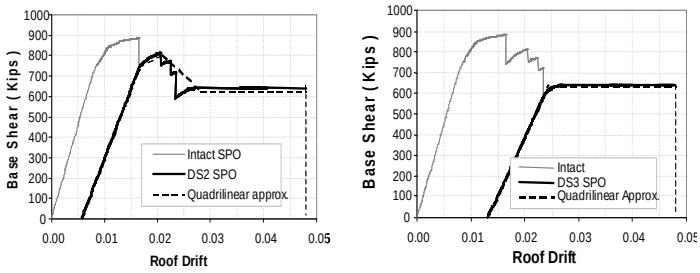

(b) $DS2$ and $DS3$

Figure 3.1: Nonlinear SPO curve for the intact, undamaged case-study building. The quadrilinear approximation is the SPO curve for the SDOF idealization of this first-mode dominated building. The four potential post-mainshock damage states and the associated peak roof drift ratios are also indicated on the figure. The SPO curves for the building in $DS2$ and $DS3$ are also shown. The SPO curve for the building in $DS1$ is assumed to be the same as that of the intact building. This figure was excerpted from Bazzurro et al. (2004b).

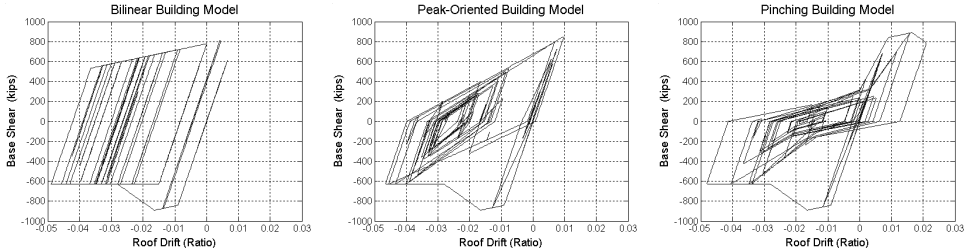

Figure 3.2: Hysteretic behavior of the bilinear, peak-oriented, and pinching SDOF building models. This figure was excerpted from Luco et al. (2004).

each θ_i. The medians are shown in Figure 3.3. The final state of the structure after this mainshock analysis will be the initial starting state for the subsequent aftershock analysis.

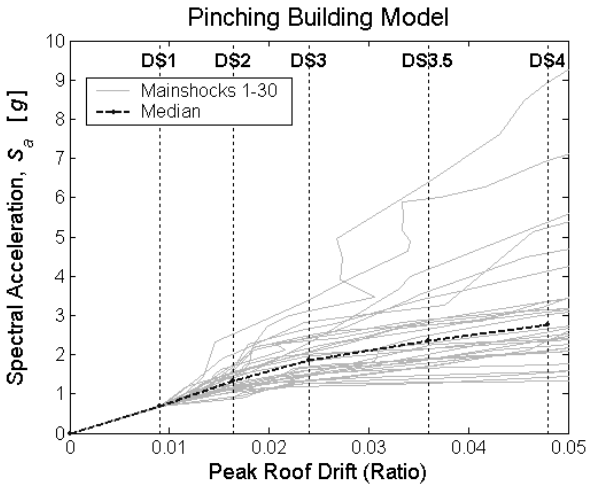

Figure 3.3: IDA curve obtained while obtaining multiple realizations of each post-mainshock damage state. This figure was excerpted from Luco et al. (2004).

Next, step 3 in Section 3.1.1 is carried out on the multiple realizations of post-mainshock damage states with aftershock earthquake ground motions, where the peak roof drift ratio associated with a worse damage state is induced by scaling each aftershock record by an appropriate factor. As discussed earlier, this procedure is iterative in general. The results are somewhat polarity sensitive. Because the scaling of aftershocks by positive and negative factors typically results in different Sa values, the smaller value is selected as per the definition of capacity described earlier as the smallest Sa that results in the transition to another damage state or worse. An example using the pinching model of the building going from $DS3$ to $DS4$, with both the mainshock and aftershock ground motion records scaled to appropriate levels, is shown in Figure 3.4.

Step 3 can be carried out for all post-mainshock damage states going to all post-aftershock damage states or worse such that we obtain all values of $\widehat{Sa}_{cap}^{DSi,DSj}$ and $\beta_R^{DSi,DSj}$. In fact, performing both steps 2 and 3 is equivalent to performing sequential IDAs for the structure with all intermediate damage states taken into consideration. Values of $\widehat{Sa}_{cap}^{DSi,DSj}$ and $\beta_R^{DSi,DSj}$ provided by Dr. Luco for a bilinear SDOF building model are shown in Figure 3.5. Here, with a bilinear SDOF model, there is some decrease in the dynamic capacity of the building in terms of $\widehat{Sa}_{cap}^{DSi,DSj}$ as the level of post-mainshock damage is increased. For

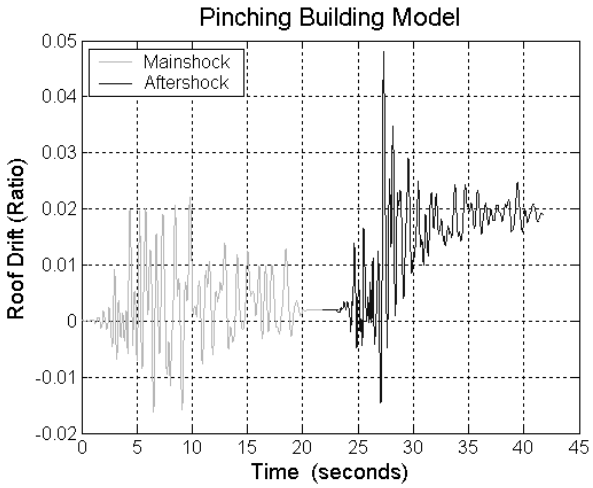

Figure 3.4: Roof drift time histories from back-to-back mainshock-aftershock dynamic analyses for building going from $DS3$ (peak roof drift ratio of 0.024) after the mainshock to $DS4$ (peak roof drift ratio of 0.048) after the aftershock. This figure was excerpted from Luco et al. (2004).

Median Spectral Acceleration (g)

From \ To	Intact	DS1	DS2	DS3	DS4
Intact	--	0.69	1.37	1.80	2.78
DS1	--	--	1.37	1.80	2.78
DS2	--	--	--	1.61	2.63
DS3	--	--	--	--	2.07
DS4	--	--	--	--	--

β_R

From \ To	Intact	DS1	DS2	DS3	DS4
Intact	--	0.00	0.27	0.33	0.39
DS1	--	--	0.27	0.33	0.39
DS2	--	--	--	0.30	0.36
DS3	--	--	--	--	0.34
DS4	--	--	--	--	--

Figure 3.5: Values of $\widehat{Sa}_{cap}^{DSi,DSj}$ and $\beta_R^{DSi,DSj}$. These results are provided by Dr. Luco.

example, $\widehat{Sa}_{cap}^{Intact,DS4} = 2.78g$ and $\widehat{Sa}_{cap}^{DS3,DS4} = 2.07g$, and the loss in dynamic capacity of the building in $DS3$ is approximately 25% as compared to that of the intact building. From Figure 3.3, the corresponding loss in maximum base shear from the SPO curves of

the intact building and the building in $DS3$ is about 33%, a percentage comparable to that of the loss in dynamic capacity. Bear in mind, however, that the results presented here use the smallest Sa that results in the transition to another damage state or worse to address the polarity issue of the scaling of the aftershock ground motions – the loss in dynamic capacity will be less otherwise. Also, as observed by Luco et al. (2004) as well as Amadio et al. (2003) and Lee and Foutch (2004) who have done similar (but less thorough) back-to-back dynamic analyses, the reduction in dynamic capacity has been generally observed to be relatively small, especially if other hysteretic behavior (other than bilinear) is assumed for the SDOF model. The performance of damaged buildings due to an aftershock is an important area of research that deserves more attention from structural engineers. Similar procedures described here should be carried out with MDOF models for different building types to study the resulting loss in dynamic capacity starting from different initial damage states. For the purpose of this report, we shall use the results in Figure 3.5 for the rest of the study. We also used the baseline $\beta_U^{Intact,DSj}$ values proposed in Bazzurro et al. (2004b) where $\beta_U^{Intact,DS1} = 0.3$, $\beta_U^{Intact,DS2} = 0.6$, $\beta_U^{Intact,DS3} = 0.6$ and $\beta_U^{Intact,DS4} = 0.5$. We assume that $\beta_U^{DSi,DSj} = \beta_U^{Intact,DSj}$.

For this example, for the purpose of illustration, we also consider a second building which is considerably weaker than the first building described earlier. This second building is assumed to have $\widehat{Sa}_{cap}^{DSi,DSj}$ values which are 50% of the corresponding values of the first building (shown in Figure 3.5), with the same $\beta_{cap}^{DSi,DSj}$(also shown in Figure 3.5). We shall refer to the first building as the original building, and this second building as the weaker building.

For numerical purposes, to illustrate the methodology to obtain the transition probabilities due to the occurrence of a mainshock for all initial states, we assume $m_m = 7.0$ and $R = 10$ km, following our base-case aftershock example described in Chapter 2. The fragility curves for each post-mainshock damage state DSi going into damage state DSj or worse in an aftershock can then be obtained and are shown in Figure 3.6 for both buildings.

Using Equation 3.4, we can also calculate the probability of transiting to each post-mainshock damage state after the above mainshock scenario for all possible initial states of both buildings. The values of these probabilities are provided in Figure 3.7. The first column indicates the initial state of the building before the mainshock. Generally, we assume that the building is intact before the occurrence of the mainshock such that only the first row of the matrix is used. If $i = 0$ refers to the intact state, the probability of

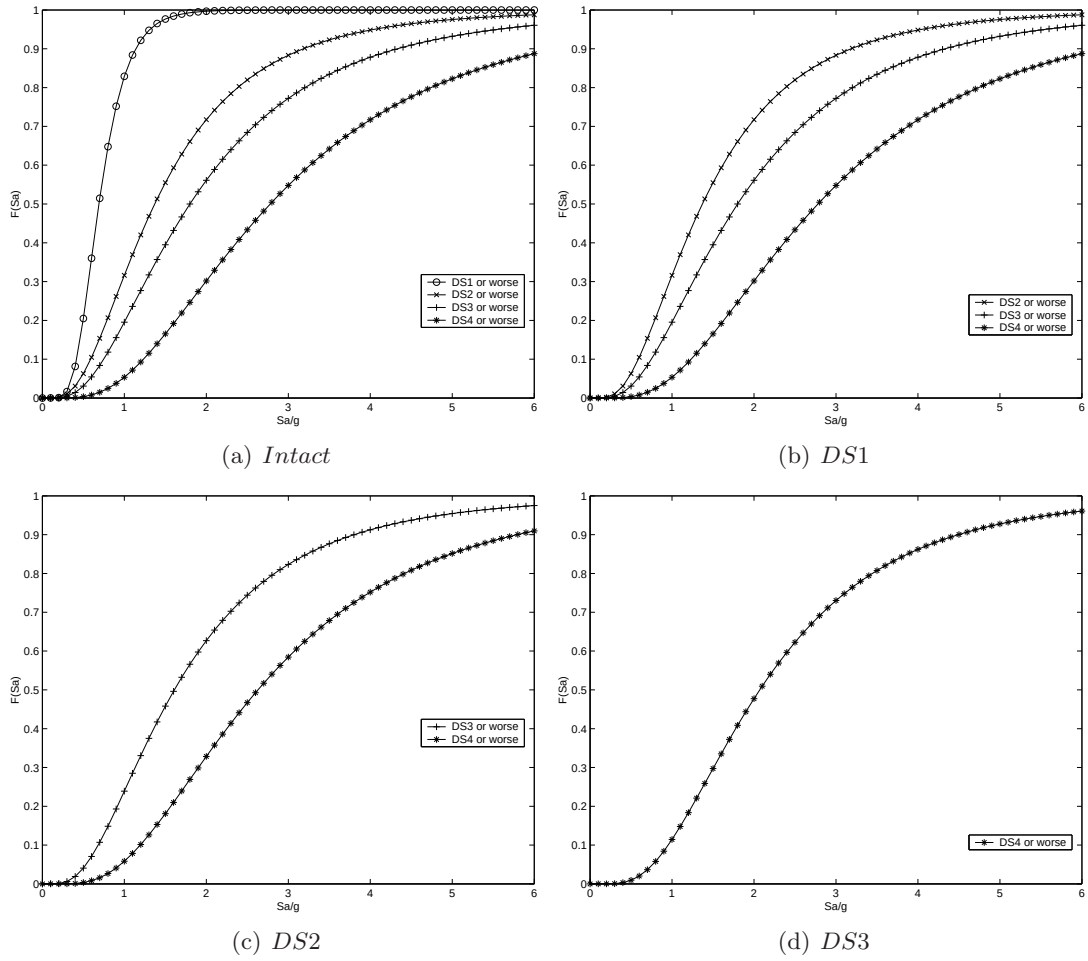

(a) *Intact* (b) $DS1$

(c) $DS2$ (d) $DS3$

Figure 3.6: Fragility curves for each post-mainshock damage state.

the intact building transiting to $DS1$, $DS2$, $DS3$ or $DS4$ (i.e., the probability of the intact building being damaged in the mainshock) is equal to $\sum_j P'_{0j}|mainshock$ for $j = 1, 2, 3, 4$, or $1 - P'_{00}|mainshock$. The probability of the first intact building being damaged after a mainshock with $m_m = 7.0$ and $R = 10$ km is equal to 0.164 and the probability of collapse is 0.0075. For the second, weaker building in the intact state, the probability of it being damaged after the same mainshock is equal to 0.554 and the probability of collapse is 0.0559. With a reduction of the values of $\widehat{Sa}_{cap}^{DSi,DSj}$ by 50%, the probability of damage of the intact building increases by more than three times, and the probability of collapse increases by more than seven times. Thus the probabilities of damage and collapse of the weakened

	Intact	*DS1*	*DS2*	*DS3*	*DS4*
Intact	8.36E-01	1.33E-01	1.41E-02	8.50E-03	7.50E-03
DS1	0	9.70E-01	1.41E-02	8.50E-03	7.50E-03
DS2	0	0	9.79E-01	1.32E-02	8.08E-03
DS3	0	0	0	9.81E-01	1.90E-02
DS4	0	0	0	0	1

Probability of being in each post-mainshock damage state given initial state of building (Original Building)

	Intact	*DS1*	*DS2*	*DS3*	*DS4*
Intact	4.46E-01	3.63E-01	7.55E-02	6.00E-02	5.59E-02
DS1	0	8.13E-01	7.68E-02	6.80E-02	4.25E-02
DS2	0	0	8.66E-01	9.17E-02	4.27E-02
DS3	0	0	0	8.63E-01	1.37E-01
DS4	0	0	0	0	1

Probability of being in each post-mainshock damage state given initial state of building (Weaker Building)

Figure 3.7: Probability of transiting to each post-mainshock damage state after a mainshock with $m_m = 7.0$ and $R = 10$ km for all possible initial states of both buildings.

building increase by a significant extent, much more than the 50% decrease in the values of $\widehat{Sa}_{cap}^{DSi,DSj}$ might imply. In this example, the mainshock rupture is extremely close to the site ($R = 10$ km) which has potentially contributed to the significant increases in the probabilities of damage and collapse.

Also, given the base-case aftershock example in Chapter 2 and using Equation 3.5, we can compute the transition probabilities of buildings for all post-mainshock damage states given the occurrence of an aftershock of random magnitude at a random location. In fact, the mainshock example described earlier can be viewed as a worst-case repeat of the mainshock in the aftershock environment, i.e., an aftershock occurred at the closest distance to the site with the mainshock magnitude. These transition probabilities for both buildings for all post-mainshock damage states are given in Figure 3.8. In this aftershock example, we assume first that both buildings remain intact after the mainshock. A reduction of the values of $\widehat{Sa}_{cap}^{DSi,DSj}$ by 50% results in the probability of damage increasing by about 60% and the probability of collapse increasing by about 70% given the occurrence of an aftershock of random magnitude at a random location. The probability of damage and collapse of the weaker building increases by a factor that is much closer to the 50% reduction in the values of $\widehat{Sa}_{cap}^{DSi,DSj}$. This observation can partly be attributed to the fact that we have considered aftershocks at random locations which can potentially be located far enough from the site such that the 50% reduction of the values of $\widehat{Sa}_{cap}^{DSi,DSj}$ does not significantly

	Intact	*DS1*	*DS2*	*DS3*	*DS4*
Intact	9.95E-01	3.95E-03	3.43E-04	1.94E-04	1.83E-04
DS1	0	9.99E-01	3.43E-04	1.94E-04	1.83E-04
DS2	0	0	9.99E-01	3.13E-04	1.96E-04
DS3	0	0	0	1.00E+00	4.24E-04
DS4	0	0	0	0	1

Transition probability for each post-mainshock damage state going to a worse damage state given an aftershock (Original Building)

	Intact	*DS1*	*DS2*	*DS3*	*DS4*
Intact	9.92E-01	5.80E-03	9.77E-04	7.04E-04	3.17E-04
DS1	0	9.99E-01	9.77E-04	7.04E-04	3.17E-04
DS2	0	0	9.99E-01	8.24E-04	3.99E-04
DS3	0	0	0	9.99E-01	1.44E-03
DS4	0	0	0	0	1

Transition probability for each post-mainshock damage state going to a worse damage state given an aftershock (Weaker Building)

Figure 3.8: Transition probabilities for all initial post-mainshock damage states for both buildings given the occurrence of an aftershock of random magnitude at a random location.

increase the probability of damage and collapse. Note also that as we progress from an intact post-mainshock state to a $DS3$ post-mainshock state, the probability of collapse due to the occurrence of an aftershock of random magnitude at a random location increases by almost two times for the original building and by almost five times for the weaker building, indicating the increasing likelihood of collapse in an aftershock of a building in $DS3$ as compared to an intact building. The results in Figures 3.7 and 3.8 will be used in later chapters.

3.3 Conclusion

This chapter provides a summary of the methodology proposed by Luco et al. (2004) to quantify the performance of damaged buildings due to potential aftershock ground motions. The methodology involves, in principle, "back-to-back" nonlinear dynamic time-history analysis of samples of records representing mainshocks and aftershocks in both cases. Iterative and/or incremental dynamic analysis are necessary to find the probability that a building goes (in the mainshock) from the intact to a pre-specified damage state, and then (in the aftershock) from that state to another. The collapse damage state is of particular interest. While in principle these nonlinear dynamic time-history analysis should be done

on MDOF models (and research is underway in this mode), in practice, less computation-intensive SDOF dynamic models and/or nonlinear-static procedures proposed in Bazzurro et al. (2004a) and Bazzurro et al. (2004b) may prove more advantageous. For example, the SPO2IDA tool developed by Vamvatsikos and Cornell (2004) which produces the median IDA curve as well as the record-to-record dispersion (if the quadrilinear backbone is available as an input) can be used by practising structural engineers who may need to obtain the approximate IDA results without resorting to time-consuming nonlinear dynamic time history analysis. This method has been used, for example, in Maffei et al. (2002).

The above procedure allows one to develop fragility curves for all post-mainshock building damage states, and it allows one to quantify the likelihood of each post-mainshock damage state after a mainshock of known magnitude and location. It also allows one to compute the transition probability of a building in a given post-mainshock damage state transiting to a worse damage state given the occurrence of an aftershock of random magnitude at a random location with a specified aftershock zone. Together with the results from APSHA, one can then obtain the rate of collapse due to aftershocks which can be used as a decision basis for building-tagging, the subject of discussion in the next chapter.

4 Life-Safety-Based Building Tagging Criteria

In this chapter, we propose a decision making/policy methodology for building evacuation and re-occupancy (i.e., building "tagging") to insure adequate life safety during a period of enhanced seismic activity. The proposed methodology for the life-safety evaluation of an earthquake-damaged building is based on the explicit quantification of the time-varying aftershock ground motion hazard at the site after a major earthquake using APSHA, the subject of discussion in Chapter 2. We also take into consideration the level of damage sustained by the building due to the mainshock and its residual capacity against collapse due to possible future aftershocks by using the methodology discussed in Chapter 3.

The proposed scheme enables us to classify buildings after an earthquake into three groups based on the frequencies of building collapse due to an aftershock. The fatality risk to an arbitrary occupant is presumed to be proportional to this number. The classification criteria are based on the value of this collapse frequency or rate relative to the tolerable value implied by current new building design. The first group of buildings is classified or "tagged" red implying that immediate entry and re-occupancy are not permitted for any personnel. The second group of buildings is tagged yellow; entry by volunteer emergency personnel for repair or retrofit purposes or for continued operation of critical facilities is allowed as long as such personnel are informed of the increased risk they face and are appropriately compensated for it. The third group of buildings is tagged green, permitting entry and re-occupancy for all personnel. The proposed methodology also provides for the change of tag color as a function of elapsed time from the mainshock due to the decreasing aftershock hazard at the site.

We also propose a methodology to allow earlier entry into a red-tagged building by

introducing the concept of a controlled work force where we limit the cumulative frequency of collapse faced by a selected informed and compensated volunteer worker. This can be achieved by limiting the duration these workers may spend in damaged buildings, followed by a required, subsequent rotation to a safer working environment.

4.1 Introduction

After an earthquake buildings might suffer significant damage without collapse. There is a need to "tag" such buildings to decide if it is necessary to evacuate their occupants based on the degree of damage sustained by the buildings. If the occupants of a damaged building are evacuated, it is also necessary to decide if and when emergency workers can enter the building for search-and-rescue or temporary shoring missions. Further, there are some critical facilities where it is essential to community recovery to ensure the continuation of their operations after the earthquake. Such facilities include water and power distribution networks etc. For such facilities, it might be extremely important to the safety of the public as a whole to allow a minimum number of workers to enter the damaged building after the earthquake to perform critical functions. This case requires special consideration.

Such tagging decisions are dependent on the damage state of the building immediately after the mainshock. The decision should be based on life-safety considerations in terms of the damaged building's ability to resist aftershocks and the likelihood of an aftershock capable of collapsing it. Unfortunately, such decisions are complicated by the significantly increased frequency of aftershocks in the post-mainshock environment. We shall use APSHA to quantify the aftershock ground motion hazard at the site in the post-mainshock scenario. We shall also consider the damage states of the building after the mainshock based on the residual capacity of the damaged building to resist aftershock ground motions. As proposed in Chapter 3, we shall use Sa_{cap}, measured in terms of spectral acceleration of the first-mode period of the building, as the measure of capacity of damaged buildings.

In this chapter, we must first introduce a proposed methodology to quantify the life-safety threats in a time-varying environment by representing them as Equivalent Constant Rates, or ECRs. We use the frequency of collapse as a proxy for the life-safety risk faced by an arbitrary building occupant. With the ability to quantify time-varying life-safety risk, we shall propose a methodology for building tagging.

4.2 Quantification of Time-Varying Rates as Equivalent Constant Rates (ECRs)

As discussed in Chapter 2, aftershock hazard is time-varying in nature, and it depends on the number of elapsed days t after the occurrence of the mainshock. Aftershock hazard is also dependent on the length of the duration T taken into consideration. Such dependence on time is inconsistent with conventional design criteria for buildings. For example, in the United States, design ground motion levels for new buildings are currently set at a frequency of exceedance of 0.0004/year (or 2% in 50 years). This frequency is implicitly assumed to be constant and indefinite in time. Individual life-safety criteria are also normally stated in terms of annual frequency of fatality. For example, NPD (1981) sets the maximum annual individual fatality risk per worker to 10^{-4} on new platforms for the offshore oil and gas industry. Again, such criteria implicitly assume time-independent fatality risks that are constant and extend indefinitely into the future. In order to compare or calibrate safety criteria in a time-varying environment (such as aftershocks) to the standard time-invariant situation, some means must be identified to transform the former into the latter.

Here, we shall develop such a methodology where time-varying rates or frequencies are changed to "equivalent" constant rates with the desired characteristics by considering an implied discounted investment in life-safety technologies for both the constant or homogeneous mainshock case and the time-varying, nonhomogeneous aftershock case on the basis of social equity. See Paté-Cornell (1984) for a discussion of the notions of social equity and investment in life-safety technologies in the context of structural safety in the typical constant rate case. Such constant rates which represent the time-varying aftershock rates are referred to as Equivalent Constant Rates, or ECRs.

Following the notation in Chapter 2, after a mainshock of magnitude m_m, $\mu(t; m_m)$ is the instantaneous daily rate of aftershocks with magnitudes between m_l and m_m at time t. Aftershocks are modeled as nonhomogeneous Poisson processes. As mentioned earlier, we propose to use the frequency of collapse as a proxy for the life-safety risk faced by an arbitrary building occupant. From Chapter 3, a building in damage state i will collapse in an aftershock with probability P'_{in} where n is defined as the collapse state. A building in damage state i is assumed to have a capacity of $Sa_{cap}^{i,n}$ to resist collapse. The median $Sa_{cap}^{i,n}$ value is $\widehat{Sa}_{cap}^{i,n}$ and the dispersion (i.e., standard deviation of the logarithm of $Sa_{cap}^{i,n}$) is $\beta_{cap}^{i,n}$. From Chapter 3, P'_{in} is defined in Equation 4.1 under certain simplifying assumptions (see

Cornell et al. (2002)).

$$P'_{in} = P(Sa_{site} > \widehat{Sa}^{i,n}_{cap} | aftershock) \exp(\frac{1}{2} k_a^2 \left[\beta^{i,n}_{cap}\right]^2) \tag{4.1}$$

$P(Sa_{site} > \widehat{Sa}^{i,n}_{cap} | aftershock)$ is the probability of exceeding $\widehat{Sa}^{i,n}_{cap}$ given an aftershock of random magnitude at a random location and it can be obtained from APSHA by integrating over the aftershock-magnitude distribution and the source-to-site distance distribution. Following the notation in Chapter 2, this is numerically equivalent to assuming that $\mu^*(t, T; m_m) = 1$. The term $\exp(\frac{1}{2} k_a^2 \left[\beta^{i,n}_{cap}\right]^2)$ is a factor to account for the dispersion of the $Sa^{i,n}_{cap}$ value, where k_a is the slope of the linearly-approximated log-log aftershock hazard curve. See Cornell et al. (2002) for details on the description of k in the mainshock case.

We define an aftershock which results in the collapse of a building in damage state i as a *fatality event*. The fatality events can be modeled as a nonhomogeneous Poisson process with intensity function $\varpi_i(t; m_m)$ in Equation 4.2.

$$\varpi_i(t; m_m) = \mu(t; m_m) P'_{in}, \ t \in [0, \infty) \tag{4.2}$$

We now wish to assess the threat due to fatality events for an arbitrary occupant of a building in damage state i in the time interval $[\tau, \tau + d\tau]$, where $\tau \in [0, \infty)$ and $d\tau$ is an infinitesimal increment from τ. The probability of a fatality event in $[\tau, \tau + d\tau]$ is approximately equal to $\varpi_i(\tau; m_m) d\tau$. We further define C as the amount of investment into "life-safety" technology at time τ in the future in order to save this occupant from building collapse due to a fatality event at the same time, analogous to Paté (1985). We assume that an investment of C at time τ instantaneously allows the building occupant to be saved. Denoting α as the inflation-adjusted discount rate appropriate for discounting societal investments in life-safety technologies in the future (see Paté-Cornell (1984) for details), we would need to invest a sum of money equal to $Ce^{-\alpha\tau}$ today to save an occupant from a fatality event at time τ. An example of such a "life-safety technology" could be temporary bracing of the building. Thus, the amount of investment society should be prepared to make today to save this arbitrary occupant from a potential fatality event in $[\tau, \tau + d\tau]$ is approximately equal to $Ce^{-\alpha\tau} \varpi_i(\tau; m_m) d\tau$[1]. We shall henceforth refer to C as the cost per life saved. If we are interested in the time interval $[t_d, \infty)$, we define

[1] In some circumstances, C might be considered a random variable, in which case, C could be replaced here by its expectation, $E(C)$.

$\widetilde{\varpi}_i(t, t_d; m_m)$ using Equation 4.3.

$$\widetilde{\varpi}_i(t, t_d; m_m) = \left\{ \begin{matrix} \varpi_i(t; m_m),\ t \in [t_d, \infty) \\ 0,\ t \notin [t_d, \infty) \end{matrix} \right\} \tag{4.3}$$

We define $\widetilde{\mu}(t, t_d; m_m)$ in a similar manner using Equation 4.4.

$$\widetilde{\mu}(t, t_d; m_m) = \left\{ \begin{matrix} \mu(t; m_m),\ t \in [t_d, \infty) \\ 0,\ t \notin [t_d, \infty) \end{matrix} \right\} \tag{4.4}$$

Thus, the investment society should make today to save this occupant due to a potential fatality event in $[t_d, \infty)$ is equal to $\int_0^\infty Ce^{-\alpha\tau}\widetilde{\varpi}_i(\tau, t_d; m_m)d\tau$.

t_d (measured from the mainshock) refers to the date at which a tagging decision is being made about the building. Therefore, t_d is the date forward from which we wish to assess the remaining life-safety threat that an occupant is exposed to. t_d includes day one after the mainshock but it may also refer to a later date when there might be better information about the damage state of the building (for example, based on better inspection and/or more sophisticated engineering analysis) to facilitate better-informed building-tagging decisions (or revisions of previous building-tagging decisions). These decisions will be based on the assessment of the remaining threat to an occupant in the building. This issue will be discussed in more details in later sections.

For a building in damage state i, we want to obtain $ECR^i_{\text{col}}(t_d; m_m)$, a constant, time-independent collapse rate from time zero to infinity which is "equivalent" to the time-dependent rate of fatality events $\widetilde{\varpi}_i(t, t_d; m_m)$. We first define "equivalence" to mean that the expected investment into life-safety technologies for saving an arbitrary building occupant in the future is the same for both cases. This definition of equivalence is based on the consideration of social equity where a building occupant in both scenarios is entitled to the same amount of investment into such technologies. Similar to the previous time-dependent case, the probability of an "equivalent" fatality event in $[\tau, \tau + d\tau]$, $\tau \in [0, \infty)$, is approximately equal to $ECR^i_{\text{col}}(t_d; m_m)d\tau$. Thus, the expected amount of investment society should make today to save this occupant due to potential equivalent fatality events in $[0, \infty)$ is equal to $\int_0^\infty Ce^{-\alpha\tau}ECR^i_{\text{col}}(t_d; m_m)d\tau$ or $\frac{[C]\left[ECR^i_{\text{col}}(t_d; m_m)\right]}{\alpha}$.

Thus, equating the expected investment into life-safety technologies for both cases, we

obtain Equation 4.5.

$$\frac{[C]\left[ECR^{i}_{\text{col}}(t_d; m_m)\right]}{\alpha} = \int_0^{\infty} Ce^{-\alpha\tau}\widetilde{\varpi}_i(\tau, t_d; m_m)d\tau \tag{4.5}$$

Notice that C cancels out from both sides of the equation such that we obtain the definition of $ECR^{i}_{\text{col}}(t_d; m_m)$ in Equation 4.6 as being independent of the value of C which has simply played a passing role in defining equivalence.

$$ECR^{i}_{\text{col}}(t_d; m_m) = \alpha \int_0^{\infty} e^{-\alpha\tau}\widetilde{\varpi}_i(\tau, t_d; m_m)d\tau \tag{4.6}$$

The social discount rate, α, remains however. It plays a crucial role as its value implies that the annual equivalent constant collapse rate, $ECR^{i}_{\text{col}}(t_d; m_m)$, is only a few percent of the expected total number of collapse in a given time interval of interest. Equation 4.6 can be approximated as Equation 4.7 because for typical parameter values, it is found that $\widetilde{\varpi}_i(\tau, t_d; m_m)$ decreases to zero rapidly relative to $e^{-\alpha\tau}$ for increasing values of τ.

$$ECR^{i}_{\text{col}}(t_d; m_m) \approx \alpha \int_0^{\infty} \widetilde{\varpi}_i(\tau, t_d; m_m)d\tau \tag{4.7}$$

Thus, $ECR^{i}_{\text{col}}(t_d; m_m)$ can be easily estimated by computing the integral in Equation 4.7. This integral is simply the expected number of fatality events in the time interval $[t_d, \infty)$ which can be computed by evaluating the area under the mean instantaneous fatality event rate curve from t_d to ∞ multiplied by the inflation-adjusted discount rate α. Note that $\widetilde{\varpi}_i(\tau, t_d; m_m)$ can potentially be defined to include mainshock hazard from other existing faults and the residual mainshock hazard from the same fault that has ruptured, but for simplicity, only the aftershock hazard (which is significantly higher as compared to mainshock hazard) is considered in this Chapter.

Alternatively, substituting Equations 4.1 and 4.4 into Equation 4.7, we obtain Equation 4.8.

$$ECR^{i}_{\text{col}}(t_d; m_m) \approx \alpha \int_0^{\infty} \widetilde{\mu}(\tau, t_d; m_m)P(Sa_{site} > \widehat{Sa}^{i,n}_{cap}|aftershock)\exp(\frac{1}{2}k_a^2\left[\beta^{i,n}_{cap}\right]^2)d\tau \tag{4.8}$$

We define $H_a^{t_d}(y; m_m)$ using Equation 4.9 which represents the "equivalent constant" aftershock rate of exceeding a Sa_{site} value of y in $[t_d, \infty)$.

$$H_a^{t_d}(y; m_m) \triangleq \alpha \int_0^{\infty} \widetilde{\mu}(\tau, t_d; m_m) P(Sa_{site} > y | aftershock) d\tau \tag{4.9}$$

Thus, Equation 4.7 can also be written as Equation 4.10.

$$ECR_{\text{col}}^{i}(t_d; m_m) \approx H_a^{t_d}(\widehat{Sa}_{cap}^{i,n}; m_m) \exp(\frac{1}{2} k_a^2 \left[\beta_{cap}^{i,n}\right]^2) \tag{4.10}$$

Thus, as described above, we have transformed the time-varying rate into an equivalent constant collapse rate, $ECR_{\text{col}}^{i}(t_d; m_m)$. Note that $ECR_{\text{col}}^{i}(t_d; m_m)$ is dependent on t_d, which has been previously defined to be the time at which the tagging decision (or revision of a previous tagging decision) is made. Note also that the lower limit of integration of $H_a^{t_d}(\widehat{Sa}_{cap}^{i,n}; m_m)$ is zero and corresponds to a high instantaneous daily aftershock rate which can potentially be an artifact of the fit of the functional form described in Chapter 2 to existing aftershock data; in subsequent sections, we will use a lower limit of integration of one day instead. While this ECR concept has been introduced here to address the aftershock problem, it is believed that it represents a potential solution to a wider class of safety problems where decisions involving time-varying life threats are involved.

4.3 Proposed Building Tagging Methodology

For a building in damage state DS, the equivalent constant collapse rate $ECR_{\text{col}}^{DS}(t_d; m_m)$ developed in the previous section is assumed to be proportional to the fatality risk to an arbitrary occupant in the damaged building, permitting life-safety decisions to be made based on comparative collapse rates even though the value of the proportionality constant is not known with precision[2]. On the basis of life-safety, given m_m and for a building in damage state DS, we will next compare the aftershock $ECR_{\text{col}}^{DS}(t_d; m_m)$ to existing tolerable mainshock collapse rates to determine if the safety criteria have been satisfied. This will form the basis of our proposed building tagging methodology.

[2]A value of about 10% has been used in earthquake loss assessments such as the HAZUS program (see FEMA (1999)) .

Given the mainshock magnitude, m_m, the location of the building, the mainshock rupture zone and the degree of damage of the building in terms of $\widehat{Sa}_{cap}^{i,n}$ and $\beta_{cap}^{i,n}$, we have above quantified the $ECR_{\text{col}}^{DS}(t_d; m_m)$ of the damaged building as a function of t_d. An occupant in a damaged building will be exposed to a time-varying collapse rate, and thus, a time-varying fatality risk. On the implicit basis of comparable life-safety, we propose to compare the equivalent constant aftershock collapse rate, $ECR_{\text{col}}^{DS}(t_d; m_m)$, to a specified tolerable collapse rate to determine the appropriate tag for the damaged building. Depending on when the tagging decision is to be made, the appropriate tag for the building may improve with an increase in the elapsed time from the mainshock because $ECR_{\text{col}}^{DS}(t_d; m_m)$ will decay as t_d increases. The possibility of considering changes of building tags arises because of this reduction of the aftershock hazard with increasing elapsed time from the mainshock.

As discussed earlier, the degree of damage of the building may be evaluated to different degrees of "accuracy" at different times. For example, shortly after the mainshock, quick visual inspection provides us with information about the damage state with high degrees of uncertainty as indicated by large $\beta_{cap}^{i,n}$ values. Better inspection (for example, inspection of the connections in a SMRF building; see Chapter 6) and better engineering analysis (for example, nonlinear time history analysis) can provide us with more information about the damage state of the building with different $\widehat{Sa}_{cap}^{i,n}$ and potentially smaller $\beta_{cap}^{i,n}$ values. This new information would provide one with an opportunity to re-assess the remaining threat to an occupant in the damaged building and to re-make the building tagging decision based on more accurate information about the damage sustained by the building and its ability to withstand future aftershocks.

We propose three possible tags for buildings after the earthquake, similar to Gallagher et al. (1999). When a building is green-tagged, all occupants may enter the building. When a building is yellow-tagged, only emergency workers may enter the building for search-and-rescue missions, or to restore operations in critical facilities such as power production and distribution facilities. Such emergency workers need to be informed of the increased risk that they face when they volunteer to perform their tasks in damaged buildings, and they also need to be appropriately compensated for the increased risk that they face. When a building is red-tagged, neither normal occupants nor emergency workers may be in the damaged building for extended periods of time. These tagging designations are analogous but not equivalent to FEMA (2000).

4.4 Tolerable Collapse Rate for Each Building Tag

We need to establish the range of tolerable collapse rates for each of the three building tags. The tolerable collapse rate for new, intact buildings designed for mainshocks (P_0) can be calculated using Equation 4.11.

$$P_0 = H_m(\widehat{Sa}_{cap}^{1,n}) \exp(\frac{1}{2} k_m^2 \left[\beta_{cap}^{1,n}\right]^2) \tag{4.11}$$

The superscripts 1 and n represent the intact and collapse state, respectively. $H_m(\widehat{Sa}_{cap}^{1,n})$ is the mainshock hazard curve evaluated at the building median capacity, $\widehat{Sa}_{cap}^{1,n}$. $\beta_{cap}^{i,n}$ is the standard deviation of the logarithm of $Sa_{cap}^{i,n}$. k_m is the slope of the linearly-approximated log-log mainshock hazard curve. We propose to specify the tolerable collapse rates for the various tagging states in terms of P_0. This number is explicit in some structural guidelines and only implicit in others. Given the discussion in Leyendecker et al. (2000), for new buildings designed to the 2000 International Building Code (IBC), the design ground motion level is typically 2% per 50 years (or 0.0004 per annum), i.e., one can use $H_m(\widehat{Sa}_{cap}^{1,n}) = 0.0004/\text{yr}$ to calculate P_0.

It is proposed that the tolerable collapse rate for existing buildings in the post-mainshock situation may be set higher than P_0 for new buildings designed for mainshocks. The proposed criteria take the following form. $\alpha_1 P_0$ represents the tolerable (equivalent) collapse rate, or $ECR_{\text{col}}^{DS}(t_d; m_m)$, for existing buildings in the post-earthquake environment. For collapse rates greater than $\alpha_1 P_0$, entry by normal occupants is not allowed. The level α_1 should be set according to the function of the building. For example, for critical community recovery facilities like water and power distribution facilities, etc., it is important for operations to continue uninterrupted. We propose a comparatively high level of α_1 for such facilities. For non-safety-critical commercial and office buildings, the level of α_1 is set to be lower than that of critical facilities. For residential buildings which are needed for shelter, the level of α_1 is set to be between that of critical facilities and commercial buildings.

We also need to set a maximum tolerable collapse rate of $\alpha_2 P_0$ beyond which entry by all personnel (including normal occupants and emergency workers) is not allowed on the basis of life-safety. For collapse rates between $\alpha_1 P_0$ and $\alpha_2 P_0$, the building will be yellow-tagged. Entry is permitted for informed, compensated and voluntary emergency workers for $ECR_{\text{col}}^{DS}(t_d; m_m)$ values in this range. Again, the relative level of α_2 should be set according to the function of the building. The building tags and their corresponding ranges of collapse

rates are shown in Figure 4.1.

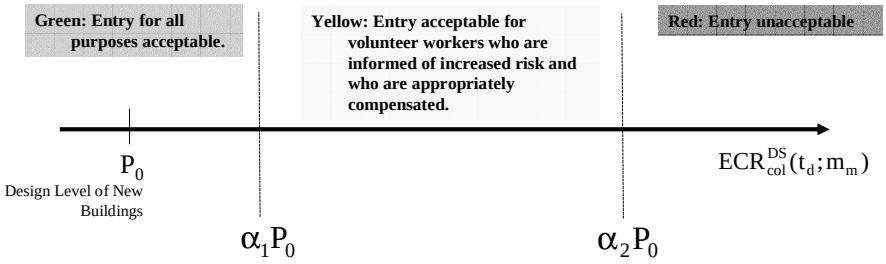

Figure 4.1: Buildings tags and their corresponding allowable collapse rates.

Representative values of α_1 and α_2 might be 5 and 10 for critical community recovery facilities, 3 and 6 for commercial and office buildings and 4 and 8 for residential buildings. The lowest α_1 value, 3, is based on the current practice of permitting existing buildings to have P_0 values of at least twice that of new buildings (e.g., DOE (2002)), plus the unusual, potentially widespread post-event circumstances.

4.5 Primary Building Tagging Basis

We now propose a tagging methodology based on quantifying the $ECR_{\text{col}}^{DS}(t_d; m_m)$ of the damaged building, first ignoring possible repair or upgrade to the building. We will consider a revised tagging methodology for buildings that might have been repaired or upgraded after the mainshock in a later section.

In order to tag the building, we first evaluate the $ECR_{\text{col}}^{DS}(t_d; m_m)$ of the building as a function of t_d. Specifically, we represent $ECR_{\text{col}}^{DS}(1; m_m)$ (one day after the mainshock) as γP_0. We compare the value of γ to the values of α_1 and α_2 for the building. If γ is less than α_1, then the building is green-tagged one day after the mainshock and occupancy of the building does not need to be restricted. If γ is less than α_2 but more than α_1, then the building is yellow-tagged and only entry by informed, compensated and voluntary emergency workers is allowed. If γ is greater than α_2, then the building will be red-tagged after the mainshock and complete evacuation of the building is necessary on the basis of life-safety.

If γ is greater than α_2 such that the building is red-tagged after the mainshock (see Figure 4.2), the tag will remain red until the $ECR_{\text{col}}^{DS}(t_d; m_m)$ decreases to a level equal

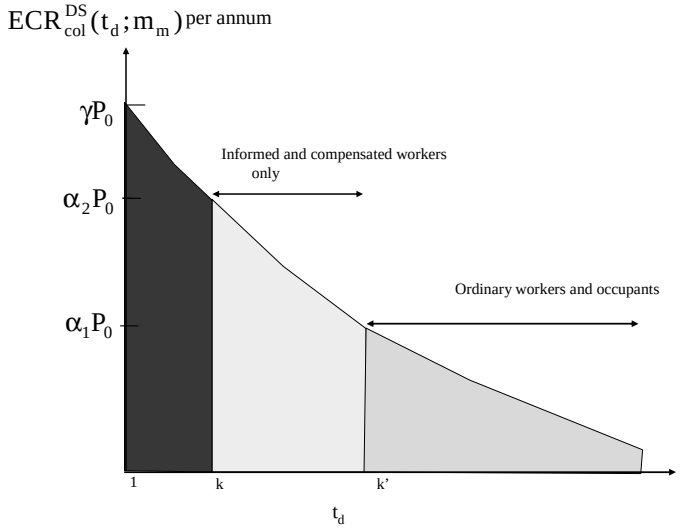

Figure 4.2: $ECR^{DS}_{\text{col}}(t_d; m_m)$ of a damaged building. The building should be tagged red from day 1 to day k, yellow between days k and k' and green from day k' on.

to $\alpha_2 P_0$ on the k^{th} day. This is when the building tag changes to yellow corresponding to an $ECR^{DS}_{\text{col}}(t_d; m_m)$ which will be less than $\alpha_2 P_0$ from that day on. Similarly, when the $ECR^{DS}_{\text{col}}(t_d; m_m)$ decreases to a level equal to $\alpha_1 P_0$ on the k'^{th} day, the building tag changes to green. The decreasing nature of $ECR^{DS}_{\text{col}}(t_d; m_m)$ ensures that the building tag will change from red to yellow to green with increasing elapsed days from the mainshock.

4.6 Special Tagging Cases: Emergency Workers

There might also be special situations where it is necessary to allow emergency workers to enter a damaged building to perform critical tasks even when the building is red-tagged. For example, it is important to ensure continued operations at power distribution networks in the post-earthquake environment, and hence it might be necessary to allow emergency workers to enter such facilities to perform short-term critical repairs or periodic monitoring or switching. In some other facilities, it might also be necessary to allow emergency workers to enter red-tagged buildings for search-and-rescue missions or collapse-prevention shoring activities.

We propose a revised tagging methodology to allow entry into buildings that have been red-tagged by providing a controlled working environment for emergency workers based on

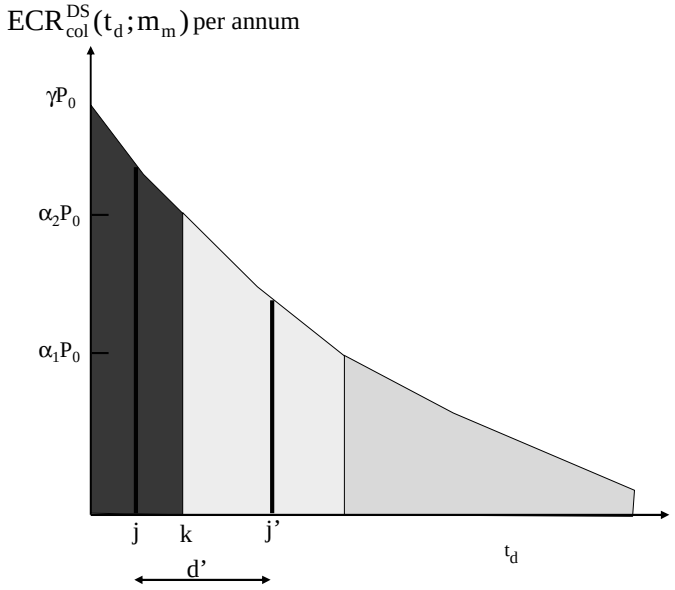

Figure 4.3: Time-varying $ECR^{DS}_{\text{col}}(t_d; m_m)$ of a damaged building. Emergency workers can enter the damaged building on day j for a total duration of d' days if their working environment is properly controlled.

the total life-safety threat that they face by entering such damaged buildings with a high $ECR^{DS}_{\text{col}}(t_d; m_m)$. Again, this methodology ignores for now possible repair or upgrade to the building after the mainshock.

Consider the $ECR^{DS}_{\text{col}}(t_d; m_m)$ for a critical facility in damage state DS as shown in Figure 4.3. The building has been red-tagged immediately after the mainshock because γ is greater than α_2. It is necessary to allow the entry of emergency workers shortly after the mainshock to perform some critical repairs which cannot wait till the k^{th} day when the building tag will change to yellow. To allow such operations, it is proposed here that these emergency workers can enter the building earlier at time j if their work schedule and exposure are properly controlled. This control requires both limiting their duration, d', in the damaged building and their subsequent rotation after departure to a "safer" environment (SE). The duration d' can be determined for an arbitrary start time j by ensuring Equation 4.12.

$$ECR^{DS}_{\text{col}}(j; m_m) - ECR^{DS}_{\text{col}}(j + d'; m_m) + ECR^{SE}_{\text{col}}(j'; m_m) \leq \alpha_2 P_0 \tag{4.12}$$

The first two terms reflect the risk accumulated with the interval in the red-tagged building and the third term reflects the time in the safer environment. The "safer" environment can be achieved by housing and/or employing the workers in a building with demonstrated higher capacity or by moving the workers to a location which is further away from the aftershock zone where the aftershock hazard is lower, or a combination of both. The $ECR_{\text{col}}^{SE}(t_d; m_m)$ of the "safer" environment needs to be evaluated based on the median assessed Sa_{cap} of the new building that they are relocated to, and/or on a APSHA which takes into consideration the location of the second building with respect to the mainshock rupture zone. If further occupancy is needed in the mainshock-damaged building, a new group of controlled workers can be engaged to begin on day j'. This new group of workers should have been controlled – in a "safer" environment – since day j.

This tagging proposal is, in effect, a limited cumulative risk concept where the employer must evaluate and control the cumulative threat to a worker due to occupancy in a damaged building and in a "safer" environment. See Cornell and Bandyopadhyay (1996) for an analogous proposal in the field of nuclear power plant safety. This scheme has been proposed to the U.S. Nuclear Regulatory Committee by the nuclear industry to rationalize the seismic assessment of temporary shoring during maintenance operations. See Amin et al. (1999) and EPRI (1998).

4.7 Tagging Basis with Repair

We next propose a building tagging criterion where we allow for possible upgrade or repair to the building after the mainshock. We show in Figure 4.4 the $ECR_{\text{col}}(t_d; m_m)$ curves for the damaged building (damage state DS) and the repaired building (repaired state is denoted as R). Note that the $ECR_{\text{col}}^{R}(t_d; m_m)$ curve for the repaired building could be either above or below that of the corresponding curve for the new intact building. Again, based on the concept of the controlled working environment, emergency repair workers can enter the building from time j for d' days when the building is red-tagged, where the duration d' can be determined based on Equation 4.12. If repair is completed on day k (after which one should consider the $ECR_{\text{col}}^{R}(t_d; m_m)$ curve for the repaired building), normal occupants can enter the building only if Equation 4.13 is true. This case is shown in Figure 4.4.

$$ECR_{\text{col}}^{R}(k; m_m) \leq \alpha_1 P_0 \tag{4.13}$$

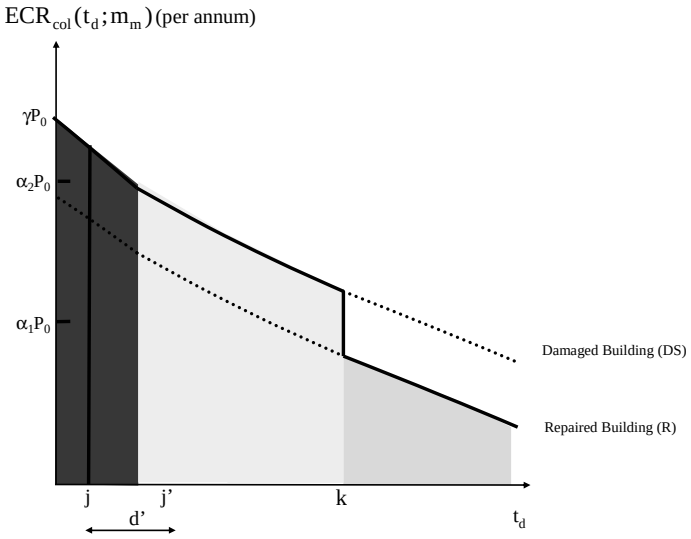

Figure 4.4: Tagging of a damaged building with possible repair or upgrade to the building.

If not, normal occupants can enter the repaired building only after the $ECR^{R}_{\text{col}}(t_d; m_m)$ for the repaired building has decreased to $\alpha_1 P_0$.

Here, we have considered a case where emergency workers are controlled and where we have further considered the possibility of repair. The proposed methodology allows us to take advantage of our knowledge of the time-varying aftershock hazard at the site and the damage state of the building to provide an appropriate tag for the mainshock-damaged building based on life-safety considerations.

4.8 Simplified Building Tagging Basis

So far, we have developed a methodology for tagging mainshock-damaged buildings based on APSHA and by comparing $ECR^{DS}_{\text{col}}(t_d; m_m)$ to P_0. If we assume that $k_a \approx k_m$ and $\beta^{1,n}_{cap} \approx \beta^{i,n}_{cap}$, then the exponential terms in Equations 4.10 and 4.11 cancel out such that we can simplify the building tagging methodology by computing the ratio of the equivalent constant aftershock ground motion hazard at $\widehat{Sa}^{DS,n}_{cap}$, $H^{1}_{a}(\widehat{Sa}^{DS,n}_{cap}; m_m)$, to the mainshock hazard at $\widehat{Sa}^{1,n}_{cap}$, $H_m(\widehat{Sa}^{1,n}_{cap})$, to determine the value of γ one day after the mainshock. Then, the building tagging procedures based on comparing γ to α_1 and α_2 follows. Alternatively, we can also compare $H^{t_d}_{a}(\widehat{Sa}^{DS,n}_{cap}; m_m)$ to $\alpha_1 H_m(\widehat{Sa}^{1,n}_{cap})$ and $\alpha_2 H_m(\widehat{Sa}^{1,n}_{cap})$ to determine the

appropriate tag of the damaged building. This forms the basis of our simplified building tagging procedure.

Also, we have shown in Chapter 2 that for cases where a single nearby fault (segment) is the dominant source of a damaging mainshock ground motion (such as the San Francisco Bay area), the aftershock hazard is approximately a fixed multiple of the mainshock hazard for all ground motion levels, all values of T_0 and all site locations. We could thus make use of the aftershock base case results in Chapter 2 to obtain a rapid but approximate estimate of the ratio of $H_a^{t_d}(\widehat{Sa}_{cap}^{DS,n}; m_m)$ to $H_m(\widehat{Sa}_{cap}^{1,n})$ for other values of m_m, t and T to tag buildings at nearby site locations under different mainshock scenarios. In order to do this, we first need to convert the ratio of aftershock hazard to mainshock hazard in Chapter 2 to a ratio of an "equivalent constant" aftershock hazard to mainshock hazard by multiplying by α. We can adjust for other values of m_m, t and T using the procedures described in Chapter 2. The proposed building tagging procedure then follows based on the damage state DS and the value of $\widehat{Sa}_{cap}^{DS,n}$ of the building.

4.9 Example

To illustrate our proposed methodology, we consider the three-story SMRF building located at the Stanford, California site as in Chapters 2 and 3. Following the example in Chapter 2, we assume that a mainshock of magnitude 7.0 has occurred on the San Andreas Fault which has ruptured the neighboring Mid-Peninsula Segment. We assume that aftershocks can occur anywhere on the mainshock rupture zone with equal likelihood. We use $\alpha = 5\%$ in this example.

The instantaneous daily aftershock rates are shown in Figure 4.5 as a function of elapsed time from the mainshock. Here, we consider aftershocks with magnitudes between 5.0 and 7.0, the mainshock magnitude. Note that, for example, the expected total number of aftershocks starting 10 days after the mainshock over a time interval of infinite length is equal to seven, i.e., the shaded area shown below in Figure 4.5.

We then perform an APSHA for Sa with $T_0 = 0.75$s, close to the structural period of our three-story SMRF building of 0.73s. We obtain the probability of exceeding Sa at the Stanford site 10 km from the ruptured segment given an aftershock of random magnitude at a random location in the aftershock zone. The results are shown in Figure 4.6. Note that this function times the aftershock rate in Figure 4.5 gives the APSHA ground motion

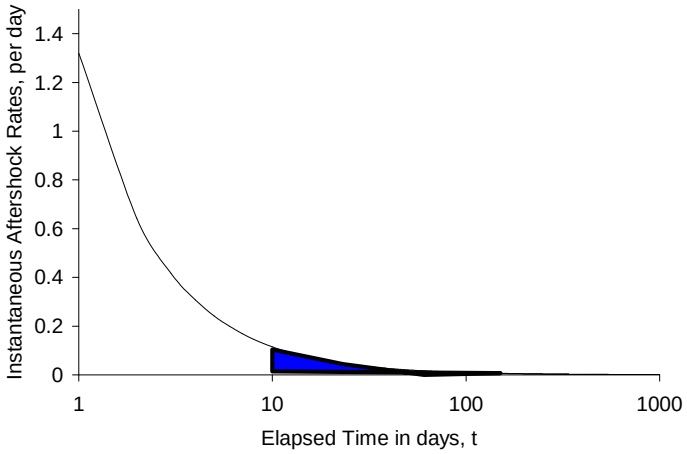

Figure 4.5: Numerical example: Instantaneous time-varying daily aftershock rate as a function of elapsed time from the mainshock of magnitude 7.0.

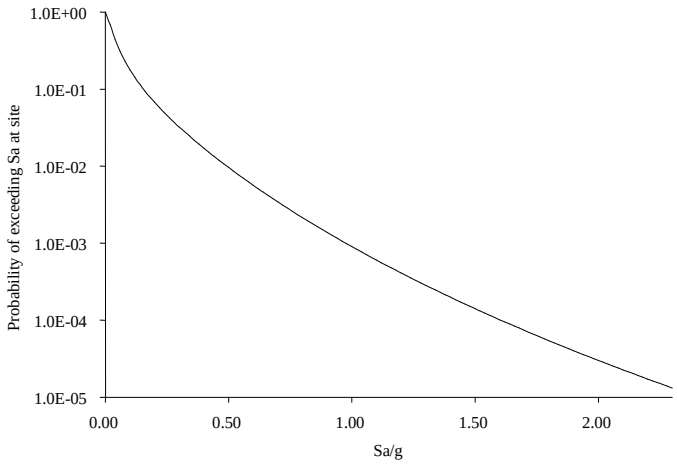

Figure 4.6: Numerical example: Probability of exceeding Sa (with $T_0 = 0.75$s) at the Stanford site given an aftershock of random magnitude at a random location relative to the site.

hazard results.

Here, we shall apply the building tagging methodology to the damaged building. Using Equation 4.10, we evaluate the $ECR^i_{\text{col}}(t_d; m_m)$ of the building given different initial post-mainshock damage states as a function of t_d. We consider the same three damage states for the building as in Chapter 3. The median assessed Sa_{cap} to bring a building in $DS1$, $DS2$

and $DS3$ to collapse in an aftershock is 1.4g, 1.2g and 1.1g, respectively, based on a separate study carried out in Maffei et al. (2002). We use the values of $\widehat{Sa}_{cap}^{1,n}$ and $\beta_{cap}^{1,n}$ obtained in Maffei et al. (2002). The resulting annual $ECR_{\text{col}}^{DS}(t_d; m_m)$ for the three damage states are shown in Figure 4.7. One can see that in the first 10 days after the mainshock, the

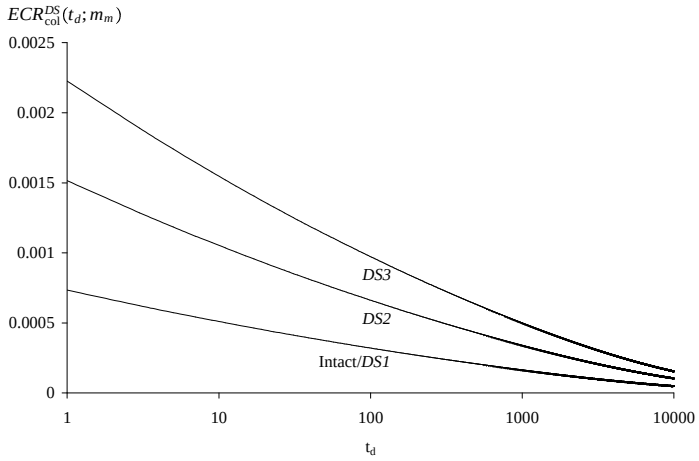

Figure 4.7: Numerical example: $ECR_{\text{col}}^{DS}(t_d; m_m)$ for three-story SMRF progressing to collapse given different post-mainshock damage states.

$ECR_{\text{col}}^{DS}(t_d; m_m)$ values decrease by about 30%. The $ECR_{\text{col}}^{DS}(t_d; m_m)$ values demonstrate a much slower rate of decay as compared to the instantaneous daily aftershock rates in Figure 4.5 which decrease by about 90% in the same duration.

We assume that the three-story SMRF building is a residential building with $\alpha_1 = 3$ and $\alpha_2 = 5$. Consider the case when the building is in $DS3$ after the mainshock. We use $P_0 = 0.0004$/year (corresponding to 2% in 50 years) and assuming no repair or upgrade to the building, we can compute γ one day after the mainshock ($ECR_{\text{col}}^{DS3}(1; m_m)$ normalized by P_0) to be equal to 5.56. This is greater than the α_2 value of 5. Thus, the building is red-tagged immediately after the mainshock. We need to wait for three days before the value of $ECR_{\text{col}}^{DS3}(t_d; m_m)$ reduces to $\alpha_2 P_0$ and the building becomes yellow-tagged. The building only becomes green-tagged 40 days after the mainshock. See Figure 4.8.

We next consider a case where we provide a controlled working environment for volunteer emergency workers so that they can enter the damaged building when it is red-tagged. We assume that the emergency workers will be relocated to a new intact building at the same site with $ECR_{\text{col}}^{Intact}(t_d; m_m)$ as shown in Figure 4.7 after completion of repair. We also

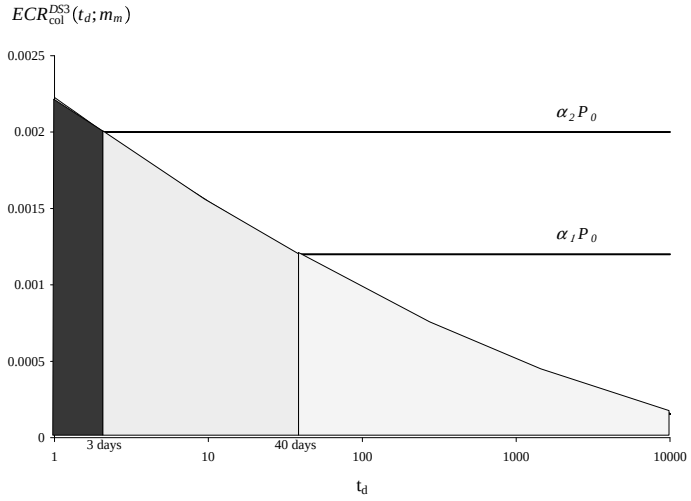

Figure 4.8: Numerical example: Tagging of damaged building in $DS3$ assuming no repair or upgrade.

assume for illustration that the building repair (e.g., temporary shoring) will be completed in two days. In this case, analogous to Equation 4.12, we compute $ECR_{\text{col}}^{DS3}(1; m_m) - ECR_{\text{col}}^{DS3}(3; m_m)$ and $ECR_{\text{col}}^{Intact}(3; m_m)$. The sum of the two values above is equal to 0.0009/year, less than $\alpha_2 P_0$ which has a value equal to 0.002/year. Hence, the emergency workers can enter the damaged building on day one when the building is red-tagged to complete the repair.

The longest allowable duration d^* for repair can be evaluated by trial and error by ensuring that $ECR_{\text{col}}^{DS3}(1; m_m) - ECR_{\text{col}}^{DS3}(1 + d^*; m_m) + ECR_{\text{col}}^{Intact}(1 + d^*; m_m)$ is less than $\alpha_2 P_0$. Also, the value of $ECR_{\text{col}}^{Intact}(3; m_m)$ is less than $\alpha_1 P_0$. This means that the building will be green-tagged three days after the mainshock if the emergency workers are (hypothetically) able to restore the building to its intact capacity (as represented by the $ECR_{\text{col}}^{Intact}(t_d; m_m)$ plot in Figure 4.7) in two days. This is shown in Figure 4.9.

In addition to the Stanford site, for other buildings at nearby site locations, one can estimate the aftershock ground motion hazard to be approximately 20 times that of the pre-mainshock hazard for $t_d = 7$ days after the mainshock and for a duration of interest, T, equal to 365 days. This conclusion is drawn based on our observation in Chapter 2 and in Section 4.8 of this chapter where we observed that the ratio of aftershock hazard to mainshock hazard at a site where the mainshock hazard is dominated by a single fault or

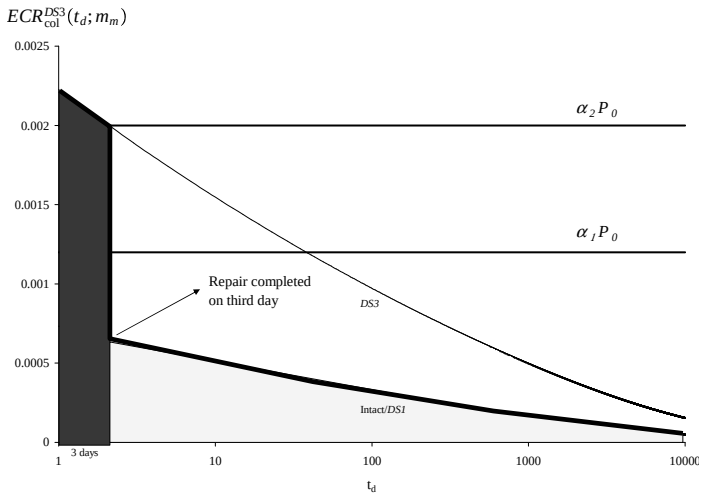

Figure 4.9: Numerical example: Tagging of damaged building in $DS3$ with 3-day repair to intact state capacity.

fault segment is constant for all T_0 and ground motion levels, as well as being insensitive to site locations. To assess γ one day after the mainshock, we need to multiply the factor 20 by α based on Equation 4.9 (to convert to a ratio of "equivalent constant" aftershock hazard to mainshock hazard) and a factor to adjust the base case results from $t_d = 7$ and $T = 365$ to the limits of integration $t_d = 1$ and $T = \infty$ (which is about a factor of 2.3 obtained from Chapter 2). We can also use the method proposed in Chapter 2 to adjust for other values of t_d. Also, if the mainshock magnitude is increased from $m_m = 7.0$ to $m_m = 8.0$, we also need to include a factor of 8.25 obtained from Chapter 2 as well. This proposed simplified methodology is an approximate alternative for rapid building-tagging immediately after the mainshock.

4.10 Conclusion

We propose a tagging methodology for damaged buildings after the mainshock based on individual life-safety considerations. We consider the aftershock hazard at the site in terms of possible future aftershock ground motions. The damage state of the building after the mainshock is also taken into account. The proposed methodology allows for entry into a red-tagged building after the mainshock by introducing the concept of a controlled working

environment for informed/compensated emergency workers. Possible repair or upgrade to the damaged building can also be introduced in the proposed methodology. We also propose a simplified approximate building tagging procedure for buildings in locations where the mainshock hazard is dominated by a single fault or segment. It is our hope that such a methodology will allow better tagging decisions to be made after the mainshock. The procedure proposed here for a given mainshock magnitude and damage state of the building is also used in Bazzurro et al. (2004a) and Bazzurro et al. (2004b) to assess *pre-mainshock* likelihoods of each of the potential future tagging states of the building.

5 Formulation of Future Life-Cycle Financial Losses due to Mainshocks and Aftershocks

In Chapter 4, we proposed a building tagging decision methodology based on quantification of the life-safety threat that an arbitrary occupant is exposed to due to occupancy of a damaged building in the nonhomogeneous aftershock environment. As part of our effort to incorporate the performance of (possibly mainshock-damaged) buildings into post- and pre-mainshock design criteria, besides life-safety considerations, we also need to take into account economic efficiency in terms of minimizing life-cycle financial losses due to earthquakes, including both mainshocks and aftershocks. The objective of this chapter is to develop formal stochastic financial loss estimation models over the lifetime of the building. The initial model is the traditional simplified homogeneous Poisson mainshock process and nonhomogeneous Poisson aftershock process with "immediate" repair of the building to the initial building state, following the discussion in Chapter 1. We then turn to a more general Markov and semi-Markov framework where we consider both Poisson and renewal processes for modeling mainshock occurrences with consideration of various building repair and/or damage progression scenarios. As in the previous chapters, aftershocks will be modeled as a nonhomogeneous Poisson process with random magnitudes which has parameters (mainshock magnitude, m_m, and location) that are conditional on the random mainshock.

The model formulation for the post-earthquake environment begins by focussing on predicting losses *given* (i.e., conditional upon) the occurrence of a mainshock with its ground motion and resulting building damage state. The financial losses include one-time transition costs, or costs from further structural and nonstructural damage to the building due to the

occurrence of an earthquake, and they may also include the costs of evacuation of the occupants of a building. Since a building could be severely damaged after a mainshock to the extent that it is red-tagged or yellow-tagged and closed to further occupancy, the financial losses also include disruption or downtime costs which are financial losses incurred by the owner of the building due to its non-operability or limited functionality. Such downtime and post-mainshock functionality depends on the life safety threat that the damaged building poses subsequent to the mainshock. As mentioned earlier, a building-tagging methodology based on nonstationary aftershock hazard, damaged-building capacity and life-safety decisions has been proposed in Chapter 4.

We will derive the expected (mean) financial losses and the corresponding moment generating functions for both the homogeneous mainshock process as well as the nonhomogeneous aftershock process in the simplified Poisson process model. We will also relax the restrictions of the simpler Poisson model by formulating a method of obtaining the expected financial losses for both the homogeneous mainshock process as well as for the nonhomogeneous aftershock processes embedded in the more general Markov process framework to describe the transitions from one building damage state to another. We also consider a (non-Poissonian) renewal mainshock process in the formulation of expected financial losses where we use an arbitrary inter-arrival time distribution for mainshock occurrences. Lastly, we will also incorporate the random aftershock losses into pre-mainshock financial loss estimation to be used as an input to *pre*-mainshock design analyses.

We consider a building in damage state i which could go to one of n damage states given the occurrence of an earthquake (either mainshock or aftershock). The intact state is typically denoted as damage state 1 and the collapse state is typically denoted as damage state n. A building in damage state i can go to damage state j with probability P'_{ij} given the occurrence of an earthquake (again, either mainshock or aftershock). The method to obtain the values of P'_{ij} given a mainshock or aftershock has been discussed in Chapter 3. Recall $P'_{ij} = 0$ for $i > j$ if we assume no repair operations, and $\sum_j P'_{ij} = 1$. The full transition matrix, $\mathbf{P'}$, is shown in Equation 5.1.

$$\mathbf{P'} = \begin{pmatrix} P'_{11} & P'_{12} & \cdots & P'_{1n} \\ \vdots & P'_{22} & \ddots & \vdots \\ \vdots & \ddots & \ddots & P'_{(n-1)n} \\ 0 & \cdots & \cdots & 1 \end{pmatrix} \tag{5.1}$$

If an earthquake occurs and the building suffers additional damage and enters damage state j, where $j > i$, we assume that there is incurred a (random) transition cost of L_{ij} which is dependent on states i and j. This transition cost can be attributed to financial losses due to further structural and nonstructural damage to the building and perhaps the costs of evacuation of the occupants of a building. While the building remains in damage state i, we assume that it incurs a constant (but random) disruption cost of R_i per unit time due to the downtime and limited functionality of the damaged structure. We further assume $E(L_{ij}) = l_{ij}$ and $E(R_i) = r_i$.

5.1 Poisson Loss Model

We first propose a simplified method to quantify the financial losses by using a Poisson model for earthquakes where the intensity function $\mu(t)$ can either be homogeneous (i.e., $\mu(t) = \mu$, a constant value independent of time for mainshocks) or nonhomogeneous (i.e., $\mu(t; m_m)$ is time-dependent and mainshock-magnitude dependent for aftershocks). For the formulation to follow, we suppress in the notation the dependence of the aftershock intensity function on m_m. Following the notation in Chapter 2, $\mu(t)$ for aftershocks represents the instantaneous daily rate of aftershocks with magnitudes between m_l and m_m at time t following a mainshock of magnitude m_m.

For a building in damage state i, an earthquake which results in the building suffering further damage and going to damage state j, where $j > i$, is considered as a *loss event*. Thus, if the intensity function of earthquakes (either mainshock or aftershock) is denoted by $\mu(t)$, then the loss events for a building in state i can be modeled as a Poisson process with intensity function $\lambda_i(t)$, where:

$$\lambda_i(t) = \mu(t) \sum_{j>i} P'_{ij} = \mu(t)(1 - P'_{ii}) \tag{5.2}$$

In order to quantify the financial losses due to the occurrence of a loss event, the total transition and disruption losses due to downtime of the building need to be taken into consideration and appropriately discounted back to the present value. The disruption loss is highly dependent on the inter-arrival times between events (i.e., either mainshocks or aftershocks) where the inter-arrival time distribution is nonstationary in nature if we consider a nonhomogeneous Poisson process with intensity function $\mu(t)$. For this initial simplified

procedure, we assume that l_{ij} includes an expected disruption loss due to transition to damage state j.

Also, as mentioned in Chapter 1, the simplified Poisson model assumes that the building is immediately "re-built" back to its original damage state after the loss event. This, again, might not be realistic in the aftershock environment where there might be incremental damage to the building due to the occurrences of aftershocks and where there might not be sufficient time for repair back to its original state. Such assumptions will be relaxed in the Markov process framework to follow.

Based on the damage states of the building, given a loss event, we can form a transition matrix $\mathbf{P}$ as defined in Equations 5.3, 5.4 and 5.5.

$$\mathbf{P} = \begin{pmatrix} 0 & P_{12} & \cdots & P_{1n} \\ \vdots & 0 & \ddots & \vdots \\ \vdots & \ddots & 0 & P_{(n-1)n} \\ 0 & \cdots & \cdots & 0 \end{pmatrix} \tag{5.3}$$

$$P_{ij} = 0, \ i \geq j \tag{5.4}$$

$$P_{ij} = \frac{\mu(t) P'_{ij}}{\lambda_i(t)} = \frac{P'_{ij}}{1 - P'_{ii}}, \ i < j \tag{5.5}$$

$\mathbf{P}$ is a stationary transition matrix, i.e., it does not change with time. The values of the lower triangular portion and the diagonals of the matrix $\mathbf{P}$ are all equal to zero because we are only considering loss events, i.e., earthquakes that result in transitions to more severe damage states, with no repair operations.

We denote $L(i)$ as the random variable of the financial losses given the occurrence of a loss event for a building in damage state i. We obtain the first two moments of $L(i)$ in Equations 5.6 and 5.7.

$$E\left[L(i)\right] = \sum_{j>i} P_{ij} l_{ij} \tag{5.6}$$

$$E\left[L^2(i)\right] = \sum_{j>i} P_{ij} l_{ij}^2 \tag{5.7}$$

Higher moments can be obtained in a similar manner such that we can characterize the full probability distribution of $L(i)$ by moment-matching to a specified probability distribution (an example of which could be the lognormal distribution).

In the formulation to follow, we consider the Poisson process of loss events with intensity function $\lambda_i(t)$ given in Equation 5.2 for a building in damage state i. We suppress the dependence on the original damage state of the building (i) for $L(i)$ such that we represent $L(i)$ as L. We use the notations in Table 5.1 for a building originally in damage state i. We consider financial losses for both mainshocks (i.e., homogeneous Poisson process) and aftershocks (i.e., nonhomogeneous Poisson process). A formulation for expected total losses assuming a renewal process for mainshocks will be discussed in a later section.

Table 5.1: Notations for Poisson model for a building in initial state i; Capital letters denote random variables

t = Time
$t_{\max}$ = Total time interval of interest, possibly life span of building
$TL_i(t_{\max})$ = Total loss in time interval $[0, t_{\max}]$
$N_i(t_{\max})$ = Number of loss events in $[0, t_{\max}]$ with Poisson intensity function $\lambda_i(t)$
L = Financial losses given occurrence of loss event
T_k = Arrival time of the kth loss event
α = Discount rate per unit time

5.1.1 Discounted Losses due to Homogeneous Poisson Mainshock Process

Expected Total Losses

First, for a building in damage state i, we start by deriving the expected total discounted financial losses for a homogeneous Poisson mainshock process $TL_i(t_{\max})$ in $[0, t_{\max}]$. The loss events are Poisson with mean rate equal to λ_i which is independent of time. The expected financial losses are important for the decision-making procedures to be discussed in Chapter 6. Here, we consider a general model where the building is in damage state i before the mainshock, where i is typically taken to be the intact state. Such a formulation will be useful in the post-mainshock scenario where the building can be in an arbitrary damage state i after the mainshock. Again, this model assumes that the building is immediately "re-built" back to damage state i after the loss event.

$TL_i(t_{\max})$ can be expressed by Equation 5.8, where L_k is the financial losses due to the k^{th} loss event occurring at T_k and appropriately discounted back to the present value by $e^{-\alpha T_k}$. $N_i(t_{\max})$ is the random number of loss events in $[0, t_{\max}]$ for a building in damage

state i.

$$TL_i(t_{\max}) = \sum_{k=1}^{N_i(t_{\max})} L_k e^{-\alpha T_k} \tag{5.8}$$

Here, $N_i(t_{\max})$ is a homogeneous Poisson process with $E\left[N_i(t_{\max})\right] = \lambda_i t_{\max}$. Given $N_i(t_{\max}) = n$, the T_k have uniform distributions in $[0, t_{\max}]$ and are independent and identically distributed (henceforth abbreviated as i.i.d.) such that all T_k have the same distribution as a common random variable T, denoted as $T_k \stackrel{D}{=} T$. See Ross (2000) for further details. Assuming L_k and T_k are independent and $L_k \stackrel{D}{=} L$, we have:

$$\begin{aligned} & E\left[TL_i(t_{\max}) | N_i(t_{\max}) = n\right] = E\left[\sum_{k=1}^{n} L_k e^{-\alpha T_k}\right] = \sum_{k=1}^{n} E\left[L_k e^{-\alpha T_k}\right] \\ = & \sum_{k=1}^{n} E\left[L_k\right] E\left[e^{-\alpha T_k}\right] = E\left[L\right] \sum_{k=1}^{n} \int_0^{t_{\max}} \frac{1}{t_{\max}} e^{-\alpha t} dt \\ = & E\left[L\right] \frac{n}{t_{\max}} \int_0^{t_{\max}} e^{-\alpha t} dt = \frac{nE\left[L\right]}{\alpha t_{\max}} \left[1 - e^{-\alpha t_{\max}}\right] \end{aligned} \tag{5.9}$$

The interchange of expectation and summation is allowed since $N_i(t_{\max}) < \infty$. Since $E\left[N_i(t_{\max})\right] = \lambda_i t_{\max}$, we have:

$$E\left[TL_i(t_{\max})\right] = \frac{E\left[N_i(t_{\max})\right] E\left[L\right]}{\alpha t_{\max}} \left[1 - e^{-\alpha t_{\max}}\right] = \frac{\lambda_i E\left[L\right]}{\alpha} \left[1 - e^{-\alpha t_{\max}}\right] \tag{5.10}$$

For small values of $\alpha t_{\max}$, Equation 5.10 can be approximated as $\frac{\lambda_i E[L]}{\alpha} \left[1 - (1 - \alpha t_{\max})\right] \approx \lambda_i t_{\max} E\left[L\right]$. Thus, $E\left[TL_i(t_{\max})\right]$ is directly proportional to $t_{\max}$ for small values of $\alpha t_{\max}$.

As $t_{\max} \to \infty$, we have:

$$E\left[TL_i(t_{\max})\right] = \frac{\lambda_i E\left[L\right]}{\alpha} \tag{5.11}$$

As discussed in Chapter 1, Equations 5.10 and 5.11 have been previously derived by Wen and Kang (2001) and Rosenblueth (1976), respectively.

Moment Generating Function of Total Losses

Using the same approach, we can also obtain the moment generating function of $TL_i(t_{\max})$. The moment-generating function uniquely determines the probability distribution of the

random variable. See Ross (2000) for details.

$$
\begin{aligned}
& M_{TL_i(t_{\max})}(\zeta) = E\left[e^{\varsigma TL_i(t_{\max})}\right] \\
= \; & E_{N_i(t_{\max})}\left(E_{L_k,T_k,1\leqslant k\leqslant N_i(t_{\max})=n}\left[\exp\left(\varsigma \sum_{k=1}^{N_i(t_{\max})=n} L_k e^{-\alpha T_k} | N_i(t_{\max})=n\right)\right]\right) \\
= \; & E_{N_i(t_{\max})}\left(E_{L_k,T_k,1\leqslant k\leqslant n}\left[\exp\left(\varsigma \sum_{k=1}^{n} L_k e^{-\alpha T_k}\right)\right]\right) \\
= \; & E_{N_i(t_{\max})}\left(\left[E_{L,T}\left[\exp\left(\varsigma L e^{-\alpha T}\right)\right]\right]^n\right) \\
= \; & \int_0^{\infty} e^{-\lambda_i t_{\max}} \frac{(\lambda_i t_{\max})^n}{n!}\left[E_L \int_0^{t_{\max}} \frac{1}{t_{\max}} \exp\left(\varsigma L e^{-\alpha t}\right) dt\right]^n dn \\
= \; & e^{-\lambda_i t_{\max}} \int_0^{\infty} \frac{1}{n!}\left[\lambda_i t_{\max} E_L \int_0^{t_{\max}} \frac{1}{t_{\max}} \exp\left(\varsigma L e^{-\alpha t}\right) dt\right]^n dn \\
= \; & e^{-\lambda_i t_{\max}} \exp\left(\lambda_i E_L \int_0^{t_{\max}} \exp\left(\varsigma L e^{-\alpha t}\right) dt\right) \\
= \; & \exp\left(-\lambda_i t_{\max} + \lambda_i \int_0^{t_{\max}} E_L\left[\exp\left(\varsigma L e^{-\alpha t}\right) dt\right]\right) \qquad (5.12)
\end{aligned}
$$

The moment generating function of $TL_i(t_{\max})$ has also been derived in Delbaen and Haezendonck (1987). From the moment generating function $M_{TL_i(t_{\max})}(\zeta)$, we have:

$$
E\left[TL_i(t_{\max})\right] = \left.\frac{dM_{TL_i(t_{\max})}(\zeta)}{d\zeta}\right|_{\zeta=0} = \frac{\lambda_i E[L]}{\alpha}\left[1 - e^{-\alpha t_{\max}}\right] \qquad (5.13)
$$

$$
\begin{aligned}
E\left(\left[TL_i(t_{\max})\right]^2\right) &= \left.\frac{d^2 M_{TL_i(t_{\max})}(\zeta)}{d\zeta^2}\right|_{\zeta=0} \\
&= \frac{\lambda_i E\left[L^2\right]}{2\alpha}\left[1 - e^{-2\alpha t_{\max}}\right] + \frac{\lambda_i^2 E[L]^2}{\alpha^2}\left[1 - e^{-\alpha t_{\max}}\right]^2 \qquad (5.14)
\end{aligned}
$$

$$
Var\left[TL_i(t_{\max})\right] = \frac{\lambda_i E\left[L^2\right]}{2\alpha}\left[1 - e^{-2\alpha t_{\max}}\right] \qquad (5.15)
$$

Higher moments can be similarly obtained by successive differentiation of the moment-generating function.

5.1.2 Discounted Losses due to Nonhomogeneous Poisson Aftershock Process

Expected Total Losses

Again, for a building in damage state i, $TL_i(t_{\max}) = \sum_{k=1}^{N_i(t_{\max})} L_k e^{-\alpha T_k}$ in $[0, t_{\max}]$, but here, $N_i(t_{\max})$ is a nonhomogeneous Poisson process with $E\left[N_i(t_{\max})\right] = \int_0^{t_{\max}} \lambda_i(t)dt$. This model for discounted losses due to the nonhomogeneous Poisson process also assumes that the building is immediately "re-built" back to damage state i after the occurrence of an aftershock loss event.

Here, we construct a new time scale such that the nonhomogeneous Poisson process becomes a homogeneous one so that we can adopt the same method of evaluating the expectations as described in Section 5.1.1. Consider a small infinitesimal time interval dt in real time t with intensity function $\lambda_i(t)$. Consider a corresponding small infinitesimal time interval $d\tau(t)$ in a transformed time scale $\tau(t)$ such that in this transformed time scale, the nonhomogeneous $\lambda_i(t)$ becomes a constant value identically equal to one. This means that we have $\lambda_i(t)dt = [1]\left[d\tau(t)\right]$ or $\frac{d\tau(t)}{dt} = \lambda_i(t)$. Thus:

$$\tau(t) = \int_0^t \lambda_i(y)dy \tag{5.16}$$

This method of "homogenizing" the nonhomogeneous Poisson process is described in Parzen (1962).

For a given mainshock magnitude, $\lambda_i(t)$ is the intensity function of loss events which can be calculated using Equation 5.2. We wish to evaluate the threat due to aftershocks after the mainshock. We can approximate the intensity function of loss events as $\frac{\lambda_i^*}{t}$ where λ_i^* is the mean rate of all loss events one day after the mainshock. The exact form of the intensity function has been discussed in Chapter 2.

Then, a suitable time scale $\tau(t)$ for "homogenizing" $\lambda_i(t)$ would be:

$$\tau(t) = \int_1^t \frac{\lambda_i^*}{y} dy = \lambda_i^* \ln(t) \tag{5.17}$$

$$t = \exp(\frac{\tau}{\lambda_i^*}) \tag{5.18}$$

Thus, we have:

$$\begin{aligned} & E\left[TL_i(t_{\max})|N_i(t_{\max}) = n\right] = E\left[TL_i(\tau\left(t_{\max}\right))|N_i(\tau\left(t_{\max}\right)) = n\right] \\ = \; & E\left[\sum_{k=1}^{n} L_k \exp\left(-\alpha e^{\frac{\tau_k}{\lambda_i^*}}\right)\right], \text{ where } \tau_k = \tau(t_k) \end{aligned} \tag{5.19}$$

Given $N_i(\tau\left[t_{\max}\right]) = n$, τ_k has a uniform distribution in $[0, \tau_{\max}]$ and are i.i.d. such that $\tau_k \overset{D}{=} \tau$. Assuming L_k and τ_k are independent and $L_k \overset{D}{=} L$, we have:

$$\begin{aligned} & E\left[TL_i(t_{\max})|N_i(t_{\max}) = n\right] = E\left[\sum_{k=1}^{n} L_k \exp\left(-\alpha e^{\frac{\tau_k}{\lambda_i^*}}\right)\right] \\ = \; & \sum_{k=1}^{n} E\left[L_k\right] E\left[\exp\left(-\alpha e^{\frac{\tau_k}{\lambda_i^*}}\right)\right] = E\left[L\right] \sum_{k=1}^{n} \int_0^{\tau_{\max}} \frac{1}{\tau_{\max}} \exp\left(-\alpha e^{\frac{\tau}{\lambda_i^*}}\right) d\tau \\ = \; & \frac{nE\left[L\right]}{\tau_{\max}} \int_0^{\tau_{\max}} \exp\left(-\alpha e^{\frac{\tau}{\lambda_i^*}}\right) d\tau \end{aligned} \tag{5.20}$$

Recall that, by construction, the homogeneous rate of loss events is unity in the transformed time space. Therefore, $E\left[N_i(t_{\max})\right] = E\left[N_i(\tau\left(t_{\max}\right))\right] = 1.\tau_{\max} = \lambda_i^* \ln(t_{\max})$. Hence, we have:

$$E\left[TL_i(t_{\max})\right] = E\left[L\right] \int_0^{\lambda_i^* \ln(t_{\max})} \exp\left(-\alpha e^{\frac{\tau}{\lambda_i^*}}\right) d\tau \tag{5.21}$$

Moment Generating Function of Total Losses

We can also obtain the moment generating function of $TL_i(t_{\max})$ in the aftershock environment.

$$M_{TL_i(t_{\max})}\left(\zeta\right) = E\left[e^{\zeta TL_i(t_{\max})}\right]$$

$$
\begin{aligned}
&= E_{N_i(t_{\max})}\left(E_{L_k,T_k,1\leqslant k\leqslant N_i(t_{\max})=n}\left[\exp\left(\varsigma\sum_{k=1}^{N_i(t_{\max})=n}L_k e^{-\alpha T_k}|N_i(t_{\max})=n\right)\right]\right)\\
&= E_{N_i(\tau_{\max})}\left(E_{L_k,\tau_k,1\leqslant k\leqslant N_i(\tau_{\max})=n}\left[\exp\left(\varsigma\sum_{k=1}^{N_i(\tau_{\max})=n}L_k e^{-\alpha e^{\frac{\tau_k}{\lambda_i^*}}}|N_i(\tau_{\max})=n\right)\right]\right)\\
&= E_{N_i(t_{\max})}\left(E_{L_k,\tau_k,1\leqslant k\leqslant n}\left[\exp\left(\varsigma\sum_{k=1}^{n}L_k\exp\left(-\alpha e^{\frac{\tau_k}{\lambda_i^*}}\right)\right)\right]\right)\\
&= E_{N_i(t_{\max})}\left(\left[E_{L,\tau}\left[\exp\left(\varsigma L e^{-\alpha e^{\frac{\tau}{\lambda_i^*}}}\right)\right]\right]^n\right)\\
&= \int_0^\infty e^{-\tau_{\max}}\frac{(\tau_{\max})^n}{n!}\left[E_L\int_0^{\tau_{\max}}\frac{1}{\tau_{\max}}e^{\varsigma L e^{-\alpha e^{\frac{\tau}{\lambda_i^*}}}}d\tau\right]^n dn\\
&= e^{-\tau_{\max}}\int_0^\infty\frac{1}{n!}\left[\tau_{\max}E_L\int_0^{\tau_{\max}}\frac{1}{\tau_{\max}}e^{\varsigma L e^{-\alpha e^{\frac{\tau}{\lambda_i^*}}}}d\tau\right]^n dn\\
&= e^{-\tau_{\max}}\exp\left(E_L\int_0^{\tau_{\max}}e^{\varsigma L e^{-\alpha e^{\frac{\tau}{\lambda_i^*}}}}d\tau\right)\\
&= e^{-\lambda_i^*\ln(t_{\max})}\exp\left(E_L\int_0^{\lambda_i^*\ln(t_{\max})}e^{\varsigma L e^{-\alpha e^{\frac{\tau}{\lambda_i^*}}}}d\tau\right)\\
&= \frac{1}{(t_{\max})^{\lambda_i^*}}\exp\left(\int_0^{\lambda_i^*\ln(t_{\max})}E_L\left[e^{\varsigma L e^{-\alpha e^{\frac{\tau}{\lambda_i^*}}}}\right]d\tau\right) \qquad (5.22)
\end{aligned}
$$

From the moment generating function $M_{TL_i(t_{\max})}(\zeta)$, we can obtain the moments of $TL_i(t_{\max})$ in the aftershock environment. For example,

$$
E\left[TL_i(t_{\max})\right]=\left.\frac{dM_{TL_i(t_{\max})}(\zeta)}{d\zeta}\right|_{\zeta=0}=E[L]\int_0^{\lambda_i^*\ln(t_{\max})}\exp\left(-\alpha e^{\frac{\tau}{\lambda_i^*}}\right)d\tau \qquad (5.23)
$$

$$
E\left(\left[TL_i(t_{\max})\right]^2\right)=\left.\frac{d^2M_{TL_i(t_{\max})}(\zeta)}{d\zeta^2}\right|_{\zeta=0}
$$

$$= E\left[L\right]^2 \left[\int_0^{\lambda_i^* \ln(t_{\max})} \exp\left(-\alpha e^{\frac{\tau}{\lambda_i^*}}\right) d\tau\right]^2 + E\left[L^2\right] \left[\int_0^{\lambda_i^* \ln(t_{\max})} \exp\left(-2\alpha e^{\frac{\tau}{\lambda_i^*}}\right) d\tau\right] \quad (5.24)$$

$$Var\left[TL_i(t_{\max})\right] = E\left[L^2\right] \left[\int_0^{\lambda_i^* \ln(t_{\max})} \exp\left(-2\alpha e^{\frac{\tau}{\lambda_i^*}}\right) d\tau\right] \quad (5.25)$$

Higher moments can be obtained by successive differentiation.

5.2 Markov Loss Models

We have pointed out that a shortcoming of the simplified Poisson model is that it assumes instant "re-build" of the building back to its original damage state before the occurrence of the next loss event. This is generally not realistic in the aftershock environment where buildings could suffer incremental damage due to aftershocks and where there is limited time available for repair. Also, the simplified Poisson model does not explicitly take into consideration the disruption cost based on the *actual* (random) downtime of the building, but instead considers it implicitly by simply including an expected disruption loss in l_{ij}.

Vanmarcke and Diaz-Padilla (1971) previously proposed a method based on Markov chains and Markov decision theory to describe the effects and evaluate the performance of structural systems subjected to mainshocks based on a homogeneous Poisson assumption. Here, we propose a more general stochastic formulation which includes both homogeneous and nonhomogeneous Markov "reward" models for mainshocks and aftershocks and semi-Markov reward models for mainshocks based on Markov descriptions of the damage states of the building. Reward models allow the characterization of the total rewards or losses where there is a reward or cost at the (random) time of transition to a different state (in our aftershock example, perhaps due to content damage in the building) as well as a reward or cost per unit time due to the duration spent in each state (in our example, perhaps due to business downtime losses). See Howard (1971) for details on such processes.

In this formulation, we allow for transitions from one damage state to another. The disruption cost is explicitly dependent on the length of time that the building remains in each damage state. We assume that the future financial losses incurred by the damaged building are dependent only on the current damage state of the building and not upon the path by which it got there, i.e., the future financial losses are *Markovian* in nature.

Here, we are interested in developing a methodology to quantify the total financial losses due to both the mainshock and aftershock processes over a time interval of specified length to serve as an input to the decision-making procedures to be developed in Chapter 6. We consider both Poisson and renewal processes for mainshock occurrences. A renewal process model for mainshocks assumes an arbitrary inter-arrival time distribution between mainshocks whereas the Poisson process assumes (specifically) an exponential inter-arrival time distribution. More details will be discussed in a later section to follow. We shall restrict our attention to analysis of the expected losses. Because the moment-generating functions are difficult to evaluate in this case, if estimates of higher moments or probability distributions are required, one can use Monte Carlo simulation to simulate the Markov reward process.

5.2.1 Expected Total Discounted Losses due to Markov Mainshock Process

Here, we compute the expected total discounted losses where potential loss events from mainshocks result in progression of the building to more severe damage states. To begin, we define U as the time of first transition out of damage state i. Again, we denote λ_i as the intensity function of loss events due to mainshocks for a building originally in damage state i. Also, we assume that a building in damage state i incurs an expected transition cost of l_{ij} and an expected constant disruption cost of r_i per unit time.

We denote $\theta_i(x)$ as the expected total losses in $[0, x]$ given that the building is initially in damage state i. Note that $\theta_i(x)$ is a simplified notation for $E[TL_i(x)]$ used in the previous section. Loss events are described by a homogeneous Poisson process with intensity function λ_i where the inter-arrival times between loss events are exponentially distributed. The probability of transition from state i to j given the occurrence of a loss event from mainshocks is given by P_{ij} from the stationary transition matrix $\mathbf{P}$ defined in Equations 5.3, 5.4 and 5.5.

Here, we use the method of formulation commonly referred to as *first transition* analysis to obtain Equation 5.26.

$$\theta_i(t_{\max}) = \left[\int_{t_{\max}}^{\infty} \lambda_i e^{-\lambda_i u} du\right]\left[\int_0^{t_{\max}} r_i e^{-\alpha t} dt\right] + \left[\int_0^{t_{\max}} \lambda_i e^{-\lambda_i u}\left(\int_0^{u} r_i e^{-\alpha t} dt\right) du\right]$$

$$+\sum_{j>i}^{n} P_{ij}\left[\int_{0}^{t_{\max}} \lambda_i e^{-\lambda_i u}\left(l_{ij}e^{-\alpha u}\right)du\right]+\sum_{j>i}^{n} P_{ij}\left[\int_{0}^{t_{\max}} \lambda_i e^{-\lambda_i u}\left[e^{-\alpha u}\theta_j(t_{\max}-u)\right]du\right] \tag{5.26}$$

See Parzen (1962) for further details. The first term in Equation 5.26 is based on conditioning on $U > t_{\max}$ where the probability that $U > t_{\max}$ is equal to $\int_{t_{\max}}^{\infty} \lambda_i e^{-\lambda_i u} du$ and the expected disruption losses given $U > t_{\max}$ is $\int_{0}^{t_{\max}} r_i e^{-\alpha t} dt$, a term dependent only on the initial building state i. The second term in Equation 5.26 conditions on $U = u$ where the expected disruption losses is equal to $\int_{0}^{u} r_i e^{-\alpha t} dt$. The expected disruption losses is then multiplied by the probability density function of U (where $f_U(u) = \lambda_i e^{-\lambda_i u}$) and integrated over possible values of u in the interval $[0, t_{\max}]$. Similarly, the third term in Equation 5.26 conditions on $U = u$ where the expected transition losses for a building going into damage state j discounted back to time zero is equal to $l_{ij}e^{-\alpha u}$. Again, the expected transition losses is multiplied by the probability density function of U and integrated over possible values of u in $[0, t_{\max}]$. Since the future damage state j is random, we need to compute the expected transition losses by multiplying by P_{ij} and summing over all possible $j > i$. The last term in Equation 5.26 accounts for losses due to future transitions. We condition on the building going to damage state j at time u. The future losses is dependent only on state j (albeit in a shortened time interval of $[u, t_{\max}]$) because of the presumed Markovian nature of the damage states of the buildings. This is equivalent to considering the expected losses (starting in state j) in a shortened time interval of $[0, t_{\max} - u]$, i.e., $\theta_j(t_{\max} - u)$, to which we apply a suitable discount factor of $e^{-\alpha u}$. Then, following similar procedures described above, we multiply by the probability density function of U, integrate over all values of u in $[0, t_{\max}]$, multiply by P_{ij} and sum up over all possible random future building states $j > i$.

Equation 5.26 for $\theta_i(t_{\max})$ has an unknown function $\theta_j(x)$ on the right-hand side of the equation. To solve the set of equations for all the unknown functions $\theta_i(x), i = 1, ..., n$, we adopt the following solution strategy analogous to Howard (1971). We denote $\theta_i^e(s)$ as the Laplace transform of $\theta_i(t_{\max})$. The Laplace transformation (or exponential transformation) of a function $f(t)$ is defined in Equation 5.27. See Howard (1971) for details.

$$f^e(s) = \int_{0}^{\infty} f(t)e^{-st}dt \tag{5.27}$$

A special multiplicative property of the Laplace transform of convolution integral is:

$$\int_0^t f_1(y) f_2(t-y) dy = f_1^e(s) f_2^e(s) \tag{5.28}$$

Using this property for the last term in Equation 5.26, we have:

$$\begin{aligned}\theta_i^e(s) = &\left(\left[\int_{t_{\max}}^{\infty} \lambda_i e^{-\lambda_i u} du \right] \left[\int_0^{t_{\max}} r_i e^{-\alpha t} dt \right] \right)^e + \left[\int_0^{t_{\max}} \lambda_i e^{-\lambda_i u} \left(\int_0^u r_i e^{-\alpha t} dt \right) du \right]^e \\ &+ \sum_{j>i}^{n} P_{ij} \left[\int_0^{t_{\max}} \lambda_i e^{-\lambda_i u} \left(l_{ij} e^{-\alpha u} \right) du \right]^e + \sum_{j>i}^{n} P_{ij} \left\{ \lambda_i e^{-\lambda_i u} e^{-\alpha u} \right\}^e \theta_j^e(s)\end{aligned} \tag{5.29}$$

We further denote:

$$\begin{aligned}\kappa_i^e(s) = &\left(\left[\int_{t_{\max}}^{\infty} \lambda_i e^{-\lambda_i u} du \right] \left[\int_0^{t_{\max}} r_i e^{-\alpha t} dt \right] \right)^e + \left[\int_0^{t_{\max}} \lambda_i e^{-\lambda_i u} \left(\int_0^u r_i e^{-\alpha t} dt \right) du \right]^e \\ &+ \sum_{j>i}^{n} P_{ij} \left[\int_0^{t_{\max}} \lambda_i e^{-\lambda_i u} \left(l_{ij} e^{-\alpha u} \right) du \right]^e, i = 1, ..., n\end{aligned} \tag{5.30}$$

$$\eta_{ij}^e(s) = P_{ij} \left[\lambda_i e^{-\lambda_i u} e^{-\alpha u} \right]^e, i = 1, ..., n, j = 1, ..., n \tag{5.31}$$

In vector form, we have:

$$\boldsymbol{\kappa}^{\mathbf{e}}(\mathbf{s}) = \begin{pmatrix} \kappa_1^e \\ \vdots \\ \vdots \\ \kappa_n^e \end{pmatrix}, \boldsymbol{\eta}^{\mathbf{e}}(\mathbf{s}) = \begin{pmatrix} \eta_{11}^e & \cdots & \cdots & \eta_{1n}^e \\ \vdots & \ddots & \ddots & \vdots \\ \vdots & \ddots & \ddots & \vdots \\ \eta_{n1}^e & \cdots & \cdots & \eta_{nn}^e \end{pmatrix}, \boldsymbol{\theta}^{\mathbf{e}}(\mathbf{s}) = \begin{pmatrix} \theta_1^e \\ \vdots \\ \vdots \\ \theta_n^e \end{pmatrix} \tag{5.32}$$

Therefore, based on Equation 5.30, we have the set of equations in Equation 5.33 with solution in Equation 5.34.

$$\boldsymbol{\theta}^{\mathbf{e}}(\mathbf{s}) = \boldsymbol{\kappa}^{\mathbf{e}}(\mathbf{s}) + \boldsymbol{\eta}^{\mathbf{e}}(\mathbf{s}) \boldsymbol{\theta}^{\mathbf{e}}(\mathbf{s}) \tag{5.33}$$

$$\boldsymbol{\theta}^{\mathbf{e}}(\mathbf{s}) = \left[\mathbf{I} - \boldsymbol{\eta}^{\mathbf{e}}(\mathbf{s})\right]^{-1} \boldsymbol{\kappa}^{\mathbf{e}}(\mathbf{s}) \tag{5.34}$$

$\theta_i(t_{\max})$ can be obtained from the appropriate row of the inverse Laplace transform of $\boldsymbol{\theta}^{\mathbf{e}}(\mathbf{s})$. This formulation allows us to obtain the expected total losses due to a homogeneous Poisson mainshock process in $[0, t_{\max}]$ for all damage states of the building. Vanmarcke and Diaz-Padilla (1971) considered homogeneous mainshocks in their study, but provided solutions only for $t_{\max} \to \infty$ for which asymptotic results exist.

It is worth noting that if we have a transition matrix $\mathbf{P}$, where $\mathbf{P}$ is given in Equation 5.35, our general Markov reward model simplifies to that of the mainshock homogeneous Poisson model described in Section 5.1.1.

$$\mathbf{P} = \begin{pmatrix} 0 & 1 \\ 1 & 0 \end{pmatrix} \tag{5.35}$$

Hence, this is indeed a more general model which allows for a much greater degree of modeling flexibility. For example, repair back to the intact state can be introduced in the above framework if we consider exponential repair times for the different building damage states. Such generalizations will be discussed in the chapter to follow, together with a more general framework for both the mainshock and aftershock environment where we consider non-exponential repair times which can start at different (deterministic) time periods after the mainshock for different building damage states. Numerical results demonstrating the above methodology will be presented in a later section.

5.2.2 Expected Total Discounted Losses due to Markov Mainshock Process Considering No More than 1 Event in $[0, t_{\max}]$

As a simple approximation to the more general formulation described in Section 5.2.1, we can approximate $\theta_i(t_{\max})$ by computing the expected total discounted losses considering no more than 1 event in $[0, t_{\max}]$ using Equation 5.36.

$$\theta_i(t_{\max}) \approx \left[\int_{t_{\max}}^{\infty} \lambda_i e^{-\lambda_i u} du\right] \left[\int_0^{t_{\max}} r_i e^{-\alpha t} dt\right] + \left[\int_0^{t_{\max}} \lambda_i e^{-\lambda_i u} \left(\int_0^{u} r_i e^{-\alpha t} dt\right) du\right]$$

$$+\sum_{j>i}^{n} P_{ij}\left[\int_{0}^{t_{\max}} \lambda_i e^{-\lambda_i u}\left(\int_{u}^{t_{\max}} r_j e^{-\alpha t} dt\right) e^{-\alpha u} du\right] + \sum_{j>i}^{n} P_{ij}\left[\int_{0}^{t_{\max}} \lambda_i e^{-\lambda_i u}\left(l_{ij} e^{-\alpha u}\right) du\right] \tag{5.36}$$

This simplification is justified because of the significant length of the inter-arrival times between mainshocks, which are typically on the order of hundreds to thousands of years such that the contribution to expected total discounted losses from the second and subsequent events will be significantly less due to the strong effect that discounting has over such an extended period of time.

Note that we have a much simpler formulation in this case as we do not have to consider the contribution to the expected total discounted losses from the second and subsequent events. Solving this equation is also much simpler as we do not have to solve simultaneous equations for the $\theta_i(x)$, i.e., to perform Laplace and inverse Laplace transformations in order to obtain the solution to the expected total losses.

5.2.3 Expected Total Discounted Losses due to Markov Mainshock Process with Repair

In Sections 5.2.1 and 5.2.2, we proposed formulations to compute the expected total discounted losses due to a Markov mainshock process. We can further include in the previous formulations the possibility of repair back to the intact state if we assume that the repair duration to the intact state is exponentially distributed. Even though this assumption might not be extremely realistic, we shall further develop the formulation to include repair with exponentially distributed repair durations, with a more realistic, non-exponential model to follow in Chapter 6.

For a building in damage state i, if the mean of the exponentially distributed repair duration is m_i, then the mean repair *rate* back to the intact state is equal to $\varphi_{i1} = \frac{1}{m_i}$. Further, l_{i1} is taken to be the repair cost for a building in damage state i. The intensity function of mainshocks is taken to be equal to μ, following Section 5.2.1. The intensity function of events resulting in transitions out of damage state i should include the possibility of the completion of repair, and it can be calculated using Equation 5.37, analogous to Equation 5.2 without repair. Again, a building in damage state i can go to damage state j with probability P'_{ij} given the occurrence of a mainshock, where values of P'_{ij} have been calculated in Chapter 3.

$$\lambda_i = \mu \sum_{j>i} P'_{ij} + \varphi_{i1} = \mu(1 - P'_{ii}) + \varphi_{i1} \tag{5.37}$$

The transition matrix $\mathbf{P}$ also needs to be modified. In this case, the matrix $\mathbf{P}$ will have positive values in the first column as shown in Equation 5.38, as opposed to the column of zeros in the first column of $\mathbf{P}$ in Equation 5.3 where repair has not been taken into consideration. Equation 5.38 can be calculated using Equations 5.39, 5.40 and 5.41.

$$\mathbf{P} = \begin{pmatrix} 0 & P_{12} & \cdots & P_{1n} \\ P_{21} & 0 & \ddots & \vdots \\ \vdots & \ddots & 0 & P_{(n-1)n} \\ P_{n1} & \cdots & \cdots & 0 \end{pmatrix} \tag{5.38}$$

$$P_{ij} = 0,\ i \geq j,\ j \neq 1 \tag{5.39}$$

$$P_{ij} = \frac{\mu P'_{ij}}{\lambda_i},\ i < j,\ j \neq 1 \tag{5.40}$$

$$P_{i1} = \frac{\varphi_{i1}}{\lambda_i} \tag{5.41}$$

Having defined λ_i and $\mathbf{P}$, we can now solve for the expected total discounted losses due to a Markov mainshock process with repair using the procedure described in Sections 5.2.1 and 5.2.2, but using λ_i from Equation 5.37 and $\mathbf{P}$ from Equation 5.38 instead.

5.2.4 Expected Total Discounted Losses due to Semi-Markov Mainshock Process

We now consider a more realistic formulation for the expected total discounted losses in the mainshock environment in $[0, t_{\max}]$ by considering an arbitrary inter-arrival time distribution as opposed to the exponential inter-arrival time distribution implied by the previous Markov formulation. We denote W as the inter-arrival time between loss events due to mainshocks, and $f(w)$ and $F(w)$ represent the probability density function and the cumulative distribution function, respectively, of W. A non-exponential inter-arrival time

distribution means that we have a non-constant hazard rate function, which is defined as:

$$r(w) = \frac{f(w)}{1 - F(w)} \tag{5.42}$$

The hazard rate function thus tells us the probability that we will have a mainshock in the next dw given that there were no mainshocks in the last w years. See Ross (2000) for details. For the exponential inter-arrival time distribution, $r(w)$ is equal to the intensity function, λ_i, of the corresponding Poisson loss event process as a result of the memoryless property of the exponential distribution. In this case, the process in essence restarts itself probabilistically at every instant in time and hence knowledge about the elapsed time since the last mainshock provides us with no further information on when the next mainshock is going to occur. The memoryless nature of the Poisson process contradicts the elastic rebound theory which suggests that it becomes more likely for a mainshock to occur when the elapsed time since the last mainshock increases due to the accumulation of stress in the faults. The elastic rebound theory suggests that a monotonically increasing hazard rate function might be appropriate for modeling the inter-arrival time distribution of mainshocks, and thus a renewal process can be used to model mainshock occurrences. Typical inter-arrival time distributions for mainshocks that have been used in literature include the lognormal, gamma, Weibull and BPT (Brownian Passage Time) models. See USGS (1990), USGS (2003), Cornell and Winterstein (1988), Kiremidjian and Anagnos (1984) and Takahashi et al. (2004) for details. The gamma and Weibull models have monotonically increasing hazard rate functions which are in accordance with the elastic rebound theory, while the lognormal and BPT models do not have strictly monotonically increasing hazard rate functions. As opposed to the Poisson process, the renewal process restarts itself probabilistically only at the times of transitions (known as regeneration points), at which points (only) it has no memory.

We now propose a alternative formulation for $\theta_i(x)$ using a renewal process to model the occurrences of loss events due to mainshocks. We shall use $f_i(w)$ and $F_i(w)$ to represent the probability density function and cumulative distribution function of the inter-arrival time W for loss events given a building in damage state i. We also denote s as the elapsed time since the last occurrence of a loss event, which is denoted as the 0^{th} event. Note that when a loss event occurs, the building will transit to a different damage state according to the same Markov transition matrix $\mathbf{P}$ defined in Equations 5.3 , 5.4 and 5.5. We define T_k as

the time of arrival of the k^{th} event. The T_k, $k = 1, 2, ...$, are non-negative random variables. We also define W_k as the inter-arrival time between the $(k-1)^{th}$ and k^{th} loss event, i.e., $W_k = T_k - T_{k-1}$. By default, $T_0 = -s$.

Following the same approach as used in Equation 5.26, first, we condition on $T_1 = t_1$, $t_1 \geq 0$ to obtain Equation 5.43.

$$\theta_i(\widetilde{t}_{\max}) = \left[\int_{\widetilde{t}_{\max}}^{\infty} f_i(w_2)dw_2\right]\left[\int_0^{\widetilde{t}_{\max}} r_i e^{-\alpha t}dt\right] + \left[\int_0^{\widetilde{t}_{\max}} f_i(w_2)\left(\int_0^{w_2} r_i e^{-\alpha t}dt\right)dw_2\right]$$
$$+ \sum_{j>i}^{n} P_{ij}\left[\int_0^{\widetilde{t}_{\max}} f_i(w_2)\left(l_{ij}e^{-\alpha w_2}\right)dw_2\right] + \sum_{j>i}^{n} P_{ij}\left[\int_0^{\widetilde{t}_{\max}} f_i(w_2)e^{-\alpha w_2}\theta_j(\widetilde{t}_{\max} - w_2)dw_2\right] \tag{5.43}$$

Here, again, $t_{\max}$ represents the length of the time interval of economic interest. The formulation here takes advantage of the memoryless properties at the regeneration points, T_k, of the renewal process. In this case, however, we have to consider the first event separately from the remaining events because its arrival time distribution is dependent on the elapsed time since the last mainshock, s. This is commonly referred to as a delayed renewal process. At $T_1 = t_1$, however, $s = 0$, and the renewal process restarts itself probabilistically. Denoting $\widetilde{t}_{\max} = t_{\max} - t_1$, we can then evaluate $\theta_i(\widetilde{t}_{\max})$ using a similar procedure as that described in Section 5.2.1 where we condition on $W_2 = w_2$, but we replace the exponential inter-arrival time distribution with $f_i(w_2)$ instead. $\theta_i(\widetilde{t}_{\max})$ represents the expected financial losses in the shortened time interval $[t_1, t_{\max}]$. Equation 5.43 can be solved for all states i by using the previously proposed method involving Laplace transformations and its inverse for $T_1 = t_1$.

Solving Equation 5.43 enables us to compute the expected financial losses in $[t_1, t_{\max}]$. We now need to compute the expected financial losses in $[0, t_{\max}]$, i.e., $\theta_i(t_{\max})$, by unconditioning on T_1. We first need to compute the conditional probability density function of T_1 given $W_1 > s$, $f_{T_1|W_1>s}(t_1|W_1 > s)$, which is given in Equation 5.44.

$$\begin{aligned} f_{T_1|W_1>s}(t_1|W_1 > s) &= f(W_1 = s + t_1|W_1 > s) \\ &= \frac{f(s+t_1)}{1-F(s)},\ t_1 \geq 0 \\ &= 0,\ \text{otherwise} \end{aligned} \tag{5.44}$$

Similar to the approach used in Equation 5.26 in Section 5.2.1. we obtain Equation 5.45.

$$\theta_i(t_{\max}) = \left[\int_{t_{\max}}^{\infty} \frac{f(s+t_1)}{1-F(s)} dt_1\right]\left[\int_0^{t_{\max}} r_i e^{-\alpha t} dt\right] + \left[\int_0^{t_{\max}} \frac{f(s+t_1)}{1-F(s)} \left(\int_0^{t_1} r_i e^{-\alpha t} dt\right) dt_1\right]$$
$$+ \sum_{j>i} P_{ij} \left[\int_0^{t_{\max}} \frac{f(s+t_1)}{1-F(s)} \left(l_{ij} e^{-\alpha t_1}\right) dt_1\right] + \sum_{j>i} P_{ij} \left[\int_0^{t_{\max}} \frac{f(s+t_1)}{1-F(s)} \left(e^{-\alpha t_1} \theta_j(\widetilde{t}_{\max})\right) dt_1\right] \tag{5.45}$$

Instead of the exponential probability density function $\lambda_i e^{-\lambda_i u}$ in Equation 5.26, here, we use the conditional probability density function in Equation 5.44. Also, here, we use $\theta_j(\widetilde{t}_{\max})$ obtained from Equation 5.43. The solution of Equation 5.45 differs from that of Equation 5.26 because we have to solve $\theta_i(\widetilde{t}_{\max})$ first for all damage states i (which entails the process of Laplace and inverse Laplace transformations described earlier) before we can solve for $\theta_i(t_{\max})$. A two-step process is required to solve Equation 5.45 due to the dependence of the conditional probability density function of T_1 on s, whereas a one-step process is required to solve Equation 5.26 due to lack of such dependence on the elapsed time since the last loss event. Numerical integration can be used to solve Equation 5.45.

The introduction of renewal arrivals of loss events with an embedded Markov transition structure results in a more general semi-Markov mainshock model for estimating the expected total discounted losses in any time interval of interest. Note that if, as in Section 5.2.2, Equation 5.36 for Poisson mainshocks, we wish to consider only one transition as a simplifying approximation, we simply need to eliminate the last term in Equation 5.45.

We may also consider a special case similar to the Poisson models described in Section 5.1.1 where we have a binary state model, i.e., either a loss event occurs or not, but where loss events due to mainshocks occur according to a renewal process. This is equivalent to using Equation 5.35 as the transition probability matrix. As discussed earlier, the implicit assumption is that the building is restored back to its original (usually intact) state before the occurrence of the second loss event. Here, we assume that there is a one-time financial loss L, with $E(L) = l$, at the times of transitions. This is equivalent to eliminating the

terms with r_i in Equation 5.43 such that we obtain Equation 5.46.

$$\theta_1(\widetilde{t}_{\max}) = \left[\int_0^{\widetilde{t}_{\max}} f_1(w_2) l e^{-\alpha w_2} dw_2\right] + \left[\int_0^{\widetilde{t}_{\max}} f_1(w_2) e^{-\alpha w_2} \theta_2(\widetilde{t}_{\max} - w_2) dw_2\right] \tag{5.46}$$

Here, $i = 1$ corresponds to the original building state, and $i = 2$ corresponds to the building damage state after a loss event. Because of the symmetry of the transition probability matrix in Equation 5.35, we can replace $\theta_2(\widetilde{t}_{\max} - w_2)$ in the second term of Equation 5.46 by $\theta_1(\widetilde{t}_{\max} - w_2)$ such that we obtain Equation 5.47.

$$\theta_1(\widetilde{t}_{\max}) = \left[\int_0^{\widetilde{t}_{\max}} f_1(w_2) l e^{-\alpha w_2} dw_2\right] + \left[\int_0^{\widetilde{t}_{\max}} f_1(w_2) e^{-\alpha w_2} \theta_1(\widetilde{t}_{\max} - w_2) dw_2\right] \tag{5.47}$$

Equation 5.47 can be solved by first taking the Laplace transform of both sides of the equation and rearranging the terms to obtain the Laplace transform of $\theta_1(\widetilde{t}_{\max})$ in Equation 5.48.

$$\theta_1^e(\widetilde{t}_{\max}) = \frac{\left[\int_0^{\widetilde{t}_{\max}} f_1(w_2) l e^{-\alpha w_2} dw_2\right]^e}{[1 - f_1(w_2) e^{-\alpha w_2}]^e} \tag{5.48}$$

$\theta_1(\widetilde{t}_{\max})$ can then be obtained by taking the inverse Laplace transform of Equation 5.48. $\theta_1(t_{\max})$ can then be obtained easily by eliminating the terms with r_i in Equation 5.45 such that we obtain Equation 5.49.

$$\theta_1(t_{\max}) = \int_0^{t_{\max}} \frac{f(s + t_1)}{1 - F(s)} \left[l + \theta_1(\widetilde{t}_{\max})\right] e^{-\alpha t_1} dt_1 \tag{5.49}$$

These results will be used in a later section.

Unlike Section 5.2.3 where we were able to include the possibility of repair to the intact state in the formulation to compute the expected total discounted losses due to a Markov mainshock process, it is not as straightforward to adopt the same procedure for the formulation proposed in this section with a semi-Markov mainshock process. A renewal process to model mainshock occurrences typically results in a non-constant hazard rate function. If we assume a constant mean repair rate to the intact state for a building in damage state i, the

intensity function of events resulting in transitions out of damage state i will be the sum of the intensity function of mainshocks resulting in incremental damage and the constant mean repair rate. This will result in a non-stationary transition matrix $\mathbf{P}$ where the proposed procedure in Section 5.2.3 will fail. A more general procedure to include non-exponential repair durations together with a renewal process model of mainshock occurrences will be introduced in Chapter 6.

5.2.5 Expected Total Undiscounted Losses due to Nonhomogeneous Markov Aftershock Process

We now begin to explore the formulation for expected total losses in the nonhomogeneous aftershock environment. We first consider a case for undiscounted losses because damaging aftershocks are unlikely to happen more than 5 years after the mainshock and the effects of discounting will therefore not be significant. Also, we anticipate that the building owner would have either repaired the damaged building to the intact state or relocated to a new building to continue operations within a period of 5 years after the mainshock such that the building owner does not incur any aftershock induced financial losses after that. The effects of discounting will also not be significant in this case. An undiscounted model provides for a degree of analytical simplicity and tractability that is lacking in the discounted model to be discussed in the next section.[1]

Here, as in Section 5.1.2, a time transformation is again necessary to "homogenize" the nonhomogeneous aftershock process. We define τ as the transformed time, υ as the time of first transition out of initial state i in transformed time and $\tau_{\max}$ as the total length of time interval of interest in transformed time.

Again, we denote $\theta_i(x)$ as the expected total losses in $[0, x]$ given that the building is initially in damage state i after the mainshock. In the aftershock environment, loss events are described by a nonhomogeneous Poisson process with intensity function $\lambda_i(t)$ defined in Equation 5.2. The probability of transition from state i to j given the occurrence of a loss event is given by P_{ij} from the stationary transition matrix $\mathbf{P}$ defined in Equations 5.3, 5.4

[1] The proposed methodologies in the nonhomogeneous Markov aftershock environment (both discounted and undiscounted) should be used for $t_{\max}$ less than or equal to 5 years. This is because aftershocks die off quickly as a function of time and because the probability of transiting to the collapse state is small relative to the probability of transitions to other intermediate damage states, the building could remain in an intermediate damage state which incurs a constant disruption cost per day for an indefinite length of time. This is not realistic for the reasons discussed above. Models which include repair operations explicitly in the formulation of financial losses will be discussed in Chapter 6.

and 5.5.

Here we define the transformed time $\tau(t)$ based on $\mu(t)$, the intensity function of aftershocks. In the transformed time $\tau(t)$, all aftershocks follow a homogeneous Poisson process with mean rate equal to one per unit time period. Thus we have $\tau(t) = \int_0^t \mu(y)dy$. We can approximate the intensity function of aftershocks as $\frac{\mu^*}{t}$ where μ^* is the mean rate of all aftershocks one day after the mainshock. Hence, we have $\tau(t) = \mu^* \ln(t)$ and $t = \exp(\frac{\tau}{\mu^*})$.[2]

In the actual time space t, the expected disruption costs in state i, r_i, is a constant per unit time. In the transformed time space $\tau(t)$, the expected disruption costs in state i, $r_i(\tau)$, is dependent on τ such that:

$$r_i dt = r_i(\tau)d\tau \tag{5.50}$$

Thus:

$$r_i(\tau) = r_i \frac{dt}{d\tau} = \frac{r_i}{\mu^*} \exp(\frac{\tau}{\mu^*}) \tag{5.51}$$

We now want to define $\lambda_i(t)$, the mean rate of loss events, in the transformed time space. In the transformed time $\tau(t)$, for a building in damage state i, we assume first that the loss events follow a homogeneous Poisson process with mean rate equal to λ_i^* which can be calculated using Equation 5.53.

$$\lambda_i^* d\tau = \lambda_i(t)dt \tag{5.52}$$

Thus:

$$\lambda_i^* = \lambda_i(t)\frac{dt}{d\tau} = \mu(t)(1 - P_{ii}^{'})\frac{1}{\mu(t)} = (1 - P_{ii}^{'}) \tag{5.53}$$

We have $\theta_i(t_{\max}) = \theta_i(\tau_{\max})$. We denote $\theta_i(t_{\max}) = \theta_i^d(t_{\max}) + \theta_i^t(t_{\max})$ and $\theta_i(\tau_{\max}) = \theta_i^d(\tau_{\max}) + \theta_i^t(\tau_{\max})$, where $\theta_i^d(t_{\max})$ is the expected disruption losses in $[0, t_{\max}]$ given that the building is initially in damage state i, and $\theta_i^t(t_{\max})$ is the expected transition losses in $[0, t_{\max}]$ given that the building is initially in damage state i. We consider the expected disruption losses and expected transition losses separately because the disruption losses do not "restart" itself after the occurrence of a loss event due to its nonstationary nature in

[2]Note that in the development of nonhomogeneous Poisson loss models in Section 5.1.2, we defined multiple transformed time scale in terms of λ_i^* for $i = 1, 2, ..., n$. It was feasible because we could consider each state i independently. Here, because we permit transitions from state to state, we used a common time scale for all states based on the mean rate of all aftershocks 1 day after the mainshock, μ^*.

the transformed time space. This will be discussed below.

Again, we condition on the time, υ, of the first transition out of state in the transformed time space. Using a similar approach as the previous homogeneous case, we have for the expected disruption losses:

$$\begin{aligned}\theta_i^d(\tau_{\max}) = &\left[\int_{\tau_{\max}}^{\infty} \lambda_i^* e^{-\lambda_i^* \upsilon} d\upsilon\right]\left[\int_0^{\tau_{\max}} \frac{r_i}{\mu^*}\exp(\frac{\tau}{\mu^*})d\tau\right] \\ &+ \left[\int_0^{\tau_{\max}} \lambda_i^* e^{-\lambda_i^* \upsilon}\left(\int_0^{\upsilon} \frac{r_i}{\mu^*}\exp(\frac{\tau}{\mu^*})d\tau\right)d\upsilon\right] \\ &+ \sum_{j>i}^{n} P_{ij}\left[\int_0^{\tau_{\max}} \lambda_i^* e^{-\lambda_i^* \upsilon} e^{\frac{\upsilon}{\mu^*}} \theta_j^d(\tau_{\max}-\upsilon)d\upsilon\right] \end{aligned} \tag{5.54}$$

Here, we have an additional factor of $e^{\frac{\upsilon}{\mu^*}}$ in the last term as the disruption losses is a function of absolute transformed time τ such that after υ, the disruption losses do not "restart" itself as if we are back at transformed time zero again. This is a unique characteristic of the nonhomogeneous Poisson process. Because of the specific form of $\frac{1}{t}$ assumed for the intensity process of aftershocks, we can obtain an exact formulation of the disruption losses incurred after $\upsilon, r_i(\tau), \tau > \upsilon$, by multiplying $e^{\frac{\upsilon}{\mu^*}}$, a factor dependent only on υ, to the disruption losses starting from transformed time zero, $r_i(\tau), \tau > 0$.[3] This is exact in the undiscounted case, but an approximation in the discounted case which we shall discuss in the next section.

Again, taking the Laplace transformation, we have:

$$\begin{aligned}\left[\theta_i^d\right]^e(s) = &\left(\left[\int_{\tau_{\max}}^{\infty} \lambda_i^* e^{-\lambda_i^* \upsilon} d\upsilon\right]\left[\int_0^{\tau_{\max}} \frac{r_i}{\mu^*}\exp(\frac{\tau}{\mu^*})d\tau\right]\right)^e \\ &+ \left[\int_0^{\tau_{\max}} \lambda_i^* e^{-\lambda_i^* \upsilon}\left(\int_0^{\upsilon} \frac{r_i}{\mu^*}\exp(\frac{\tau}{\mu^*})d\tau\right)d\upsilon\right]^e \\ &+ \sum_{j>i}^{n} P_{ij}\left[\int_0^{\tau_{\max}} \lambda_i^* e^{-\lambda_i^* \upsilon} e^{\frac{\upsilon}{\mu^*}}\right]^e \left[\theta_j^d\right]^e(s) \end{aligned} \tag{5.55}$$

[3] In general, the formulation will require us to multiply a factor dependent on both υ and τ to obtain $r_i(\tau), \tau > \upsilon$.

We further denote:

$$\begin{aligned}\left[\kappa_i^d\right]^e(s) &= \left(\left[\int_{\tau_{\max}}^{\infty}\lambda_i^* e^{-\lambda_i^*\upsilon}d\upsilon\right]\left[\int_0^{\tau_{\max}}\frac{r_i}{\mu^*}\exp(\frac{\tau}{\mu^*})d\tau\right]\right)^e \\ &+\left[\int_0^{\tau_{\max}}\lambda_i^* e^{-\lambda_i^*\upsilon}\left(\int_0^{\upsilon}\frac{r_i}{\mu^*}\exp(\frac{\tau}{\mu^*})d\tau\right)d\upsilon\right]^e, i=1,...,n, \end{aligned} \tag{5.56}$$

$$\left[\eta_{ij}^d\right]^e(s) = P_{ij}\left[\lambda_i^* e^{-\lambda_i^*\upsilon}e^{\frac{\upsilon}{\mu^*}}\right]^e, i=1,...,n, j=1,...,n \tag{5.57}$$

In vector form, we have:

$$\left[\boldsymbol{\kappa}^{\mathbf{d}}\right]^{\mathbf{e}}(\mathbf{s}) = \begin{pmatrix}\left[\kappa_1^d\right]^e\\ \vdots \\ \vdots \\ \left[\kappa_n^d\right]^e\end{pmatrix}, \left[\boldsymbol{\eta}^{\mathbf{d}}\right]^{\mathbf{e}}(\mathbf{s}) = \begin{pmatrix}\left[\eta_{11}^d\right]^e & \cdots & \cdots & \left[\eta_{1n}^d\right]^e\\ \vdots & \ddots & \ddots & \vdots \\ \vdots & \ddots & \ddots & \vdots \\ \left[\eta_{n1}^d\right]^e & \cdots & \cdots & \left[\eta_{nn}^d\right]^e\end{pmatrix}, \left[\boldsymbol{\theta}^{\mathbf{d}}\right]^{\mathbf{e}}(\mathbf{s}) = \begin{pmatrix}\left[\theta_1^d\right]^e\\ \vdots \\ \vdots \\ \left[\theta_n^d\right]^e\end{pmatrix} \tag{5.58}$$

Therefore, we have:

$$\left[\boldsymbol{\theta}^{\mathbf{d}}\right]^{\mathbf{e}}(\mathbf{s}) = \left[\mathbf{I} - \left[\boldsymbol{\eta}^{\mathbf{d}}\right]^{\mathbf{e}}(\mathbf{s})\right]^{-1}\left[\boldsymbol{\kappa}^{\mathbf{d}}\right]^{\mathbf{e}}(\mathbf{s}) \tag{5.59}$$

Similarly, for the transition losses:

$$\theta_i^t(\tau_{\max}) = \sum_{j>i}^{n}P_{ij}\left[\int_0^{\tau_{\max}}\lambda_i^* e^{-\lambda_i^*\upsilon}l_{ij}d\upsilon\right] + \sum_{j>i}^{n}P_{ij}\left[\int_0^{\tau_{\max}}\lambda_i^* e^{-\lambda_i^*\upsilon}\theta_j^t(\tau_{\max}-\upsilon)d\upsilon\right] \tag{5.60}$$

$$\left[\theta_i^t\right]^e(s) = \sum_{j>i}^{n}P_{ij}\left[\int_0^{\tau_{\max}}\lambda_i^* e^{-\lambda_i^*\upsilon}l_{ij}d\upsilon\right]^e + \sum_{j>i}^{n}P_{ij}\left[\lambda_i^* e^{-\lambda_i^*\upsilon}\right]^e\left[\theta_j^t\right]^e(s) \tag{5.61}$$

We further denote:

$$\left[\kappa_i^t\right]^e(s) = \sum_{j>i}^{n}P_{ij}\left[\int_0^{\tau_{\max}}\lambda_i^* e^{-\lambda_i^*\upsilon}l_{ij}d\upsilon\right]^e, i=1,...,n \tag{5.62}$$

$$\left[\eta_{ij}^d\right]^e(s) = P_{ij}\left[\lambda_i^* e^{-\lambda_i^*\upsilon}\right]^e, i=1,...,n, j=1,...,n \tag{5.63}$$

In vector form, we have:

$$\left[\boldsymbol{\kappa}^{\mathbf{t}}\right]^{\mathbf{e}}(\mathbf{s}) = \begin{pmatrix} \left[\kappa_1^t\right]^e \\ \vdots \\ \vdots \\ \left[\kappa_n^t\right]^e \end{pmatrix}, \left[\boldsymbol{\eta}^{\mathbf{t}}\right]^{\mathbf{e}}(\mathbf{s}) = \begin{pmatrix} \left[\eta_{11}^t\right]^e & \cdots & \cdots & \left[\eta_{1n}^t\right]^e \\ \vdots & \ddots & \ddots & \vdots \\ \vdots & \ddots & \ddots & \vdots \\ \left[\eta_{n1}^t\right]^e & \cdots & \cdots & \left[\eta_{nn}^t\right]^e \end{pmatrix}, \left[\boldsymbol{\theta}^{\mathbf{t}}\right]^{\mathbf{e}}(\mathbf{s}) = \begin{pmatrix} \left[\theta_1^t\right]^e \\ \vdots \\ \vdots \\ \left[\theta_n^t\right]^e \end{pmatrix} \tag{5.64}$$

Therefore, we have:

$$\left[\boldsymbol{\theta}^{\mathbf{t}}\right]^{\mathbf{e}}(\mathbf{s}) = \left[\mathbf{I} - \left[\boldsymbol{\eta}^{\mathbf{t}}\right]^{\mathbf{e}}(\mathbf{s})\right]^{-1} \left[\boldsymbol{\kappa}^{\mathbf{t}}\right]^{\mathbf{e}}(\mathbf{s}) \tag{5.65}$$

By linearity of the Laplace transformation, we have $\boldsymbol{\theta}^{\mathbf{e}}(\mathbf{s}) = \left[\boldsymbol{\theta}^{\mathbf{d}}\right]^{\mathbf{e}}(\mathbf{s}) + \left[\boldsymbol{\theta}^{\mathbf{t}}\right]^{\mathbf{e}}(\mathbf{s})$. $\theta_i(t_{\max})$ can be obtained from the appropriate row of the inverse Laplace transform of $\boldsymbol{\theta}^{\mathbf{e}}(\mathbf{s})$. This formulation allows us to obtain the expected total undiscounted losses due to a nonhomogeneous aftershock process in $[0, t_{\max}]$ for all damage states of the building. We then need simply to convert the result back to the original time scale by using $t = \exp(\frac{\tau}{\mu^*})$. Numerical results demonstrating the above methodology will be presented in a later section.

5.2.6 Expected Total Discounted Losses due to Nonhomogeneous Markov Aftershock Process

The formulation for the discounted case is similar to that for the undiscounted case except that we need to include the appropriate discount factor defined based on the actual time scale.

For $\theta_i^d(\tau_{\max})$, we have:

$$\begin{aligned} \theta_i^d(\tau_{\max}) \approx & \left[\int_{\tau_{\max}}^{\infty} \lambda_i^* e^{-\lambda_i^* \upsilon} d\upsilon\right] \left[\int_0^{\tau_{\max}} \frac{r_i}{\mu^*} \exp(\frac{\tau}{\mu^*}) e^{-\alpha \exp(\frac{\tau}{\mu^*})} d\tau\right] \\ & + \left[\int_0^{\tau_{\max}} \lambda_i^* e^{-\lambda_i^* \upsilon} \left(\int_0^{\upsilon} \frac{r_i}{\mu^*} \exp(\frac{\tau}{\mu^*}) e^{-\alpha \exp(\frac{\tau}{\mu^*})} d\tau\right) d\upsilon\right] \\ & + \sum_{j>i}^{n} P_{ij} \left[\int_0^{\tau_{\max}} \lambda_i^* e^{-\lambda_i^* \upsilon} e^{-2\alpha \exp(\frac{\upsilon}{\mu^*})} e^{\frac{\upsilon}{\mu^*}} \theta_j^d(\tau_{\max} - \upsilon) d\upsilon\right] \end{aligned} \tag{5.66}$$

An additional factor of $e^{-2\alpha \exp(\frac{\upsilon}{\mu^*})} e^{\frac{\upsilon}{\mu^*}}$ exists in the last term of the above equation

to approximately account for the transformed-time-dependent discounted $r_i(\tau)$ which is a function of the absolute transformed time and does not "restart" itself as if the process is at transformed time zero when there is a transition to another damage state. It is an approximation because $r_i(\tau)$ after the arrival time of the first event in transformed time υ is discounted at a constant discount factor of $e^{-\alpha \exp(\frac{\upsilon}{\mu^*})}$ so that we can take advantage of the unique "repetitive" structure of first transition in Markov processes. To be exact, this discount factor after υ would need to be dependent on absolute transformed time τ which cannot be properly accounted for in the first transition analysis of Markov process. This is a conservative estimate which is fairly accurate for small values of λ_i^* and $\tau_{\max}$ such that υ is reasonably close to the value of $\tau_{\max}$ so that the effects of discounting are not significant.

Also, we note that $\int_0^{\tau_{\max}} \exp(\frac{\tau}{\mu^*}) e^{-\alpha \exp(\frac{\tau}{\mu^*})} d\tau = \frac{\mu^*}{\alpha}\left(e^{-\alpha} - e^{-\alpha \exp(\frac{\tau_{\max}}{\mu^*})}\right)$. Thus:

$$\begin{aligned}\theta_i^d(\tau_{\max}) \approx & \frac{r_i}{\alpha} e^{-\lambda_i^* \tau_{\max}} \left(e^{-\alpha} - e^{-\alpha \exp(\frac{\tau_{\max}}{\mu^*})}\right) \\ & + \left[\int_0^{\tau_{\max}} \lambda_i^* \frac{r_i}{\alpha} e^{-\lambda_i^* \upsilon} \left(e^{-\alpha} - e^{-\alpha \exp(\frac{\upsilon}{\mu^*})}\right) d\upsilon\right] \\ & + \sum_{j>i}^{n} P_{ij} \left[\int_0^{\tau_{\max}} \lambda_i^* e^{-\lambda_i^* \upsilon} e^{-2\alpha \exp(\frac{\upsilon}{\mu^*})} e^{\frac{\upsilon}{\mu^*}} \theta_j^d(\tau_{\max} - \upsilon) d\upsilon\right] \end{aligned} \tag{5.67}$$

Again, we need to perform Laplace transforms in order to obtain the solution as per the homogeneous Markov case. Here, because of algebraic complexity, we fitted Legendre polynomials to $e^{-\lambda_i^* \upsilon}\left(e^{-\alpha} - e^{-\alpha \exp(\frac{\upsilon}{\mu^*})}\right)$ and $\lambda_i^* e^{-\lambda_i^* \upsilon} e^{-2\alpha \exp(\frac{\upsilon}{\mu^*})} e^{\frac{\upsilon}{\mu^*}}$ to allow Laplace transform to be obtained.

For $\theta_i^t(\tau_{\max})$, we have:

$$\begin{aligned}\theta_i^t(\tau_{\max}) = & \sum_{j>i}^{n} P_{ij} \left[\int_0^{\tau_{\max}} \lambda_i^* e^{-\lambda_i^* \upsilon} \left(l_{ij} e^{-\alpha \exp(\frac{\upsilon}{\mu^*})}\right) d\upsilon\right] \\ & + \sum_{j>i}^{n} P_{ij} \left[\int_0^{\tau_{\max}} \lambda_i^* e^{-\lambda_i^* \upsilon} e^{-\alpha \exp(\frac{\upsilon}{\mu^*})} \theta_j^t(\tau_{\max} - \upsilon) d\upsilon\right] \end{aligned} \tag{5.68}$$

This is exact because the transition cost remains as a constant value independent of τ in transformed time space. We performed Legendre polynomial fit to $\lambda_i^* e^{-\lambda_i^* \upsilon} e^{-\alpha \exp(\frac{\upsilon}{\mu^*})}$ in order for Laplace transformations to be performed.

Similar computations involving the Laplace transformations and formulation in vector format follow as per Section 5.2.5 to obtain the desired solution, followed by a transformation to the original time scale.

To introduce repair to the formulations in Sections 5.2.5 and 5.2.6, one would have to assume exponential repair durations in the *transformed time space*. This assumption would imply that the mean repair duration would change as time after the mainshock progressed. An exponential repair duration in the transformed time space is not realistic; a more general methodology with an arbitrary probability distribution for the repair duration will be introduced in Chapter 6. Nonetheless, the formulations in Sections 5.2.5 and 5.2.6 are still valid up to the time of commencement of repair, which can be as long as two years after the mainshock (see Comerio (2000)).

5.3 Incorporation of Losses due to Aftershocks into Pre-Mainshock Loss Estimation

We would now like to incorporate the financial losses from nonhomogeneous Poisson aftershock processes due to future potential mainshocks from different faults into a global pre-mainshock loss estimation formulation. This will be used as an input for establishing an optimal pre-mainshock design criterion to be discussed in Chapter 6.

We first assume that there are h seismic sources that contribute to the pre-mainshock hazard at a site. Takahashi et al. (2004) used a renewal process to model the occurrences of characteristic mainshocks which they have shown to be the main contributors to expected total discounted losses. Thus, here, we also assume that the significant financial losses from aftershocks are mainly due to characteristic ruptures of each of the h sources, where the characteristic magnitude of source q is deterministic with magnitude m_q. We also assume that the rate of loss events for source q is $\lambda_i(q)$ for a building originally in damage state i assuming we use the homogeneous Poisson process to model mainshock occurrences. Alternatively, we can also assume that the inter-arrival time probability density function and cumulative distribution function of loss events from seismic source q are $f_i^q(w)$ and $F_i^q(w)$, respectively, for a building originally in damage state i if we use a renewal process to model mainshock occurrences. W is the inter-arrival time between loss events and s_q is the elapsed time since the last loss event from seismic source q. We also assume that the (closest) source-to-site distance R^q for each of the h seismic sources is known.

Based on the above assumption, for source q, $\theta_i(q, t_{\max})$ from the previous section is equal to the expected financial losses in $[0, t_{\max}]$ from aftershocks for a building in damage state i due to a characteristic rupture of source q from a mainshock of deterministic mainshock magnitude m_q. In Chapter 3, we have shown how to compute the probability of a building originally in damage state i going into damage state j due to a mainshock of known magnitude and source-to-site distance, $P'_{ij}|mainshock$, as well as an aftershock of random magnitude at a random location, $P'_{ij}|aftershock$. In this case, for source q, we can compute the probability of a building in damage state i going to damage state j due to a characteristic mainshock rupture of source q, $P'_{ij}(q)|mainshock$, from which Equations 5.4 and 5.5 can be used to obtain the transition probability matrix $\mathbf{P^m}(q)$. Thus, for seismic source q and a building originally in damage state i, we can compute $\gamma_i(q, t_{\max})$ which we define as the expected financial losses from both mainshocks and aftershocks given the characteristic rupture of source q. We let l_{ij}^m be the expected cost due to a transition from damage state i to damage state j. The superscript m in $\mathbf{P^m}(q)$ and l_{ij}^m specifically denotes that we are considering the appropriate quantities from the characteristic mainshock rupture of source q.

$$\gamma_i(q, t_{\max}) = \sum_{j>i} P_{ij}^m(q) \left[\theta_j(q, t_{\max}) + l_{ij}^m\right] \tag{5.69}$$

We assume that there is no seismic interaction between the h seismic sources, i.e., the rupture of one source is independent of the rupture of another source. We also assume that the inter-arrival time between mainshocks from source q is sufficiently long such that by the time of the next mainshock, there are no more aftershocks resulting from the previous mainshock and that the building would have been restored to its original state i before the occurrence of a subsequent mainshock.

Thus, for a building in damage state i and considering seismic source q, we represent the expected total discounted financial losses from both mainshocks and aftershocks in $[0, t_{\max}]$ as $\delta_i(q, t_{\max})$ in Equation 5.70, where $N_i(q,, t_{\max})$ is the (random) number of loss events from source q in the time interval $[0, t_{\max}]$ for a building originally in damage state i. T_k is the arrival time of the k^{th} loss event from a mainshock.

$$\delta_i(q, t_{\max}) = E \sum_{k=1}^{N_i(q,, t_{\max})} \gamma_i(q, t_{\max} - T_k) e^{-\alpha T_k} \tag{5.70}$$

5.3.1 Formulation using Homogeneous Poisson Process for Mainshock Occurrences

First, we consider using a homogeneous Poisson process to model mainshock occurrences. Under this assumption, given $N_i(q,, t_{\max}) = n$, T_k has a uniform distribution in $[0, t_{\max}]$ and are i.i.d. such that $T_k \overset{D}{=} T$. Thus, we have:

$$\begin{aligned}
&E\sum_{k=1}^{n}\gamma_i(q, t_{\max} - T_k)e^{-\alpha T_k} \\
&= E\left[\gamma_i(q, t_{\max} - T_1)e^{-\alpha T_1} + \gamma_i(q, t_{\max} - T_2)e^{-\alpha T_2} + ... + \gamma_n(q, t_{\max} - T_n)e^{-\alpha T_n}\right] \\
&= n\int_0^{t_{\max}} \frac{1}{t_{\max}}\gamma_i(q, t_{\max} - t)e^{-\alpha t}dt = \frac{n}{t_{\max}}\int_0^{t_{\max}} \gamma_i(q, t_{\max} - t)e^{-\alpha t}dt
\end{aligned} \tag{5.71}$$

Hence:

$$\delta_i(q, t_{\max}) = \lambda_i(q)\int_0^{t_{\max}} \gamma_i(q, t_{\max} - t)e^{-\alpha t}dt \tag{5.72}$$

$\delta_i^*(t_{\max})$ represents the expected total financial losses from both mainshocks and aftershocks in $[0, t_{\max}]$ from all h sources and is equal to:

$$\delta_i^*(t_{\max}) = \sum_{q=1}^{h}\delta_i(q, t_{\max}) \tag{5.73}$$

Here, $\int_0^{t_{\max}} \gamma_i(q, t_{\max} - t)e^{-\alpha t}dt$ can be easily obtained by numerical integration. Again, based on the discussion in Section 5.2.5, we recommend that for $t_{\max} - t$ greater than 5 years, we use $\gamma_i(q, 5 \text{ years})$ in the numerical integration instead. As a conservative approximation, we can also replace $\gamma_i(q, t_{\max} - T_k)$ for all values of T_k by $\gamma_i(q, 5 \text{ years})$ for relatively long inter-arrival times between mainshocks from source q because there is significant discounting effects over such an extended period of time. Based on this assumption, $\delta_i^*(t_{\max})$ is given by:

$$\delta_i^*(t_{\max}) = \sum_{q=1}^{h}\frac{\lambda_i(q)\gamma_i(q, 5 \text{ years})}{\alpha}\left[1 - e^{-\alpha t_{\max}}\right] \tag{5.74}$$

5.3.2 Formulation Using Renewal Process for Mainshock Occurrences

In this case, we use Equations 5.46 to 5.48 derived previously in Section 5.2.4 with slight modification to obtain $\delta_i^*(t_{\max})$. Assuming long inter-arrival times between mainshocks such that the building is restored to state i between occurrences, we obtain Equation 5.75.

$$\delta_i(q,\widetilde{t}_{\max}) = \left[\int_0^{\widetilde{t}_{\max}} f_i^q(w_2)\gamma_i(q,\widetilde{t}_{\max}-w_2)e^{-\alpha w_2}dw_2\right] + \left[\int_0^{\widetilde{t}_{\max}} f_i^q(w_2)\left[e^{-\alpha w_2}\delta_i(q,\widetilde{t}_{\max}-w_2)\right]dw_2\right] \tag{5.75}$$

$$\delta_i^e(q,\widetilde{t}_{\max}) = \frac{\left[\int_0^{\widetilde{t}_{\max}} f_i^q(w_2)\gamma_i(q,\widetilde{t}_{\max}-w_2)e^{-\alpha w_2}dw_2\right]^e}{\left[1-f_i^q(w_2)e^{-\alpha w_2}\right]^e} \tag{5.76}$$

We can then obtain $\delta_i(q,t_{\max})$ as shown in Equation 5.77.

$$\delta_i(q,t_{\max}) = \int_0^{t_{\max}} \frac{f_i^q(s_q+t_1)}{1-F_i^q(s_q)}\left[\gamma_i(q,\widetilde{t}_{\max})+\delta_i(q,\widetilde{t}_{\max})\right]e^{-\alpha t_1}dt_1 \tag{5.77}$$

Again, for $\widetilde{t}_{\max}-w_2$ greater than 5 years, we recommend using $\gamma_i(q,5\text{ years})$ in the numerical integration instead.

One has to solve $\delta_i(q,\widetilde{t}_{\max})$ for different discretized values of $T_1 = t_1$ before solving Equation 5.77 by numerical integration. This will require the computations of aftershock-induced financial losses for as many iterations as we have discretized value of $T_1 = t_1$. Thus, to simplify the computation and as a conservative estimate, we can again replace $\gamma_i(q,\widetilde{t}_{\max}-w_2)$ by $\gamma_i(q,5\text{ years})$ to reduce the number of computations of aftershock-induced financial losses that are required. If we further assume that there is only one characteristic mainshock rupture in $[0,t_{\max}]$ (which is reasonable given the assumption of a renewal process model for mainshocks), then Equation 5.77 simplifies to Equation 5.78.

$$\delta_i(q,t_{\max}) = \int_0^{t_{\max}} \frac{f_i^q(s_q+t_1)}{1-F_i^q(s_q)}\left[\gamma_i(q,\widetilde{t}_{\max})\right]e^{-\alpha t_1}dt_1 \tag{5.78}$$

$\delta_i^*(t_{\max})$ can then be computed easily. Numerical results will be shown in the next section.

5.4 Example

A simple numerical example is presented here to illustrate the above formulations. Unless otherwise specified, we will consider the original, stronger building described in Chapter 3. The transition probabilities for the original, stronger SMRF building located at the site described in Chapter 2 given a characteristic mainshock on the Mid-Peninsula Segment are shown in Figure 3.7. The transition probabilities for the original, stronger SMRF building in Figure 3.8 given an aftershock of random magnitude at a random location are obtained for the mainshock rupture and site location in Chapter 2. We assume that the characteristic rupture described in Chapter 2 is the main contributor to the mainshock hazard at the site. The value of the building structure is taken to be \$160M and the value of the contents of the building is taken to be \$50M, making the total value of the building equal to \$210M. The expected financial losses are shown in Table 5.2. We denote $i = 1$ as the intact building state. Expected transition losses, l_{ij}, $i \neq 1$, are found by taking the difference between $l_{1j} - l_{1i}$. For example, if the building transits from $DS1$ to $DS2$, then the resulting expected transition losses is $l_{1DS2} - l_{1DS1} = 0.5 \text{ x } 210 - 0.25 \text{ x } 210 = \$52.5\text{M}$, and the expected disruption losses in $DS2$ is \$0.075M/day. The annual discount rate is taken to 3.5%.

Table 5.2: Potential financial losses for each building damage state

i	*Expected Disruption Losses*($\$M/day$), r_i	$\frac{Expected\ Transition\ Losses,\ l_{1i}}{Total\ Value\ of\ Building}$
$DS1$	0.05	0.25
$DS2$	0.075	0.5
$DS3$	0.1	0.75

Using the procedure described in Sections 5.2.1 and 5.2.2 assuming $\mu = 0.0067$/year, we compute the expected total discounted losses for the intact building due to a homogeneous mainshock Poisson process with Markov damage states using the transition matrix in Figure 3.7. We first compute the expected present values of the losses for different values of $t_{\max}$ assuming an unlimited random number of transitions in $[0, t_{\max}]$. The results for $t_{\max} \leq 10$ years and $t_{\max} \leq 100$ years are shown in Figure 5.1. It can be seen that both the expected transition losses and disruption losses increase with $t_{\max}$ and they approach a constant due to the significant effects of discounting for large values of $t_{\max}$. For $t_{\max} \leq 10$ years where discounting is not significant and where we expected no more than one transition, the expected transition losses are almost linear, agreeing with our conclusion in Section

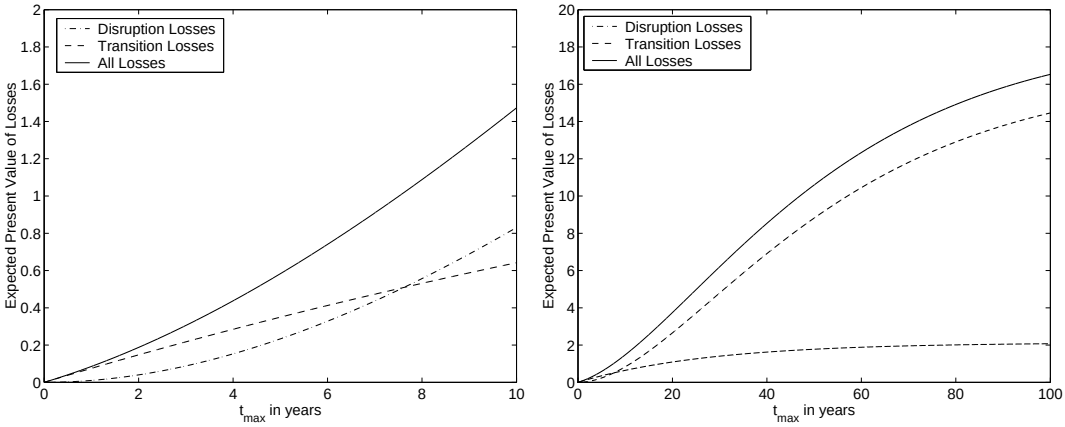

(a) $t_{\max} \leq 10$ years (b) $t_{\max} \leq 100$ years

Figure 5.1: Expected total mainshock losses ($M) for the intact building assuming an unlimited random number of transitions for different values of $t_{\max}$ in the pre-mainshock environment. Both transition and disruption losses are shown as well.

5.1.1. Note also that for $t_{\max} \leq 8$ years, the expected transition losses are slightly higher than the expected disruption losses, but for $t_{\max} \geq 8$ years, the reverse is true instead. This observation can be attributed to the fact that if the intact building transits to $DS1$ or worse, it starts to incur a daily disruption cost which increases in value for the duration that the building remains in that damage state. Note that if the building remains in the intact state, there are no disruption losses. Such accumulation of disruption losses for damaged buildings are more significant than one-time transition losses, which explains why the expected disruption losses are larger than the expected transition losses for $t_{\max} \geq 8$ years as the probability of a transition to a worse damage state is increased for increasing values of $t_{\max}$. Note that we have not considered any repair operations here.

The low rate of mainshocks implies that more than two mainshocks in 100 years is unlikely such that the formulation assuming no more than one transition gives only slightly lower results than the formulation assuming an unlimited random number of transitions, especially for low values of $t_{\max}$. The results are shown in Figure 5.2.

We next consider a mainshock example with exponentially distributed repair durations back to the intact state. We consider mean repair durations of 18 days, 60 days and 270 days for $DS1$, $DS2$ and $DS3$, respectively, and we use the formulation in Section 5.2.3, with both transition and disruption losses taken into account. The expected total losses

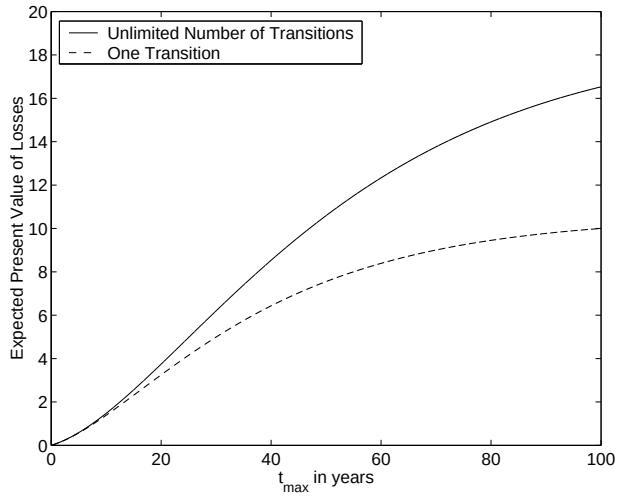

Figure 5.2: Expected total mainshock losses for the intact building assuming no more than one transition and assuming an unlimited random number of transitions for different values of $t_{\max}$ in the pre-mainshock environment.

(including both transition and disruption losses) with no repair and with repair are shown in Figure 5.3. It is clear that the expected total losses are much lower in value if we consider

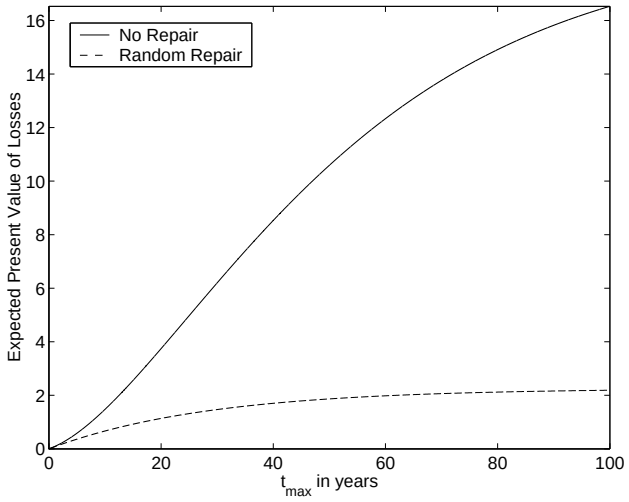

Figure 5.3: Expected total mainshock losses for the intact building assuming no repair and repair (with exponentially distributed repair durations) for different values of $t_{\max}$ in the pre-mainshock environment.

the possibility of repair back to the intact state for damaged buildings.

We also consider a case with instant repair. Note that the instant repair formulation in Section 5.1.1 only includes one-time transition losses. Hence, to be consistent with the formulation in Section 5.1.1, we consider only transition losses (and not disruption losses) in the formulation with no repair and the formulation with repair (with exponentially distributed repair durations) as well. The resulting expected total transition losses are shown in Figure 5.4. It is worthwhile noting that the expected total transition losses are

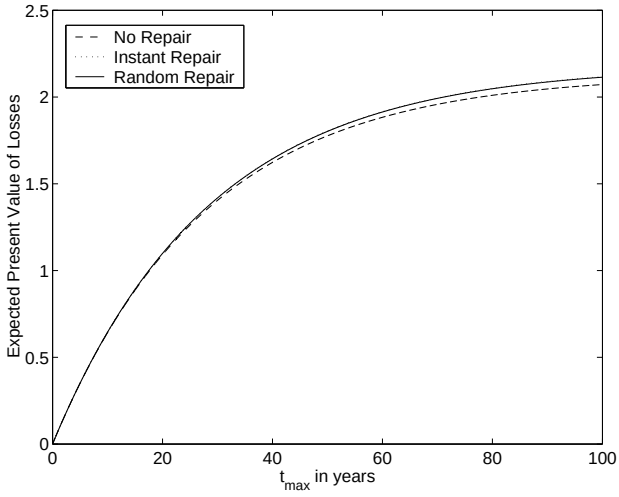

Figure 5.4: Expected total mainshock transition losses for the intact building assuming no repair, instant repair and random repair with exponentially distributed repair durations for different values of $t_{\max}$ in the pre-mainshock environment.

very similar for all three formulations. The cases with instant repair and random repair are almost indistinguishable in Figure 5.4 because the mean repair rates for damaged buildings are considerably higher than the mean transition rates to a worse damage state due to mainshock occurrences for a damaged building, or in other words, the mean time to repair is small relative to the mean time between events. Hence the likelihood of repair back to the intact state is considerably higher than the likelihood of progressive damage. Note, also, in this case, the counter-intuitive results where the expected transition losses with repair are slightly higher than the expected transition losses without repair. This conclusion can be attributed to the fact that the intact building is five times more likely to be progressively damaged as compared to other damage states (see the transition matrix in Figure 3.7) and the expected transition losses are assumed to be the same when we progress from state i to state $i+1, ..., n$, for all values of i. Thus, the formulation with repair increases the likelihood

of transiting to the intact state which actually increases the expected total transition losses. Note that we are not considering disruption losses here – the inclusion of disruption losses will significantly reduce the expected total losses with repair, since the intact state does not incur any disruption cost. The example with both disruption losses and transition losses has been shown previously in Figure 5.3.

Next we use a Brownian Passage Time (BPT) renewal process to model mainshock occurrences, following USGS (2003). The inter-arrival time distribution is shown in Equation 5.79.

$$f_{BPT}(t) = \sqrt{\frac{\varkappa}{2\pi\alpha^2 t^3}} e^{-\frac{(t-\varkappa)^2}{2\varkappa t\alpha^2}} \tag{5.79}$$

$\varkappa$ is the mean inter-arrival time defined as $\frac{1}{\mu}$ and α is the aperiodicity or coefficient of variation defined as the ratio of the standard deviation to the mean. Consistent with $\mu = 0.0067$/year, we use $\varkappa = 150$ years. Further, we assume $\alpha = 0.5$. We also use a exponential inter-arrival time distribution with the same value of $\varkappa$ (corresponding to a Poisson mainshock process) as well as a gamma distribution with the same value of $\varkappa$ and α to approximate the BPT model, following Takahashi et al. (2004). The probability density functions are shown in Figure 5.5 and the hazard rate functions are shown in Figure 5.6.

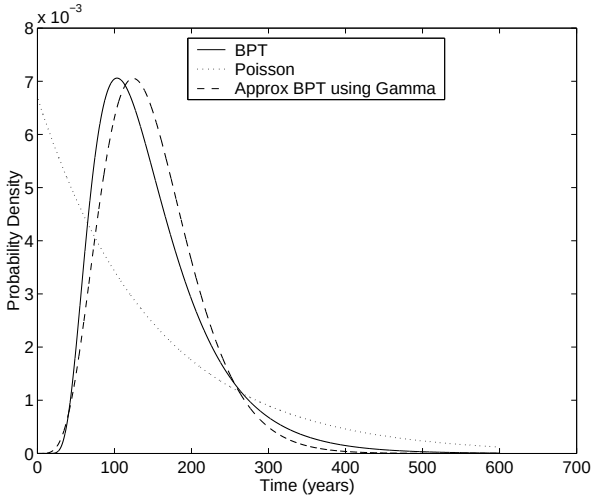

Figure 5.5: Probability density functions for interrarrival times of BPT model, Poisson model and gamma approximation of the BPT model.

Note that the gamma distribution provides a good approximation to the BPT inter-arrival time distribution, so we shall use it for subsequent computations. Note also that the hazard

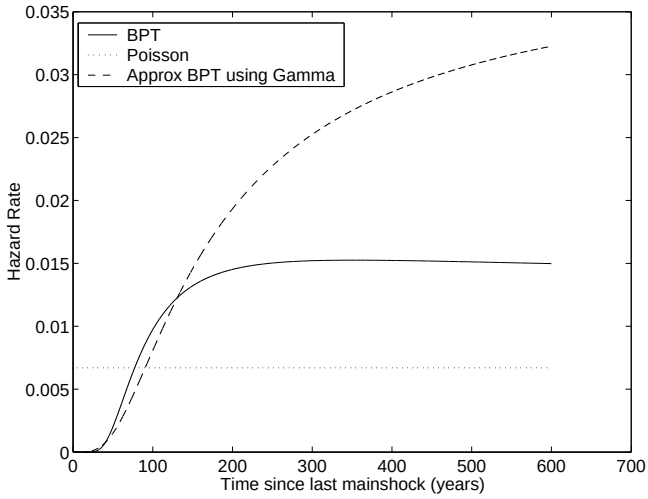

Figure 5.6: Hazard rate functions for interrarrival times of BPT model, Poisson model and gamma approximation of the BPT model.

rate function of the BPT model approaches an asymptotic limit and is not monotonically increasing, as compared to the monotonically increasing nature of the gamma inter-arrival time distribution.

We next compute the expected financial losses for different values of $t_{\max}$ using the Poisson model and the BPT model (approximated by the gamma distribution) for elapsed time since the last mainshock, s, equal to 0 years, 98 years (the last rupture of the Mid-Peninsula segment was in 1906) and 150 years. The results for the intact building are shown in Figure 5.7. The BPT model with $s = 0$ gives considerably lower values of expected losses as compared to the Poisson model because the hazard rate function starts from zero and takes about 100 years (corresponding to about $\frac{2}{3}\varkappa$) before it increases to the level implied by the Poisson model. This means that a mainshock in $[0, t_{\max}]$ (for $t_{\max} \leq 100$ years) is highly unlikely for $s = 0$ as compared to the Poisson model, thus leading to much lower values of expected losses. In contrast, for $s = 98$ years and $s = 150$ years, the hazard rate functions are higher than that implied by the Poisson model such that a mainshock is more likely in $[0, t_{\max}]$ for the corresponding BPT models as compared to the Poisson model, thus resulting in higher values of expected losses. We have not considered repair in this example.

We now turn our attention to the losses in the *aftershock* environment using the transition matrix in Figure 3.8. We first compute expected losses, both undiscounted and discounted, due to aftershocks given the mainshock rupture and site location described in

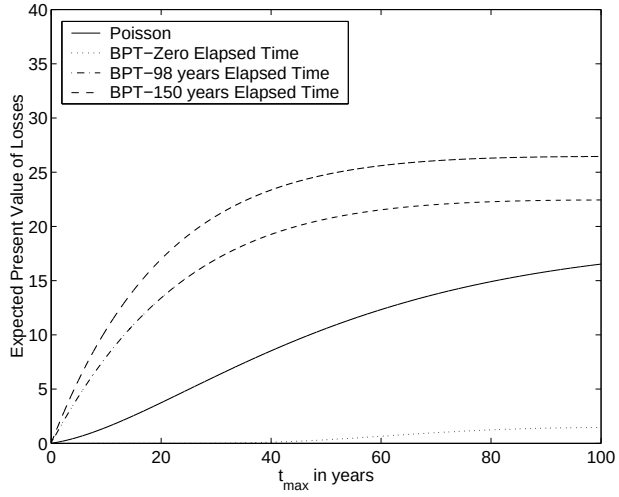

Figure 5.7: Expected total mainshock losses ($M) for the intact building using Poisson and BPT model for different values of $t_{\max}$ in the pre-mainshock environment.

Chapter 2 using the formulation in Sections 5.2.5 and 5.2.6. We shall also compare the results with those obtained using stochastic dynamic programming, a numerical procedure which will be described in detail in the next chapter, which provides us with more accurate results. The resulting graphs for different values of $t_{\max}$ are shown in Figure 5.8. One can see that for all initial post-mainshock damage states, the undiscounted and discounted losses obtained using the analytical formulations agree almost exactly with those obtained using the numerical dynamic programming procedure for $t_{\max}$ less than five years. The analytical formulations with and without discounting also agree very well with each other for $t_{\max} \leq 5$ years. For $t_{\max}$ more than five years, the formulation with no discounting provides a conservative estimate of expected discounted losses. The expected losses obtained using the analytical formulation with discounting also agree very well with the results obtained from numerical dynamic programming (in Chapter 6) for all initial post-mainshock damage states. In this case, we have not considered the possibility of any repair operations.

The procedure using dynamic programming (from Chapter 6) also allows us to incorporate repair operations back to the intact state. The time to repair is treated as a random variable with, for example, a longer average time to repair for $DS2$ to intact than $DS1$ to intact. Details of the formulation including such repair operations will be described in Chapter 6. Here, we provide a plot from Chapter 6 in Figure 5.9 for the weaker building described in Chapter 3 which demonstrates the significant reduction of expected losses if

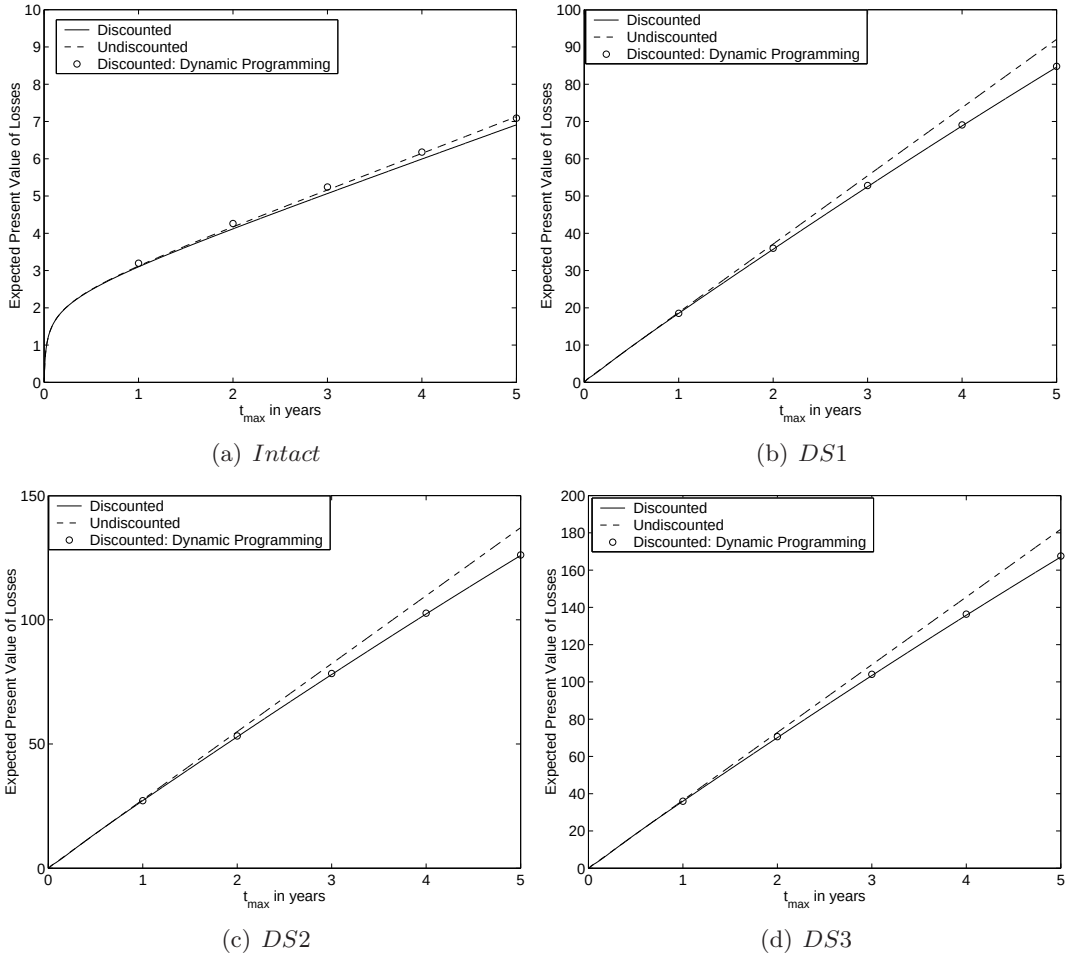

(a) *Intact* (b) $DS1$

(c) $DS2$ (d) $DS3$

Figure 5.8: Discounted and undiscounted expected aftershock losses ($M) for different values of $t_{\max}$ in the post-mainshock environment for all post-mainshock damage states.

we introduce the possibility of repair back to the intact state.

We next use the formulation in Section 5.3.1 to compute the pre-mainshock expected losses due to both mainshocks and aftershocks for different values of $t_{\max}$. We assume that mainshocks are modeled as a homogeneous Poisson process. The results for the original building in Chapter 3 are shown in Figure 5.10. We consider both the exact and approximate formulations described in Section 5.3.1. We observe that both formulations agree very well with each other for all values of $t_{\max}$. We also compute the expected aftershock losses and pre-mainshock losses for the original building and the weaker building described in Chapter 3, assuming an initial intact state. The results are shown in Figure 5.11. One can see that

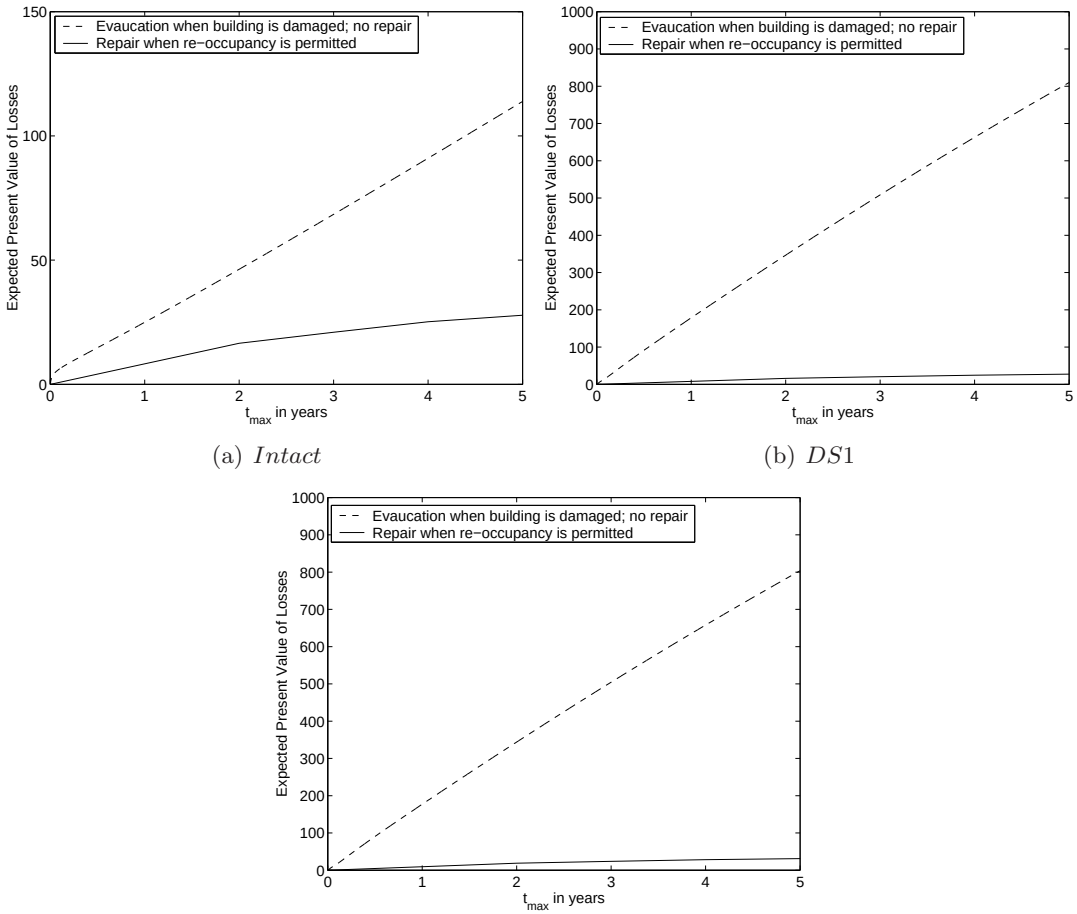

(a) *Intact* (b) $DS1$

(c) $DS2$

Figure 5.9: Expected total financial losses ($M) for all post-mainshock damage states with repair (solid line) and without repair (dotted line) for different values of $t_{\max}$ in the post-mainshock environment. In the former case, repair requires a random duration after arriving in a particular damage state. (Numerical assumptions are given in Chapter 6.)

the expected losses are considerably higher for the weaker building. Such pre-mainshock loss estimation can be used as an input to pre-mainshock design criteria to be described in Chapter 6.

We next study the contribution of aftershocks to pre-mainshock financial loss estimation. We consider only transition costs in the analysis, and we compute the expected total transitions losses considering only mainshocks as well as the expected total transition losses considering both mainshocks and the subsequent aftershocks. The results are shown in

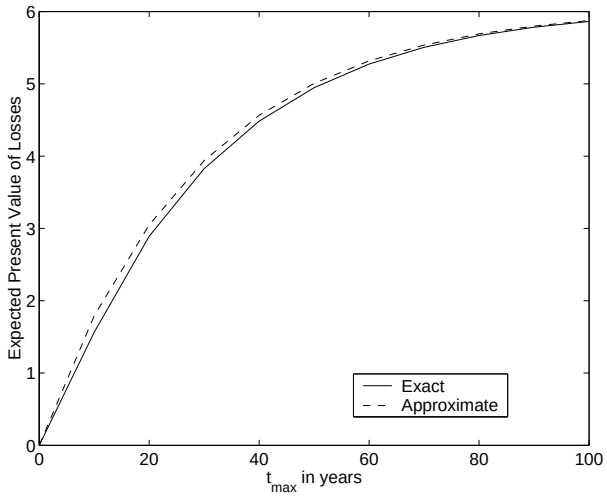

Figure 5.10: Expected financial losses ($M) from both mainshock and aftershocks using the exact and approximate formulation for different values of $t_{\max}$ in the pre-mainshock environment.

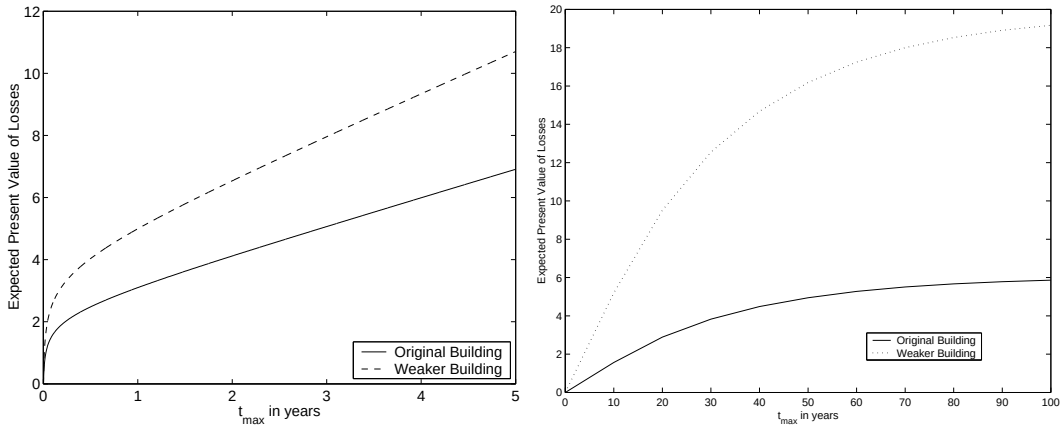

(a) (b)

Figure 5.11: (a) Expected aftershock losses. (b) Expected pre-mainshock losses for both buildings for different values of $t_{\max}$ assuming intact initial state.

Figure 5.12. One can see from Figure 5.12 that the inclusion of future aftershocks increases the expected financial losses by about 25% as compared to the case where no aftershocks have been taken into consideration. Hence, using the particular assumptions made here, the consideration of financial losses due to future aftershocks has an impact on pre-mainshock

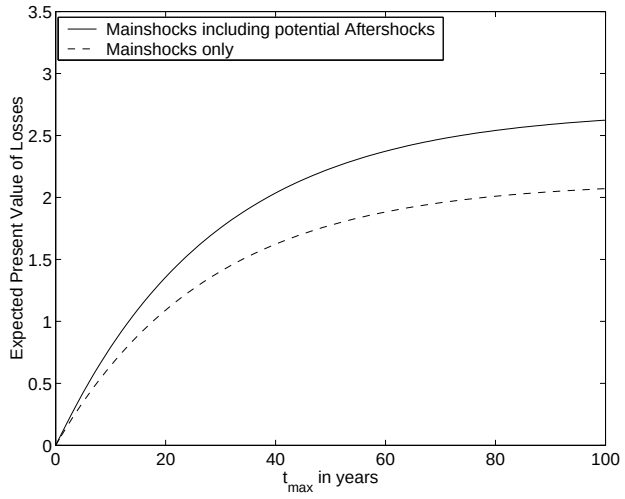

Figure 5.12: Expected total pre-mainshock transition losses ($M) considering (1) Mainshocks only and (2) Mainshocks and subsequent aftershocks. The results are obtained for different values of $t_{\max}$.

financial loss estimation as well.

Lastly, we compute pre-mainshock losses incorporating future potential aftershocks assuming several cases for the mainshocks: the homogeneous Poisson model and BPT model with $s = 0,98$ and 150 years for mainshocks. The results for the original building are shown in Figure 5.13. Similar to the earlier observation in Figure 5.7, the BPT model with $s = 0$ results in considerably lower expected losses as compared to the Poisson model, while the BPT models with $s = 98$ and 150 years result in considerably higher expected losses. This observation can again be attributed to the magnitude of the hazard rate function with $s = 0,98$ and 150 years when compared to the constant hazard rate function for the Poisson model.

5.5 Conclusion

We present a sequence of gradually improving financial life-cycle loss models starting from homogeneous Poisson mainshocks and nonhomogeneous Poisson aftershocks to models using renewal processes to describe mainshock occurrences with Markov descriptions of a building's damage states. We also developed models to estimate pre-mainshock losses by incorporating future aftershock losses from potential future mainshocks. Such financial

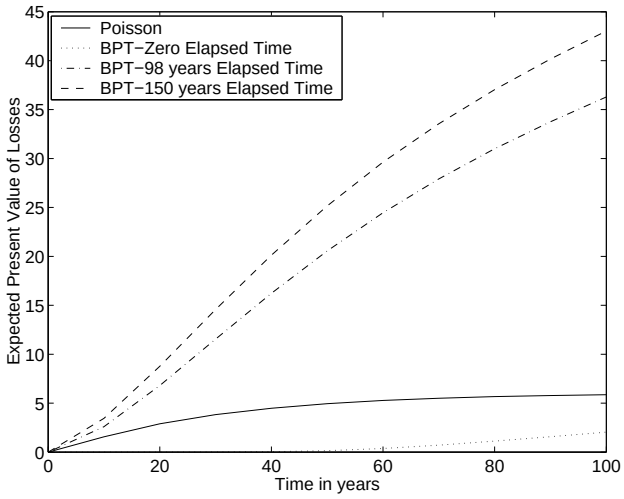

Figure 5.13: Expected total pre-mainshock financial losses ($M) including potential aftershock losses using Poisson and BPT model for different values of $t_{\max}$.

loss models serve as an input to the decision making methodology (both post- and pre-mainshock) that will be the subject of discussion in the next chapter.

6 Seismic Decision Analysis

In Chapter 4, we proposed a building tagging methodology for making evacuation and re-occupancy decisions based on the life-safety threat posed by the aftershock environment. The building tagging decision is an example of decision making in earthquake risk management. The proposed decision basis for building tagging is the rate of collapse due to aftershocks, where the collapse rate is used as a proxy for individual fatality risk. There are other examples of decision making in seismic risk management where different decision bases are used to select the most desirable action. Such decision-analytic frameworks are generally probabilistic in nature where there is explicit quantification of the stochastic nature of earthquake occurrences and the large uncertainty in seismic demand and structural capacity. Potential costs and benefits are also quantified. The "optimal" decision is generally selected to be the one that minimizes the expected value of a certain quantity, generally defined in terms of financial losses as well as fatalities.

The building tagging methodology in Chapter 4 is based on the assumption that there is complete knowledge of the post-event damage state of the building. In practice, one is unlikely to have perfect information immediately after the mainshock. More information about the building's damage state (e.g., with detailed inspection and/or engineering analysis) may potentially allow one to make better tagging decisions. Hence, the methodology developed in this chapter is designed to be sensitive to the state of information about the damage sustained by the building. Other decisions in seismic risk management can potentially be sensitive to the state of information about uncertain quantities as well. We next discuss a few representative past economic risk management studies.

Chou et al. (1973) formulated the structural design problem of a seismic structure as a decision analysis problem with two discrete options in which the choice was between steel or reinforced concrete for the design of a (linear) one-story building structure based on minimizing the total cost of construction and expected failure cost and the probability of

yielding. They considered the randomness in earthquake magnitude and duration in the decision analysis process.

In a multi-year project, Whitman et al. (1974) developed procedures for making rational choices of seismic design requirements in building codes based on the quantification of the risk of earthquake shaking (using the modified Mercalli intensity), the likelihood of building damage and the cost of increasing levels of earthquake resistance. They considered decision bases such as expected total financial losses, percentage of lives lost, etc.

Paté and Shah (1980) presented a method of probabilistic cost-benefit analysis for making decisions about building code requirements and retrofit strategies of old existing structures. They used the expected cost per life saved as a decision basis for making such decisions. Paté (1985) further studied the cost and benefits of seismic upgrading of unreinforced masonry warehouses and reinforced concrete buildings in the Boston area. She concluded that on the basis of minimizing the expected cost per life saved, the optimal decision is to strengthen the unreinforced masonry buildings.

PEER is currently spearheading an effort to develop a quantitative PBEE methodology which will allow stakeholders to make better informed decisions by providing them with probabilistic descriptions of system-level performance metrics. A consistent probabilistic framework is used to explicitly and rigorously quantify the inherent uncertainties and randomness in earthquake intensity measures (IMs), engineering demand parameters (EDPs), damage measures (DMs) and decision variables (DVs). Details of the PEER methodology can be found in Moehle and Deierlein (2004) and Porter (2003).

These past studies did not explicitly recognize the role of information in potentially reducing the uncertainty in quantities such as post-earthquake building damage. The availability of more information can potentially have a significant influence on the decision making process. In this chapter, we shall address the information-sensitive nature of decision making and introduce a method to quantify the impact (and consequently, the financial desirability) of additional information (at potentially higher costs) on the quality of decision. We shall also outline procedures for making optimal decisions in both the post- and pre-mainshock scenarios that explicitly include both financial losses and human fatalities. Examples of such decisions are pre-mainshock design and post-quake repair and re-occupancy. The nonhomogeneous aftershock ground motion hazard which had not been considered in previous studies will be explicitly quantified using APSHA. We use procedures based on minimization of expected financial losses subject to a constraint on minimal level

of individual life-safety as well as procedures where the cost of fatality is explicitly included. The formulations of mean rate of collapse due to aftershocks developed in Chapter 4 and life-cycle financial losses developed in Chapter 5 will be used. The ability to make optimal decisions in both post- and pre-mainshock scenarios potentially has an important impact on earthquake policy decision making.

6.1 Decision Analysis Using Decision Trees

Methods of making decisions under uncertainty, commonly referred to as *decision analysis*, are well-established procedures. Decision analysis is a quantitative tool developed in management science and operations research for selecting optimal decisions based on the specification of the *alternatives*, $information$ and $preferences$ of the decision maker. See, for example, Howard and Matheson (1984) and Raiffa and Schlaifer (1961) on the theory of decision analysis. In this chapter, we shall focus on the most essential aspects of modern decision theory as applied to earthquake engineering. It is worthwhile noting that decision analysis continues to be an active area of research with applications in many diverse fields such as medicine, engineering, business and finance.

The first step of decision analysis is to identify the alternatives that are available to the decision maker. For example, in the post earthquake scenario, the building owner or engineer can choose either to evacuate building occupants or not. Another decision faced by the building owner is whether or not to repair the building, and if so, when repair should commence. Pre-mainshock decisions include new building design alternatives and whether or not to retrofit a building prior to the occurrence of an earthquake, etc.

The second step of decision analysis is to quantify the probabilities of occurrence of events and the probability distributions of uncertain quantities. In the context of decision analysis, probabilities represent individual, subjective degrees of belief of the chance of occurrence of an event or an uncertain quantity taking on a certain specified value. Thus, probabilities assigned to random variables are conditioned on the current state of information. With more information, such probabilities can potentially be "updated", or revised from previous estimate, using Bayes' rule which will be discussed in an example to follow. This view of probability is commonly referred to as the "Bayesian" view, which differs from the classical "frequentist" view where probabilities are based on long-run frequencies of occurrences with fixed (albeit uncertain) values. In the Bayesian view, because probabilities

can potentially be changed with increasing levels of information, the decision maker might be faced with the option to decide if obtaining more information (at potentially higher costs) is financially desirable. Decision analysis provides a quantitative tool to calculate the *value of information*, a concept which can be used to determine if more detailed information gathering can potentially improve the decision making process. This will be discussed later as well.

The third step of decision analysis is to quantify the preferences of the decision maker. For example, the decision maker (the building owner, for example) may want to minimize the expected monetary financial losses or the fatalities[1] due to potential earthquakes. He will then select the optimal decision as the one that minimizes that quantity. The above approach to decision analysis provides a methodology to select the optimal decision based on explicit quantification of the alternatives, information and preferences of the decision maker. We shall adopt this procedure to several examples in seismic decision making with a focus on examples involving post-mainshock decisions and the aftershock threats. One objective of these examples is to demonstrate that these procedures have a role in the formulation and solution of a variety of problems confronting the earthquake community.

6.1.1 Example

We adopt for illustration the base case aftershock scenario in Chapter 2 and the three-story SMRF building described in Chapters 3 and 4. In Chapter 3, we have already calculated the probability of each post-mainshock damage state due to a characteristic mainshock ($m_m = 7.0$) rupturing the Mid-Peninsula segment of the San Andreas fault. We have also computed the damage state transition probabilities due to the occurrence of an aftershock of random magnitude at a random location on the aftershock zone (given the above characteristic rupture) for different post-mainshock damage states. We shall use these values in the example.

[1] In addition to monetary values and fatalities, classical decision theory suggests that the expected *utility* of the decision maker is the quantity that ought to be maximized. The utility function of a decision maker takes into account his risk attitude, and is not considered in this study. If the expected financial losses is chosen to be the quantity to be minimized, the implicit assumption is that the decision maker is *risk-neutral*. See Howard (1998) for details.

Updating Example

After a mainshock, a commonly faced decision by building owners and engineers is whether or not to evacuate building occupants. In Chapter 4, we assumed that the post-mainshock damage state of the building was known. Here, we shall assume that after the mainshock, the damage state is not known with certainty and we model the decisions and uncertainties involved using a "decision tree" in Figure 6.1. The two decisions (evacuate or not)

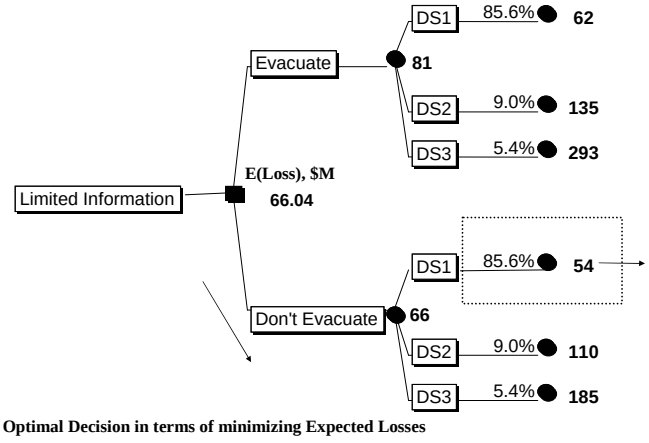

Figure 6.1: Decision tree with limited information about the post-mainshock damage state of the building. Continued in Figure 6.2.

are indicated on the first "branch" of the tree. We assume that the building has not collapsed but has suffered partial damage, the exact degree of which is unknown. Based on this limited information, we can calculate the probabilities of the building being in damage state $DS1$, $DS2$ or $DS3$ given that the building has not collapsed ($\overline{C}$) and is not intact ($\overline{Intact}$). These conditional probabilities are calculated to be: $P(DS1|\overline{C}, \overline{Intact}) = 85.6\%, P(DS2|\overline{C}, \overline{Intact}) = 9.0\%$ and $P(DS3|\overline{C}, \overline{Intact}) = 5.4\%$. For example, using the values obtained in Chapter 3, $P(DS3|\overline{C}, \overline{Intact}) = \frac{0.0085}{0.133+0.0141+0.0085} = 5.4\%$. These conditional probabilities are commonly referred to as the *prior* distribution (on the state variable) which is conditioned on the current state of information that is available. We have very limited information in this case, since we only know that the building has not collapsed and has suffered partial damage. These conditional probabilities are indicated on the second set

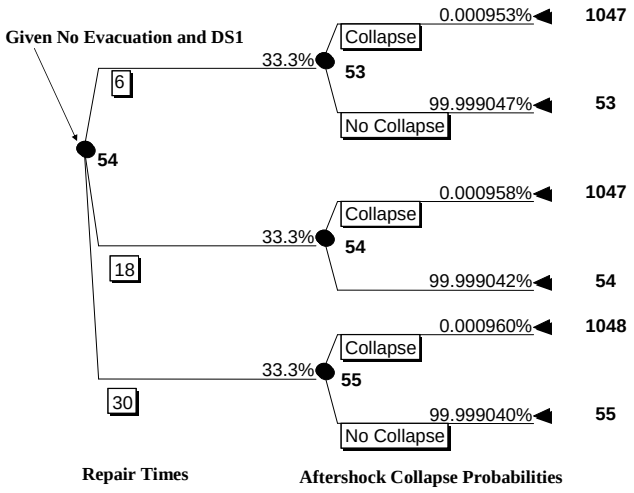

Figure 6.2: Continuation of decision tree in Figure 6.1 assuming no evacuation and $DS1$.

of branches of the decision tree in Figure 6.1[2]. We shall henceforth suppress the condition on $\overline{C}$ and $\overline{Intact}$.

The other major uncertainties are the length of the repair period and whether the building collapses in an aftershock for each post-mainshock damage state of the building. We assume here (simplistically) that repair can commence immediately after the mainshock, and that the possible durations for repair for $DS1, DS2, DS3$ are 6, 18 or 30 days, 30, 60 or 90 days and 180, 270 or 360 days, respectively. Each of these three sets of durations for repair is assumed to be equally likely. The broad range may reflect in part the post-quake disruption in the construction industry. As defined in Chapter 4, the rate of collapse is approximated by $ECR_{\text{col}}^{DSi}(t_d; m_m = 7.0)$ for a building in damage state DSi.

We use the same cost information as in Chapter 5. Again, the value of the building is assumed to be \$160M and the value of the contents of the building is assumed to be \$50M. The expected downtime and damage costs from Chapter 5 are reproduced in Table 6.1, together with the expected repair costs for each post-mainshock damage state. The expected disruption cost if the building is evacuated is taken to be \$0.5M/day. We assume that the number of building occupants is 400. In this example, we consider financial losses due to fatalities explicitly by assuming a cost per life saved equal to \$2M/person[3]. If

[2]Note that the decision nodes on the tree are denoted by solid squares and nodes from which uncertain current (or future) states branch are denoted by solid circles.

[3]The economic value of human life is a much debated issue in economics and is not the main purpose

Table 6.1: Potential financial losses for each building damage state

i	$Expected\ Disruption\ Losses(\$M/day)$, r_i	$\frac{Expected\ Transition\ Losses,\ l_{1i}}{Total\ Value\ of\ Building}$
$DS1$	0.05	0.25
$DS2$	0.075	0.5
$DS3$	0.1	0.75

i	$Expected\ Repair\ Cost(\$M)$
$DS1$	0.5
$DS2$	0.1
$DS3$	0.15

building occupants are not evacuated and the building collapses in an aftershock, we assume for simplicity that the collapse occurs mid-way during the process of repair, all building occupants are killed and the remaining value of the building is lost. If building occupants are not evacuated and the building is further damaged due to the occurrence of an aftershock, we assume that the expected transition losses, l_{ij}, for $i \neq 1$, can be found by taking the difference between $l_{1j} - l_{1i}$. If building occupants are evacuated and the building collapses in an aftershock, we assume that only one-fourth of the remaining value of the building is lost as expensive equipment might have been removed from the building. If building occupants are evacuated and the building is further damaged due to the occurrence of an aftershock, we assume that the expected transition losses are one-fourth of that as from the case where there is no evacuation.

In a next example, we assume that a structural engineer can provide the owner with perfect information on the true damage state of the building, perhaps with very detailed inspection results. This means that if the building is in DSi, then the probability that the engineer says that the building is in DSi is equal to 1. In the example to follow, we shall consider less than perfect information in which case this number is less than 1. In general, we denote this conditional probability as $P(\text{“}DSi\text{”}|DSi)$, where “$DSi$” represents the event that the engineer says that the building is in DSi. This conditional probability is known as the *likelihood* function. In this case, we should re-draw our decision tree in Figure 6.1 as Figure 6.3 such that the first branch represents the event that the engineer says that

of this report. One possible way to compute the economic value of human life is to approximate it by the amount of investment into safety technologies necessary to reduce the risk of fatality by a given amount, i.e., cost per life saved. See Paté-Cornell (1984) and a brief discussion in Chapter 4.

the building is in post-mainshock damage state DSi (an event with the prior probabilities indicated previously), followed by the decision to evacuate or not after obtaining the information from the engineer. The information provided by the engineer is "perfect" in

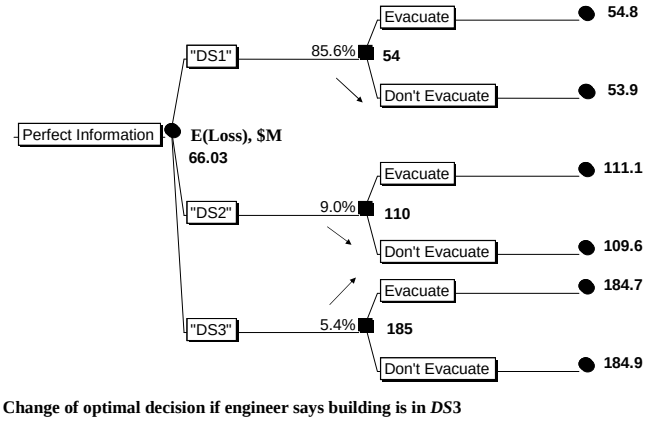

Figure 6.3: Decision tree with perfect information from engineer.

this case, and the engineer is referred to in decision analysis literature as being a *clairvoyant*. The complete state of perfect information provided by him is commonly referred to as "clairvoyance".

In this example, if the engineer says that the building is in $DS1$ or $DS2$, the optimal decision will be to not evacuate building occupants; if he says that the building is in $DS3$, the optimal decision will be to evacuate building occupants. Note that the optimal decisions in this case depend on what the engineer says after his inspection. The optimal decisions have changed from the previous case when we had limited information about the post-mainshock damage state of the building and where the optimal decision is to not evacuate building occupants. The minimum expected financial losses is also reduced when we are able to obtain the information about the true damage state of the building from the engineer.

Since we are able to reduce the minimum expected financial losses by approximately \$10,000 with perfect information from the engineer, this new information regarding the true damage state of the building is useful to us. This sum of \$10,000 is referred to as the value of "perfect information" or value of "clairvoyance". Thus, we ought to be willing to pay the engineer up to a sum of \$10,000 for the information about the true damage state of the building as it lowers our minimum expected financial losses. The ability to compute the value of clairvoyance allows one to decide if it is financially desirable to pay for perfect

information.

Of course, in most cases, the information that we receive from engineers is not perfect. For example, let us assume (for the sake of argument) that the engineer is not perfect but still accurate with his assessment such that if the building is in DSi, then the probability that he says that the building is in DSi (the likelihood function discussed earlier) is equal to 98%, or $P(\text{“}DSi\text{”}|DSi) = 98\%$ (as opposed to a probability of one previously). Other assumed values of $P(\text{“}DSj\text{”}|DSi)$ are given in Table 6.2.

Table 6.2: Likelihood functions of “imperfect” engineer

$P(\text{“}DS1\text{”}\|DS1)$	0.980	$P(\text{“}DS1\text{”}\|DS2)$	0.005	$P(\text{“}DS1\text{”}\|DS3)$	0.005
$P(\text{“}DS2\text{”}\|DS1)$	0.015	$P(\text{“}DS2\text{”}\|DS2)$	0.980	$P(\text{“}DS2\text{”}\|DS3)$	0.015
$P(\text{“}DS3\text{”}\|DS1)$	0.005	$P(\text{“}DS3\text{”}\|DS2)$	0.015	$P(\text{“}DS3\text{”}\|DS3)$	0.980

Now, using the prior distribution shown in Figure 6.1, we can calculate the probability that the engineer will tell us that the building is in a particular state, $P(\text{“}DSi\text{”})$, using Equation 6.1 by the total probability theorem.

$$P(\text{“}DSi\text{”}) = \sum_j P(DSj)P(\text{“}DSi\text{”}|DSj) \tag{6.1}$$

For example, $P(\text{“}DS2\text{”})$ is equal to $(0.856)\,(0.015) + (0.09)\,(0.98) + (0.054)\,(0.015) = 0.102$. This probability, $P(\text{“}DSi\text{”})$, is referred to as the *pre-posterior* probability of state DSi. The set of probabilities, for all DSi, is the pre-posterior distribution. Now, suppose that we hire the engineer and he says that the building is in DSi, i.e., the outcome is “DSi”, one can use Bayes' Rule (see Benjamin and Cornell (1970)) to calculate the *posterior* probability, defined as $P(DSj|\text{“}DSi\text{”})$, using Equation 6.2.

$$P(DSj|\text{“}DSi\text{”}) = \frac{P(DSj)P(\text{“}DSi\text{”}|DSj)}{\sum_j P(DSj)P(\text{“}DSi\text{”}|DSj)} = \frac{P(DSj)P(\text{“}DSi\text{”}|DSj)}{P(\text{“}DSi\text{”})} \tag{6.2}$$

Thus, given that the engineer *says* that the building is in $DS2$, the probability that it is indeed in $DS2$ is equal to $\frac{(0.09)(0.98)}{0.102} = 0.866$. With this new information provided by the engineer, the probability that the building is in $DS2$ increases from 0.09 to 0.87. Obtaining more information commonly (but not always) increases the probability of one or more

states, sharpening or narrowing the probability distribution on the possible states[4]. This procedure of updating our probabilities with new information is commonly referred to as *Bayesian updating*.

We re-draw our decision tree in Figure 6.1 as Figure 6.4 such that the first branch represents the event that the engineer says that the building is in damage state DSi with probabilities $P(\text{“}DSi\text{”})$ obtained from Equation 6.1. The second branch represents the two

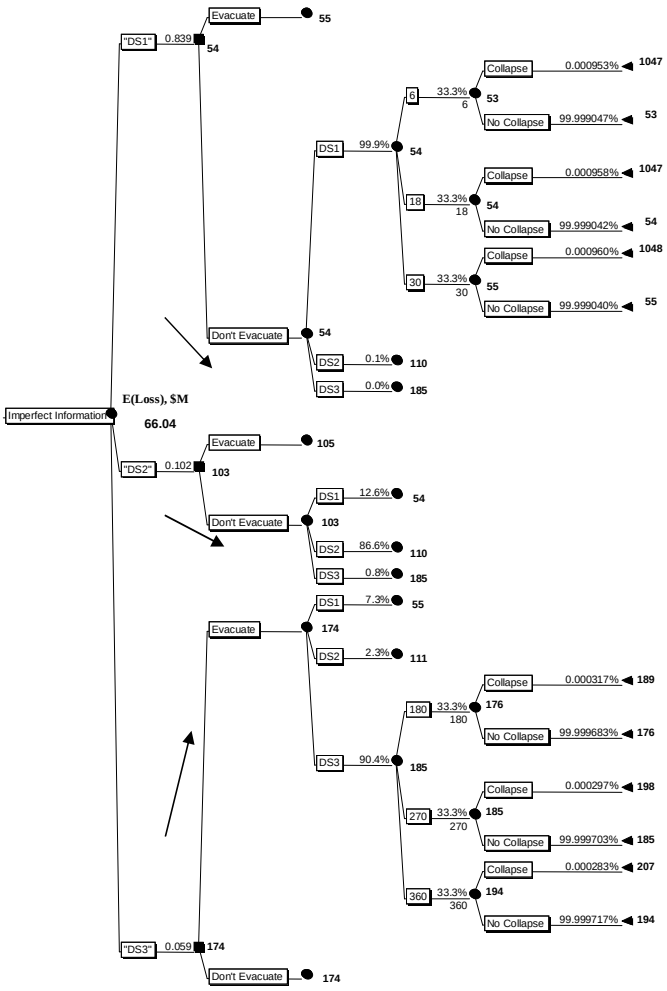

Figure 6.4: Partial decision tree with imperfect information from engineer.

[4]The exception is when the state “indicated” by the engineer’s study previously had a low probability. While this state’s probability will be increased, it may not become the most likely state. The net effect may be to broaden the distribution on the states.

decisions to evacuate or not after obtaining the information from the engineer. The third branch represents the events that the building is in DSj given that the engineer says that the building is in DSi, with conditional posterior probabilities $P(DSj|\text{“}DSi\text{”})$ calculated from Equation 6.2. In this case, the information provided by the engineer is “imperfect”. This explains why it is necessary to include the third branch of the decision tree which is not necessary in Figure 6.3 with “perfect” information. The optimal decisions are different from the initial case with limited information but are the same as those obtained with information from the clairvoyant engineer. The differences between the minimum expected financial losses with perfect and imperfect information and the minimum expected financial losses with limited information are approximately \$10,000 and \$5,000, respectively. Even though the engineer can only provide us with imperfect information, his input still allows us to reduce the minimum expected financial losses by \$5,000. This means that his input is of value to us, though not as “valuable” as the input of his clairvoyant counterpart. The value of “imperfect” information in this case is equal to \$5,000. This means that we ought to be willing to pay him up to a sum of \$5,000 (less than the value of clairvoyance of \$10,000 previously) for his information.

Fractured SMRF Connection Inspection Example

A more realistic representation of the information gathering scenario could involve partial inspection to estimate the percentage of the top-beam-flange connections that have fractured in the building. We follow the approach described in Luco et al. (2002) for a steel-moment-resisting-frame building. We shall assume in our simple example that knowing the (true) proportion of fractured top-beam-flange connections in the building allows one to quantify the true damage state of the building. For example, with a full inspection of all m connections in the building with n fractured connections, we can define the percentage of fractured connections as $f = \frac{m}{n}$. We assume (very simplistically and for the purpose of illustration) $0 < f < 0.2$ corresponds to the intact state, $0.2 < f < 0.5$ corresponds to $DS1$, $0.5 < f < 0.75$ corresponds to $DS2$, $0.75 < f < 0.9$ corresponds to $DS3$ and $0.9 < f < 1$ corresponds to collapse. But full inspection is very expensive and time-consuming. Partial inspections are more common in practice. From a partial inspection of n' connections, where $n' < n$, we will find the number, m', of top-flange fractures. The ratio, $f' = \frac{m'}{n'}$, is an estimate of the true fraction, f, of the percentage of fractures in the building. Without a complete inspection, however, the percentage of top flange fractures in the whole building

is a random variable which we denote as F. Using the prior distribution based on the probabilities of each post-mainshock damage state obtained in Chapter 3, we can obtain an approximate probability density function of F by mapping each damage state to the corresponding values of f described above. Next, we obtain the cumulative distribution function of F to which we fit a beta cumulative distribution function. The beta probability density function (with parameters a and b) has the form shown in Equation 6.3, and it will be used as our prior probability density function for F.

$$\begin{aligned} f_F(z) &= \frac{\Gamma(a+b)}{\Gamma(a)\Gamma(b)} z^{a-1} (1-z)^{b-1}, \ 0 \leq z \leq 1 \\ \Gamma(x) &= \int_0^\infty u^{x-1} e^{-u} du, x > 0 \end{aligned} \tag{6.3}$$

See Rice (1995). The resulting fit of the beta model to the cumulative distribution is shown in Figure 6.5. Based on the fit, we obtain $a = 1$ and $b = 4$.

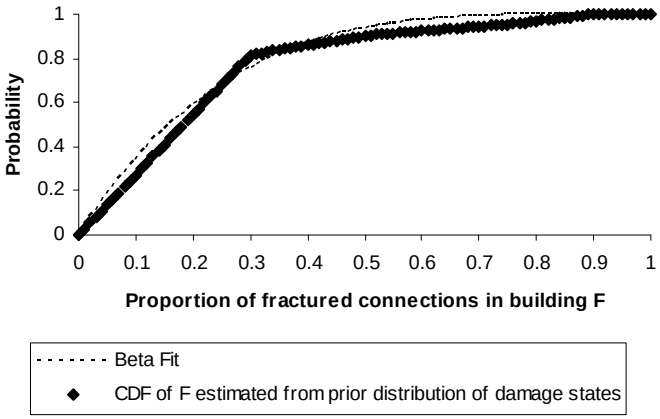

Figure 6.5: Beta distribution fit to cumulative distribution function estimated from the prior probabilities of being in each post-mainshock damage state.

In order to study the benefits of a given degree of inspection, consider the case in which we have decided to inspect m' connections, out of which a random number, X, of them can be fractures. We assume that conditioned on the true fraction $F = z$, the probability mass function of X is a binomial distribution with the probability mass function in Equation 6.4.

$$p_{X|z}(x|z) = \binom{m'}{x} z^x (1-z)^{m'-x}, \ x = 0, 1, 2, ..., m' \tag{6.4}$$

The likelihood function in this case is the "likelihood" of a true fraction $F = z$ given a sample with $X = x$ observed fractures. This likelihood function is assumed to be proportional to the probability of $X = x$ given $F = z$, i.e., the probability mass function of X conditioned on $F = z$. We shall use Equation 6.4 as the likelihood function[5].

The adoption of the beta and binomial functional forms for the prior distribution and likelihood function, respectively, means that the posterior distribution after Bayesian updating is also a beta distribution, but with different values of a and b, i.e., the beta distribution is a *conjugate prior* for the binomial distribution. See Rice (1995) for details. To confirm this claim, we can calculate the posterior distribution, $f_{F|X}(z|x)$, using Bayes' rule as shown in Equation 6.5, similar to Equation 6.2.

$$f_{F|X}(z|x) = \frac{f_F(z)p_{X|z}(x|z)}{\int_0^1 f_F(z)p_{X|z}(x|z)dz}, \ 0 \leq z \leq 1 \tag{6.5}$$

Note that the term $\int_0^1 f_F(z)p_{X|z}(x|z)dz$ in Equation 6.5 is equal to $p_X(x)$, the probability of observing any value of X in a sample of m' connections, i.e., the pre-posterior probability. $p_X(x)$ can be calculated using Equation 6.6.

$$\begin{aligned} p_X(x) &= \int_0^1 f_F(z)p_{X|z}(x|z)dz \\ &= \int_0^1 \frac{\Gamma(a+b)}{\Gamma(a)\Gamma(b)} z^{a-1}(1-z)^{b-1}\binom{m'}{x} z^x (1-z)^{m'-x}\, dz \\ &= \frac{\Gamma(a+b)}{\Gamma(a)\Gamma(b)} \frac{\Gamma(a+x)\Gamma(b+m'+x)}{\Gamma(a+b+m')} \binom{m'}{x}, \ x = 0, 1, 2, ..., m' \end{aligned} \tag{6.6}$$

Then, the posterior distribution, $f_{F|X}(z|x)$, can be calculated using Equation 6.5 such that we obtain Equation 6.7.

$$f_{F|X}(z|x) = \frac{f_F(z)p_{X|z}(x|z)}{p_X(x)}$$

[5]If the connections to inspect have been randomly selected (i.e., sampling involves a sequence of independent Bernoulli trials, each with a probability z of being a fracture) and a connection which has been inspected can potentially be inspected again (i.e., sampling is performed with "replacement"), then the use of Equation 6.4 to model X will be exact. However, because the above conditions are usually not satisfied, the binomial assumption only serves as an approximation.

$$= \frac{\Gamma(a+b+m')}{\Gamma(a+x)\Gamma(b+m'+x)} z^{a+x-1}(1-z)^{b+m'-x-1},\ 0 \le z \le 1 \qquad (6.7)$$

Note that Equation 6.7 is also a beta probability density function (which verifies our above claim), but with $a' = a+x$ and $b' = b+m'-x$. The posterior probability of being in DSi can then be approximated by integrating the posterior beta distribution over the above-stated ranges defined for each post-mainshock damage state.

As an example, we assume that there are 100 connections in our building. To demonstrate the effect of increased sampling, consider inspection sample sizes of 0, 20, 50 and 80 (i.e., 0%, 20%, 50% and 80% of the total number) and suppose in each case the result of the inspection is 40% fractured connections (e.g., 8, 20 and 32 out of 20, 50 and 80 inspected connections). We can compute the posterior distribution using Equation 6.7 and plot the resulting updated probability density functions in Figure 6.6. We can see that when the

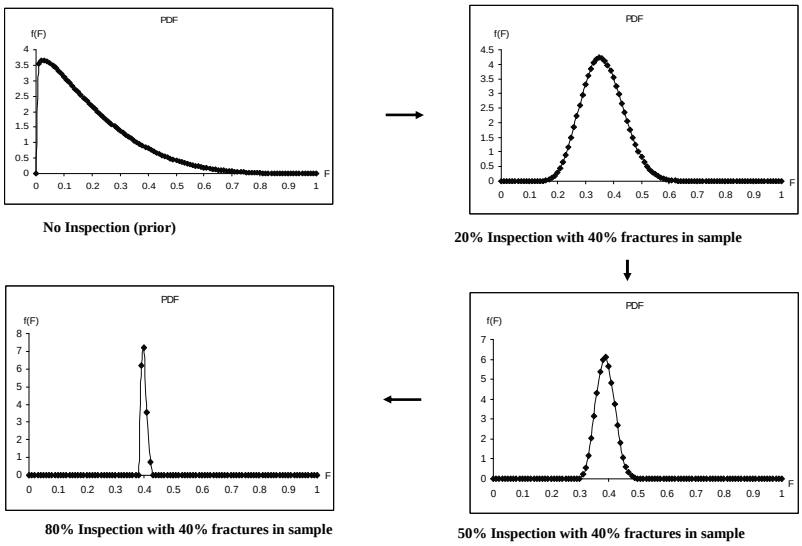

Figure 6.6: Posterior distributions of fraction of fractured connections, F, with different levels of inspection and a fixed fraction (40%) of observed fractures.

level of inspection increases, the posterior probability density function becomes more and more concentrated around 40%, the pre-specified percentage of fractures.

Next, we consider the case where we have decided to inspect 5% of the connections at random. In this case, $m' = 5$ and X is a discrete integer random variable with values between 0 and 5. We can re-draw our decision tree by incorporating the information that we obtain

from the engineer. The new decision tree is shown in Figure 6.7. The first branch of the tree

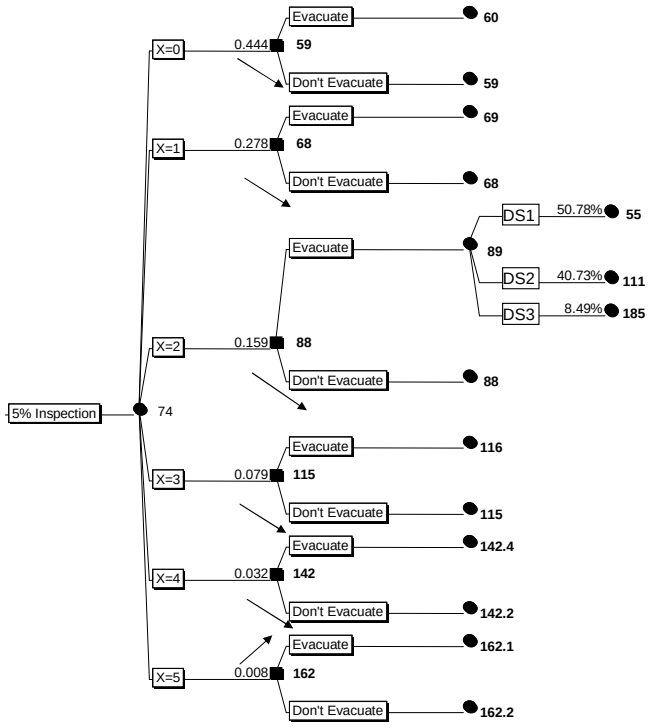

Figure 6.7: Partial decision tree with 5% inspection of connections. X represents the number of fractures in the sample.

is the pre-posterior probabilities (calculated using Equation 6.6) that the engineer inspects and observes $X = 0, 1, 2, 3, 4$ and 5 fractured connections. The second branch indicates the two actions to evacuate building occupants or not. The third branch is the posterior, updated probabilities of being in each damage state. In this case, if the engineer observes five fractured connections, the optimal decision will be to evacuate building occupants; if he observes less than five fractured connections, the optimal decision will be not to evacuate. The minimum expected financial losses is \$74M. Without any inspection, the minimum expected financial losses is \$80M. Thus the value of inspection is equal to \$6M. If inspection can be carried out for \$6M or less, it would be economically desirable to do so. Notice that the values of the minimum expected financial losses that we obtain here are different from those obtained previously: this difference can be attributed to the particular way the fractions, f, have been related to the damage states.

This example serves to illustrate the potential application of decision analysis to quantify the value of inspection. If one were to perform the same analysis with several different levels of inspection (at increasing cost for more detailed inspection), one could use the analysis of the value of inspection to determine the optimal level of inspection. The analysis of the value of inspection can also be used to decide if further inspections might be beneficial after new results are obtained.

Example with Improving Knowledge of Mainshock Site Spectral Acceleration, $Sa_{mainshock}$

We have introduced above a methodology to quantify the value of new information on the post-mainshock damage state. In this section, we shall use the same procedure to quantify the value of increasing levels of information on the mainshock site spectral acceleration, $Sa_{mainshock}$.

As discussed in Chapter 3, the post-mainshock damage state probabilities of the building after a mainshock of known magnitude and location are dependent on the mean and standard deviation of $\ln Sa_{mainshock}$, i.e., $E(\ln Sa_{mainshock})$ and $\sigma_{\ln(Sa_{mainshock})}$. The probabilities computed in Chapter 3 are based on using the magnitude and distance of the mainshock to estimate $E(\ln Sa_{mainshock})$ and $\sigma_{\ln(Sa_{mainshock})}$ from a standard ground motion attenuation law (in this case, Abrahamson and Silva (1997)). Thus, if we can quantify $Sa_{mainshock}$ with more confidence (as demonstrated by a reduction in the value of $\sigma_{\ln(Sa_{mainshock})}$), the post-mainshock damage state probabilities, and consequently, the minimum expected financial losses, will change. Thus, the optimal evacuation decision described earlier can potentially be changed by such improved information.

For example, the use of "ShakeMap", an online, automatically-generated spatial map which relies on shaking levels recorded at an array of existing seismic stations to estimate the spatial distribution of shaking, can potentially provide us with more information on $Sa_{mainshock}$ than simply the use of an attenuation law. See USGS (2004) and Wald et al. (1999) for details on ShakeMaps. Even better is to have a dedicated ground motion accelerometer at the site of the structure which will provide an exact value of $Sa_{mainshock}$. Thus, on-site instrumentation will likely provide us with the most information about $Sa_{mainshock}$, followed by the use of ShakeMaps, and, followed by the use of ground motion attenuation laws.

We shall now study the impact of more information on $Sa_{mainshock}$ on the decision-making process. We have previously computed the minimum expected financial losses where we estimated $Sa_{mainshock}$ using an attenuation law. We used the mainshock rupture scenario described in Chapter 2. The median value of $Sa_{mainshock}$ is computed to be 0.38g, $\sigma_{\ln(Sa_{mainshock})}$ is computed to be 0.568 and the minimum expected financial losses is equal to about \$66M. As an illustrative example, we assume that an instrument present at the site of our building provides us with the exact value of $Sa_{mainshock}$, taken to be equal to $0.5g$ in our example. $\sigma_{\ln(Sa_{mainshock})}$ can be taken to be equal to 0. The revised decision tree is shown in Figure 6.8, where the revised post-mainshock damage state probabilities are also shown. The minimum expected financial loss in this case is reduced to about \$56M.

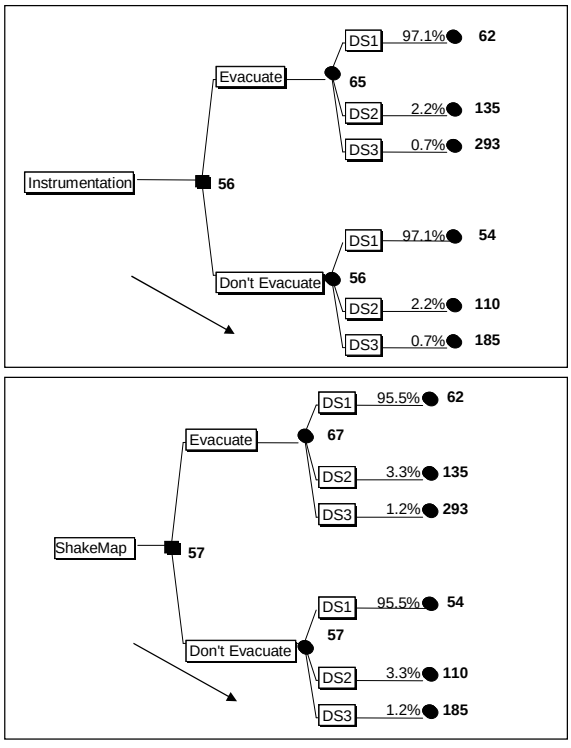

Figure 6.8: Partial decision tree with information about $Sa_{mainshock}$ from on-site instrumentation and a ShakeMap-based interpolation.

As a second case, for the sake of illustration, we assume that the online ShakeMap after the mainshock provides us with the same median $Sa_{mainshock}$ as that obtained from the use of an attenuation law (0.38g), but with $\sigma_{\ln(Sa_{mainshock})}$ reduced by 50%. This value might

result from the use of interpolation of the spatial array of instruments and the use of spatial statistical analysis to evaluate the implied standard deviation (see, for example, Journel (1978)). This results in the revised post-mainshock damage state probabilities and decision tree, also shown in Figure 6.8, where the minimum expected financial losses is reduced to about $57M. In both cases, the availability of more information results in the same optimal no-evacuation decision, but increases the probability of being in $DS1$ from 85.6% (attenuation law) in Figure 6.1 to 95.5% (ShakeMap) and 97.1% (instrumentation) despite the higher median estimate assumed in the on-site instrumentation case, i.e., 0.5g rather than 0.38g. Thus, in our illustrative example, more information on $Sa_{mainshock}$ improves our knowledge of the post-mainshock damage state and reduces the minimum expected financial losses.

The proposed framework can be used to quantify the potential benefits of ShakeMaps and building instrumentation in terms of reducing the total expected financial losses. If in addition one quantifies the cost of on-site instrumentation and/or the implementation of ShakeMaps, the proposed framework can then be used to determine if such setups are financially desirable.

6.2 Decision Analysis Allowing Damage-State Transitions

The decision tree procedure described in the previous section is based on the expected financial losses given the occurrence of a mainshock in which we consider the possibility of aftershocks that can potentially result in the collapse of the building. We have not taken into consideration the possibility of incremental damage to the building due to the sequence of aftershocks that follows the mainshock. To address this shortcoming, we can use the mathematical formulation in Chapter 5 to explicitly quantify the expected financial losses in a fixed period of time after the mainshock, allowing for multiple aftershocks and damage state progression. This procedure assumes a fixed action for each possible post-mainshock damage state immediately after the mainshock. For example, we continue to use the cost information described in Section 6.1, except that we exclude the cost of fatalities – the cost implications of evacuation are limited to economic disruption. We consider the original, stronger building described in Chapter 3. One possible decision is to evacuate building occupants as long as the building has been damaged in any way whatsoever; the second possible decision is to not evacuate building occupants if the building has been partially

damaged. The expected financial losses as a function of $t_{\max}$ after the mainshock (for $t_{\max}$ less than or equal to five years) for each post-mainshock damage state is shown in Figure 6.9. We assume that we have no information about the post-mainshock damage state of

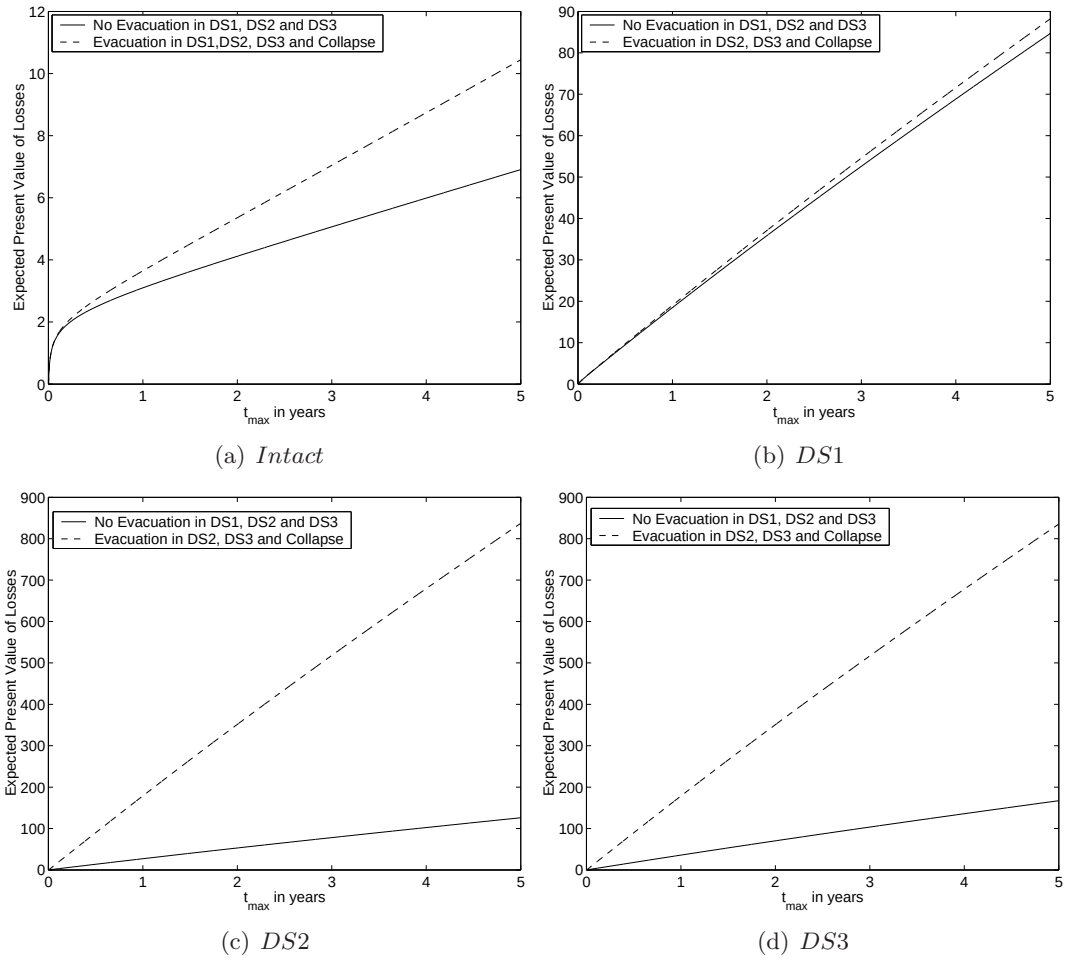

(a) *Intact* (b) $DS1$

(c) $DS2$ (d) $DS3$

Figure 6.9: Expected financial losses ($M) for each post-mainshock damage state for two possible post-mainshock evacuation decisions. The expected financial losses are plotted as a function of $t_{\max}$.

the building. Then the expected financial losses for each decision is shown in Figure 6.10, where we have weighed over each possible post-mainshock damage state. On the basis of minimizing the expected financial losses, the optimal decision is to not evacuate building occupants even if the building is damaged. We have not considered the possibility of revising decisions after the mainshock when potentially more information about the post-mainshock

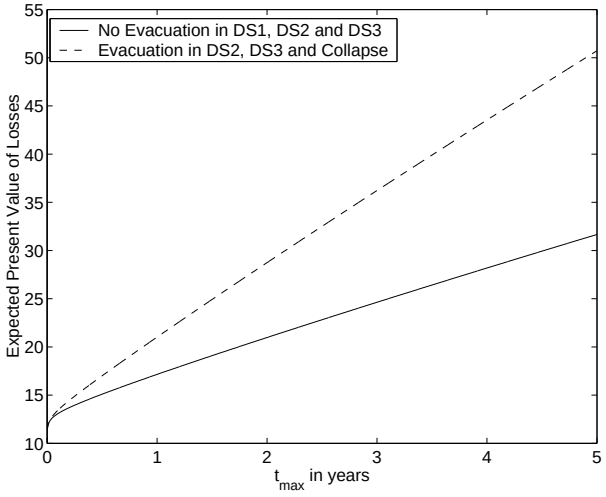

Figure 6.10: Expected financial losses ($M) for both decisions assuming no prior information about the post-mainshock damage state as a function of $t_{\max}$.

damage state of the building and the subsequent aftershock sequence parameters might become available. We shall address these issues in a more sophisticated model to follow.

The previous examples were concerned with the post-mainshock environment. We can also use *pre*-mainshock expected life-cycle cost optimization (prior to the mainshock) to decide on the optimal level of design taking into consideration performance of the damaged building in the aftershock sequence. For example, one can use pre-mainshock life-cycle cost to decide if it is desirable to expend additional funds to provide a structure with enhanced aftershock performance (e.g., to introduce self-centering connections that reduce the residual displacement which is known to increase building capacity to withstand aftershocks – see Kwan and Billington (2003a) and Kwan and Billington (2003b)). As an example, we consider the two possible discrete building designs discussed in Chapter 3, the original building being considerably stronger. We assume that the post-mainshock decision is to not evacuate building occupants if the building has been partially damaged. For a building in damage state i, we consider both a (random) transition cost of L_{ij} ($E(L_{ij}) = l_{ij}$) as well as a constant (but random) disruption cost of R_i per unit time ($E(R_i) = r_i$). We use the same cost figures as shown in Table 6.1 and Chapter 5. We also assume that only the Mid-Peninsula segment contributes to the mainshock hazard at the site: more potential seismic sources can be included very easily based on our model in Chapter 5. The resulting expected life-cycle costs for both designs are shown in Figure 6.11. If the design life-span

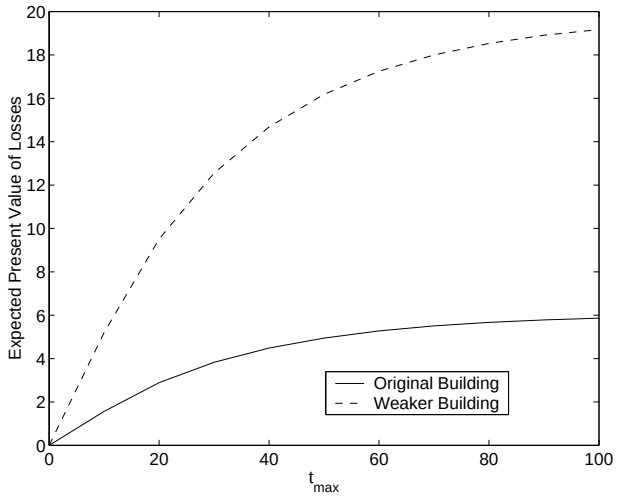

Figure 6.11: Expected financial losses ($M) from both mainshocks and aftershocks for both building designs as a function of $t_{\max}$ in the pre-mainshock environment.

of the building is 30 years, for example, one can determine the optimal choice between the two designs based on the expected financial losses in Figure 6.11 and the cost of design and construction for each design. Recall (in contrast to Section 6.1) that there has been no consideration of fatalities. Such pre-mainshock life-cycle decision making potentially has a significant impact on earthquake policy making and seismic design code development.

6.3 Decision Analysis Using Stochastic Dynamic Programming

The procedure described in Sections 6.1 and 6.2 assumes a fixed stationary policy at the start of the mainshock and aftershock sequence for each post-mainshock damage state; e.g., one will evacuate if the damage state is $DS1$ or worse at all times in the future. This assumption might not be realistic. Here, we introduce a decision analysis procedure based on stochastic dynamic programming in which we allow for the flexibility of re-considerations of previously made decisions at any time after the mainshock. Such revisions of decisions at different points in time in the future may have a significant impact on the expected financial losses in the nonhomogeneous aftershock environment. For example, after initial

evacuation, allowing subsequent re-occupancy of a damaged building is a decision which reduces downtime financial losses. Such re-occupancy decisions may be appropriate because of the decaying aftershock ground motion hazard, or because more information about the aftershock sequence (perhaps from aftershock sequence parameter updates based on Gerstenberger et al. (2002)) may reduce the perceived hazard. Also, inspection results after the mainshock might provide us with more accurate information about the post-mainshock damage state of the building such that previous evacuation decisions can potentially be changed. Thus, the availability of more information after the mainshock about the aftershock sequence and damage sustained by the building might offer a chance to revise the previously made decisions which were based on more limited information. Here, we develop a methodology which allows us to determine the optimal action and when it should be taken after the mainshock.

Further, in Chapter 5, the formulation of financial losses for a building in damage state i involves transitions to only a worse damage state j, where $j > i$, due to the occurrence of aftershocks. We have not included the possibility of repair to the intact state in the previous formulation. In order to use a analogous formulation developed in Chapter 5 which incorporates repair, one will have to assume exponential repair time distributions in the transformed time space which might not be realistic. Here, we introduce a more flexible formulation which incorporates non-exponential repair times, and includes the case with exponential repair time distributions as a special case.

6.3.1 Methodology

Our goal in this section is to propose a much more general methodology based on stochastic dynamic programming which allows one to determine the optimal action to be taken at each discrete set of points in time so as to minimize the expected financial losses at time zero, while still ensuring a tolerable level of individual life-safety for occupants of damaged building. This methodology also allows us to obtain, as a by-product, the expected financial losses in the aftershock environment where the building either can be incrementally damaged due to the occurrence of aftershocks, or it can be repaired back to the intact state (damage state 1) with a non-exponential repair time distribution. The individual life-safety constraint will be based on the concept of $ECR^{DS}_{\text{col}}(t_d; m_m)$ developed in Chapter 4. This more general procedure allows decisions such as evacuation or re-entry decisions to be made at optimal times so as to minimize financial losses without compromising life-safety. An output of the

methodology to be proposed below is the expected financial loss at time zero with the set of optimal actions to be taken at optimal times for each post-mainshock damage state. This formulation encompasses several procedures that we have described earlier. For example, the building-tagging methodology procedure described in Chapter 4 is a special case of this new methodology if individual life-safety consideration in terms of limiting $ECR_{\text{col}}^{DS}(t_d; m_m)$ is the only constraint, and we do not seek to minimize financial losses. The formulations for expected financial losses in Chapter 5 are special cases of the formulation in this section in which we assess the expected loss under certain simplifying restrictions such as (1) the decision to occupy or not can be taken only once, at the time of the mainshock, and (2) the possibility of repair is ignored. The proposed methodology is motivated by Cantaluppi (1981).

We use the same notations as in Chapter 5. We assume an expected transition cost of l_{ij} and a expected constant disruption cost of r_i per unit time for a building in state i transiting to state j. A building in damage state i ($i = 1$ denotes the intact state) can go to one of n damage states given the occurrence of an aftershock. A building in damage state i goes to damage state j with probability P'_{ij} given the occurrence of an aftershock. $\mu(t)$ is the intensity function of all aftershocks above some lower bound magnitude given a mainshock of known magnitude

Here, we allow further generality by allowing the costs and transition matrix to be "action-dependent". This means that at any point in time, we allow certain actions to be taken which will alter the transition probability matrix and the cost structure of a building originally in damage state i. We first consider a finite set of actions, $A(i)$, from which we select action a. We allow the set $A(i)$ to be dependent on the damage state i of the building.

For example, we can denote the evacuation of building occupants at time y as action a. If action a is decided upon, the cost structure after y will be altered because of a one-time expected transition cost $l_{ij}(y, a)$ due to relocation and an expected disruption cost $r_i(a)$ per unit time due to downtime and non-operability of the damaged building. We can also represent the decision to start repair as action a. The repair duration back to the intact state, T, for a building originally in damage state i is assumed to be a random variable with probability density function $f_i(t, a)$. The repair process is assumed to be a nonhomogeneous Poisson process with intensity function $\varphi_{i1}(t, a)$, where $f_1(t, a) = 0$ and $\varphi_{11}(t, a) = 0$ for all t, i.e., no repair is necessary for the intact state. Given an arbitrary $f_i(t, a)$ with corresponding cumulative distribution function $F_i(t, a)$, one can calculate $\varphi_{i1}(t, a)$ based on the definition

of hazard rate function described in Chapter 5, reproduced here as Equation 6.8.

$$\varphi_{i1}(t,a) = \frac{f_i(t,a)}{1 - F_i(t,a)} \tag{6.8}$$

The possibility of repair will alter the transition law of the building as it now has the possibility at some future time of transiting to the intact state. We represent this new transition law by the transition matrix $\mathbf{P}(\mathbf{t}, \mathbf{a})$. The dependence on the action a is explicitly included both in the transition matrix and the intensity function of the repair process. Given either the occurrence of a loss event or completion of repair for a building in damage state i, we first evaluate the mean rate of transitions out of state i, $\gamma_i(t,a)$ using Equation 6.9.

$$\gamma_i(t,a) = \varphi_{i1}(t,a) + \mu(t)(1 - P'_{ii}) \tag{6.9}$$

We can then form a transition probability matrix $\mathbf{P}(\mathbf{t}, \mathbf{a})$ given either the occurrence of a loss event or completion of repair using Equations 6.10, 6.11, 6.12 and 6.13.

$$\mathbf{P}(\mathbf{t}, \mathbf{a}) = \begin{pmatrix} 0 & P_{12}(t,a) & \cdots & P_{1n}(t,a) \\ P_{21}(t,a) & 0 & \ddots & \vdots \\ \vdots & \ddots & 0 & P_{(n-1)n}(t,a) \\ P_{n1}(t,a) & \cdots & \cdots & 0 \end{pmatrix} \tag{6.10}$$

$$P_{ik}(t,a) = 0, \ i \geq k, \ k \neq 1 \tag{6.11}$$

$$P_{ik}(t,a) = \frac{\mu(t) P'_{ik}}{\gamma_i(t,a)}, \ i < k, \ k \neq 1 \tag{6.12}$$

$$P_{i1}(t,a) = \frac{\varphi_{i1}(t,a)}{\gamma_i(t,a)} \tag{6.13}$$

$\gamma_i(t,a)$, $i = 1, ..., n$, and $\mathbf{P}(\mathbf{t}, \mathbf{a})$ allow us to describe both the aftershock process and the repair process for all post-mainshock damage states. Note that if $\varphi_{i1}(t,a) = \varphi_{i1}(a)$, a constant independent of time, then the repair duration is assumed to be exponentially distributed. Also, if $\mu(t) = \mu$, the above formulation generalizes to the case for Poisson mainshocks, and for $\mu(t)$ which is time-dependent (corresponding to a renewal process to model mainshock occurrences), the above formulation is also appropriate.

We now consider discretizing $\gamma_i(t, a)$ in "small" time steps so that for numerical purposes, we can approximate it by piecewise *constant* functions at discrete points in time t_j, where $0 \leq t_j \leq t_{\max}$ and j is an integer. As mentioned, we also consider the possibility of taking a different action a at each discretization point in time, the actions being selected from the finite set of actions $A(i)$.

Figure 6.12 is a schematic plot of the discretization for the case where we consider only loss events from aftershocks. Similar discretizations generalize to the case with repair. Since the intensity function between t_j and t_{j+1} is constant with $\gamma_{i,t_j}(a)$, the interarrival times of aftershocks in $[t_j, t_{j+1}]$ are exponentially distributed with (constant) intensity functions $\gamma_{i,t_j}(a)$. This is due to the memoryless nature of the nonhomogeneous Poisson assumption for both the loss events and repair process.

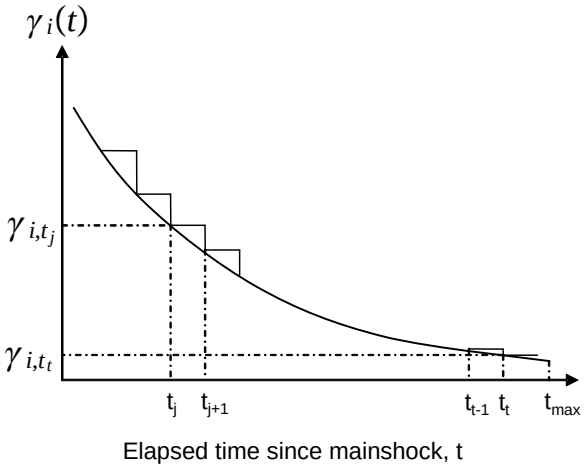

Figure 6.12: Schematic plot of discretization points in time of $\gamma_i(t, a)$, assuming $\varphi_{i1}(t, a) = 0$ for all i.

Again, $t_{\max}$ is the total length of the time interval of interest. The length of each discrete time interval $[t_j, t_{j+1}]$ is selected to be small enough such that the probability of two or more events (here, we refer to both loss events as well as completion of repairs) in $[t_j, t_{j+1}]$ is small based on the intensity function $\gamma_{i,t_j}(a)$. t_t is selected so that the probability of any event in $[t_t, t_{\max}]$ is small. Note here that our proposed formulation requires the formation of an augmented state space where we include both damage state and time.

Now, consider the discrete time interval $[t_j, t_{j+1}]$ with intensity function $\gamma_{i,t_j}(a)$. We

have a building in damage state i at time t_j when we take action a, $a \in A(i)$. We denote $L_{i,a}^{t_j}$ as the expected financial losses in $[t_j, t_{\max}]$ given initial building damage state i at time t_j when action a is taken. We wish to obtain $[L_i^{t_j*}, a_i^{t_j*}]$, where $a_i^{t_j*}$ is the optimal action to take if one is in state i at time t_j; $a_i^{t_j*}$ minimizes the expected financial losses in $[t_j, t_{\max}]$ to $L_i^{t_j*}$. We also wish to limit $ECR_{\text{col}}^i(t_j; m_m)$ to $\alpha_1 P_0$ or less, where $\alpha_1 P_0$ is the tolerable level of collapse rate that we have discussed in Chapter 4. In order to obtain the optimal actions and minimum expected financial losses for all values of t_j, we employ the technique known as stochastic dynamic programming by which we first obtain, for each state i, the optimal action at t_{t-1}, $a_i^{t_{t-1}*}$. $a_i^{t_{t-1}*}$ minimizes the expected losses in the final time interval $[t_{t-1}, t_{\max}]$ to $L_i^{t_{t-1}*}$, subject to the constraint $ECR_{\text{col}}^i(t_{t-1}; m_m) \leq \alpha_1 P_0$, where $a_i^{t_{t-1}*}$ is selected from $a \in A(i)$. Then, based on $a_i^{t_{t-1}*}$ and $L_i^{t_{t-1}*}$ for all i, we can next work backwards in time to obtain the optimal action at t_{t-2} and minimum expected losses in $[t_{t-2}, t_{\max}]$ by recognizing that we have already chosen the optimal action to take at time t_{t-1} for each state we might be in at t_{t-1}, while ensuring that the ECR constraint is also satisfied at t_{t-2}. We can do the same for t_{t-3}, t_{t-4}, etc. Such a procedure where we work backwards in time is known as the method of backward induction in stochastic dynamic programming. See Bertsekas (2000) for more details on dynamic programming.

Using the principle of stochastic dynamic programming, since we have selected the length of $[t_j, t_{j+1}]$ to be small enough such that the probability of two or more events is small, we can obtain $[L_i^{t_j*}, a_i^{t_j*}]$ by considering two mutually exclusive, collectively exhaustive cases where either one event happens in $[t_j, t_{j+1}]$ such that the building transits from state i to

state k, or no event happens in $[t_j, t_{j+1}]$, using Equation 6.14. We denote $\Delta t_j = t_{j+1} - t_j$.

$$[L_i^{t_j*}, a_i^{t_j*}] = \min_{\substack{a \epsilon A(i), \\ ECR^i_{\text{col}}(t_j) \leq \alpha_1 P_0}} \left\{ \begin{array}{l} \sum_{k=1}^{n} P_{ik}(a) \int_0^{\Delta t_j} \gamma_{i,t_j}(a) e^{-\gamma_{i,t_j}(a)u} l_{ik}(a) e^{-\alpha u} du \\ \quad + \int_0^{\Delta t_j} \gamma_{i,t_j}(a) e^{-\gamma_{i,t_j}(a)u} \left[\int_0^{u} r_i(a) e^{-\alpha t} dt \right] du \\ + \sum_{k=1}^{n} P_{ik}(a) \int_0^{\Delta t_j} \gamma_{i,t_j}(a) e^{-\gamma_{i,t_j}(a)u} \left[\int_u^{\Delta t_j} r_k(a) e^{-\alpha t} dt \right] e^{-\alpha u} du \\ \quad + \sum_{k=1}^{n} P_{ik}(a) \left[\int_0^{\Delta t_j} \gamma_{i,t_j}(a) e^{-\gamma_{i,t_j}(a)u} du \right] L_k^{t_{j+1}*} e^{-\alpha \Delta t_j} \\ \quad + \left[\int_{\Delta t_j}^{\infty} \gamma_{i,t_j}(a) e^{-\gamma_{i,t_j}(a)u} du \right] \left[\int_0^{\Delta t_j} r_i(a) e^{-\alpha t} dt \right] \\ \quad + \left[\int_{\Delta t_j}^{\infty} \gamma_{i,t_j}(a) e^{-\gamma_{i,t_j}(a)u} du \right] L_i^{t_{j+1}*} e^{-\alpha \Delta t_j} \end{array} \right\} \tag{6.14}$$

Equation 6.14, while initially of imposing appearance, is analogous to similar equations described in Chapter 5. For the case where we assume that there is one event in $[t_j, t_{j+1}]$, we denote the time of first transition in $[t_j, t_{j+1}]$ as $t_j + u$, where u is exponentially distributed with intensity function $\gamma_{i,t_j}(a)$.

The first four terms in Equation 6.14 are based on conditioning on having one event resulting in a transition from damage state i to damage state k occurring in the interval $[t_j, t_{j+1}]$ at $t_j + u$. The first term accounts for the expected transition cost, $l_{ik}(a)$, discounted to time t_j, where $\gamma_{i,t_j}(a)e^{-\gamma_{i,t_j}(a)u}$ is the probability density function of u. The second term accounts for the expected disruption cost of $r_i(a)$ per unit time up to time $t_j + u$ before the event happens, also discounted back to time t_j. The third term accounts for the expected disruption cost from time $t_j + u$ to t_{j+1} after the building has transited to state k. This is discounted back to time t_j as well. The fourth term is a unique characteristic of stochastic dynamic programming. Now, conditioned on having a transition to a new state k, we assume that we have taken the optimal action $a_k^{t_{j+1}*}$ at t_{j+1} such that all future losses from t_{j+1} on is denoted by $L_k^{t_{j+1}*}$. $L_k^{t_{j+1}*}$ will be known because (as per the backward induction procedure), before solving for $[L_i^{t_j*}, a_i^{t_j*}]$ at the time step t_j, we will have already solved the problem at t_{j+1}. The last two terms of Equation 6.14 are based on conditioning on having no events in the interval $[t_j, t_{j+1}]$, and the formulation follows along the same line of argument. Note that $\int_{\Delta t_j}^{\infty} \gamma_{i,t_j}(a) e^{-\gamma_{i,t_j}(a)u} du$ is the probability of having no events in

$[t_j, t_{j+1}]$, and can be simplified to $e^{-\gamma_{i,t_j}(a)\Delta t_j}$.

We simplify Equation 6.14 by neglecting the effects of discounting for durations less than Δt_j. Then Equation 6.14 can be approximated as Equation 6.15.

$$[L_i^{t_j*}, a_i^{t_j*}] = \min_{\substack{a\epsilon A(i),\\ ECR^i_{\text{col}}(t_j)\leq \alpha_1 P_0}} \left\{ \begin{array}{c} \sum_{k=1}^{n} P_{ik}(a)\left[\gamma_{i,t_j}(a)\Delta t_j\right] l_{ik}(a) \\ +\frac{1}{2}\left[r_i(a)\Delta t_j\right]\left[\gamma_{i,t_j}(a)\Delta t_j\right] \\ +\sum_{k=1}^{n} P_{ik}(a)\frac{1}{2}\left[r_k(a)\Delta t_j\right]\left[\gamma_{i,t_j}(a)\Delta t_j\right] \\ +\sum_{k=1}^{n} P_{ik}(a)\left[\gamma_{i,t_j}(a)\Delta t_j\right] L_k^{t_{j+1}*} e^{-\alpha\Delta t_j} \\ +\left[1-\gamma_{i,t_j}(a)\Delta t_j\right]\left[r_i(a)\Delta t_j\right] \\ +\left[1-\gamma_{i,t_j}(a)\Delta t_j\right] L_i^{t_{j+1}*} e^{-\alpha\Delta t_j} \end{array} \right\} \quad (6.15)$$

Similar to Equation 6.14, the first term of Equation 6.15 accounts for the expected transition cost, $l_{ik}(a)$, where $\left[\gamma_{i,t_j}(a)\Delta t_j\right]$ is the probability of the occurrence of one event in $[t_j, t_{j+1}]$. The second term accounts for the expected disruption cost of $r_i(a)$ per unit time up to time $t_j + u$ before the event happens, where conditioned upon the occurrence of one event in $[t_j, t_{j+1}]$, the expected arrival time of the event is at $t_j + \frac{1}{2}\Delta t_j$, such that the expected disruption loss is equal to $\frac{1}{2}\left[r_i(a)\Delta t_j\right]$. The third and fourth terms can be obtained analogously. The last two terms of Equation 6.15 are based on conditioning on having no events in the interval $[t_j, t_{j+1}]$, where the probability of no events is approximately equal to $\left[1-\gamma_{i,t_j}(a)\Delta t_j\right]$.

Using the same simplifying assumptions, we can also further simplify the dynamic programming formulation by using a discrete-time Markov chain to approximate the continuous-time Markov chain; in the latter model, an event can happen at any time in the time-interval $[t_j, t_{j+1}]$, whereas in the former model, transitions are restricted to fixed points in time. We assume then that all events (inclusive of both aftershock occurrences and completion of repairs) can only happen at discrete points in time t_j, t_{j+1}, ..., for all t_j up to $t_{\max}$. We first denote the vector of actions taken for all initial states as $\mathbf{a}$, where $\mathbf{a}$ is given in Equation 6.16. We then denote $\mathbf{Q}(\mathbf{t_j}, \mathbf{a})$ as the transition matrix for the probability of an event resulting in a transition from state i to state j, for all i and j, in the time interval $[t_j, t_{j+1}]$, assuming that action a_i is taken at t_j and the event occurs at t_{j+1}. $\mathbf{Q}(\mathbf{t_j}, \mathbf{a})$ is obtained

using Equations 6.17 to 6.21 for $i = 1, 2, ..., n$.

$$\mathbf{a} = \begin{pmatrix} a_1 \\ \vdots \\ \vdots \\ a_n \end{pmatrix} \tag{6.16}$$

$$\mathbf{Q}(\mathbf{t_j}, \mathbf{a}) = \begin{pmatrix} Q_{11}(t_j, a_1) & Q_{12}(t_j, a_1) & \cdots & Q_{1n}(t_j, a_1) \\ Q_{21}(t_j, a_2) & Q_{22}(t_j, a_2) & \ddots & \vdots \\ \vdots & \ddots & \ddots & \vdots \\ Q_{n1}(t_j, a_n) & \cdots & \cdots & Q_{nn}(t_j, a_n) \end{pmatrix} \tag{6.17}$$

$$Q_{ik}(t_j, a_i) = 0,\ i > k,\ k \neq 1 \tag{6.18}$$

$$Q_{ik}(t_j, a_i) = \mu(t_j)\Delta t_j P'_{ik},\ i < k,\ k \neq 1 \tag{6.19}$$

$$Q_{i1}(t_j, a_i) = \varphi_{i1}(t_j, a_i)\Delta t_j \tag{6.20}$$

$$Q_{ii}(t_j, a_i) = 1 - \mu(t_j)\Delta t_j(1 - P'_{ii}) - \varphi_{i1}(t_j, a_i)\Delta t_j \tag{6.21}$$

Recall that the equations also assume that the "probabilities" $\mu(t_j)\Delta t_j$ and $\varphi_{i1}(t_j, a_i)$ are small. Note that $Q_{ii}(t_j, a_i)$, the probability of no state transitions, is then close to unity.

The vector of optimal actions for all initial states at time t_j is denoted as $\mathbf{a}^{\mathbf{t}^*_\mathbf{j}}$ and the vector of minimum financial losses from t_j to $t_{\max}$ for all initial states is denoted as $\mathbf{L}^{\mathbf{t}^*_\mathbf{j}}$. These vectors are defined in Equation 6.22.

$$\mathbf{a}^{\mathbf{t}^*_\mathbf{j}} = \begin{pmatrix} a_1^{t_j^*} \\ \vdots \\ \vdots \\ a_n^{t_j^*} \end{pmatrix},\ \mathbf{L}^{\mathbf{t}^*_\mathbf{j}} = \begin{pmatrix} L_1^{t_j^*} \\ \vdots \\ \vdots \\ L_n^{t_j^*} \end{pmatrix} \tag{6.22}$$

Furthermore, the expected financial loss incurred in $[t_j, t_{j+1}]$ assuming that action a_i is taken at t_j and the event occurs at t_{j+1} for a building originally in state i is denoted as $C_i^{t_j}(a_i)$. $C_i^{t_j}(a_i)$ can be calculated using Equation 6.23 as the sum of the disruption losses while in state i and the expected value of transition loss at the end of the interval. We further denote $\mathbf{C}^{\mathbf{t_j}}(\mathbf{a})$ as the vector of expected financial losses incurred in $[t_j, t_{j+1}]$ for all

initial states, represented by Equation 6.24.

$$C_i^{t_j}(a_i) = r_i(a_i)\Delta t_j + \sum_{k=1}^{n} Q_{ik}(t_j, a_i) l_{ik}(a_i) \tag{6.23}$$

$$\mathbf{C^{t_j}(a)} = \begin{pmatrix} C_1^{t_j}(a) \\ \vdots \\ \vdots \\ C_n^{t_j}(a) \end{pmatrix} \tag{6.24}$$

Then, similar to Equations 6.14 and 6.15, the dynamic programming formulation can be written in a much simpler format as Equation 6.25. As $\Delta t_j \to 0$, Equation 6.25 converges to Equations 6.14 and 6.15.

$$[\mathbf{L^{t_j^*}}, \mathbf{a^{t_j^*}}] = \min_{\substack{i=1,\ldots,n,\ a_i \epsilon A(i), \\ ECR^i_{\text{col}}(t_j) \leq \alpha_1 P_0}} \left\{ \ \mathbf{C^{t_j}(a)} + \mathbf{Q(t_j, a)} \mathbf{L^{t_{j+1}^*}} \ \right\} e^{-\alpha \Delta t_j} \tag{6.25}$$

Thus, using backward induction from t_t back to time zero based on Equations 6.14, 6.15 or 6.25, this procedure allows us to obtain the optimal action to take at any of the discrete points in time for buildings that could be in any damage state. It also allows us to obtain the minimum expected financial losses from any point in time to $t_{\max}$, under the assumption that we will have taken the optimal actions at all points in time to $t_{\max}$. As we have discussed earlier, this is a more general case of the previously proposed building-tagging procedure and decision-making procedure based on computing the expected financial losses in the aftershock environment. Thus, this methodology allows for much wider loss and event modeling flexibility.

6.3.2 Example

We apply the procedure in Section 6.3.1 to the "weaker" building described in Chapter 3 to determine if the building should be evacuated or if continued occupancy is permitted; the decision is evaluated at multiple discrete points in time from day one for a duration, $t_{\max}$, equal to five years after the mainshock. We use the same cost information as in Section 6.1. For this example, however, we consider the mainshock magnitude, m_m, to be equal to 7.3, α_1 from Chapter 4 for building tagging based on individual life-safety consideration to be equal to 5, and the discount rate, α, to be equal to 5% per year. With available information on

the aftershock ground motion hazard at the site and the building's transition probabilities given the occurrence of an aftershock, for all post-mainshock damage states, we can use the dynamic programming procedure to determine the optimal decisions at all points in time from day one and forward. We shall consider three separate cases about the treatment of the economic and life-safety elements of the decision.

In the first case (Case 1), we impose only the individual life-safety constraint without any explicit minimization of financial losses. The constraint is imposed at all discrete points in time (i.e., ensuring $ECR^{i}_{\text{col}}(t_j) \leq \alpha_1 P_0$ for all t_j). As discussed earlier, adopting the dynamic programming methodology in this manner is the same as using the building-tagging criteria described in Chapter 4. In our example, for all post-mainshock damage states, the "optimal" decision at day one is to evacuate building occupants because of the high aftershock hazard. We say "optimal" even though there is in Case 1 no explicit minimization of cost; rather it simply assumed re-occupancy will occur as soon as it is feasible, i.e., as soon as the life-safety constraint is satisfied. From the results obtained using the dynamic programming algorithm, if the building is in the intact, $DS1$ and $DS2$ post-mainshock damage states, the optimal action changes from building evacuation to allowing re-occupancy after 3, 6 and 10 days (respectively) from the occurrence of the mainshock, as shown in Table 6.3. The

Table 6.3: Case 1: Times in days after mainshock when the optimal decision changes from having evacuation to allowing re-occupancy. The individual life-safety constraint is enforced in this case without explicit minimization of financial losses.

Damage state i	Points in time when optimal decision changes from building evacuation to allowing re-occupancy (days)
Intact	3
$DS1$	6
$DS2$	10

change in optimal decision is attributable simply to the reduction in the aftershock hazard.

Having determined the points in time when re-occupancy is permitted by the individual life-safety constraint, we now wish to evaluate the expected financial losses for each post-mainshock damage state assuming repair operations commence immediately after re-occupancy is allowed. We consider repair only for $DS1$ and $DS2$ – the intact building does not require repair and we assume for this example that the building in $DS3$ is so severely

damaged that repair is not economically feasible. We use the probability density functions of the repair duration, $f_i(t)$, in Figure 6.13, and compute the corresponding repair duration intensity functions, $\varphi_{i1}(t)$ (also shown in Figure 6.13), using Equation 6.8. We show

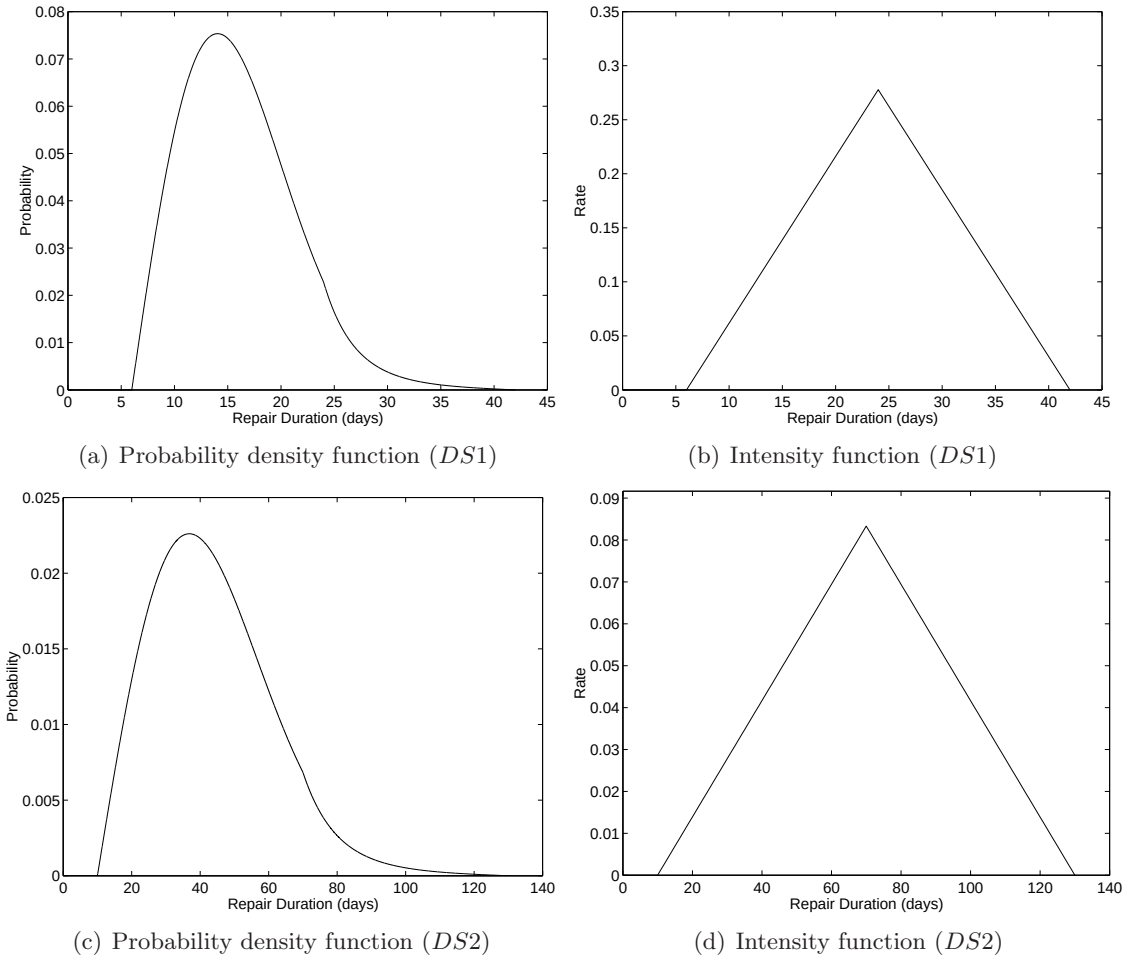

(a) Probability density function ($DS1$)

(b) Intensity function ($DS1$)

(c) Probability density function ($DS2$)

(d) Intensity function ($DS2$)

Figure 6.13: Probability density functions and corresponding intensity functions for the duration of the repair to intact condition for post-mainshock damage states $DS1$ and $DS2$.

in Figure 6.14 the expected financial losses for the intact, $DS1$ and $DS2$ post-mainshock damage states using the optimal decision policy obtained from dynamic programming with repair. The expected financial losses using the optimal policy with repair are significantly lower in value as compared to the expected financial losses where the policy is to evacuate building occupants as long as the building has been damaged by the mainshock, with no consideration of repair. We can also take into account the repair cost for $DS1$ and $DS2$ to

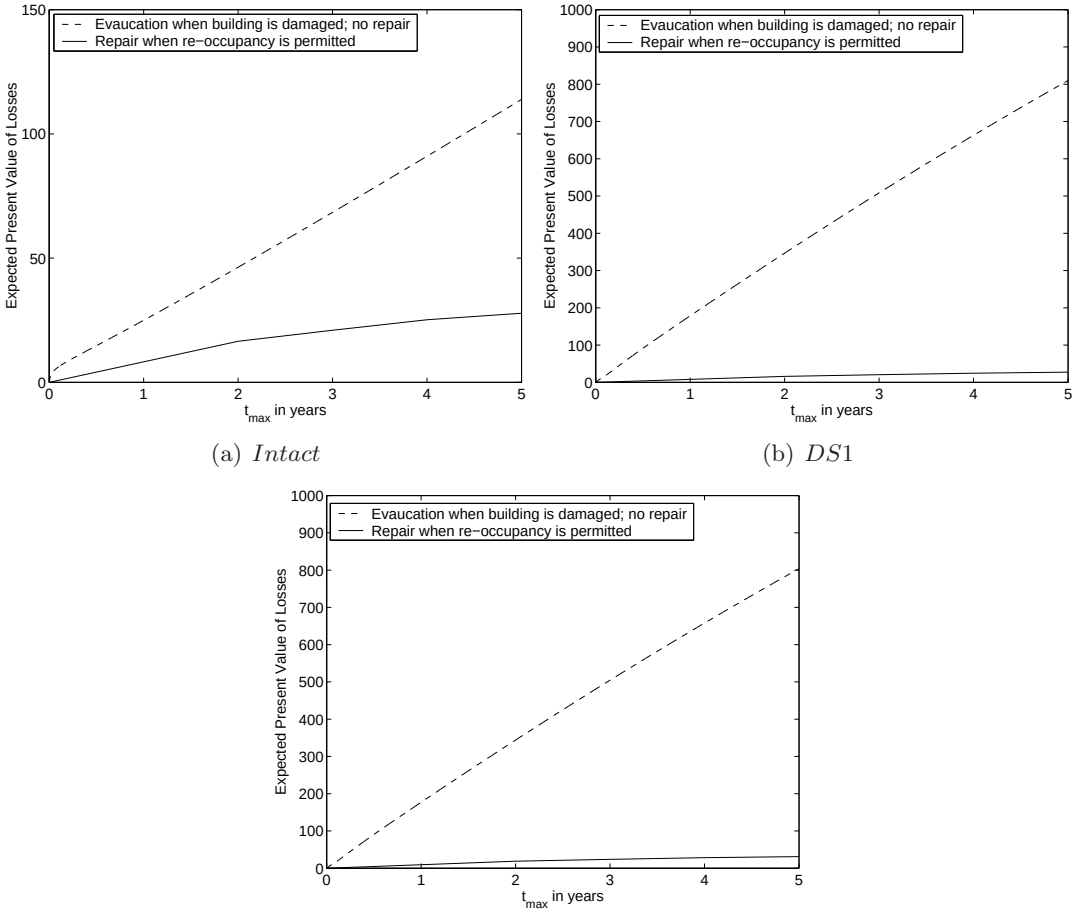

(a) *Intact* (b) $DS1$

(c) $DS2$

Figure 6.14: Expected financial losses (\$M) for *Intact*, $DS1$ and $DS2$ for (1) Repair when re-occupancy is permitted using optimal policy (solid line) (2) Evacuation when building is damaged with no repair (dotted line). The losses are plotted as a function of $t_{\max}$ in years.

decide if repair is financially feasible.

A second case (Case 2) of the application of the dynamic programming formulation seeks to obtain the optimal policy based on minimizing the expected financial losses (including the cost per life saved), but without considering repair or enforcing the individual life-safety constraint. We assume 400 occupants in the building, and we consider a range of cost per life saved from \$0M (i.e., only economic losses are considered) to \$10M. A typical output of the optimal policy as a function of elapsed days after the mainshock for all post-mainshock damage states is shown in Table 6.4 for the case where the cost per life saved is equal

to \$2M. The conclusion is that, except for the case where the cost per life saved is not

Table 6.4: Typical output of dynamic programming algorithm for the case where the individual life-safety constraint is not imposed, and where a cost per life saved of \$2M is used. The optimal policy is shown as a function of elapsed days after the mainshock for all post-mainshock damage states.

Days after mainshock	Intact	$DS1$	$DS2$	$DS3$
1	Evacuate	Evacuate	Evacuate	Evacuate
2	Evacuate	Evacuate	Evacuate	Evacuate
3	Evacuate	Permit re-occupancy	Permit re-occupancy	Permit re-occupancy
4	Permit re-occupancy	Permit re-occupancy	Permit re-occupancy	Permit re-occupancy
5	Permit re-occupancy	Permit re-occupancy	Permit re-occupancy	Permit re-occupancy
⋮	⋮	⋮	⋮	⋮
⋮	⋮	⋮	⋮	⋮

included, for all post-mainshock damage states, the optimal decision is to evacuate building occupants immediately after the mainshock. For the building in the intact, $DS1$ and $DS2$ damage states after the mainshock, the points in time when the optimal decision changes from evacuation of building occupants to allowing re-occupancy are shown in Table 6.5.

Table 6.5: Case 2: Times in days after mainshock when the optimal decision changes from having evacuation to allowing re-occupancy. The individual life-safety constraint is not enforced in this case.

	Cost per life saved (\$M)				
	0	1	2	5	10
Damage state i	Points in time when optimal decision changes from building evacuation to allowing re-occupancy (days)				
Intact	3	3	4	6	9
$DS1$	Never Evacuate	2	3	5	10
$DS2$	Never Evacuate	2	3	6	11

When the cost per life saved is not included, if the building is in $DS1$ or $DS2$, the optimal action is to permit continued occupancy at all times. If the building is in the intact state, however, the optimal decision is to evacuate building occupants for the first two days after the mainshock (when the aftershock hazard is high), and permit re-occupancy after that. This conclusion is counter-intuitive, but we shall illustrate why it is logical based on the cost values and state transition matrix that we use. The example helps to understand just how the dynamic programming analysis works.

The counter-intuitive optimal policy obtained from the dynamic programming formulation in the case where we seek to minimize only economic losses is to evacuate building occupants in the intact building for the first two days after the mainshock, and permit re-occupancy from the third day on, whereas no such evacuation is suggested if the building is damaged! Without performing any analysis, one would expect the optimal policy to be to permit continued indefinite occupancy in the intact building also. These two policies differ only in the first two days after the mainshock. We shall make an approximation of the expected financial losses in the first two days after the mainshock assuming (1) building occupants are evacuated and (2) building occupants are not evacuated. The expected number of aftershocks (based on the formulation in Chapter 2) in the first two days after the mainshock with magnitudes between 5.0 and the mainshock magnitude, m_m=7.3, can be estimated to be about 3. Given the occurrence of an aftershock, we see from the state transition matrix of the weaker building in Chapter 3 (Figure 3.8) that the probability of transiting to $DS1$ and $DS2$ is almost an order of magnitude higher than the probability of transiting to $DS3$ and $DS4$, respectively. Thus, as a first estimate, we shall only concentrate on the possibility of the intact building transiting to $DS1$ and $DS2$ due to the occurrence of an aftershock. From the same state transition matrix, the probability of the intact building transiting to $DS1$ and $DS2$ given the occurrence of an aftershock is equal to 0.0058 and 0.001, respectively. Thus the expected number of aftershocks in the first two days that would result in a transition from the intact state to $DS1$ and $DS2$ is approximately equal to 3 x 0.0058 $\approx$ 0.02 and 3 x 0.001 = 0.003 respectively. Thus, we can approximate the probability of an aftershock resulting in a transition from the intact state to $DS1$ and $DS2$ in the first two days after the mainshock to be about 0.02 and 0.003, respectively. The expected transition financial loss from the intact state to $DS1$ and $DS2$ is about \$52.5M and \$105M respectively if building occupants have not been evacuated, and one-fourth that (i.e., \$13M and \$26M) if building occupants have been evacuated (see

Section 6.1). If building occupants are evacuated, we have assumed an expected daily disruption cost of \$0.5M (see Section 6.1); on the other hand, if building occupants are not evacuated, there is no disruption cost. Thus, the expected financial losses in the first 2 days after the mainshock (where the effect of discounting is negligible) can be approximated by the sum of the expected transition losses and the expected disruption losses. If building occupants have been evacuated, the expected transition losses (due to transitions to $DS1$ and $DS2$) can be estimated to be 0.02 x \$13M + 0.003 x \$26M $\approx$ \$0.34M and the expected disruption losses can be estimated to be about 2 x \$0.5M = \$1M, making the total expected financial losses to be about \$1.34M. On the other hand, if building occupants have not been evacuated, the expected transition losses (due to transitions to $DS1$ and $DS2$) can be estimated to be 0.02 x \$52.5M + 0.003 x \$105M $\approx$ \$1.37M and since there are no disruption losses, the total expected financial losses is about \$1.37M as well. Thus, it can be seen as a first approximation that the optimal policy for the first 2 days based on minimizing the expected financial losses is indeed to evacuate building occupants. This counter-intuitive conclusion, namely that one should evacuate when the building is intact but not when it is damaged ($DS1$ or $DS2$) is due in part to there being no life-safety constraint, in part to the particular cost values adopted in this chapter and in Chapter 5, and in part to the particular values in the state transition matrix of the building in Chapter 4. Note that it is in fact about 5 times more likely (given an aftershock) that the intact building goes to a worse damage state than it is that a damaged building does so. The cost assigned to making these unanticipated damage state transitions is high. Therefore (for these numbers), the optimal policy (economically) is to avoid the risk of a costly transition from intact to a worse damage state by making a cheaper planned evacuation on day one.

Referring again to Table 6.5, when we introduce non-zero values for the cost per life saved (say, \$2M), the optimal decision is to evacuate the building for the first four days if the building is in the intact state, three days if the building is in the $DS1$ or $DS2$ damage state, and permit re-occupancy after that (Again, the factors described just above cause this unexpected longer evacuation time for the intact than the damaged cases). As must be expected, the length of elapsed time required before re-occupancy is permitted increases as we use increasing values for the cost per life saved, which increases the expected losses for the continued-occupancy decision.

A third example (Case 3) of the application of the dynamic programming formulation

couples the first two cases just described in that the individual life-safety constraint (ensuring $ECR^i_{\text{col}}(t_j) \leq \alpha_1 P_0$ for all t_j) is imposed, and the expected financial losses (including the cost per life saved) are minimized. The points in time when the optimal decision changes are shown in Table 6.6. Note that because we are now posing a constrained economic opti-

Table 6.6: Case 3: Times in days after mainshock when the optimal decision changes from having evacuation to allowing re-occupancy. The individual life-safety constraint is also enforced in this case.

	Cost per life saved ($M)				
	0	1	2	5	10
Damage state i	Points in time when optimal decision changes from building evacuation to allowing re-occupancy (days)				
Intact	3	3	4	6	9
$DS1$	6	6	6	6	10
$DS2$	10	10	10	10	11

mization problem, these times where revisions of decision occur are as long or longer than the results obtained from each of the two previous cases where we either only imposed the individual life-safety constraint, or only minimized the expected financial losses (including the cost per life saved). By using such an approach, we are determining the optimal policy by ensuring that expected financial losses (including the cost per life saved) are minimized without violating the individual life-safety constraint. Again, from Table 6.6, as we use increasing values for the cost per life saved, the length of time before re-occupancy is permitted is also increased. By comparing Tables 6.3, 6.5 and 6.6, one can see that when we use a cost per life saved of $2M, $5M and $10M for the intact building, the minimization of expected financial losses (including the cost per life saved) determines the points in time when the optimal decision changes from building evacuation to permitting re-occupancy. For the building in $DS1$ or $DS2$, the individual life-safety constraint determines the points in time when the optimal decision changes from building evacuation to permitting re-occupancy for values of cost per life saved between $0M and $5M; for a cost per live saved of $10M, the minimization of expected financial losses governs instead.

6.4 Conclusion

The objectives of this chapter are, first, to introduce earthquake engineers to elementary decision analysis concepts – beyond simply the expected economic loss analyses that they use now – which hold promise for informed earthquake engineering decisions, especially with regard to information gathering and the value of new information. We introduce different methods of decision analysis with examples in both the post- and pre-mainshock environment. We use different decision bases for comparing different decisions, and we consider both the losses per event (via the use of decision trees) as well as life-cycle losses using the analytic formulations described in Chapter 5. Throughout this chapter, we have emphasized the role of information in potentially improving our decision-making capability. We have introduced the value of information which can be used to determine if obtaining more information is financially desirable. A second major chapter objective has been the introduction of a general methodology using stochastic dynamic programming to allow for the flexibility of revisions of previously made decisions with the availability of more information. This methodology enables us to determine the optimal policy at all times after the mainshock, and it also allows us to determine the optimal policy based on minimizing the expected financial losses (which can include the cost per life saved) while not violating the individual life-safety constraint. The proposed procedures can potentially be applied to earthquake policy and decision making, especially in terms of quantifying the value of additional information in the information-gathering process.

7 Summary, Limitations, and Future Work

7.1 Summary

In this report, we study the role of aftershocks in performance-based earthquake engineering. We begin by introducing Aftershock Probabilistic Seismic Hazard Analysis (APSHA) in Chapter 2. APSHA is a procedure analogous to conventional mainshock PSHA to characterize aftershock ground motion hazard. The proposed methodology takes into consideration the time-varying nature of the aftershock occurrence rate which decreases with increased elapsed time from the initial occurrence of the mainshock. The aftershock ground motion hazard at a site is also dependent on the magnitude and location of the causative mainshock, the location of aftershocks being limited to an aftershock zone dependent on the location and magnitude of the initial mainshock. We use APSHA in Chapter 4 to quantify the rate of building collapse caused by aftershocks following the initial rupture to make decisions for building tagging, including entry of damaged buildings for rescue, repair or normal occupancy.

Chapter 3 introduces a methodology generalizing the work of Luco et al. (2004) to characterize the performance of (possibly) mainshock-damaged buildings in the aftershock environment under different levels of ground shaking due to potential aftershocks. The probabilistic capacity of mainshock-damaged buildings to withstand future aftershock ground shaking is quantified by considering several levels of mainshock-sustained damage. The methodology used here involves back-to-back nonlinear dynamic time-history analysis and fragility curves can be developed for all initial building damage states. The proposed methodology allows one to quantify the likelihood of each post-mainshock damage state after a mainshock of known magnitude and location. The novelty of the methodology is

that it also allows one to compute the transition probability of a building in a given post-mainshock damage state transiting to a worse damage state given the occurrence of an aftershock of random magnitude at a random location with a specified aftershock zone.

Chapter 4 describes a risk management building tagging policy based on the quantification of life-safety threat in the aftershock environment using the probability of collapse as a proxy for fatality risk. The proposed methodology enables us to classify buildings after a mainshock earthquake into three groups with red, yellow and green building tags. The objective of yellow or red-tagging a building after an earthquake is to insure adequate life safety during a period of enhanced seismic activity. A methodology for the life-safety evaluation of an earthquake-damaged building is proposed based on APSHA and the residual capacity of (possibly) mainshock-damaged buildings against collapse due to possible future aftershocks. We also propose a methodology to allow earlier entry into a red-tagged building by introducing the concept of a controlled work force where we limit the total probability of collapse faced by an informed and compensated volunteer worker.

Chapter 5 presents formal stochastic financial life-cycle loss models in both the aftershock and pre-mainshock scenarios over the lifetime of the building. We begin our formulation using the traditional homogeneous Poisson mainshock process. We extend this previous model to include nonhomogeneous Poisson aftershock process with "immediate" repair of the building to the initial building state. We then generalize our formulation to include Markov and semi-Markov frameworks where we use both Poisson and renewal processes to model mainshock occurrences with consideration of various building repair and/or damage progression scenarios. Such financial loss models serve as an input to the decision making methodology (both post- and pre-mainshock) that is the subject of discussion in Chapter 6.

Chapter 6 presents a decision analytic framework under improving states of information for post- and pre-mainshock decision making. Decisions such as post-mainshock building tagging and retrofit decisions prior to the occurrence of a mainshock are fundamentally dependent on the life-safety threat due to building occupancy and financial life-cycle losses which can potentially be incurred due to building damage and downtime. Different decision bases are proposed to compare different decisions. Throughout this chapter, we emphasize the role of information in potentially improving our decision-making capability. For example, we study the impact of increasing levels of information of the post-mainshock building

damage state (based, for example, on inspection and/or engineering analysis) on evacuation decisions. Finally, we also introduce a general methodology using stochastic dynamic programming to allow for the flexibility of revisions of previously made decisions with the availability of more information. The proposed procedures have important implications in terms of earthquake policy and decision making, especially in terms of quantifying the value of additional information in the information-gathering process.

7.2 Conclusions

The methodologies proposed in this report are illustrated by a continuing example of a three-story SMRF building located on the Stanford site. We observe that aftershock hazard rate (e.g., per day or week) after the mainshock can be significantly higher than the pre-mainshock hazard, especially for a short elapsed number of days after the mainshock. The ratio of aftershock hazard to pre-mainshock hazard is less striking if we use a proposed new concept, that of Equivalent Constant Rates (ECRs), introduced in Chapter 4 to address the time-varying nature of the aftershock threat. This notion has potential application to other time-varying safety problems as well.

We also believe that building-tagging should be based on explicit quantification of the performance of (potentially) damaged building in the post-mainshock environment and the quantitative evaluation of the enhanced time-varying aftershock hazard at the site. These two factors have a direct impact on the life-safety threat that an arbitrary building occupant would be exposed to if he were to occupy a damaged building, and thus should be taken into consideration in the building-tagging process. In this report, we have used the rate of building collapse as a proxy for the life-safety threat in the aftershock environment.

Besides life-safety considerations, we should also take into account financial losses and disruption losses due to downtime in the performance-based earthquake engineering framework. Aftershock life safety (implicitly at least) drives building evacuation decisions which can potentially result in loss of revenues due to downtime. The financial formulations developed in Chapters 5 and 6 explicitly took into consideration both the one-time losses (such as financial losses due to structural and content damage) and continuing disruption losses (due, for example, to downtime of the building). The economic analysis models developed in Chapter 5 provide explicit analytical equations which can be solved easily via the use of computer software packages for the homogeneous Poisson and semi-Markov mainshock

environment. Solving the same set of equations for the nonhomogeneous Poisson aftershock environment requires a time-transformation and the use of Legendre expansions. These formulations are more limited, however, in the modeling assumptions – specifically, with regard to the accurate representation of realistic repair durations which require a non-realistic exponential assumption in the previous formulations. The numerical analysis model developed in Chapter 6 is more flexible, and while numerically recursive in discretized time, is actually less demanding computationally than the Chapter 5 models. We recommend the use of the Chapter 6 model over the models developed in Chapter 5.

7.3 Limitations

This study presents an analytic framework for the incorporation of aftershocks into PBEE. Since the subject of investigation is at its infancy, at every stage, a broad framework is presented and certain assumptions are made. These assumptions define the limitations and scope of this work as well as possible scheme for future research.

We assume that aftershocks can be appropriately modeled by a nonhomogeneous Poisson process. The time-varying nature of aftershock occurrence rates has been studied, for example, in Reasenberg and Jones (1989) and Reasenberg and Jones (1994), but the Poissonian nature of aftershocks has yet to be validated by any studies to the author's knowledge. The time transformation described in Chapter 5 can be used to homogenize the time-varying rate of aftershocks such that the Poissonian nature of aftershocks can be verified on the transformed time scale, using standard procedures in, for example, Ross (2000). We also use the aftershock parameters obtained by Reasenberg and Jones for California to estimate the aftershock ground motion hazard at our site. The ability to estimate site-specific, event-specific aftershock parameters based on Gerstenberger et al. (2002) might potentially allow us to obtain a more accurate representation of a particular aftershock hazard. Their work is based on Bayesian updating to use accumulated aftershock information to update the coefficients in the Omori Law.

The example in this work uses the values of the median capacity $\widehat{Sa}_{cap}^{DSi,DSj}$ and dispersion $\beta_R^{DSi,DSj}$ for a bilinear SDOF building model to compute the probability of being in each post-mainshock damage state and the transition probabilities of the (potentially) damaged building in the aftershock environment. Ideally, the values of $\widehat{Sa}_{cap}^{DSi,DSj}$ and $\beta_R^{DSi,DSj}$ should have been obtained using the results obtained from nonlinear dynamic time-history

analysis of a MDOF representation of the building. Such studies are under way by Dr. Nicolas Luco. The understanding of structural analysis and behavior of damaged buildings is a rich area for future research. The quantification of the epistemic uncertainty, β_U^{DSi}, also deserves more in-depth studies. We also propose default values of coefficients α_1 and α_2 in Chapter 4 to establish the ranges of acceptable collapse rate for buildings of different functionality. The determination of appropriate levels of α_1 and α_2 is an issue of public policy and requires more input from informed government regulatory bodies and social scientists.

The stochastic financial loss models developed in this work focus on obtaining the expected values of life-cycle cost. If full probability distributions are required, we recommend Monte-Carlo simulation to be used (see, for example, Porter (2003)). The damage states used in this study are defined based on peak roof drift ratios. It might be necessary to consider a vector of engineering demand parameters to better define the damage states of the building and its subsequent damage progression due to the occurrences of future earthquakes. The progression of damage states due to the occurrences of both mainshocks and aftershocks is also assumed to be Markovian in nature. This needs to be further verified; it might be necessary to use a vector of engineering demand and response parameters in order to make the Markovian assumption of the damage progression process more accurate. The earthquake occurrence model used in this work also assumes no fault and/or segment interaction.

The decision analytic framework described in Chapter 6 uses decision bases consisting of expected life-cycle cost and rate of collapse. As mentioned earlier in Chapter 6, decision analysis and economics theory suggest that the expected utility of the decision maker should be the quantity to be optimized. The utility function of a decision maker describes his/her attitude towards risk; the process of soliciting the preferences of a decision maker in terms of a utility function is described in Howard (1998). We have also stressed the role of information on the decision making process. This is an area that deserves more attention as Bayesian updating can potentially have an important influence on all aspects of seismic decision making and the information gathering process.

7.4 Future Work

There are several areas of further research that would improve the incorporation of aftershocks into the current PBEE framework. Here, we briefly describe two important areas.

The values of $\widehat{Sa}_{cap}^{DSi,DSj}$ and $\beta_R^{DSi,DSj}$ obtained using the bilinear SDOF model in this work do not demonstrate much reduction in the values of the median capacities of the building with increased levels of sustained damaged for all initial post-mainshock damage states. This finding is contrary to most engineers' current perceptions. The study of the capacities of damaged buildings and the effects of multiple earthquake ground motions on structures are areas that need more research by the structural engineering community.

Another important area of research is to identify potential areas of Bayesian updating in seismic risk management decision making to develop the applications in depth. Subjects might include the impact of ground motion information, inspection levels and analysis depth on the knowledge of seismic capacity of intact and damaged buildings. A quantitative approach to decision making in both the post- and pre-mainshock scenarios allows one to identify the areas in which more information gathering is required, which will help to reduce epistemic uncertainty and improve the quality of the decision.

References

Abrahamson, N.A. and Silva, W.J. 1997. Empirical response spectral attenuation relations for shallow crustal earthquakes. *Seismological Research Letters*, **68**(1), 94–127.

Amadio, C., Fragiacomo, M. and Rajgelj, S. 2003. The effects of repeated earthquake ground motions on the non-linear response of SDOF systems. *Earthquake Engineering and Structural Dynamics*, **32**, 291–308.

Amin, M., Budnitz, R.J., Cornell, C.A., Kennedy, R.P., Olson, D.E. and Tang, H.T. 1999. Reduced seismic loads for temporary conditions. *Nuclear Engineering and Design*, **192**(2-3), 167–178.

Ang, A.H-S. and Leon, D.D. 1996. Development of risk-based cost-effective criteria for design and upgrading of structures. *In: Proceedings of the 11th World Conference on Earthquake Engineering, Acapulco, Mexico.*

Bazzurro, P., Cornell, C.A., Menun, C., Luco, N. and Motahari, M. 2004a (September). *Advanced seismic assessment guidelines.* Tech. rept. 2004/03. Pacific Earthquake Engineering Research Center (PEER).

Bazzurro, P., Cornell, C.A., Menun, C. and Motahari, M. 2004b. Guidelines for seismic assessment of damaged buildings. *In: Proceedings of the 13th World Conference on Earthquake Engineering, Vancouver, Canada.*

Benjamin, J.R. and Cornell, C.A. 1970. *Probability, Statistics and Decision for Civil Engineers.* McGraw-Hill.

Bertsekas, D.P. 2000. *Dynamic Programming and Optimal Control: Vol one.* Second edition. Athena Scientific.

Cantaluppi, L.J. 1981. *Semi-markov decision chains with holding-time-dependent policies.* Ph.D. thesis, Stanford University.

Chou, I.H., Goldberg, J.E. and Yao, J.T.P. 1973. Design decisions for seismic structures. *In: Proceedings of the 5th World Conference on Earthquake Engineering, Rome, Italy.*

Comartin, C.D. 2004. Applications of performance-based engineering to risk management decisions. *In: International Workshop on Performance-Based Design: Bled, Slovenia.*

Comerio, M.C. 2000. *The economic benefits of a disaster resistant university: Earthquake loss estimation for UC Berkeley.* Institute of Urban and Regional Development (IURD) Working Paper Series 2000-02. UC Berkeley.

Cornell, C. A. and Winterstein, S. 1988. Temporal and magnitude dependence in earthquake recurrence models. *Bulletin of the Seismological Society of America*, **78**(4), 1522–1537.

Cornell, C.A. 2004. Hazard analysis, ground motions and probabilistic assessments for PBSD. *In: International Workshop on Performance-Based Design: Bled, Slovenia.*

Cornell, C.A. and Bandyopadhyay, K.K. 1996. Should we relax seismic criteria for shorter system exposure times? *In: Proceedings of Pressure Vessels and Piping Conference: New York: ASME.*

Cornell, C.A., Jalayer, F., Hamburger, R.O. and Foutch, D.A. 2002. The probabilistic basis for the 2000 SAC/FEMA steel moment frame guidelines. *ASCE Journal of Structural Engineering*, **128**(4), 526–533.

Delbaen, F. and Haezendonck, J. 1987. Classical risk theory in an economic environment. *Insurance: Mathematics and Economics*, **6**(2), 85–116.

DOE. 2002 (January). *Natural phenomena hazards design and evaluation criteria for Department of Energy facilities.* Tech. rept. DOE-STD-1020-2002. U.S. Department of Energy, Washington, D.C.

Dreger, D. and Savage, B. 1998. Aftershocks of the 1952 Kern County, California, Earthquake Sequence. *Bulletin of the Seismological Society of America*, **89**, 1094–1108.

EPRI. 1998. *Guidelines for reduced seismic loads to assess temporary conditions in nuclear power plants.* Tech. rept. TR-108904. Electric Power Research Institute.

FEMA. 1999. *HAZUS 99 Technical Manual*. Prepared by Federal Emergency Management Agency, Washington, DC.

FEMA. 2000. *FEMA 352: Recommended Post-Earthquake Evaluation and Repair Criteria for Welded Steel Moment-Frame Buildings*. Prepared by the SAC Steel Project.

Gallagher, R.P., Reasenberg, P.A. and Poland, C.D. 1999. *Earthquake Aftershocks- Entering Damaged Buildings: ATC TechBrief 2*. Applied Technology Council (ATC).

Gerstenberger, M., Wiemer, S. and Jones, L. 2002. STEP - An online, realtime, short term earthquake hazard modeling procedure. *Submitted to USGS*.

Hauksson, E., Jones, L.M., Hutton, K. and Phillips, D.E. 1993. The 1992 Landers earthquake sequence: Seismological observations. *Journal of Geophysical Research*, **98**(B11), 19835–19858.

Hough, S.E. and Dreger, D.S. 1995. Source parameters of the 23 April 1992 M 6.1 Joshua Tree, California, earthquake and its aftershocks: Empirical Green's function analysis of GEOS and TERRAscope Data. *Bulletin of the Seismological Society of America*, **85**(6), 1576–1590.

Howard, R.A. 1971. *Dynamic Probabilistic Systems Volume II: Semi-Markov and Decision Processes*. John Wiley and Sons, Inc.

Howard, R.A. 1998. *The Foundations of Decision Analysis*. Tech. rept.

Howard, R.A. and Matheson, J.E. 1984. *Readings on the Principles and Applications of Decision Analysis*. Tech. rept. Strategic Decisions Group.

Journel, A.G. 1978. *Mining Geostatistics*. Academic Press.

Kiremidjian, A. and Anagnos, T. 1984. Stochastic slip-predictable model for earthquake occurrences. *Bulletin of the Seismological Society of America*, **74**(2), 739–755.

Kramer, S.L. 1995. *Geotechnical Earthquake Engineering*. John Wiley and Sons Inc.

Kwan, W.P. and Billington, S.L. 2003a. Unbonded post-tensioned concrete bridge piers: Part I: Monotonic and cyclic analyses. *ASCE Journal of Bridge Engineering*, **8**(2), 92–101.

Kwan, W.P. and Billington, S.L. 2003b. Unbonded post-tenstioned concrete bridge piers: Part II: Seismic Analyses. *ASCE Journal of Bridge Engineering*, **8**(2), 102–111.

Lee, K. and Foutch, D.A. 2004. Performance evaluation of damaged steel frame buildings subjected to seismic loads. *ASCE Journal of Structural Engineering*, **130**(4), 588–599.

Lew, M., Naeim, F., Huang, S.C., Lam, H.K. and Carpenter, L.D. 2000. Geotechnical and geological effects of the 21 September 1999 Chi-Chi earthquake, Taiwan. *The Structural Design of Tall Buildings*, **9**, 89–106.

Leyendecker, E.V., Hunt, R.J., Frankel, A.D. and Rukstales, K.S. 2000. Development of maximum considered earthquake ground motion maps. *Earthquake Spectra*, **1**(16), 21–40.

Luco, N., Cornell, C.A. and Yeo, G.L. 2002. Annual Limit-Sate Frequencies for Partially-Inspected Earthquake-Damage Buildings. *Structural Safety*, **24**(2-4), 281–296.

Luco, N., Bazzurro, P. and Cornell, C.A. 2004. Dynamic versus static computation of the residual capacity of a mainshock-damaged building to withstand an aftershock. *In: Proceedings of the 13th World Conference on Earthquake Engineering, Vancouver, Canada.*

Mackie, K. and Stojadinovic, B. 2004. Post-earthquake function of highway overpass bridges. *In: International Workshop on Performance-Based Design: Bled, Slovenia.*

Maffei, J.R., Mohr, D.S. and Holmes, W.T. 2002. *Test application of advanced seismic assessment guidelines for 3-story steel moment-frame: Draft.* Rutherford and Chekene; Oakland, California.

Merz, H.A. 1973. *Aftershocks in engineering seismic risk analysis.* M.Sc thesis, Massachusetts Institute of Technology.

Moehle, J. and Deierlein, G.G. 2004. A framework methodology for performance-based earthquake engineering. *In: International Workshop on Performance-Based Design: Bled, Slovenia.*

NPD. 1981. *Guidelines for safety evaluation of platform conceptual design: Oslo, Norway.* Norwegian Petroleum Directorate.

Okrent, D. 1987. The safety goals of the U.S. Nuclear Regulatory Commission. *Science*, **236**, 296–300.

Omori, F. 1894. On the aftershocks of earthquakes. *Journal of Coll. Science Imperial University Tokyo*, **7**, 111–120.

Parzen, E. 1962. *Stochastic Processes*. Holden-Day, Inc.

Paté, M.E. 1985. Costs and benefits of seismic upgrading of some buildings in the Boston area. *Earthquake Spectra*, **1**(4), 721–740.

Paté, M.E. and Shah, H.C. 1980. Public policy issues: Earthquake Engineering. *Bulletin of the Seismological Society of America*, **70**(5), 1955–1968.

Paté-Cornell, M.E. 1984. Discounting in Risk Analysis: Capital vs. Human Safety. *In: Structural Technology and Risk. Waterloo: University of Waterloo Press.*

Porter, K. 2003. An overview of PEER's Performance-based earthquake engineering methodology. *In: Ninth International Conference on Applications of Statistics and Probability in Civil Engineering (ICASP9): San Francisco, California, U.S.A.*

Raiffa, H. and Schlaifer, R. 1961. *Applied Statistical Decision Theory.* Harvard University, Boston, MA.

Reasenberg, P.A. and Jones, L.M. 1989. Earthquake hazard after a mainshock in California. *Science*, **243**, 1173–1175.

Reasenberg, P.A. and Jones, L.M. 1994. Earthquake aftershocks: Update. *Science*, **265**, 1251–1252.

Rice, J.A. 1995. *Mathematical Statistics and Data Analysis.* Second edition. Duxbury Press.

Rosenblueth, E. 1976. Optimum design for infrequent disturbances. *ASCE Journal of Structural Engineering*, **102**(9), 1807–1825.

Ross, S.M. 2000. *Introduction to Probability Models.* Seventh edition. Academic Press.

Takahashi, Y., A. Der Kiureghian and Ang, A.H-S. 2004. Life-cycle cost analysis based on a renewal model of earthquake occurrences. *Earthquake Engineering and Structural Dynamics*, **33**, 859–880.

USGS. 1986. *USGS Circular 971: Strong-motion program report, January-December 1983.*

USGS. 1990. *Probabilities of Large Earthquakes in the San Francisco Bay Region*. Open file report 90-1053 edition. Working Group on California Earthquake Probabilities.

USGS. 1999. *Earthquake Probabilities in the San Francisco Bay Region: 2000 to 2003*. Open file report 99-517 edition. Working Group on California Earthquake Probabilities.

USGS. 2000. *USGS Circular 1193: Implications for earthquake risk reduction in the United States from the Kocaeli, Turkey, earthquake of August 17, 1999*.

USGS. 2003. *Earthquake Probabilities in the San Francisco Bay Region: 2002-2031*. Open file report 03-214 edition. Working Group on California Earthquake Probabilities.

USGS. 2004. *ShakeMap Website*. http://www.trinet.org/shake/.

Utsu, T. 1995. The centenary of the Omori Formula for a decay law of aftershock activity. *Journal of the Physics of the Earth*, **43**, 1–33.

Vamvatsikos, D. and Cornell, C.A. 2004. Practical estimation of the seismic demand and capacity of oscillators with multi-linear static pushovers through incremental dynamic analysis. *In: Proceedings of the 7th U.S. National Conference on Earthquake Engineering, Boston, MA*.

Vanmarcke, E.H. and Diaz-Padilla, J. 1971 (December). *Markov decision models in seismic design*. Research Report R71-20. Massachusetts Institute of Technology.

Wald, D.J., Quitoriano, V., Heaton, T.H., Kanamori, H., Scrivner, C.W. and Worden, C.B. 1999. TriNet ShakeMaps: Rapid Generation of Instrumental Ground Motion and Intensity Maps for Earthquakes in Southern California. *Earthquake Spectra*, **15**, 537–556.

Weimer, S. 2000. Introducing probabilistic aftershock hazard mapping. *Geophysical Research Letters*, **27**(20), 3405–3408.

Wells, D.L. and Coppersmith, K.J. 1994. New empirical relationships among magnitude, rupture length, rupture width, rupture area and surface displacement. *Bulletin of the Seismological Society of America*, **84**(4), 974–1002.

Wen, Y.K. and Kang, Y.J. 2001. Minimum building life-cycle cost design criteria. I: Methodology. *ASCE Journal of Structural Engineering*, **127**(3), 330–337.

Whitman, R.V., Biggs, J.M., Brennan, J., Cornell, C.A., de Neufville, R. and Vanmarcke, E.H. 1974 (July). *Seismic design decision analysis: Methodology and pilot application.* Research Report MIT-CE-R74-15. Massachusetts Institute of Technology.

Whittaker, A., Bertero, V.V., Wright, J. and Higashino, M. 1997. *Earthquake damage distribution.* http://nisee.berkeley.edu/kobe/damage.html.

Woodward-Clyde. 1991. *Evaluation of site response and design earthquake motions, Stanford University, Palo Alto, California.*

PEER REPORTS

PEER reports are available from the National Information Service for Earthquake Engineering (NISEE). To order PEER reports, please contact the Pacific Earthquake Engineering Research Center, 1301 South 46th Street, Richmond, California 94804-4698. Tel.: (510) 665-3405; Fax: (510) 665-3420.

PEER 2006/01 *Bracing Berkeley. A Guide to Seismic Safety on the UC Berkeley Campus.* Mary C. Comerio, Stephen Tobriner, and Ariane Fehrenkamp. January 2006.

PEER 2005/15 *CPT-Based Probabilistic Assessment of Seismic Soil Liquefaction Initiation.* R. E. S. Moss, R. B. Seed, R. E. Kayen, J. P. Stewart, and A. Der Kiureghian. April 2006.

PEER 2005/13 *Stochastic Characterization and Decision Bases under Time-Dependent Aftershock Risk in Performance-Based Earthquake Engineering.* Gee Liek Yeo and C. Allin Cornell. July 2005.

PEER 2005/12 *PEER Testbed Study on a Laboratory Building: Exercising Seismic Performance Assessment.* Mary C. Comerio, editor. November 2005.

PEER 2005/11 *Van Nuys Hotel Building Testbed Report: Exercising Seismic Performance Assessment.* Helmut Krawinkler, editor. October 2005.

PEER 2005/10 *First NEES/E-Defense Workshop on Collapse Simulation of Reinforced Concrete Building Structures.* September 2005.

PEER 2005/08 *Damage Accumulation in Lightly Confined Reinforced Concrete Bridge Columns.* R. Tyler Ranf, Jared M. Nelson, Zach Price, Marc O. Eberhard, and John F. Stanton. April 2006.

PEER 2005/07 *Experimental and Analytical Studies on the Seismic Response of Freestanding and Anchored Laboratory Equipment.* Dimitrios Konstantinidis and Nicos Makris. January 2005.

PEER 2005/06 *Global Collapse of Frame Structures under Seismic Excitations.* Luis F. Ibarra and Helmut Krawinkler. September 2005.

PEER 2005/05 *Performance Characterization of Bench- and Shelf-Mounted Equipment.* Samit Ray Chaudhuri and Tara C. Hutchinson. May 2006.

PEER 2005/04 *Numerical Modeling of the Nonlinear Cyclic Response of Shallow Foundations.* Chad Harden, Tara Hutchinson, Geoffrey R. Martin, and Bruce L. Kutter. August 2005.

PEER 2005/03 *A Taxonomy of Building Components for Performance-Based Earthquake Engineering.* Keith A. Porter. September 2005.

PEER 2005/02 *Fragility Basis for California Highway Overpass Bridge Seismic Decision Making.* Kevin R. Mackie and Bozidar Stojadinovic. June 2005.

PEER 2005/01 *Empirical Characterization of Site Conditions on Strong Ground Motion.* Jonathan P. Stewart, Yoojoong Choi, and Robert W. Graves. June 2005.

PEER 2004/09 *Electrical Substation Equipment Interaction: Experimental Rigid Conductor Studies.* Christopher Stearns and André Filiatrault. February 2005.

PEER 2004/08 *Seismic Qualification and Fragility Testing of Line Break 550-kV Disconnect Switches.* Shakhzod M. Takhirov, Gregory L. Fenves, and Eric Fujisaki. January 2005.

PEER 2004/07 *Ground Motions for Earthquake Simulator Qualification of Electrical Substation Equipment.* Shakhzod M. Takhirov, Gregory L. Fenves, Eric Fujisaki, and Don Clyde. January 2005.

PEER 2004/06 *Performance-Based Regulation and Regulatory Regimes.* Peter J. May and Chris Koski. September 2004.

PEER 2004/05 *Performance-Based Seismic Design Concepts and Implementation: Proceedings of an International Workshop.* Peter Fajfar and Helmut Krawinkler, editors. September 2004.

PEER 2004/04 *Seismic Performance of an Instrumented Tilt-up Wall Building.* James C. Anderson and Vitelmo V. Bertero. July 2004.

PEER 2004/03 *Evaluation and Application of Concrete Tilt-up Assessment Methodologies.* Timothy Graf and James O. Malley. October 2004.

PEER 2004/02 *Analytical Investigations of New Methods for Reducing Residual Displacements of Reinforced Concrete Bridge Columns.* Junichi Sakai and Stephen A. Mahin. August 2004.

PEER 2004/01 *Seismic Performance of Masonry Buildings and Design Implications.* Kerri Anne Taeko Tokoro, James C. Anderson, and Vitelmo V. Bertero. February 2004.

PEER 2003/18 *Performance Models for Flexural Damage in Reinforced Concrete Columns.* Michael Berry and Marc Eberhard. August 2003.

PEER 2003/17 *Predicting Earthquake Damage in Older Reinforced Concrete Beam-Column Joints.* Catherine Pagni and Laura Lowes. October 2004.

PEER 2003/16 *Seismic Demands for Performance-Based Design of Bridges.* Kevin Mackie and Božidar Stojadinovic. August 2003.

PEER 2003/15 *Seismic Demands for Nondeteriorating Frame Structures and Their Dependence on Ground Motions.* Ricardo Antonio Medina and Helmut Krawinkler. May 2004.

PEER 2003/14 *Finite Element Reliability and Sensitivity Methods for Performance-Based Earthquake Engineering.* Terje Haukaas and Armen Der Kiureghian. April 2004.

PEER 2003/13 *Effects of Connection Hysteretic Degradation on the Seismic Behavior of Steel Moment-Resisting Frames.* Janise E. Rodgers and Stephen A. Mahin. March 2004.

PEER 2003/12 *Implementation Manual for the Seismic Protection of Laboratory Contents: Format and Case Studies.* William T. Holmes and Mary C. Comerio. October 2003.

PEER 2003/11 *Fifth U.S.-Japan Workshop on Performance-Based Earthquake Engineering Methodology for Reinforced Concrete Building Structures.* February 2004.

PEER 2003/10 *A Beam-Column Joint Model for Simulating the Earthquake Response of Reinforced Concrete Frames.* Laura N. Lowes, Nilanjan Mitra, and Arash Altoontash. February 2004.

PEER 2003/09 *Sequencing Repairs after an Earthquake: An Economic Approach.* Marco Casari and Simon J. Wilkie. April 2004.

PEER 2003/08 *A Technical Framework for Probability-Based Demand and Capacity Factor Design (DCFD) Seismic Formats*. Fatemeh Jalayer and C. Allin Cornell. November 2003.

PEER 2003/07 *Uncertainty Specification and Propagation for Loss Estimation Using FOSM Methods.* Jack W. Baker and C. Allin Cornell. September 2003.

PEER 2003/06 *Performance of Circular Reinforced Concrete Bridge Columns under Bidirectional Earthquake Loading*. Mahmoud M. Hachem, Stephen A. Mahin, and Jack P. Moehle. February 2003.

PEER 2003/05 *Response Assessment for Building-Specific Loss Estimation.* Eduardo Miranda and Shahram Taghavi. September 2003.

PEER 2003/04 *Experimental Assessment of Columns with Short Lap Splices Subjected to Cyclic Loads*. Murat Melek, John W. Wallace, and Joel Conte. April 2003.

PEER 2003/03 *Probabilistic Response Assessment for Building-Specific Loss Estimation.* Eduardo Miranda and Hesameddin Aslani. September 2003.

PEER 2003/02 *Software Framework for Collaborative Development of Nonlinear Dynamic Analysis Program.* Jun Peng and Kincho H. Law. September 2003.

PEER 2003/01 *Shake Table Tests and Analytical Studies on the Gravity Load Collapse of Reinforced Concrete Frames.* Kenneth John Elwood and Jack P. Moehle. November 2003.

PEER 2002/24 *Performance of Beam to Column Bridge Joints Subjected to a Large Velocity Pulse.* Natalie Gibson, André Filiatrault, and Scott A. Ashford. April 2002.

PEER 2002/23 *Effects of Large Velocity Pulses on Reinforced Concrete Bridge Columns.* Greg L. Orozco and Scott A. Ashford. April 2002.

PEER 2002/22 *Characterization of Large Velocity Pulses for Laboratory Testing.* Kenneth E. Cox and Scott A. Ashford. April 2002.

PEER 2002/21 *Fourth U.S.-Japan Workshop on Performance-Based Earthquake Engineering Methodology for Reinforced Concrete Building Structures*. December 2002.

PEER 2002/20 *Barriers to Adoption and Implementation of PBEE Innovations.* Peter J. May. August 2002.

PEER 2002/19 *Economic-Engineered Integrated Models for Earthquakes: Socioeconomic Impacts.* Peter Gordon, James E. Moore II, and Harry W. Richardson. July 2002.

PEER 2002/18 *Assessment of Reinforced Concrete Building Exterior Joints with Substandard Details.* Chris P. Pantelides, Jon Hansen, Justin Nadauld, and Lawrence D. Reaveley. May 2002.

PEER 2002/17 *Structural Characterization and Seismic Response Analysis of a Highway Overcrossing Equipped with Elastomeric Bearings and Fluid Dampers: A Case Study.* Nicos Makris and Jian Zhang. November 2002.

PEER 2002/16 *Estimation of Uncertainty in Geotechnical Properties for Performance-Based Earthquake Engineering.* Allen L. Jones, Steven L. Kramer, and Pedro Arduino. December 2002.

PEER 2002/15 *Seismic Behavior of Bridge Columns Subjected to Various Loading Patterns.* Asadollah Esmaeily-Gh. and Yan Xiao. December 2002.

PEER 2002/14 *Inelastic Seismic Response of Extended Pile Shaft Supported Bridge Structures.* T.C. Hutchinson, R.W. Boulanger, Y.H. Chai, and I.M. Idriss. December 2002.

PEER 2002/13 *Probabilistic Models and Fragility Estimates for Bridge Components and Systems.* Paolo Gardoni, Armen Der Kiureghian, and Khalid M. Mosalam. June 2002.

PEER 2002/12 *Effects of Fault Dip and Slip Rake on Near-Source Ground Motions: Why Chi-Chi Was a Relatively Mild M7.6 Earthquake.* Brad T. Aagaard, John F. Hall, and Thomas H. Heaton. December 2002.

PEER 2002/11 *Analytical and Experimental Study of Fiber-Reinforced Strip Isolators*. James M. Kelly and Shakhzod M. Takhirov. September 2002.

PEER 2002/10 *Centrifuge Modeling of Settlement and Lateral Spreading with Comparisons to Numerical Analyses***.** Sivapalan Gajan and Bruce L. Kutter. January 2003.

PEER 2002/09 *Documentation and Analysis of Field Case Histories of Seismic Compression during the 1994 Northridge, California, Earthquake.* Jonathan P. Stewart, Patrick M. Smith, Daniel H. Whang, and Jonathan D. Bray. October 2002.

PEER 2002/08 *Component Testing, Stability Analysis and Characterization of Buckling-Restrained Unbonded Braces™*. Cameron Black, Nicos Makris, and Ian Aiken. September 2002.

PEER 2002/07 *Seismic Performance of Pile-Wharf Connections.* Charles W. Roeder, Robert Graff, Jennifer Soderstrom, and Jun Han Yoo. December 2001.

PEER 2002/06 *The Use of Benefit-Cost Analysis for Evaluation of Performance-Based Earthquake Engineering Decisions*. Richard O. Zerbe and Anthony Falit-Baiamonte. September 2001.

PEER 2002/05 *Guidelines, Specifications, and Seismic Performance Characterization of Nonstructural Building Components and Equipment*. André Filiatrault, Constantin Christopoulos, and Christopher Stearns. September 2001.

PEER 2002/04 *Consortium of Organizations for Strong-Motion Observation Systems and the Pacific Earthquake Engineering Research Center Lifelines Program: Invited Workshop on Archiving and Web Dissemination of Geotechnical Data, 4–5 October 2001*. September 2002.

PEER 2002/03 *Investigation of Sensitivity of Building Loss Estimates to Major Uncertain Variables for the Van Nuys Testbed.* Keith A. Porter, James L. Beck, and Rustem V. Shaikhutdinov. August 2002.

PEER 2002/02 *The Third U.S.-Japan Workshop on Performance-Based Earthquake Engineering Methodology for Reinforced Concrete Building Structures*. July 2002.

PEER 2002/01 *Nonstructural Loss Estimation: The UC Berkeley Case Study.* Mary C. Comerio and John C. Stallmeyer. December 2001.

PEER 2001/16 *Statistics of SDF-System Estimate of Roof Displacement for Pushover Analysis of Buildings.* Anil K. Chopra, Rakesh K. Goel, and Chatpan Chintanapakdee. December 2001.

PEER 2001/15 *Damage to Bridges during the 2001 Nisqually Earthquake.* R. Tyler Ranf, Marc O. Eberhard, and Michael P. Berry. November 2001.

PEER 2001/14 *Rocking Response of Equipment Anchored to a Base Foundation.* Nicos Makris and Cameron J. Black. September 2001.

PEER 2001/13 *Modeling Soil Liquefaction Hazards for Performance-Based Earthquake Engineering.* Steven L. Kramer and Ahmed-W. Elgamal. February 2001.

PEER 2001/12 *Development of Geotechnical Capabilities in OpenSees.* Boris Jeremi . September 2001.

PEER 2001/11 *Analytical and Experimental Study of Fiber-Reinforced Elastomeric Isolators*. James M. Kelly and Shakhzod M. Takhirov. September 2001.

PEER 2001/10 *Amplification Factors for Spectral Acceleration in Active Regions.* Jonathan P. Stewart, Andrew H. Liu, Yoojoong Choi, and Mehmet B. Baturay. December 2001.

PEER 2001/09 *Ground Motion Evaluation Procedures for Performance-Based Design.* Jonathan P. Stewart, Shyh-Jeng Chiou, Jonathan D. Bray, Robert W. Graves, Paul G. Somerville, and Norman A. Abrahamson. September 2001.

PEER 2001/08 *Experimental and Computational Evaluation of Reinforced Concrete Bridge Beam-Column Connections for Seismic Performance*. Clay J. Naito, Jack P. Moehle, and Khalid M. Mosalam. November 2001.

PEER 2001/07 *The Rocking Spectrum and the Shortcomings of Design Guidelines.* Nicos Makris and Dimitrios Konstantinidis. August 2001.

PEER 2001/06 *Development of an Electrical Substation Equipment Performance Database for Evaluation of Equipment Fragilities*. Thalia Agnanos. April 1999.

PEER 2001/05 *Stiffness Analysis of Fiber-Reinforced Elastomeric Isolators.* Hsiang-Chuan Tsai and James M. Kelly. May 2001.

PEER 2001/04 *Organizational and Societal Considerations for Performance-Based Earthquake Engineering.* Peter J. May. April 2001.

PEER 2001/03 *A Modal Pushover Analysis Procedure to Estimate Seismic Demands for Buildings: Theory and Preliminary Evaluation.* Anil K. Chopra and Rakesh K. Goel. January 2001.

PEER 2001/02 *Seismic Response Analysis of Highway Overcrossings Including Soil-Structure Interaction.* Jian Zhang and Nicos Makris. March 2001.

PEER 2001/01 *Experimental Study of Large Seismic Steel Beam-to-Column Connections.* Egor P. Popov and Shakhzod M. Takhirov. November 2000.

PEER 2000/10 *The Second U.S.-Japan Workshop on Performance-Based Earthquake Engineering Methodology for Reinforced Concrete Building Structures.* March 2000.

PEER 2000/09 *Structural Engineering Reconnaissance of the August 17, 1999 Earthquake: Kocaeli (Izmit), Turkey*. Halil Sezen, Kenneth J. Elwood, Andrew S. Whittaker, Khalid Mosalam, John J. Wallace, and John F. Stanton. December 2000.

PEER 2000/08 *Behavior of Reinforced Concrete Bridge Columns Having Varying Aspect Ratios and Varying Lengths of Confinement*. Anthony J. Calderone, Dawn E. Lehman, and Jack P. Moehle. January 2001.

PEER 2000/07 *Cover-Plate and Flange-Plate Reinforced Steel Moment-Resisting Connections.* Taejin Kim, Andrew S. Whittaker, Amir S. Gilani, Vitelmo V. Bertero, and Shakhzod M. Takhirov. September 2000.

PEER 2000/06 *Seismic Evaluation and Analysis of 230-kV Disconnect Switches.* Amir S. J. Gilani, Andrew S. Whittaker, Gregory L. Fenves, Chun-Hao Chen, Henry Ho, and Eric Fujisaki. July 2000.

PEER 2000/05 *Performance-Based Evaluation of Exterior Reinforced Concrete Building Joints for Seismic Excitation.* Chandra Clyde, Chris P. Pantelides, and Lawrence D. Reaveley. July 2000.

PEER 2000/04 *An Evaluation of Seismic Energy Demand: An Attenuation Approach.* Chung-Che Chou and Chia-Ming Uang. July 1999.

PEER 2000/03 *Framing Earthquake Retrofitting Decisions: The Case of Hillside Homes in Los Angeles.* Detlof von Winterfeldt, Nels Roselund, and Alicia Kitsuse. March 2000.

PEER 2000/02 *U.S.-Japan Workshop on the Effects of Near-Field Earthquake Shaking.* Andrew Whittaker, ed. July 2000.

PEER 2000/01 *Further Studies on Seismic Interaction in Interconnected Electrical Substation Equipment.* Armen Der Kiureghian, Kee-Jeung Hong, and Jerome L. Sackman. November 1999.

PEER 1999/14 *Seismic Evaluation and Retrofit of 230-kV Porcelain Transformer Bushings*. Amir S. Gilani, Andrew S. Whittaker, Gregory L. Fenves, and Eric Fujisaki. December 1999.

PEER 1999/13 *Building Vulnerability Studies: Modeling and Evaluation of Tilt-up and Steel Reinforced Concrete Buildings.* John W. Wallace, Jonathan P. Stewart, and Andrew S. Whittaker, editors. December 1999.

PEER 1999/12 *Rehabilitation of Nonductile RC Frame Building Using Encasement Plates and Energy-Dissipating Devices.* Mehrdad Sasani, Vitelmo V. Bertero, James C. Anderson. December 1999.

PEER 1999/11 *Performance Evaluation Database for Concrete Bridge Components and Systems under Simulated Seismic Loads.* Yael D. Hose and Frieder Seible. November 1999.

PEER 1999/10 *U.S.-Japan Workshop on Performance-Based Earthquake Engineering Methodology for Reinforced Concrete Building Structures.* December 1999.

PEER 1999/09 *Performance Improvement of Long Period Building Structures Subjected to Severe Pulse-Type Ground Motions.* James C. Anderson, Vitelmo V. Bertero, and Raul Bertero. October 1999.

PEER 1999/08 *Envelopes for Seismic Response Vectors.* Charles Menun and Armen Der Kiureghian. July 1999.

PEER 1999/07 *Documentation of Strengths and Weaknesses of Current Computer Analysis Methods for Seismic Performance of Reinforced Concrete Members.* William F. Cofer. November 1999.

PEER 1999/06 *Rocking Response and Overturning of Anchored Equipment under Seismic Excitations.* Nicos Makris and Jian Zhang. November 1999.

PEER 1999/05 *Seismic Evaluation of 550 kV Porcelain Transformer Bushings.* Amir S. Gilani, Andrew S. Whittaker, Gregory L. Fenves, and Eric Fujisaki. October 1999.

PEER 1999/04 *Adoption and Enforcement of Earthquake Risk-Reduction Measures.* Peter J. May, Raymond J. Burby, T. Jens Feeley, and Robert Wood.

PEER 1999/03 *Task 3 Characterization of Site Response General Site Categories.* Adrian Rodriguez-Marek, Jonathan D. Bray, and Norman Abrahamson. February 1999.

PEER 1999/02 *Capacity-Demand-Diagram Methods for Estimating Seismic Deformation of Inelastic Structures: SDF Systems.* Anil K. Chopra and Rakesh Goel. April 1999.

PEER 1999/01 *Interaction in Interconnected Electrical Substation Equipment Subjected to Earthquake Ground Motions.* Armen Der Kiureghian, Jerome L. Sackman, and Kee-Jeung Hong. February 1999.

PEER 1998/08 *Behavior and Failure Analysis of a Multiple-Frame Highway Bridge in the 1994 Northridge Earthquake.* Gregory L. Fenves and Michael Ellery. December 1998.

PEER 1998/07 *Empirical Evaluation of Inertial Soil-Structure Interaction Effects.* Jonathan P. Stewart, Raymond B. Seed, and Gregory L. Fenves. November 1998.

PEER 1998/06 *Effect of Damping Mechanisms on the Response of Seismic Isolated Structures.* Nicos Makris and Shih-Po Chang. November 1998.

PEER 1998/05 *Rocking Response and Overturning of Equipment under Horizontal Pulse-Type Motions.* Nicos Makris and Yiannis Roussos. October 1998.

PEER 1998/04 *Pacific Earthquake Engineering Research Invitational Workshop Proceedings, May 14–15, 1998: Defining the Links between Planning, Policy Analysis, Economics and Earthquake Engineering.* Mary Comerio and Peter Gordon. September 1998.

PEER 1998/03 *Repair/Upgrade Procedures for Welded Beam to Column Connections.* James C. Anderson and Xiaojing Duan. May 1998.

PEER 1998/02 *Seismic Evaluation of 196 kV Porcelain Transformer Bushings.* Amir S. Gilani, Juan W. Chavez, Gregory L. Fenves, and Andrew S. Whittaker. May 1998.

PEER 1998/01 *Seismic Performance of Well-Confined Concrete Bridge Columns.* Dawn E. Lehman and Jack P. Moehle. December 2000.